# Direct and indirect measurements of on-road vehicle emissions in the UK: Implications for outdoor and within-vehicle air quality and human health

by

Vasileios N. Matthaios

A thesis submitted to
the University of
Birmingham for the
degree of
DOCTOR OF PHILOSOPHY


UNIVERSITY OF BIRMINGHAM

School of Geography, Earth and Environmental Sciences
University of Birmingham
May 2020

# Abstract

Urban air quality and particularly human exposure to traffic related emissions is one of the biggest problems in modern societies. This thesis is dedicated to advancing understanding of human exposure to traffic related air pollution in developed cities. The conceptual framework covers aspects of exposure spanning from roadside to within-vehicle exposure, while focusing on providing new modelling tools and methods that can be used to assist and better manage air quality. To investigate roadside exposure, a trend analysis of nitric oxide, nitrogen dioxide, ozone and temperature was performed across the UK for the period 2009 - 2016 and a new methodology was introduced to quantify for the first time the impact of cold weather-related vehicle primary nitrogen dioxide emissions on urban air quality. To study within-vehicle exposure, a set of field experiments were conducted, where four vehicles were driven on a consistent route encompassing contrasting road types, measuring, under different ventilation options, simultaneous within-vehicle and ambient levels of particulate matter, aerosol lung surface deposited area, nitric oxide and nitrogen dioxide. The data from these experiments were used to build a mass balance model to estimate personal exposure to air pollution within vehicle cabins, while state-of-the-art machine learning algorithms were also used to introduce new predictive capabilities for air pollution exposure.

*This thesis is dedicated to the memory of my father Nikolaos Matthaios, who I miss dearly and to my mother and brother*

# Acknowledgements

First and foremost, I would like to express gratitude to my supervisor Bill Bloss for giving me the opportunity to pursue my research curiosity. I thank him not only for putting up with me over the last few years but also for his guidance and the trust that he showed me to make my own decisions. I have enjoyed his challenging scientific questions that have shaped my way of thinking. Due to his support and encouragement I had the chance to visit numerous conferences and research institutions throughout my PhD years. This helped interact with other research groups and shape new ideas that assisted my PhD research. During my visit in EU joint Research Centre in Ispra, Italy, I would like to thank Bart Degraeuwe, Enrico Pisoni and Marco Trombetti for hosting me there. I will miss the usual coffee breaks that taught me a lot about policy related research and vehicle emission control systems. During my visit in University of Queensland in Brisbane, Australia I would like to thank Luke Knibbs who hosted me there and supported my research with his ideas.

I would like to show my appreciation to NERC for a studentship that allowed me to advance my studies to a PhD level and the School of Geography, Earth and Environmental Sciences at the University of Birmingham for making it possible.

As much as I enjoy research, these past few years could not have been as fruitful an experience without the people I have met along the way and worked alongside on a day to day basis. I want to thank Louisa Kramer, Leigh Crilley and Roberto Sommariva for all their help during my PhD and also for the useful discussions that we had all

these years either in their office or over a beer. I also want to thank Colin and Michael who I have shared an office and few beers with along the way, but also Clemens, Grigoris, Argiris and Stelios that made my time in Birmingham much more enjoyable. Most of all, I would like to thank Christina for her moral support and patience during my final years of my PhD.

Finally, I would like to thank my brother and my parents for always supporting me in my decisions and for their endless love, and encouragement all these years that thereby helped me to achieve my goals. I would forever be thankful to my father who gave me the initial spark to study environmental sciences and to my mother for her prayers and putting up with all my idiosyncrasies all these years.

# List of abbreviations

| | |
|---|---|
| AC | Air Condition on |
| AC_R | Air Condition on with recirculation on |
| CCRT | Catalysed continuously regenerated trap |
| CRT | Catalysed regenerated trap |
| DOC | Diesel Oxidation Catalysts |
| DPF | Diesel Particulate Filter |
| EGR | Exhaust Gas Recirculation |
| EU | European Union |
| FAN | Fan on |
| FAN_R | Fan on with recirculation on |
| HC | Hydrocarbons |
| I/O | Inside to outside ratio |
| LDV | Light Duty Vehicle |
| LNT | Lean NOx Trap |
| LSDA | Lung surface deposited area |
| MCM | Master Chemical Mechanism |
| ML | Machine Learning |
| NONE | No Ventilation setting |
| OPC | Optical Particle Counter |
| OPEN | Windows open |
| PEMS | Portable Emission System |
| PM | Particulate Matter |
| PN | Particle number |
| ppb | Parts per billion |
| ppm | Parts per million |
| PSS | photo-stationary steady state |
| SCR | Selective Catalytic Reduction |
| TWC | Three Way catalyst |
| UFP | Ultrafine particles |
| WHO | World Health Organisation |

# Author Contributions

This thesis is based on two published papers and one that is in preparation for submission. These works are shown below along with information of my individual contributions.

1. **Chapter 2 contributions:** The idea for the study was developed by VNM with contributions from WJB and FDP. The conceptual methodological design for the primary $NO_2$ from roadsides under cold weather was developed by VNM. The $NO_x$ - $O_3$ model calculations were conducted by LJK, while the MCM modelling was performed by RS. VNM collected the data, carried out the analysis, interpreted results and wrote the paper with contributions from all co-authors. The results of this chapter have been published in Atmospheric Environment as:

*Matthaios N. V., Kramer J. L., Sommariva R., Pope D. F., Bloss J. W., 2019. Investigation of vehicle cold starts primary NO2 emissions from ambient monitoring data in the UK and their implications for urban air quality. Atmospheric Environment 199, 402-414, DOI: 10.1016/j.atmosenv.2018.11.*

2. **Chapter 3 contributions:** The initial idea was formulated by WJB and VNM, and developed by VNM, LJK, and LRC. The experimental design and methodology was developed by VNM, LRC and LJK, while the experimental work was carried out by VNM, LJK, LRC and RS. VNM carried out the analysis, interpreted the results and wrote the

paper with contributions from all co-authors. The results of this chapter have been published in Atmospheric Environment as:

*Matthaios, V. N., Kramer, L. J., Crilley, L. R., Sommariva, R., Pope, F. D., Bloss, W. J. (2020). Quantification of within-vehicle exposure to NOx and particles: Variation with outside air quality, route choice and ventilation options. Atmospheric Environment, 117810. doi:10.1016/j.atmosenv.2020.117810*

3. **Chapter 4 contributions:** The initial idea was formulated by VNM and developed by VNM, LK and WJB. Both modelling approaches were developed by VNM. LJK and LRC helped with the data collection. VNM carried out the analysis, interpreted the results and wrote the results with contributions from WJB. The work is in preparation for submission as:

*Matthaios N. V., Knibbs L., Kramer J. L., Crilley R. L., Bloss J. W., Predicting within-vehicle exposure with mass-balance and machine learning approaches using inside to outside vehicle and roadside air quality data.*

# Table of Contents

# List of Figures

# Chapter 1



# Chapter 2

# Chapter 3

# Chapter 4

# List of Tables

# Chapter 1

# Chapter 2



# Chapter 3

# Chapter 4

# Preface

***“Love is in the air, but the air is highly polluted”***

Air pollution is not only a problem of our time but might arguably be the biggest challenge of the modern world and the 21st century. The discovery of fire created problems by polluting the air of the surrounding inhabited areas due to incomplete combustion processes. The Roman philosopher and statesman Seneca wrote in 61 A.D:

*"No sooner had I left behind the oppressive atmosphere of the city of Rome and that reek of smoking cookers which pour out, along with clouds of ashes, all the poisonous fumes they've accumulated in their interiors whenever they're started up, than I noticed the change in my condition"*

*In the 16th century the British poet Percy Bysshe Shelley writes:*

*"Hell is a city much like London, a populous and a smoky city"*

A century later John Evelyn made a study of the effects of coal smoke on health, plant life and buildings. Evelyn's paper: *"Fumifugium; or the Inconveniencie of the Aer and Smoak of London Dissipated"* published in 1661 might represent the first complete study of air pollution.

In the 20th century there were several high profile air pollution episodes around the globe. In December 1930, in Meuse valley, Belgium, a five-day smog event coincidentally in conjunction with strong temperature inversions in the atmosphere and heavy sulfur dioxide ($SO_2$) emissions from coal burning resulted in 63 deaths and 6000 people suffering from illness. In 1948 in the United States, there was another

disaster due to air pollution, when a pall of $SO_2$ and suspended particulate matter stabilized for five days over the city of Donora. About 6,000 residents out of the city's 14,000 people became ill, while 20 of them died. The worst of these $20^{th}$ century air pollution episodes occurred in London in 1952. At the time, the city used low quality coal for everything from generating power to heating homes, while much industry and power generation was within the city. As a result, a week of high levels of air pollution caused by stagnant conditions in the atmosphere led to as many as 12,000 deaths, all attributable to air pollution. When the increased use of petrol as a fuel for internal combustion engines grew as a result of the increase in vehicle numbers in big cities, the problem of pollution became more severe and another type of pollution, photochemical air pollution, appeared. This type of secondary air pollution was first seen in the early 1940s, was derived from the mix of vehicular or internal combustion engine emissions and industrial emissions. It affects many cities globally including Mexico City in Mexico, Santiago in Chile, Tokyo in Japan, Beijing in China, Athens in Greece and Los Angeles in the USA.

Nowadays, the major threat to clean air in developed cities is posed by traffic emissions. Petrol and diesel-engine vehicles emit a wide variety of pollutants, principally oxides of nitrogen ($NO_x$) as a sum of nitrogen oxide (NO) and nitrogen dioxide ($NO_2$), volatile organic compounds (VOCs) and particulate matter with aerodynamic diameters ranging from coarse ≤ 10 μm ($PM_{10}$) to fine ≤ 2.5 μm ($PM_{2.5}$) and ultrafine ≤ 300 nm (UFP), which have a significant impact upon human health. In addition, many of these emissions are responsible for the formation of tropospheric ozone ($O_3$), a secondary pollutant generated through photochemical processing of

nitrogen dioxide and VOCs. $O_3$ normally particularly affects suburban and rural areas and has significant impact upon human health, vegetation and climate change.

In the UK road transport is the second largest $NO_2$ source of outdoor urban air pollution. According to the Department for Transport, 68% of the working population use road transport to go to work on a daily basis spending on average at least 38 minutes inside the vehicle cabins. As people use vehicles, outdoor air undergoes exchange with the air inside vehicle cabins, thus exposing vehicle occupants to outdoor air pollution levels to varying extents during this time. However, since the majority of the time (about 90%) is spent in other microenvironments such as houses, work places and schools, many fundamental indoor air quality studies have been primarily focused towards these microenvironments. Thus, little quantitative information is available on air pollution exposure within vehicles and how this varies compared with outside air composition and ventilation preferences or travel route. The overarching aim of this thesis is to understand the impacts of vehicle emissions on air quality in urban environments, and develop understanding of how outdoor air quality is a determinant of health and personal air pollution exposure in passenger cars.

# Thesis overview

Chapter 1 provides an introduction to the thesis. It touches upon some basic atmospheric principles regarding the atmosphere and the main sources of air pollution. Particular focus is given to vehicle emissions, where an extensive introduction to the techniques used to measure vehicle emissions is provided. Vehicle exhaust after-treatment systems and their operation conditions are also discussed. The chapter also considers indoor air pollution with particular emphasis to within-vehicle air quality and exposure. Finally chapter 1 discusses current state of the art techniques that are used to estimate air pollution and personal exposure.

Chapter 2 provides a new analysis of roadside $NO_2/NO_x$ ratios in the UK and how these have changed over the last decade with regard to new polices and vehicle technologies. The analysis covers hourly data from 45 monitoring sites across the UK acquired for the period 2009-2016. About three million hourly data points for each of NO, $NO_2$, $O_3$ and temperature were included in the analysis, while trends of the aforementioned species were also analysed. This chapter presents a methodology to investigate the impact of enhanced cold-weather vehicle primary $NO_2$ emissions upon urban air quality. The work described in this chapter has been published as:

*Matthaios, V. N., Kramer, L. J., Sommariva R., Pope, F. D., Bloss, W. J., 2019. Investigation of vehicle cold start primary NO2 emissions from ambient monitoring data in the UK and their implications for urban air quality. Atmospheric Environment. 199, 402-414.*

Chapter 3 provides an analysis of within-vehicle air pollution exposure relative to air pollution directly outside the vehicles in Birmingham, UK. The instrumentation and experimental setup are described, and the results of 83 hours of successful driving experiments are presented. These results are used to assess within-vehicle exposure based on observations of ultrafine particles (UFP), lung surface deposited area (LSDA), particulate matter ($PM_{10}$, $PM_{2.5}$, $PM_1$) and nitrogen oxides ($NO_x$ = NO + $NO_2$), under different ventilation settings and routes. The chapter concludes by calculating the inhalation dose of vehicle occupants in comparison with that of cyclists and pedestrians following equivalent routes around the city of Birmingham. The work in this chapter has been published as:

*Matthaios N. V., Kramer J. L., Crilley R. L., Sommariva R., Pope D. F., Bloss J. W., 2020. Quantification of within-vehicle exposure to NOx and particles: variation with outside air quality, route choice and ventilation options.*

Chapter 4 builds upon the measurements of chapter 3 and develops a mass-balance model that can be used to estimate air pollution exposure within vehicle cabins and other microenvironments in general. The model accounts for vehicle ventilation setting and takes into account basic gas-phase reactions and processes such as deposition, infiltration and vehicle leakage. State-of-the-art machine learning algorithms are also used to provide insights into new modelling prediction tools for air quality. These data driven algorithms, based on a training dataset, showed skill in

predicting within-vehicle air pollution exposure from input observations from local authority air quality monitoring stations.

Chapter 5 provides a synthesis of the research performed, some concluding remarks for the thesis, and identifies potential future research gaps.

# Chapter 1. Introduction

## Graphical thesis abstract

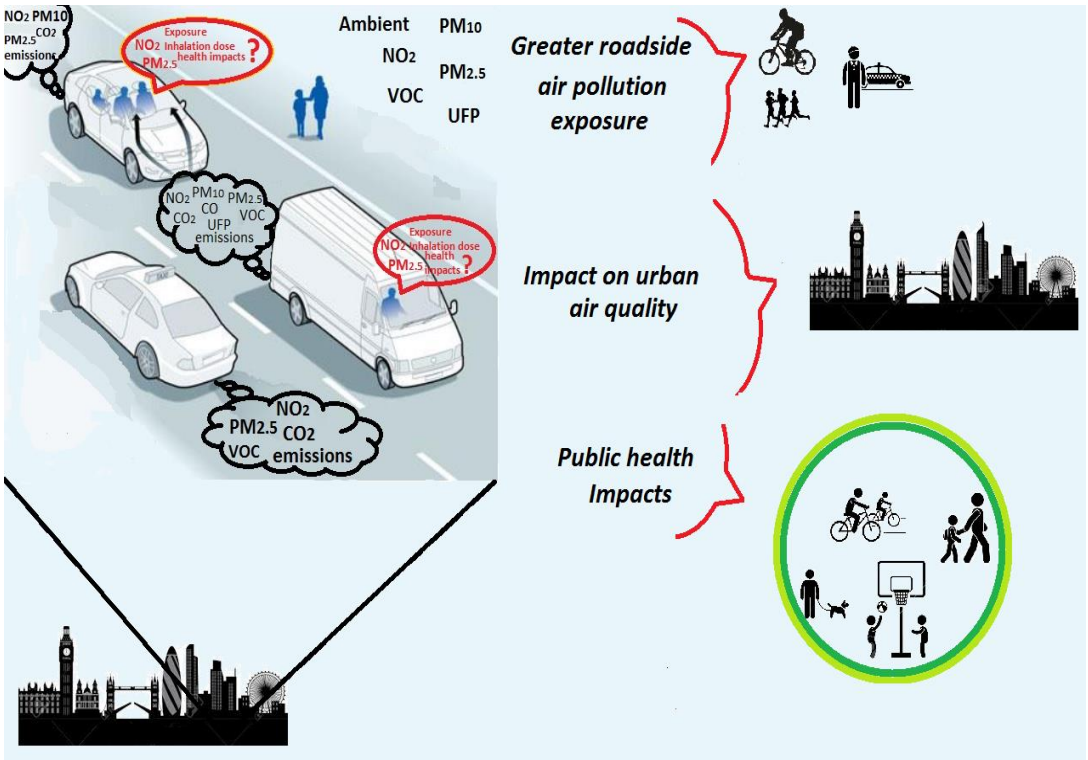

# 1.1 Background

According to World Health Organization (WHO), outdoor air pollution is responsible for at least 4.2 million deaths per year, however recent studies have shown that this number can be as high as 8.8 million per year (Lelieveld et al., 2019). Worldwide, ambient air pollution accounts for 29% of all deaths and diseases from lung cancer, 17% of all deaths and diseases from acute lower respiratory infection, 24% of all deaths from stroke, 25% of all deaths and diseases from ischaemic heart disease and 43% of all deaths and disease from chronic obstructive pulmonary disease (WHO, 2016). Globally, more than 80% of urban residents are exposed to unhealthy outdoor air pollution levels that exceed the WHO limits (WHO, 2016), while recent evidence (Apte et al., 2018) claim that air pollution on average reduces human life expectancy by a year.

In the European Union the first directive for air quality 96/62/EC (EC, 1996), which is commonly referred to as the Air Quality Framework Directive, defines air pollution as:

*"pollution' shall mean the direct or indirect introduction of substances, vibrations, heat or noise into the air, water or land which may be harmful to human health or the quality of the environment, result in damage to material property, or impair or interfere with amenities and other legitimate uses of the environment."*

Air pollution is caused by natural and anthropogenic sources. Natural sources can be a volcano eruption, wildfires or dust transfer from various deserts, etc. Anthropogenic air pollution sources are mainly associated with: means of transport, generation of electricity, domestic cooking and heating, industry, high temperature combustion activities and agricultural activities.

Urban environments in developing nations are dominated by sources mainly related to domestic activities such as heating or cooking. Such activities make a significant contribution to local PM levels and may also be substantial contributors to other pollutant concentrations such as soot, polyaromatic hydrocarbons (PAH) or CO, especially when wood or pellet or other alternative combustion materials are used as fuel (Bloss, 2009). On the other hand, in developed nations, road transport is a major and probably the predominant source of air pollutants and toxic mixtures in urban areas that have direct and indirect detrimental impacts on human health and ecosystems. To minimise negative impacts to human health arising from transport pollution, all vehicles, by law, are required to maintain emissions under a certain threshold. Before being released on the market, vehicles are put through testing procedures to prove they can maintain low emissions. However, in 2014, it was found that some car manufacturers were implementing software in vehicles which could recognise when a test was being performed and then adjusted the engine to emit less than if it were being driven normally. This finding resulted in a number of scandals in which actual vehicle emissions were found to be much greater than reported by individual manufacturers, the most famous of those being the Volkswagen “Dieselgate” in 2014. Since then, there is a growing body of research that reports an

underestimation of real world driving emissions and their implications for air quality and human health (e.g. Anenberg et al., 2017; Matthaios et al., 2019; Grange et al., 2019), particularly in highly exposed groups such as professional drivers, cyclists and pedestrians.

The following sections provide an introductory basis for the primary focus of this thesis, namely investigation of direct and indirect vehicle emissions under real-world driving conditions and their implications for passenger air quality and human health.

## 1.2 The Earth's atmosphere - structure and key pollutants

The Earth's atmosphere consists of four main vertical layers, namely the thermosphere, mesosphere, stratosphere and troposphere, each with different properties such as composition, temperature and pressure. The major gaseous constituents of the atmosphere are nitrogen $N_2$ (78% v/v), oxygen $O_2$ (21% v/v), argon (0.9% v/v) and carbon dioxide (0.04% v/v) when the atmosphere is dry, while water vapour also comprises a variable fraction up to 4% v/v. The troposphere is the lowest part of the atmosphere and the one that is most directly affected by human activities.

It contains 75% of the atmosphere's mass and 99% of the total mass of water vapour and aerosols. The lowest part of the troposphere that responds directly to the flows of mass, energy and momentum from the Earth's surface, characteristically at timescales of an hour or less, is called the atmospheric boundary layer (Stull, 1988). Most pollutants are emitted into, or chemically produced within this layer, while its diurnal evolution plays a critical role for the determination of pollutant dispersion pathways (Salmond and McKendry, 2005) and the air quality of a region (Aidaui et al., 2015).

The boundary layer and hence the atmosphere is considered polluted when harmful or excessive quantities of substances including gases (such as carbon dioxide, sulfur dioxide, nitrogen oxides, methane), particulates (both organic and inorganic or mixed), and other biological material are introduced into the Earth's atmosphere. The main two pollutants of greatest concern to health, that also dominate the urban atmosphere in developed and developing nations, are nitrogen dioxide and particulate matter.

Nitrogen oxides ($NO_x$ = NO + $NO_2$) are widely present in the troposphere, and are generated from both natural and anthropogenic sources (Jacobson, 2012). Natural $NO_x$ emission sources include lightning, wild fires and volcanic activities. Human activities contribute substantially to tropospheric $NO_x$ levels. $NO_x$ emissions (as NO) from anthropogenic sources contribute 77% of the global $NO_x$ emission (Holloway and Wayne, 2010) and they are mainly associated with high temperature combustion processes emitted from power plants, ships and road transportation.

PM with aerodynamic diameters ranging from coarse ≤ 10 µm ($PM_{10}$) to fine ≤ 2.5 µm ($PM_{2.5}$) and ultrafine ≤ 300 nm (UFP), is a complex mixture of primary and

secondary particles that includes both organic and inorganic components, and includes sources such as dust, pollen, soot, smoke, and liquid droplets that vary greatly in size, composition and origin. All are emitted either from natural sources or by human activities (Seinfeld and Pandis, 1998). Primary PM are emitted from sources directly into the atmosphere; it includes dust erosion, sea spray, soot from fuel combustion, fugitive dust from metallurgical processes or open pit mine activities, and freshly emitted organic compounds condensed on particles. Secondary PM, on the other hand, are formed in the atmosphere through condensation, oxidation, and reaction with precursor gases such as volatile organic compounds, and sulfur and nitrogen oxides (Harrison et al., 1997).

## 1.3 Basic gas phase reactions in urban environments

$NO_x$ emissions are of particular importance to urban air quality, since they do not only contribute to local and regional scale air pollution, but also to the formation of secondary pollutants such as ozone ($O_3$) and components of secondary PM. $NO_x$, associated with internal combustion engine vehicles, are produced primarily from tailpipe exhaust emissions, and normally dominate gas-phase processes in urban environments (Bloss, 2009).

During daylight hours, $NO_x$ concentrations together with that of ozone (and in the absence of other atmospheric chemical reactions) are in steady state, also known as a photostationary state (PSS), and represent a null cycle for NO, $NO_2$, O, and $O_3$ following the three reactions:

$$NO + O_3 \rightarrow NO_2 + O_2 \quad (1)$$

$$NO_2 + hv \rightarrow NO + O \quad (2)$$

$$O + O_2 + M \rightarrow O_3 + M \quad (3)$$

The timescales of these PSS reactions are a few minutes under typical boundary layer daylight conditions, thus they define an equilibrium between NO, $O_3$ and $NO_2$ with the following relationship:

$$[NO_2]/[NO] = k[O_3]/j_{NO_2}$$

This relationship between $NO_x$ and $O_3$ is also known as the Leighton relationship. In a typical urban environment, in the early morning, $NO_2$ levels are relatively high in the atmosphere, while NO and $O_3$ levels are low. When the sunrise starts, $NO_2$ levels rapidly drop due to solar photolysis, and NO and $O_3$ levels maximise from late morning to afternoon. As the sunlight begins to fade, $NO_2$ levels rise again through this null cycle, alongside reducing NO and $O_3$ levels. Due to the rapid

interchange of $O_3$ and $NO_2$, it can be helpful to consider the total level of oxidant, $O_x$ ($O_x = O_3 + NO_2$), and its variation with $NO_x$ levels. Elevated levels of $O_x$ may result from a) regional ozone production or b) potential local sources. These include direct primary emissions of $NO_2$. These regional and local contributions to $O_x$ may be distinguished through their dependence upon $NO_x$ levels (Figure 1). $O_x$ as a function of $NO_x$ determines the regional ($NO_x$ - independent) contribution from the ordinate intercept, and the local ($NO_x$ - dependent) contribution from the gradient (Clapp and Jenkin, 2001).

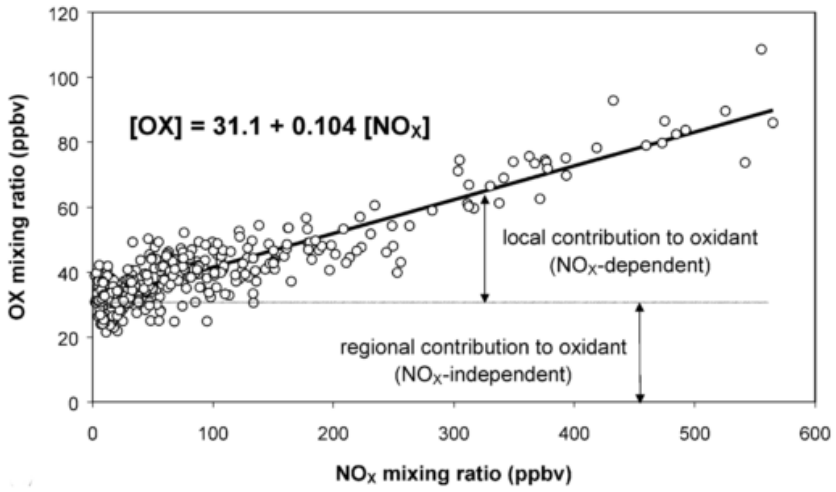


Figure 1.1: Variation of daylight average mixing ratios of oxidant ($O_x$) with the level of $NO_x$. The line is calculated by the regression analysis (Source: Clapp and Jenkin, 2001).

# 1.4 Vehicle emissions

In urban environments in developed nations, vehicle and road transport emissions in general are the dominant source of atmospheric air pollution. Increasing urbanisation, and (in many societies) growth in vehicle ownership and passenger-journeys, have contributed to growth in traffic-related ambient air pollution abundance, counteracting in some cases improvements in emissions abatement technologies. The predominant primary air pollutant emissions from vehicles include nitrogen oxides ($NO_x$, the sum of nitrogen monoxide (NO) and nitrogen dioxide ($NO_2$)), carbon dioxide ($CO_2$), particulate matter (PM) including ultrafine particles (UFP) mainly referred as soot in diesel vehicles, and volatile organic compounds (VOCs), derived primarily from exhaust (tailpipe) sources, alongside mechanical (brake, tyre) inputs and road dust resuspension in the case of PM.

Vehicle emissions are formed as a result of burning the heterogeneous air/fuel mixture and depend on the prevailing conditions not only during combustion, but also during the expansion. Several processes contribute to the emissions formation including, mixture preparation during the ignition delay, fuel ignition quality, residence time at different combustion temperatures, expansion duration and general engine design. In principle, the concentration of the different emission species in the exhaust is the result of their formation, and their reduction in the exhaust system.

Incomplete combustion products include mainly formation of PM, while primary mechanisms of combustion-produced $NO_x$ include thermal, prompt and fuel $NO_x$. Thermal $NO_x$ only require nitrogen in the air to combine with O and OH radicals, which are in abundant supply in a flame. The combustion $NO_x$ reactions are highly temperature dependent, so the hotter the combustion, the more $NO_x$ is formed. Prompt $NO_x$ is the reaction of atmospheric nitrogen with combustion radicals occurring in the earliest stages of combustion. Fuel $NO_x$ are the result of nitrogen being chemically bonded to the untreated fuel, which largely converts to $NO_x$ in the exhaust.

Particulate matter or soot emissions are formed during the high temperature pyrolysis or combustion of hydrocarbons at extreme air/oxygen deficiency that is locally inside diesel engines; soot formation increases as the air/fuel ratio decreases. Soot is produced by oxygen deficient thermal cracking of long-chain molecules. A separation of hydrogen leads to C-structures showing an increasing lack of hydrogen. Alkynes and other polymerization processes lead to formation of molecules rich in carbon that form soot (Homann, 1985). Soot consists of solid (organically insoluble) and liquid (organically soluble) phases and its composition is largely dependent on the operating point and the combustion process.

Vehicular pollutants have been reported to have substantial adverse impacts on human health (Papapostolou et al., 2011), with exposure to $NO_2$ known to lead to reduced lung function and increased risk of cancer (Adam et al., 2015; Hamra et al., 2015; WHO, 2013). The latest evidence across Europe suggests that $NO_2$ is responsible for hundreds of thousands of premature deaths each year (EEA, 2016; RCP, 2016; COMEAP, 2010). Moreover, the International Agency for Research on Cancer has

recently classified diesel engine exhaust as a Group I carcinogen, based on its association with lung cancer (Attfield et al., 2012; Silverman et al., 2012). Despite the fact that there is a general overall decrease in the diesel passenger car share across the European Union in recent years, the diesel passenger share is still above 50%, according to the European Automobile Manufacturers Association (ACEA, 2017).

Within the EU, a series of legislative measures have been introduced to address this challenge and it is now over 20 years since the introduction of the first $NO_x$ guidelines in Europe, originally for ambient concentrations and eventually for direct vehicle emissions. The first directive 96/62/EC (EC, 1996), which is commonly referred as the Air Quality Framework Directive, and its daughter directives, established standards in the period up to 2004 for the abundance of a range of pollutants including $NO_2$ in ambient air. The first three daughter directives were consolidated into a single ambient air quality directive adopted as 2008/50/EC (EC, 2008a) and together with the fourth daughter directive 2004/107/EC they provide the current framework for the control of ambient concentrations of air pollution. However, the need for better and more accurate measures to minimize $NO_2$ mixing ratios led to more rigorous vehicle legislation directives, which gradually aimed to decrease emissions from vehicles (EC, 2008b; 2011). European Union emission regulations for new light duty vehicles, including passenger cars and light commercial vehicles, were specified in Directive 70/220/EEC with a number of amendments adopted in 2004. In 2007, this directive was repealed and replaced by Regulation 715/2007 (Euro 5/6). Some of the important regulatory steps for implementing emission standards for light-duty vehicles were: Euro 1 standards (also known as EC 93): Directives 91/441/EEC (passenger cars only) or

93/59/EEC (passenger cars and light trucks). Euro 2 standards (EC 96): Directives 94/12/EC or 96/69/EC. Euro 3/4 standards (2000/2005): Directive 98/69/EC, further amendments in 2002/80/EC. Euro 5/6 standards (2009/2014): Regulation 715/2007 ("political" legislation) and several comitology regulations.

EU regulations introduce different emission limits for compression ignition (diesel) and spark ignition (gasoline, ethanol, etc.) vehicles. Diesels have more stringent CO standards but are allowed higher $NO_x$ emissions. Positive ignition vehicles were exempted from PM standards through the Euro 4 stage. Euro 5/6 regulations introduce PM mass emission standards, equal to those for diesels, for positive ignition vehicles with direct injection (DI) engines. EU emission standards are summarized in the following tables (1.1 and 1.2). All dates listed in the tables refer to new type approvals.

Table 1.1: EU emission standards for passenger cars. DI: Direct injection engine, IDI: indirect injection. *: and Non methane hydrocarbons = 0.068 g/km, **: applied only in vehicles with DI engines

| Stage | Date | CO g/km | HC | HC +NOx | NOx | PM | PN #/km |
|---|---|---|---|---|---|---|---|
| | | | Spark Ignition (Gasoline) | | | | |
| Euro 1 | 07.1992 | 2.72 (3.16) | - | 0.97 (1.13) | - | - | - |
| Euro 2 | 1996.01 | 2.2 | - | 0.5 | - | - | - |
| Euro 3 | 2000.01 | 2.30 | 0.20 | - | 0.15 | - | - |
| Euro 4 | 2005.01 | 1.0 | 0.10 | - | 0.08 | - | - |
| Euro 5 | 2009.09 | 1.0 | 0.10* | - | 0.06 | 0.005** | - |
| Euro 6 | 2014.09 | 1.0 | 0.10* | - | 0.06 | 0.005** | $6.0\times10^{11}$ |
| | | | Compression Ignition (Diesel) | | | | |
| Euro 1 | 1992.07 | 2.72 (3.16) | - | 0.97 (1.13) | - | 0.14 (0.18) | - |
| Euro 2, IDI | 1996.01 | 1.0 | - | 0.7 | - | 0.08 | - |
| Euro 2, DI | 1996.01 | 1.0 | - | 0.9 | - | 0.10 | - |
| Euro 3 | 2000.01 | 0.64 | - | 0.56 | 0.50 | 0.05 | - |
| Euro 4 | 2005.01 | 0.50 | - | 0.30 | 0.25 | 0.025 | - |
| Euro 5 | 2011.09 | 0.50 | - | 0.23 | 0.18 | 0.005 | $6.0\times10^{11}$ |
| Euro 6 | 2014.09 | 0.50 | - | 0.17 | 0.08 | 0.005 | $6.0\times10^{11}$ |

Table 1.2: EU emission standards for light duty vehicles. DI: Direct injection engine, IDI: indirect injection.

| Category | Stage | Date | CO g/km | HC | HC+NOx | NOx | PM | PN #/km |
|---|---|---|---|---|---|---|---|---|
| | | | Spark Ignition (Gasoline) | | | | | |
| N1, Class I | Euro 1 | 1994.10 | 2.72 | - | 0.97 | - | - | - |
| ≤1305 kg | Euro 2 | 1997.01 | 2.2 | - | 0.50 | - | - | - |
| | Euro 3 | 2000.01 | 2.3 | 0.20 | - | 0.15 | - | - |
| | Euro 4 | 2005.01 | 1.0 | 0.10 | - | 0.08 | - | - |
| | Euro 5 | 2009.09 | 1.0 | 0.10 | - | 0.06 | 0.005 | - |
| | Euro 6 | 2014.09 | 1.0 | 0.10 | - | 0.06 | 0.005 | $6.0\times10^{11}$ |
| N1, Class II | Euro 1 | 1994.10 | 5.17 | - | 1.40 | - | - | - |
| 1305-1760 kg | Euro 2 | 1998.01 | 4.0 | - | 0.65 | - | - | - |
| | Euro 3 | 2001.01 | 4.17 | 0.25 | - | 0.18 | - | - |
| | Euro 4 | 2006.01 | 1.81 | 0.13 | - | 0.10 | - | - |
| | Euro 5 | 2010.09 | 1.81 | 0.13 | - | 0.075 | 0.005 | - |
| | Euro 6 | 2015.09 | 1.81 | 0.13 | - | 0.075 | 0.005 | $6.0\times10^{11}$ |
| N1, Class III | Euro 1 | 1994.10 | 6.90 | - | 1.70 | - | - | - |
| >1760 kg | Euro 2 | 1998.01 | 5.0 | - | 0.80 | - | - | - |
| | Euro 3 | 2001.01 | 5.22 | 0.29 | - | 0.21 | - | - |
| | Euro 4 | 2006.01 | 2.27 | 0.16 | - | 0.11 | - | - |
| | Euro 5 | 2010.09 | 2.27 | 0.16 | - | 0.082 | 0.005 | - |
| | Euro 6 | 2015.09 | 2.27 | 0.16 | - | 0.082 | 0.005 | $6.0\times10^{11}$ |
| N2 | Euro 5 | 2010.09 | 2.27 | 0.16 | - | 0.082 | 0.005 | - |
| | Euro 6 | 2015.09 | 2.27 | 0.16 | - | 0.082 | 0.005 | $6.0\times10^{11}$ |
| | | | Compression Ignition (Diesel) | | | | | |
| N1, Class I | Euro 1 | 1994.10 | 2.72 | - | 0.97 | - | 0.14 | - |
| ≤1305 kg | Euro 2 IDI | 1997.01 | 1.0 | - | 0.70 | - | 0.08 | - |
| | Euro 2 DI | 1997.01 | 1.0 | - | 0.90 | - | 0.10 | - |
| | Euro 3 | 2000.01 | 0.64 | - | 0.56 | 0.50 | 0.05 | - |
| | Euro 4 | 2005.01 | 0.50 | - | 0.30 | 0.25 | 0.025 | - |
| | Euro 5a | 2009.09 | 0.50 | - | 0.23 | 0.18 | 0.005 | - |
| | Euro 5b | 2011.09 | 0.50 | - | 0.23 | 0.18 | 0.005 | $6.0\times10^{11}$ |
| | Euro 6 | 2014.09 | 0.50 | - | 0.17 | 0.08 | 0.005 | $6.0\times10^{11}$ |
| N1, Class II | Euro 1 | 1994.10 | 5.17 | - | 1.40 | - | 0.19 | - |
| 1305-1760 kg | Euro 2 IDI | 1998.01 | 1.25 | - | 1.0 | - | 0.12 | - |
| | Euro 2 DI | 1998.01 | 1.25 | - | 1.30 | - | 0.14 | - |
| | Euro 3 | 2001.01 | 0.80 | - | 0.72 | 0.65 | 0.07 | - |
| | Euro 4 | 2006.01 | 0.63 | - | 0.39 | 0.33 | 0.04 | - |
| | Euro 5a | 2010.09 | 0.63 | - | 0.295 | 0.235 | 0.005 | - |
| | Euro 5b | 2011.09 | 0.63 | - | 0.295 | 0.235 | 0.005 | $6.0\times10^{11}$ |
| | Euro 6 | 2015.09 | 0.63 | - | 0.195 | 0.105 | 0.005 | $6.0\times10^{11}$ |
| N1, Class III | Euro 1 | 1994.10 | 6.90 | - | 1.70 | - | 0.25 | - |
| >1760 kg | Euro 2 IDI | 1998.01 | 1.5 | - | 1.20 | - | 0.17 | - |
| | Euro 2 DI | 1998.01 | 1.5 | - | 1.60 | - | 0.20 | - |
| | Euro 3 | 2001.01 | 0.95 | - | 0.86 | 0.78 | 0.10 | - |
| | Euro 4 | 2006.01 | 0.74 | - | 0.46 | 0.39 | 0.06 | - |
| | Euro 5a | 2010.09 | 0.74 | - | 0.350 | 0.280 | 0.005 | - |
| | Euro 5b | 2011.09 | 0.74 | - | 0.350 | 0.280 | 0.005 | $6.0\times10^{11}$ |
| | Euro 6 | 2015.09 | 0.74 | - | 0.215 | 0.125 | 0.005 | $6.0\times10^{11}$ |
| N2 | Euro 5a | 2010.09 | 0.74 | - | 0.350 | 0.280 | 0.005 | - |
| | Euro 5b | 2011.09 | 0.74 | - | 0.350 | 0.280 | 0.005 | $6.0\times10^{11}$ |
| | Euro 6 | 2015.09 | 0.74 | - | 0.215 | 0.125 | 0.005 | $6.0\times10^{11}$ |

Studies over the past decade in the UK have shown that the ambient $NO_x$ mixing ratios have dropped significantly (DEFRA, 2017), however, this decrease is not observed for ambient $NO_2$ levels. In fact, it is observed that $NO_2$ hourly values exceeded both the hourly average limit of $NO_2$ > 200 μg/$m^3$ and the limit of 35 exceedances per year. It was also observed that there were increasing amounts of $NO_2$ for a given $NO_x$ mixing ratio in the roadside sites (primary $NO_2$), with $NO_2/NO_x$ ratios increasing from about 5-6% in 1997 to 17% in 2003 (Carslaw, 2005). Similar results were obtained for individual fleet categories, with observed increases in the $NO_x$ emission factors for Euro 4/5 cars compared to previous Euro classes (Carslaw et al., 2011). Such behaviour was observed in a range of European cities such as Paris, Milan, Athens, Barcelona, London, and Stuttgart (Anttila et al, 2011; Grice et al., 2009; Hueglin et al, 2006). Nevertheless, some of the latest results (Carslaw et al., 2016b; Grange et al., 2017; Matthaios et al., 2019) give more optimistic conclusions in the reduction of traffic related pollution. New Euro limits (Euro 5 and Euro 6), and after-treatment technologies, in conjunction with factors such as aged catalyst technologies having reduced oxidative capacity of $NO_x$ via thermal deactivation, have a positive impact in the reduction of particulate pollution (Harrison and Beddows, 2017) and ambient as well as primary $NO_2$ from traffic (DEFRA, 2017; Carslaw et al., 2016b). Figure 1.2 shows the $NO_2/NO_x$ ratio in roadside stations across Europe. Despite the fact that roadside $NO_2/NO_x$ emissions are showing reductions over the recent years 2009-2016 (Grange et al., 2017), there is still an on-going debate as studies also reveal that under cold or hot weather conditions vehicle emissions are greater when comparing

them with normal conditions, which is probably due to how the emission after-treatment control systems operate (Grange et al., 2019, Dallman et al., 2019).

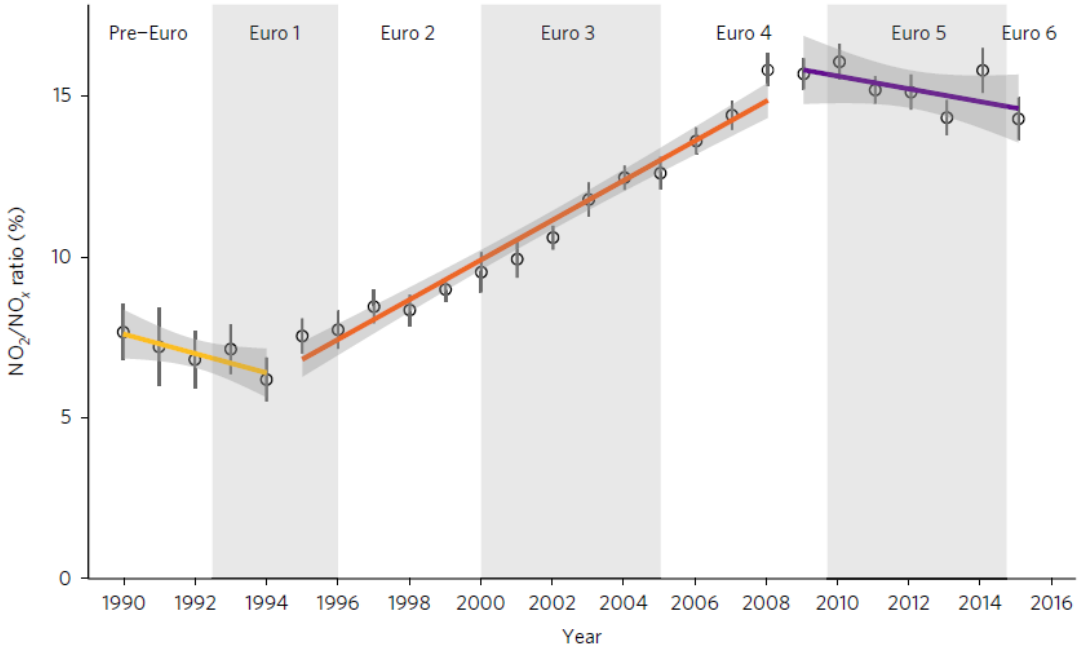


Figure 1.2: Mean $NO_2/NO_x$ ratio for all roadside monitoring sites for the 61 European urban areas analysed between 1990 and 2015. The error bars represent the 95% confidence intervals (from Grange et al., 2017).

# 1.5 Emission controls of vehicle pollutants

Vehicle technologies have evolved to reduce fuel consumption, improve engine performance, and (primarily through the addition of after-treatment systems) reduce emission of air pollutants such as $NO_x$ in order to comply with the Euro class and other

vehicle emission standards. In internal combustion engines the pollutants are emitted when the combustion process is incomplete, and a big role to that plays the air to fuel ratio. The determination of the excess air or excess fuel in a combustion system is defined by the stoichiometric air-fuel ratio (1:1 is the ideal combustion). The stoichiometric ratio is the ideal fuel ratio where the chemical mixing proportion is correct and when burned, all fuel and air is consumed without any excess or left over. In case where the air content is higher that the stoichiometric ratio, the mixture is defined as fuel-lean, while, when the air content is less than the stoichiometric ratio, the mixture is fuel-rich.

Of the two principal categories of internal combustion engine, the emission problem is more straightforward to address for gasoline (positive/spark ignition) vehicles in comparison to diesel (compression ignition) vehicles. Most gasoline vehicles now employ a three-way catalyst (TWC), one of the most important abatement technologies introduced in the 1980's and applied in the 1990's manufactured vehicles to reduce vehicle tailpipe emissions. Under stoichiometric conditions (ideal combustion process where fuel is burned completely) TWC are designed to simultaneously convert carbon monoxide (CO) to $CO_2$, hydrocarbons (HC) to $CO_2$ and water and $NO_x$ species to nitrogen. Theoretically, TWC can cut CO, HC and $NO_x$ emissions by over 99% (under stoichiometric conditions) if the air to fuel ratio in the exhaust stream is accurately controlled, although they have been associated with emissions of the greenhouse gas nitrous oxide ($N_2O$) (Berges et al., 1993; Jimenez et al., 2000).

Diesel after-treatment systems face more challenges in reducing emissions from the exhaust system mainly due to the high amount of oxygen in the combustion process, as diesel engines have an air-fuel ratio leaner than stoichiometric. A schematic of these systems is illustrated in Figure 1.3. Diesel vehicles (Euro 3 and later) use diesel oxidation catalysts (DOC), which normally contain palladium, platinum and aluminium oxide, all of which serve as catalysts to oxidize the HC and CO with $O_2$ to form $CO_2$ and $H_2O$. However, this oxidation can lead to increased $NO_2$ emissions when no further after-treatment technology is applied. In modern engines DOC is often used as an auxiliary catalyst in other after treatment systems (see DPF and SCR below).

Exhaust gas recirculation (EGR) was introduced as a further emission control technology introduced in larger size Euro 3 engines, and became the standard in Euro 4 and later diesel passenger cars and light duty vehicles (LDV). The EGR system principally channels and recirculates a portion of the exhaust gas into the new filtered, high-pressure, fresh combustion air at the engine intake. The higher the engine load, the better the EGR performance and the greater the $NO_x$ reduction (Yokomura et al., 2003).

Diesel particle filters (DPF), introduced in 2009 to achieve Euro 5 limits, physically capture diesel particles and prevent their release to the atmosphere. However, the stored PM must be oxidized in order not to completely block the filter and damage the vehicle operation. This oxidation is achieved via reaction with $O_2$ at high temperatures (600 $^{O}$C) and via reaction with $NO_2$ at low temperatures (250 – 450 $^{O}$C). Mainly, the oxidation in DPF is accomplished by $NO_2$, due to the amount of $NO_2$ needed in the DPF to burn the soot. For this reason, the DPF is usually attached after

the DOC system, forming a continuously regenerated trap (CRT) or catalyzed continuously regenerated trap (CCRT), which reduces PM, CO and HC. The secondary $NO_2$ formation as a by-product of the catalysis, however, is a major issue in these systems and can lead to increased $NO_2$ emissions from the vehicle.

The latest after-treatment technologies involve Lean $NO_x$ trap (LNT) and Selective catalytic reduction (SCR) technologies, and are needed to achieve Euro 6 limits. LNT technology achieves $NO_x$ storage during lean engine operation, $NO_x$ reduction during rich operation phases. During lean engine operation, $NO_x$ is stored in the storage components in the form of nitrates and nitrites. In a subsequent, short fuel-rich period, the $NO_x$ trap is regenerated by $NO_x$ release and reaction with HCs achieves reduction to $N_2$. Since fuel consumption for $NO_x$ trap regeneration depends on the regeneration frequency, which is a function of $NO_x$ trap performance parameters, the impact of catalyst aging must be considered in the operation strategy.

Selective catalytic reduction (SCR) is an after-treatment system which catalyses $NO_x$ ($NO + NO_2$) reduction using reactive nitrogen compounds, such as ammonia or urea $(NH_2)_2CO$; (commercial name AdBlue). In SCR, the mixture of ammonia/urea reacts with $NO_x$ to form $N_2$, $CO_2$, and $H_2O$. The SCR process requires precise control of the ammonia/urea injection rate; an insufficient injection rate may result in unacceptably low $NO_x$ conversions, while too large an injection rate results in releases of undesirable ammonia (“ammonia slip”) to the atmosphere and increased SCR reductant consumption. All after-treatment systems need to reach a certain temperature threshold (regular operating conditions) in order to effectively reduce $NO_x$ vehicle emissions. This difference in the temperature, for both the engine and the

catalytic converter, to which the vehicle is operated comparing to regular operating conditions can be expressed as a “cold – start” and can be defined as when the engine is started with the temperature of the oil, coolant and all elements of the engine at the ambient temperature. At lower ambient temperatures, the engine and catalyst warm up period is prolonged and this can have adverse effect on vehicle emissions. Modern gasoline and diesel vehicles are equipped with TWC and DOC after-treatment systems. Under cold operation, disproportionally higher levels of gaseous pollutants are produced, since the temperature of the catalyst is not high enough to ensure efficient $NO_x$ conversion. Currently in the EU, only the emissions from gasoline Euro 3/4 vehicles under cold-start in low ambient temperature are regulated under the Directive 98/69/EC (EC, 1998), as identified elsewhere (e.g. Dardiotis et al., 2013; Bielaczyc et al., 2011; 2012).

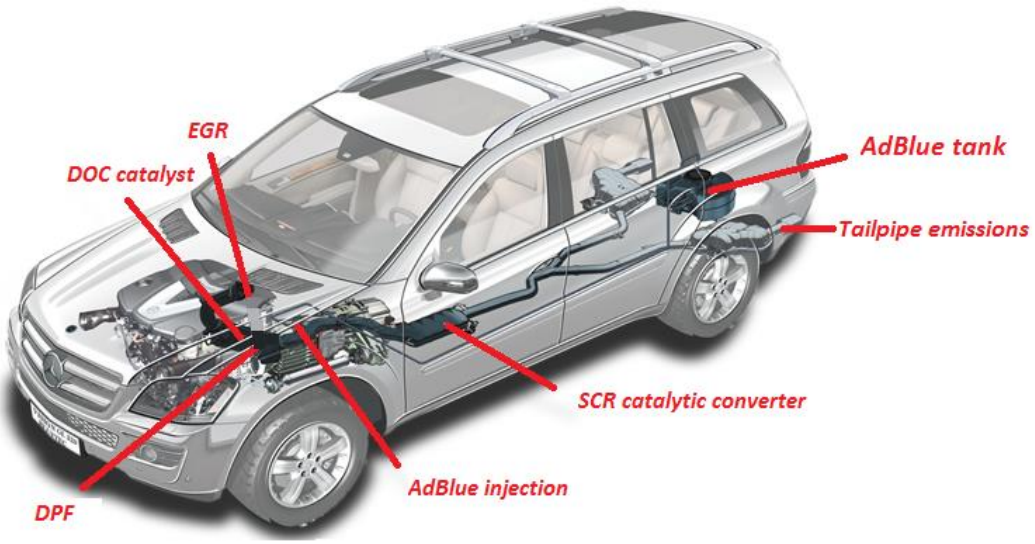


Figure 1.3: Schematic representation of vehicle’s emission after-treatment systems. EGR: Exhaust gas recirculation, DOC: Diesel oxidation catalyst, DPF: Diesel particulate filter, SCR: Selective catalytic reduction.

# 1.6 Vehicle tailpipe emission measurement approaches

There are many different approaches to estimate vehicle combustion (tailpipe) emissions. A review on the techniques that are used to measure vehicle emissions can be found in Franco et al., (2013), here, we briefly introduce the key approaches to provide context for the methodology used in this work. Firstly, there are the approved bench (chassis dynamometer) tests (see Figure 1.4), where the tested vehicle follows a certain driving cycle (sequence of speed/acceleration/deceleration over a pre-defined period of time that corresponds to notional urban driving or extra-urban driving behaviour) and relevant analysers sample directly from the exhaust to determine $NO_x$ emissions (Nine et al., 1999; Yanowitz et al, 2000). However, such tests are very short (approximately 20 min each test) and as has been widely reported, fail to capture the real driving $NO_x$ emissions by accident or design (Andersson et al., 2014; Degraeuwe and Weiss, 2017). Thus, it is thought that emission factors based solely upon such tests may not be representative of real-world on-road vehicle behaviour.

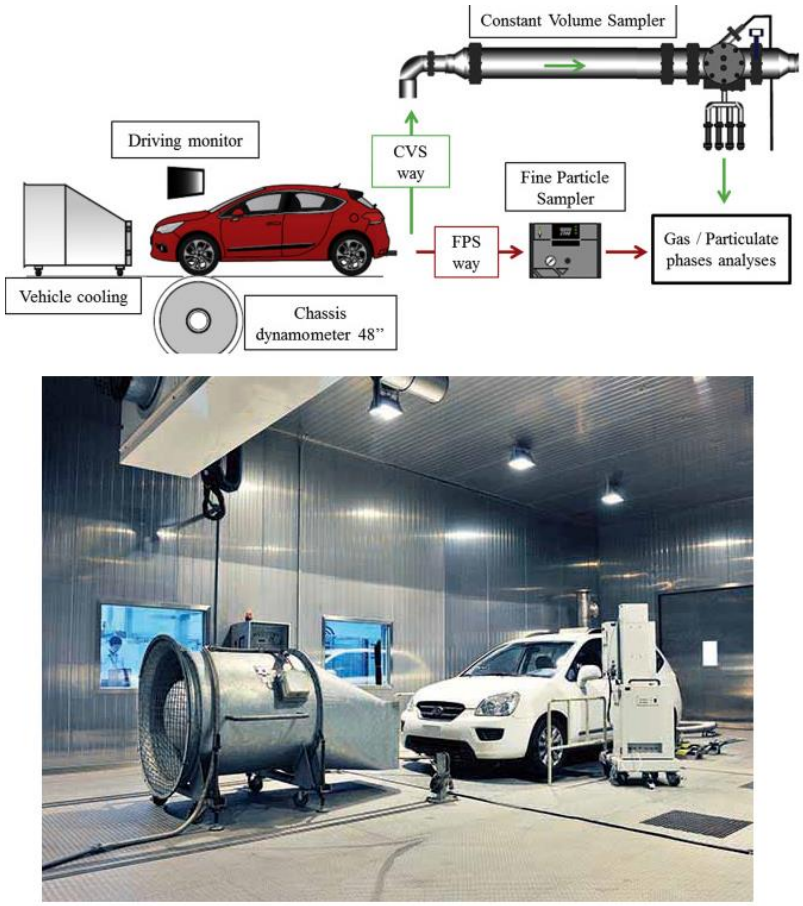


Figure 1.4: Illustration of the chassis dynamometer vehicle emission control test. a) Schematic representation and description, b) real lab vehicle testing at European Vehicle Emission Laboratory test chambers (adopted from Luis et al., 2017).

Secondly, portable emission systems (PEMS) are devices mounted to individual test vehicles which measure directly from the exhaust/tailpipe during on-road driving (Weiss et al, 2011). PEMS systems can be installed externally or internally of the tested vehicle (see Figure 1.5). PEMS capture individual vehicle emissions under real driving conditions. However they are expensive and can only be fitted in one car at a time. Normally they also require tailpipe adaptations to sample directly, and may suffer power limitations if powered by the vehicle on-board low voltage power supply

system. A related approach is the chase measurement method. In this approach, instruments are mounted in a second, monitoring vehicle and an inlet is used in order to sample from ambient air, while following individual (or a group of) target vehicles (Brantley et al., 2014). Chase approaches can, compared with test bench measurements and PEMS approaches, more readily give accurate information about fleet emissions from a number of vehicles and variations with driving behaviour (e.g. urban, rural, motorway), but suffer from limitations from the need to account for mixing with background air (commonly achieved via use of $CO_2$ as an exhaust tracer), and overlap of multiple potential target vehicle plumes.

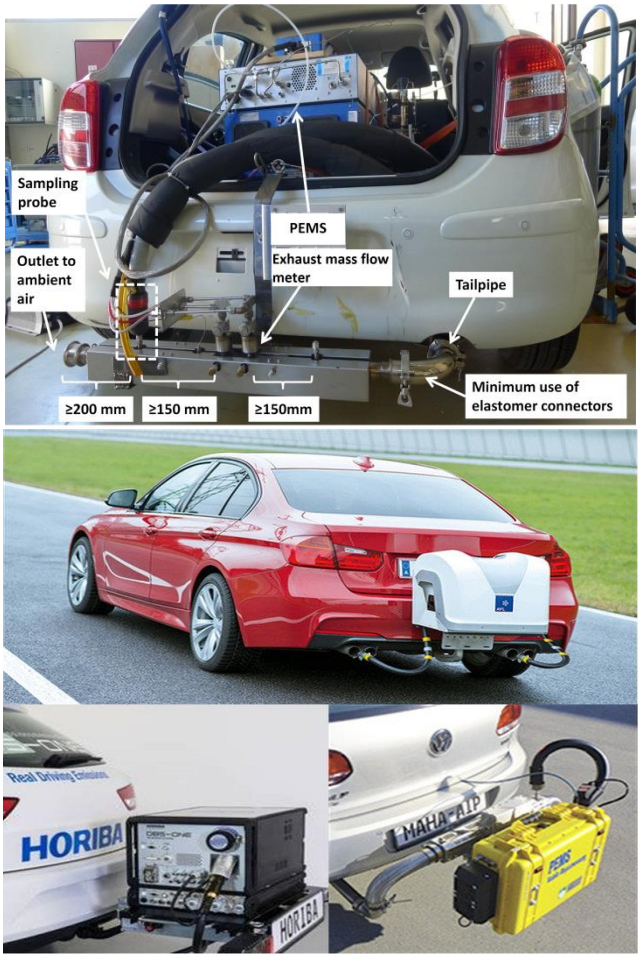


Figure 1.5: Illustration of real world driving emission tests. (top) Internal installation and configuration of PEMS, (bottom) external installation and driving with mounted PEMS (adopted from Giechaskiel et al., 2016).

Thirdly, remote sensing technologies (Bishop et al, 1989), where infrared and/or ultraviolet light of specific wavelengths from a source passes through the exhaust plume of an individual or series of target vehicles prior to measurement at a detector, wherein the amount of light absorbed is proportional to the concentration of gases in the plume (Carslaw and Rhys-Tyler, 2013). An alternative recently-developed top-down geometry, which can sample individual vehicle lanes, has also recently been demonstrated with similar results (Ropkins et al., 2017). Figure 1.6 illustrates both

horizontal and vertical vehicle emission remote sensing measurements. Both approaches are commonly coupled with vehicle sensing and number plate recognition tools to identify speed, acceleration and vehicle/engine characteristics. Although remote sensing methodologies are in many senses the “gold standard” approach, in that they can measure the real-world on-road emissions from large numbers of individual vehicles under favourable operating conditions, they suffer from constraints of cost, complexity and potentially perturbations to traffic flow/behaviour. Furthermore, many of the relevant pollutants do not have UV or IR spectra, while such techniques have issues when located on multiple lane roads as emissions from vehicles alongside the target vehicle can interfere with the result, in particular when the wind is in an unfavourable direction.

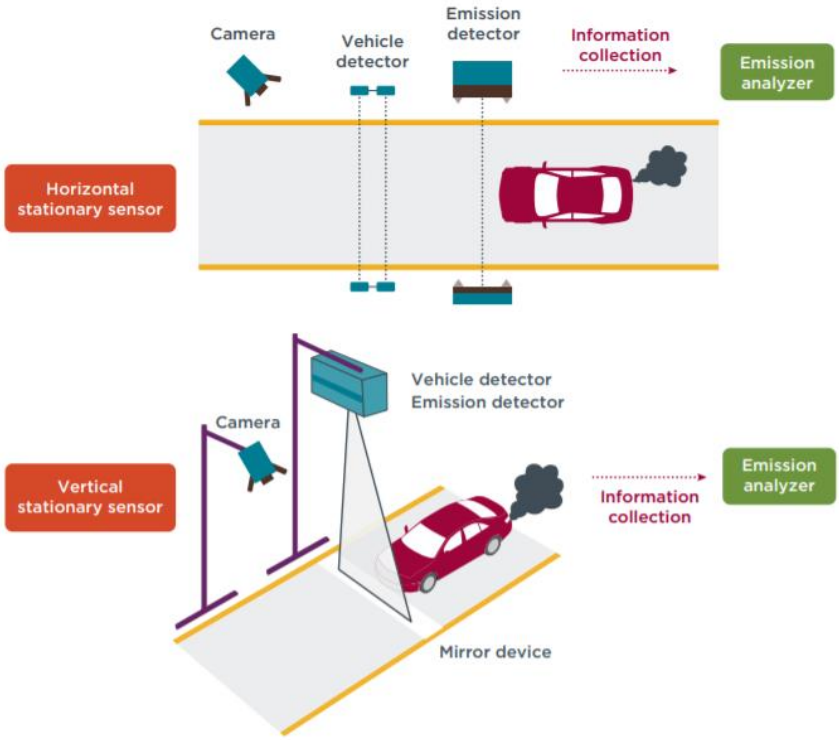


Figure 1.6: Illustration of horizontal and vertical remote sensing vehicle emission measurements (from Dallman et al., 2019).

Lastly, vehicle emissions may be inferred from the analysis of ambient air quality measurements, using monitoring sites located in suitable proximity to the road. This method has the advantage of exploiting the data that in most of the cases are used to report the ambient air pollution levels to the government authorities and EU. This method is relatively cheap compared to the aforementioned approaches and no additional experiments are needed. One major advantage is that it still remains the cheapest and most reliable method for long term observations and the most efficient approach to check the efficacy of policy making legislations. However, it cannot give as

detailed information for the vehicle fleet (e.g. size and type of vehicles) or the driving behaviour (speed/acceleration of the passing vehicles), as the previous approaches, and therefore needs to be coupled with additional measurements/observations. Since the UK has an extensive and dense air quality network for different locations (e.g. urban, urban-traffic, industrial, etc.), coupling those air quality measurements with meteorological observations can provide local to regional insights.

## 1.7 Indoor air quality

People in developed countries spend the majority of their time (about 90%) indoors, at schools, work, homes, shops, restaurants or transport/commuting, with vulnerable groups such as elderly people, young children and people with diagnosed health issues typically spending an even larger portion of their time at home. Therefore, the impact of outdoor air on the indoor environment, and of indoor sources such as tobacco smoking, gas cooking and heating, as well as household paints, adhesives and cleaning products on human health might be very significant (Vardoulakis, 2009).

The concentration of an indoor air pollutant is a function of numerous processes including indoor emissions, exchanges with outdoor air, deposition to indoor

surfaces, evaporation, condensation, removal by filtration and indoor chemistry (Weschler and Carslaw, 2018). Indoor sources can be very diverse and highly variable depending on the nature and strength of the source, ventilation rates and location of the indoor environment. A broad categorisation of indoor sources can be the following: a) fuel, wood and tobacco combustion emissions that include volatile and semi-volatile compounds, carbon monoxide (CO), particulate matter, $NO_2$ and sulphur dioxide ($SO_2$); b) emissions from the building materials and the furnishing materials that include asbestos fibres, formaldehyde or other polyaromatic hydrocarbons (PAH) and persistent organic pollutants (PCB); c) cooking emissions; d) emissions from electronic devices such as ultrafine particles from painters or vacuum cleaners, or $O_3$ from photocopiers e) emissions from beauty products, insecticide, pesticides, air refreshers, cleansing products (Volatile Care Products, VCPs); f) biological emitted pollutants such as mould, bacteria, dust resuspension, viruses. In addition to the aforementioned indoor sources, air pollutants can enter the indoor environment from the outdoor environment (e.g. traffic related air pollutants, dust resuspension/transport from nearby construction works) or from the ground beneath the building (e.g. radon, methane or other soil gases). Finally, one has to consider reactive chemistry as a source of chemicals that might not otherwise be present indoors and can be responsible for the formation of oxygenated VOCs (such as organic nitrates, carbonyls, etc.) and secondary organic aerosol (SOA).

Generally, there is more effective air mixing between the rooms of a house than the air exchange between indoors and outdoors, hence air pollution levels can be assumed equal between the rooms inside the houses. Consequently, population

exposure in such microenvironments can be roughly estimated by the ambient (outdoor) levels and the indoor:outdoor ratio (I/O) or the ambient levels and the calculated air exchange and deposition rates. Singer et al., (2004) found a strong correlation between air pollutant concentrations inside houses and traffic-related outdoor air pollution in areas which are dominated by traffic emissions. Some typical median indoor air pollution levels and I/O ratios are reported in Table 1.3.

Table 1.3: Median indoor/Outdoor concentration ratios reported in literature. * non-smokers, ** smokers.

| **Air pollutant** | **Indoor levels** | **Outdoor levels** | **I/O ratio** | **Reference** | **Place** |
|---|---|---|---|---|---|
| Formaldehyde ($\mu g/m^3$) | 20.10 | 6.42 | 3.1 | Liu et al. 2006 | USA (homes) |
| $PM_{2.5}$ ($\mu g/m^3$) | 23.2 | 23.4 | 1.0 | Janssen et al. 2001 | Netherlands (schools) |
| $NO_2$ ($\mu g/m^3$) | 17.5 | 38.5 | 0.5 | Janssen et al. 2001 | Netherlands (schools) |
| Benzene ($\mu g/m^3$) | 2.9 | 2.1 | 1.4 | Janssen et al. 2001 | Netherlands (schools) |
| Benzene ($\mu g/m^3$) | 1.5–2.2 | 1.1–1.6 | 1.2–1.4 | Schneider et al. 2001 | Germany (homes) |
| Toluene ($\mu g/m^3$) | 20.5–37.3 | 4.5–5.0 | 5.0–7.6 | Schneider et al. 2001 | Germany (homes) |
| m,p-Xylene ($\mu g/m^3$) | 2.9–4.2 | 1.2–1.8 | 2.1–1.8 | Schneider et al. 2001 | Germany (homes) |
| Benzo[a]pyrene* ($ng/m^3$) | 0.09 | 0.10 | 0.9 | Fromme et al. 2004 | Germany (homes) |
| Benzo[a]pyrene** ($ng/m^3$) | 0.30 | 0.10 | 2.7 | Fromme et al. 2004 | Germany (homes) |

In a commuting context, people also spend a certain amount of time inside cars, trains and buses. In Europe, 56% of all people use cars as their main

transportation option on a daily basis (Fiorello et al., 2016). According to the data reported by TomTom traffic index (https://www.tomtom.com/en_gb/traffic-index/), which is an index now in its 8$^{th}$ year that gives insight into congestion and travel times by vehicles in urban centres globally. Traveling by vehicle has increased in urban areas from 2018 to 2019 by a range of 2% to 18% (TomTom, 2019). As a consequence, the time spent within vehicles in large cities (population > 800 000) worldwide has increased during morning and evening rush hours by up to 42 minutes (TomTom, 2019). Knowing that despite spending only 6% of our time daily in transport, this accounts for 25% of our total daily exposure (Dons et al., 2011); Vehicle occupants in urban environments might experience elevated exposure to vehicular combustion air pollution since both commuting time and time spending within vehicles has increased. Table 1.4 shows within-vehicle air pollutant concentrations measured at locations around the globe. The results show that, within-vehicle air quality is poor compared to the legislative limits (despite not being directly related). Research into within-vehicle exposure over the past two decades has mainly focused on CO, PM and UFP, and has been well documented and reported in several review studies (e.g. Knibbs et al., 2011; El-Fadel and Abi-Esber, 2009; Kaur et al., 2007). Notable findings are of Riediker et al., 2004, who investigated the effects of $PM_{2.5}$ in young healthy non-smoking police officers by adding $PM_{2.5}$ monitors inside their cars and sampling the police officers' blood 14 hours after each shift while keeping them monitored until the next shift. They found that the within-vehicle exposure to $PM_{2.5}$ even in these young healthy individuals can cause changes that involve inflammation, coagulation and irregularities in cardiac rhythm.

Only a few studies in the literature report within-vehicle cabin $NO_x$ concentrations. First Petersen and Sabersky, (1975), investigated the Los Angeles smog components of CO, $O_3$, NO and $NO_x$ inside the cars, by collecting samples in a bag, and reported $NO_2$ values (assuming it is the difference between $NO_x$ and NO) of ~0.20 ppm. Almost two decades later, Chan et al., (1991), reported within-cabin $NO_2$ concentrations of ~60 ppb, 100 ppb and 120 ppb for morning, noon and afternoon hours, in North Carolina USA. In the late 90's – early 20's two more studies reported levels of in-vehicle cabin $NO_x$. Chan et al., (1999), who measured nitrogen oxides in different commuter microenvironments and reported mean levels of 643 ppb, 544 ppb and 69 ppb for $NO_x$, NO and $NO_2$ respectively in passenger cars for the city of Hong Kong, and Chan and Chung, (2003), who reported relationships of indoor/outdoor NO and $NO_2$ for driving environments of highway, countryside, urban street and tunnel for the city of Hong Kong. Since those findings, only recently have two studies reported in-vehicle cabin $NO_x$ (Yamada et al., 2016; Martin et al., 2016). Yamada et al., (2016), drove a passenger car in a regional road and a highway in Tokyo, Japan and reported concentrations of $NO_2$ around 0.10 ppm, which is almost equal to the WHO 1-hour standard; this concentration increased to 0.89 ppm while driving inside an urban tunnel for about 20 min. In the second recent study by Martin et al., 2016, nine passenger cars were driven in a route in Sydney, Australia that included long and short tunnels and busy roads. They reported average concentrations of $NO_2$ as high as 200 ±23 ppb for major tunnels (3.8 ±1.2 min inside tunnels) and 100 ±14 ppb for minor tunnels and busy roads.

Table 1.4: Within vehicle cabin air pollutant concentrations reported in the literature. WO: windows open; WC: Windows closed; AC: Air conditioning; RC: recirculation. Note that some studies reported ranges and others did not report standard deviations. In the absence of mean and standard deviation, the median was included (indicated where reported). Bold highlight: Exposure above the legislative limits. CO limits: 10 $mg/m^3$ (maximum daily running 8 hour mean); $PM_{2.5}$ limits: 25 $\mu g/m^3$ (annual mean).

| Pollutant | City/Country | Mean±SD/ Range | Ventilation | Reference |
|---|---|---|---|---|
| CO ($mg/m^3$) | Raleigh/USA | **13±5.9/-** | Not reported | Chan et al., 1991 |
| | Riyadh/Saudi Arabia | **36±12.9/29-39** | Not reported | Koushki et al., 1992 |
| | California/ USA | 9.8±5.8/- | WO, WO 1/3 | Ott et al., 1994 |
| | Taipei/Taiwan | **11±3.6/4.5-20** | Not reported | Liu et al., 1994 |
| | Mexico/Mexico | **-/55.2 – 57** | Not reported | Fernandez and Ashmore, 1995 |
| | Nottingham/UK | -/4.8 - 11.3 | Not reported | Clifford et al., 1997 |
| | Hong Kong/China | **10.1±4.2/-** | Not reported | Chan et al., 1999 |
| | Kuopio/Finland | **11.5±2.3/1.4 – 13** | WC, fan on | Alm et al., 1999 |
| | Paris/France | 4.4±1.1/- | Not reported | Zagury et al., 2000 |
| | Hong Kong/China | 3.8±1.2/- | AC on | Chan and Liu, 2001 |
| | Hong Kong/China | 2.2/1 - 3.6 | AC on | Chan et al., 2002a |
| | Guangzhou/China | **21.5±6.2/10.5 - 46.1** | WC, AC on | Chan et al., 2002b |
| | | **33±11.7/11.9 - 39.8** | WO, AC off | |
| | Athens/Greece | **21.4±4/14.6-40** | Not reported | Duci et al., 2003 |
| | London/UK | 1.5±5.8/0-2.5 | Not reported | Kaur et al., 2005 |
| | Beirut/Lebanon | **17.7±2.4/2-34.5** | WO ½ | Abi Esber and El-Fadel, 2008 |
| | | **30.2±3.2/3.5-55.5** | AC on RC on | |
| | | **20.5±4/0-120.5** | AC on | |
| | Andhra Pradesh/India | 1.5±1.15 /- (Car) | WO | Kolluru et al., 2018 |
| | | 2.1±1.5/- (Car) | AC on | |
| | Mexico City/Mexico | 2.1±0.2/- (Car) | Not reported | Velasco et al., 2019 |
| | | 1.8±0.3/- (Bus) | | |
| $PM_{2.5}$ ($\mu g/m^3$) | London, UK | **33.36±20.73/- (Taxi)** | Not reported | Pfeifer et al., 1999 |
| | London, UK | **38.9/5.9-97.4 (bus)** | Not reported | Adams et al., 2001 |
| | | **35.7/6.6-94.4** | | |
| | Hong Kong, China | **93±12/78-109 (bus)** | AC off | Chan et al., 2002a |
| | | **97±38/48-138 (mini-bus)** | | |
| | | **51±19/30-98 (bus)** | AC on | |
| | | **45±14/27-67 (mini-bus)** | | |
| | Guangzhou, China | **145±56/- Bus** | AC off | Chan et al., 2002b |
| | | **106±28/- Taxi** | | |
| | | **101±61/- Bus** | AC on | |
| | | **73±30/- Taxi** | | |
| | Aberdeen, UK | **38 (median) Bus** | Not reported | Dennekamp et al., 2002 |
| | | **11 (median) Car** | | |
| | Boston, USA | **≈100/≈75-175 Bus** | Not reported | Levy et al., 2002 |
| | | **≈100/≈90-130 Car** | | |
| | Sidney, Australia | 24.8/9.1-45.2 | Not reported | Chertok et al., 2004 |
| | Mexico City, Mexico | **68±15/12-106 (Mini Bus)** | Not reported | Gomez-Parales et al., 2004 |
| | | **71±21/23-137 (Bus)** | | |
| | Northampton, UK | 15.5±15/- | Not reported | Gulliver and Briggs, 2004 |
| | Trujillo, Peru | **161±35/- Bus** | Not reported | Han et al., 2005 |
| | London, UK | **34.5/6-64.6 (Bus)** | Not reported | Kaur et al., 2005 |
| | | **38/15.2-58.5 (Car)** | | |
| | | **41.5/17.9-71.8 (Taxi)** | | |
| | Leicester, UK | -/9.7-25.6 Van | Not reported | Krausse and Mardaljevic, 2005 |
| | Netherlands | **48.9±22.5/-** | Not reported | Boogard et al., 2009 |
| | Ispra, Italy | 26.9±6.2/0.9-94.4 (Car) | Not reported | Geiss et al., 2010 |
| | Beijing, China | **31.6±13/- Taxi** | Not reported | Huang et al., 2012 |
| | Jakarta, Indonesia | **92±39/-** | Not reported | Both et al., 2013 |
| | Beirut, Lebanon | **71±29/-** | Not reported | Abi-Esber and El-Fadel, 2013 |
| | Guntur, India | 29 ± 12/ 9–109 (Car) | WO | Kolluru and Patra, 2020 |
| | | 24 ± 8/ 9–300 | AC on | |
| | | 10 ± 4/ 4–35 | RC on | |
| | Mexico City/ Mexico | **41±3/ - (Bus)** | Not reported | Velasco et al., 2019 |
| | | **26±3/- (Car)** | | |
| | Lisbon/Portugal | **34±8.6/-** | Not reported | Correia et al., 2020 |

| | | | | |
|---|---|---|---|---|
| UFP (pt/cm$^3$) | Kuopia, Finland | (morning)<br>107000±19000/59000-214000<br>(afternoon)<br>52000±21000/15000-155000 | Not reported | Alm et al., 1999 |
| | London, UK | 349000/- | | Dickens, 2000 |
| | Aberdeen, UK | 53000 (median) Bus<br>23000 (median) Car<br>50000 (median) Landrover | Not reported | Dennekamp et al., 2002 |
| | Boston, USA | -/80000-120000 (Bus)<br>-/83000-120000 (car) | Not reported | Levy et al., 2002 |
| | Leeds, UK | Off-peak (10:00-13:00)<br>43600±24200/9980-143000 (bus)<br>58300±48700/8000-282000 (car)<br>Peak(14:30-16:30)<br>40800±25500/12400-181700 (bus)<br>52000±36000/15800-230800 (car) | Not reported | Mackay, 2004 |
| | London, UK | 101364/64463-158685 (bus)<br>99736/36474-151810 (car)<br>87545/51506-114022 (taxi) | Not reported | Kaur et al., 2005 |
| | Hong Kong, China | 782000/-<br>245000/-<br>465000/- | AC on<br>AC off<br>WO | Kaminsky et al., 2009 |
| | Mexico City/ Mecixo | 38300±7800/ - (Bus)<br>16500±12400/- (Car) | Not reported | Velasco et al., 2019 |
| | Lisbon/Portugal | 28400±20900 (Bus)<br>18500±14700 (Car) | Not reported | Correia et al., 2020 |

# 1.8 Human exposure to air pollution

Humans are exposed to air pollution for a short (acute) or a long (chronic) period of time. Acute exposure is the short contact with a pollutant which is in the scale of a few seconds or a few hours. Chronic exposure is the continuous or repeated contact with an air pollutant over a long period of time (months or years). Both types of exposure may cause adverse health effects. Chronic exposures normally occur at home, where individuals are exposed to household furniture or carpeting chemicals.

Traditionally, indoor air quality studies have been focused on environments such as homes (Schieweck et al., 2018; Kurti et al., 2016; Morawska et al., 2013), work places (Mandin et al., 2017, Salonen et al., 2019) and schools (Ben-David and Waring, 2016; Romagnoli et al., 2014), where most of the chronic exposure occurs. However, human beings are also spending dissimilar proportions of their time in other indoor environments such as shopping malls, restaurants, supermarkets, and during commuting in micro-environments such as cars, buses, metros etc. The distribution of time that each person dedicates to these activities or any other daily activities such as running, walking, cycling etc. is different for each individual, making human beings dynamic receptors of air pollution exposure.

Exposure to air pollution depends on the amount of time and the frequency in each microenvironment/activity, the concentration of the air pollutants in that specific micro-environment and the activity based uptake (breathing rate x tidal volume) of each individual. Breathing rates, and hence exposure are influenced by a number of factors such as age, gender, weight, physical condition and activity level. The typical breathing rate per day for adult males is usually higher than for adult females, while typical breathing rates are lower for children compared to adults, although contaminant uptake per mass body weight is normally larger for children.

The accurate assessment of human exposure is a critical aspect to conduct a subsequent risk analysis and health impact assessment study, which in turn can help individuals, local authorities and policy makers to apply effective strategies to reduce such exposure. Typically there are two broad categories of assessment methodologies: a) the direct, which may involve people carrying personal exposure devices to measure

their exposure to air pollution on a typical day (e.g. Delgado-Saborit, 2012; Dons et al., 2011) and b) the indirect, which normally involves certain assumptions and proxies around the sources (e.g. distance of pedestrians from the roadsides) and/or the ambient air pollution levels (e.g. population exposure is equivalent to that reported on the air quality monitoring stations) and normally uses air pollution/air quality modelling techniques as tools to assess exposure.

## 1.9 Air quality modelling

The definition of the world that surrounds us depends on how it is perceived by individuals, and may consist of objects, phenomena, processes or even a combination of the above. These can be represented by photographs, drawings, tables, written or oral speech, or various mathematical formulas and so on. In order to understand each such world or environment, it has to be broken down into smaller and simplified parts and each part in turn has to be divided into even smaller and more simplified ones and so on. Each such part is called a reality of the world which has been defined in the beginning of the process, and every representation of a reality is called a model of that reality.

The atmosphere, in order to describe it, is considered such a reality (Figure 1.7). The atmosphere is mainly described and studied by a combination of three things: a) measurements of the atmosphere, carried out by different instruments and provide detailed state of the atmosphere in one area, b) laboratory studies, which provide detailed information on the various phenomena occurring in the atmosphere (transport, photochemical transformations, etc.) and finally, c) simulations of these phenomena, which help us to better understand the atmosphere, allowing the study of individual cases.

Simulations of atmospheric phenomena are carried out with the help of appropriate mathematical models, which are an alternative way to study the atmosphere and the laws that govern it. Atmospheric models are a family of mathematical descriptions of atmospheric circulation, atmospheric transport, dispersion, diffusion, wet and dry deposition processes, precipitation and photochemical and physical pollutant transformations. They can be used to predict the weather, investigate the climate and estimate the air quality. The main objective in the development of models is to achieve a balance between the complexity of their mathematical description (equations, resolution) and the capabilities of the computational systems which are required for the numerical solution of these equations.

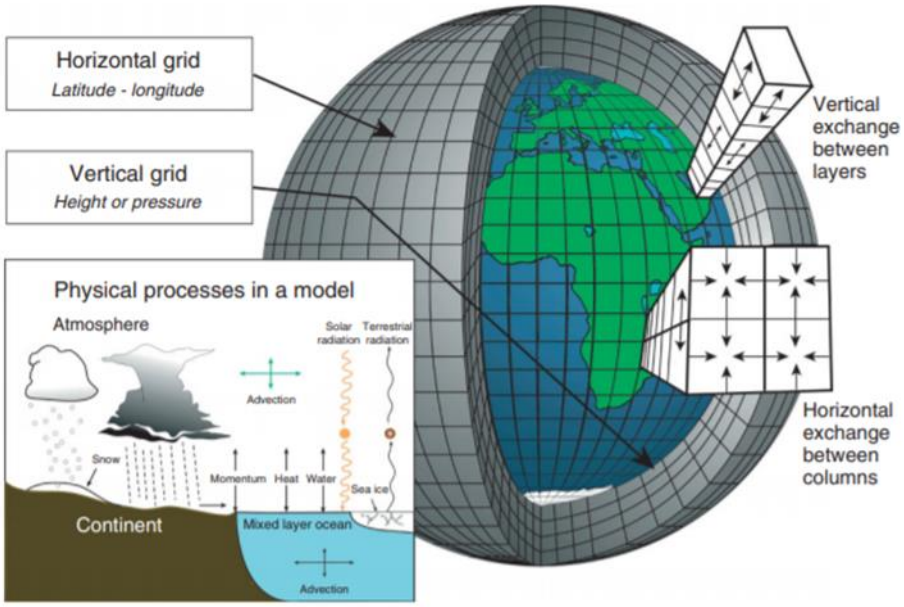


Figure 1.7: Schematic representation of a Cartesian grid in an air quality model (adopted from Edwards, 2011).

Air quality models use mathematical equations and numerical techniques, and based on inputs of meteorological data and source information like emission rates, simulate the physical and chemical processes that affect air pollutants as they disperse and react in the atmosphere. Models are evaluated by making comparisons between atmospheric measurements and model predictions (Papalexiou and Moussiopoulos, 2006; Sokhi et al., 2006; Matthaios et al., 2018). This has led to the improvement of field campaigns and to more laboratory experiments, as well as the need to improve the approaches and parametrisations of the mathematical models.

Air quality models are a very important tool which can be used routinely in order to estimate air quality (or for air quality management), apply environmental friendly policies, emission reduction scenarios and environmental impact assessment

studies. These models are also useful as decision support systems in cases of pollution episodes (e.g., San Jose et al., 2005) and/or accidents in industrial or other facilities. Depending on their nature air quality models can roughly be categorised into: Box models, Gaussian models, Eulerian models (including large-eddy simulation models and computational fluid dynamics models), and Lagrangian models (Russell and Dennis 2000; Seaman, 2000). Air quality models can also be used, or coupled with other models, to estimate the exposure of people to air pollution (Renquia et al., 2017) and with some adaptations predict the cleanest commuting road (Boniardi et al., 2019) or give an activity based exposure (de Nazelle et al., 2013), the so called "exposure modelling techniques".

Exposure modelling is an indirect method for assessing human exposure to air pollution based on a range of indicators, such as proximity to the source, road traffic density, indoor and outdoor pollutant concentrations, etc. Although the complexity of exposure models varies widely, they usually involve some mathematical simulations that require input information as well as independent exposure monitoring datasets for validation (Vardoulakis, 2009). Models are particularly useful for assessing exposure in areas where measurements are not available, as well as for testing exposure scenarios and mitigation strategies, reconstructing past exposures and providing exposure predictions for epidemiological studies (e.g. Jerret et al., 2005; Nieuwenhuijsen et al., 2006).

Exposure models can be broadly classified into the following categories: (a) source-oriented models (e.g. photochemical models); (b) geostatistical interpolation and land-use regression models; (c) receptor-oriented models (including chemical

mass balance and statistical factor analysis models); and (d) time–activity (or micro-environmental) models. Source-oriented models generally rely on information associated with the pollution source, for example proximity to an industrial source, emission rates, stacks height, etc., to predict pollutant concentrations at outdoor locations. Geospatial interpolation and land-use regression models use statistical techniques to interpolate air quality data obtained from a network of monitoring sites. Receptor models analyse air quality data obtained from one or more receptor locations to identify contributing emission sources. Finally, time–activity models use a combination of air quality measurements, dispersion model simulations and questionnaires to reconstruct the personal exposure of individuals or population sub-groups. There are different ways of classifying models, and some exposure models (sometimes called hybrid) may combine more than one of the above approaches, while there is a growing body of studies that involve learning algorithms (e.g. deep learning, machine learning algorithms) to improve the predictive skill of these models (Aquilina et al., 2018; Stingone et al., 2017). However, in most learning algorithms the quality of their output is highly dependent on the quality of the input data.

# 1.10 Objectives of the thesis

The main aim of this thesis is to increase our understanding of real-world on-road vehicle emissions and their impact on urban/roadside and within-vehicle concentrations/exposure. To address this, the study aims to complete the following objectives:

**Determine vehicle primary $NO_2/NO_x$ emissions in the UK under normal and cold weather conditions and their impact upon urban air quality.** In chapter 2 of this thesis, the inferred trends in cumulative UK fleet $NO_x$ emissions and their response to temperature are presented and discussed extensively. In doing so the study builds upon previous, related work applying a similar approach to infer changes in relative vehicle emissions (e.g. Carslaw et al., 2016b; Carslaw and Beevers, 2005; Jenkin, 2004), and potential signatures of increased diesel vehicle penetration and tightening of emission standards (e.g. Carslaw et al., 2016b; Grange et al., 2017). The focus upon $NO_x$ / $NO_2$ is driven by the current exceedance of air quality limits for NO2 in many urban locations across the UK. Although there are several studies in the literature investigating the primary $NO_2/NO_x$ vehicle emissions from ambient monitoring stations, there is little to no information available regarding their response to cold weather (Grange et al., 2019). This chapter of the thesis develops a methodology to investigate the primary $NO_2/NO_x$ vehicle emissions under cold weather conditions and quantifies their impact on urban air quality.

**Quantify within-vehicle air pollution exposure to $NO_x$ and particles and investigate their variation with outdoor air pollution, route and ventilation settings in Birmingham, UK.** Chapter 3 of this thesis reports direct and indirect methods to assess the air pollution exposure of several activities in the urban area of Birmingham UK. The chapter presents and discusses extensively the direct exposure of vehicle occupants to air pollution and how individuals can moderate their air pollution exposure by changing the ventilation settings of vehicles and/or driving routes. The chapter also applies indirect methods, to calculate the inhalation dose of cyclists and pedestrians and compares the dose to that of vehicle occupants to provide detail and comparable insights about activity based exposure to PM and $NO_2$. The focus is upon these species as the air pollutants responsible for the largest human health impacts in the UK. Several studies have addressed the issue of within-vehicle air pollution, however most of the studies in the literature are either limited by the fact that they are using personal exposure devices that normally have big discrepancies with the referenced air quality instruments or by not taking into account the variation of the on-road air pollution and/or air exchange rate that occurs inside the vehicle. Studies that take into account the on-road air pollution variations/air exchange in the vehicle are only focusing on one species which is either $NO_x$ (Martin et al., 2016; Yamada et al., 2016) or particles (Knibbs et al., 2012; de Nezelle et al., 2012; Hudda et al., 2012). The chapter of this thesis aims to improve the understanding of the combined effect that $NO_x$ and particles have to within-vehicle exposure in the UK, as this is of great significance in order to implement accurate health-impact assessment studies (COMEAP, 2018).

**Predict within-vehicle air pollution of $NO_x$ and particles with traditional and data driven modelling techniques.** Chapter 4 of this thesis reports the direct measurements of chapter 3 to develop an indirect tool to estimate personal exposure inside vehicles. Specifically, chapter 4 develops a source-oriented mass balance exposure model that takes into account basic atmospheric processes and photochemistry in mircoenvironments to estimate vehicle occupant exposure to outside air pollution under different ventilation settings. The chapter also applies the state-of-the-art machine learning algorithms based upon a training dataset to improve the model predictions and enhance its capabilities to predict within vehicle air pollution exposure from the reported air quality levels of the nearby monitoring stations. Several attempts have been made to model within-vehicle exposure with different mass-balance approximations (Knibbs et al., 2011; Xu and Zhu, 2009; Hudda et al., 2012), however there are no studies that include basic gas-phase reactions within-vehicles. This chapter aims to develop a mass-balance model that can be used to estimate both particulate and gas concentrations inside vehicles with respect to the outside pollution variations and the choice of ventilation. Another area that this chapter aims to contribute is the predictions of microenvironment exposure with data-driven models. These models are gaining more attention in air pollution exposure studies (Aquilina et al., 2018; Stingone et al., 2017), however since their output depends on the quality of their input, applying them to microenviroment exposure studies such as the one reported in chapter 3 will provide novel prediction capabilities to human air pollution exposure estimations.

# Chapter 2: Roadside $NO_x$ and primary $NO_2$ emissions in the UK and their implications for urban air quality

In this chapter, an analysis of the trends in $NO_x$ and $NO_2$ mixing ratios between 2009 and 2016 for urban monitoring stations across the UK is presented and discussed. Changes in the ambient $NO_2/NO_x$ ratio were also assessed, and the total oxidant approach was applied to the ambient data to quantify trends in inferred primary or directly emitted $NO_2$ from vehicles. The air quality data were coupled with meteorological observations and a methodology was introduced to assess the potential changes in vehicle emissions associated with "cold–start" operation, as indicated by ambient temperature. The material presented in this chapter has been published as:

*Matthaios N. V., Kramer J. L., Sommariva R., Pope D. F., Bloss J. W., 2019. Investigation of vehicle cold starts primary $NO_2$ emissions from ambient monitoring data in the UK and their implications for urban air quality. Atmospheric Environment 199, 402-414, DOI: 10.1016/j.atmosenv.2018.11.*

## Graphical abstract

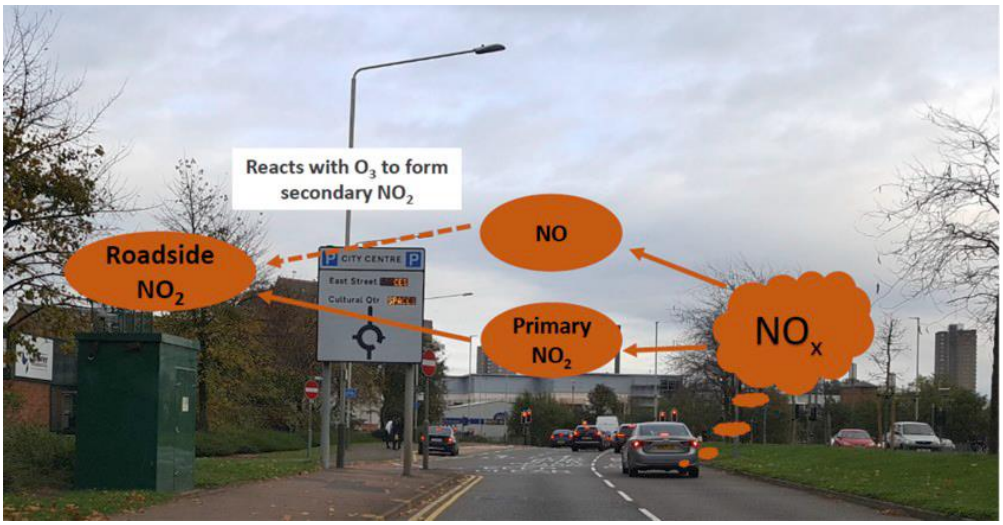


# 2.1 Introduction

In the last two decades, the European vehicle fleet has undergone significant dieselisation (Cames and Helmers, 2013; EEA, 2015; ICCT, 2015) mainly with the incentive of better fuel efficiency, lower $CO_2$ emissions and increased driving performance over alternative fuels and technologies (Koetse and Hoen, 2014). In the UK, although recent statistics show that there was a 17% decrease in new diesel car

registrations in 2017, following by a second 30% decline in the number of diesel cars being registered for the first time in 2018 compared to 2017 (DfT, 2019), diesel vehicles still comprise 54% of the total fleet in England and about 57% in Scotland, Wales and Northern Ireland (NAEI, 2018).

Road transport is the second largest source of $NO_x$ emissions in the UK, contributing 30% of total emissions in 2015 (DEFRA, 2018). However, emissions from road transport have fallen by 34% between 1990 and 2000 and by 50% from 2000 to 2015 which is very important for urban areas. This is due to improvements in engine design and fitting of new after-treatment systems such as three way catalysts (TWC), and selective catalytic reduction (SCR) and lean $NO_x$ trap (LNT) to petrol and diesel cars respectively, to meet the increasingly strict European standards. As mentioned in Chapter 1, internal combustion engine vehicles emit $NO_x$ which consist from $NO_2$ and NO. The $NO_2$ that is emitted directly from vehicles is the primary $NO_2$, while the $NO_2$ that is formed shortly after the tailpipe emissions in the atmosphere, via the reaction of NO with $O_3$, is called secondary $NO_2$. In UK many roadside locations do not comply with the annual EU $NO_2$ limits (DEFRA, 2017). In order to improve local urban air quality it is essential to know the primary $NO_2/NO_x$ ratio that is emitted from vehicles and how that has changed over the years with the applied mitigating policies/changing in vehicle exhaust treatment technologies.

A recent focus for vehicle emissions research has been the quantification of the discrepancy between type approval and real-world emissions performance of diesel passenger cars, where on-road $NO_x$ emissions from diesel vehicles have been found to be much higher in real-world situations than in the type approval laboratory based

emission tests (Degraeuwe and Weiss, 2017; O'Driscoll et al., 2018). Although the reason for this disagreement is inadequately understood, as the main reason was believed to be the cycle recognition defeat devices that many manufacturers used, however recent evidence suggest that $NO_x$ emissions from vehicles, from laboratory and real-world driving tests, are also highly dependent on ambient temperature and specifically low temperatures (< 5 $^{o}$C) (Suarez-Bertoa and Astorga, 2018; Grange et al., 2019, Dallman et al., 2019).

Currently within the EU, vehicle type approval test do not include $NO_x$ emissions at low temperatures. Furthermore, techniques such as the laboratory tests, PEMS or remote sensing methods that are traditionally used to estimate $NO_x$ emissions from vehicles and their dependence upon low temperature are very expensive, and not practical, especially when it comes to methods that can be used to estimate the extra burden of these elevated vehicle emissions to air quality and human health. As a result, the implications arising from increased $NO_x$ vehicle emissions at lower temperatures for air quality remain very significant but very poorly recognised. In the United Kingdom the most recent (until 2019) National Atmospheric Emissions Inventory (NAEI) does not account for any dependence of vehicular emissions upon ambient temperature, which would result in less than ideal modelling of emissions and hence ambient concentrations in air quality models. This in turn will result in errors in the estimation of human exposure to vehicular air pollution and thus less accurate air pollution - human health impact studies. Therefore, this chapter explores an alternative methodology to estimate the low temperature vehicle $NO_2/NO_x$ emissions

as this understanding will promote effective strategies a) to mitigate these emissions and b) to control our personal exposure to air pollution.

## 2.2 Data and methodology

### 2.2.1 Experimental data

Atmospheric mixing ratios of $NO_x$ and $O_3$ are monitored across the UK by the Automatic Urban and Rural Network (AURN), which is operated and maintained by the Department for Environment, Food and Rural Affairs (DEFRA), the Scottish Executive, the National Assembly for Wales and the Department of the Environment for Northern Ireland. Ambient mixing ratios are reported at hourly resolution, with measurements made by well-established conventional techniques, UV photometry for $O_3$ and chemiluminescence for $NO_x$ with a molybdenum converter (see section 2.2, for $NO_2$ selectivity). The measurement uncertainty for $NO_x$ and $O_3$ from the AURN stations is <15%, following the European Committee for Standardisation (documents BS EN14211:2012 - $NO_x$ and BS EN14625:2012 - $O_3$).

The analysis presented here uses hourly data; about three million hourly data points for each of NO, $NO_2$, $O_3$ were included in the analysis from every urban-traffic monitoring station (defined as stations that are located at roadside and kerbside locations) in the UK AURN network. For each urban-traffic station, background data were obtained from a nearby background site, defined as the urban or rural background site (applying the AURN classification) closest to the location of the urban traffic monitoring station. Further data availability constraints of coverage from the start of 2009 to the end of 2016, and overall data capture greater than 75% were applied (75 % selected as this is the minimum requirement for a valid aggregated value over a day and a year according to the EU air quality reports (EEA, 2016; Font and Fuller, 2016)), Additionally, for each urban traffic monitoring site, meteorological measurements (UK Met-Office, downloaded from the British Atmospheric Data Centre (BADC) were used, in order to couple the air pollution measurements with local meteorology. In total, 17 urban traffic stations were included, which were paired with 10 urban background sites and 5 rural sites from the AURN network, alongside the 14 meteorological sites. The rural stations were required as not all urban traffic sites have a proximate urban background station. The difference in the numbers of urban background and meteorological stations arises as for London two urban background sites were used for four urban traffic stations, and one meteorological station for the whole area. The map of the stations used is shown in Figure 2.1, and their details are listed in Table 2.1.

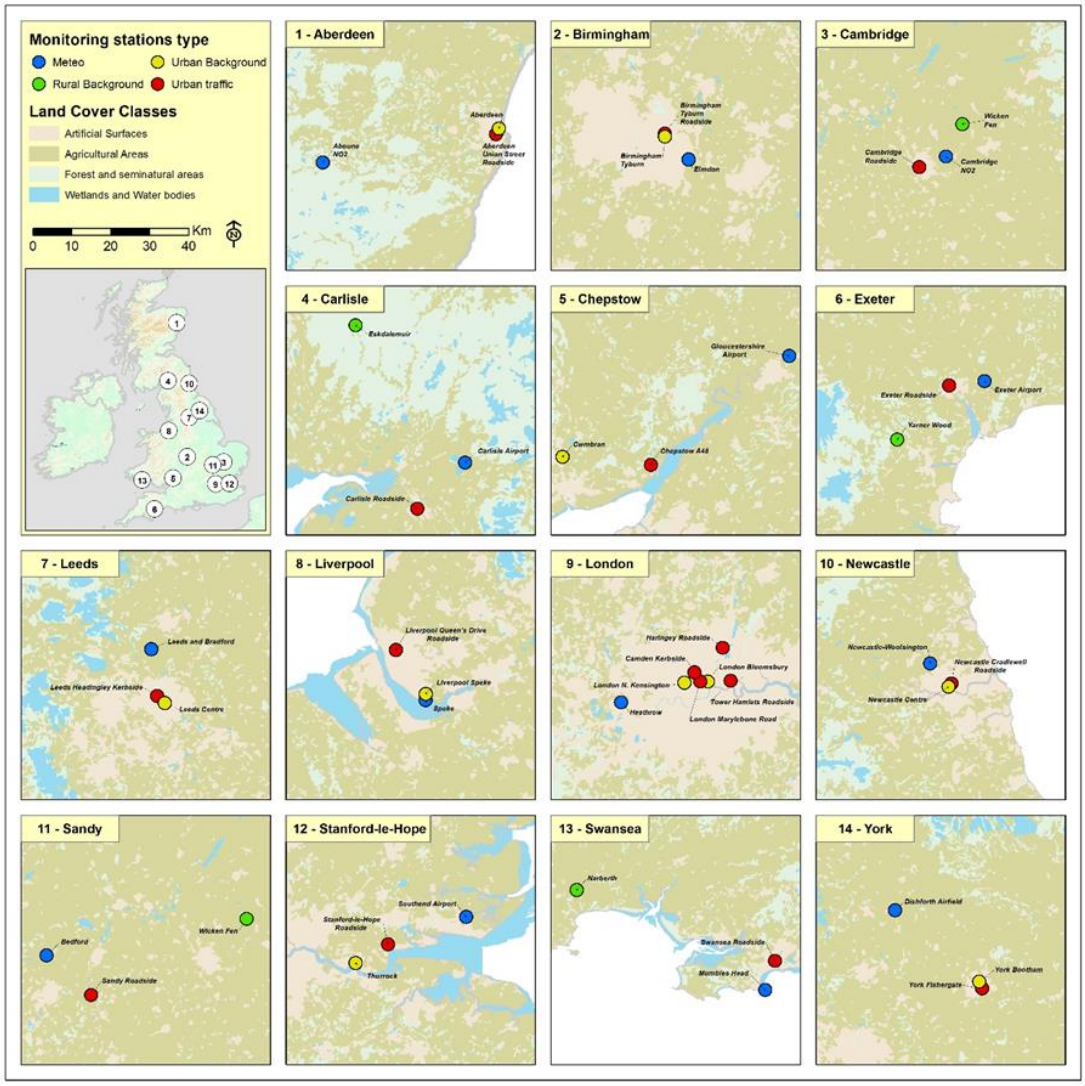


Figure 2.1: Monitoring sites used in this study. Blue colour indicates the meteorological stations, red colour the urban traffic sites, yellow the urban background and green the rural sites

Table 2.1: Names, location and type (AURN classification) of the UK urban traffic dominated monitoring sites included in this study.

| Name | Latitude | Longitude | Type | Area |
|---|---|---|---|---|
| Aboune NO2 | 57.076 | -2.83948 | Meteo | Aberdeen |
| Elmdon | 52.4524 | -1.74099 | Meteo | Birmingham |
| Cambridge NO2 | 52.2249 | 0.22563 | Meteo | Cambridge |
| Carlisle Airport | 55.0023 | -2.75675 | Meteo | Carlisle |
| Gloucestershire Airport | 51.8915 | -2.16713 | Meteo | Chepstow |
| Exeter Airport | 50.7366 | -3.40458 | Meteo | Exeter |
| Leeds and Bradford | 53.9282 | -1.5979 | Meteo | Leeds |
| Speke | 53.3316 | -2.8455 | Meteo | Liverpool |
| Heathrow | 51.4787 | -0.44904 | Meteo | London |
| Newcastle-Woolsington | 55.033 | -1.68393 | Meteo | Newcastle |
| Bedford | 52.2265 | -0.46376 | Meteo | Sandy |
| Southend Airport | 51.5748 | 0.73213 | Meteo | Stanford le hope |
| Mumbles Head | 51.5651 | -3.98056 | Meteo | Swansea |
| Dishforth Airfield | 54.1346 | -1.41293 | Meteo | York |
| Liverpool Queen's Drive | 53.44694 | -2.9625 | Urban traffic | Liverpool |
| Liverpool Speke | 53.34633 | -2.844333 | Urban Background | Liverpool |
| Aberdeen Union Street | 57.14455 | -2.106472 | Urban traffic | Aberdeen |
| Aberdeen | 57.15736 | -2.094278 | Urban Background | Aberdeen |
| Birmingham Tyburn Roadside | 52.51219 | -1.830861 | Urban traffic | Birmingham |
| Birmingham Tyburn | 52.51172 | -1.830583 | Urban Background | Birmingham |
| Cambridge Roadside | 52.20237 | 0.124456 | Urban traffic | Cambridge |
| Wicken Fen | 52.2985 | 0.290917 | Rural Background | Cambridge |
| Carlisle Roadside | 54.89472 | -2.945861 | Urban traffic | Carlisle |
| Eskdalemuir | 55.31531 | -3.206111 | Rural Background | Carlisle |
| Chepstow A48 | 51.63809 | -2.678731 | Urban traffic | Chepstow |
| Cwmbran | 51.6538 | -3.006953 | Urban Background | Chepstow |
| Exeter Roadside | 50.72508 | -3.532465 | Urban traffic | Exeter |
| Yarner Wood | 50.5976 | -3.71651 | Rural Background | Exeter |

| | | | | |
|---|---|---|---|---|
| Stanford-le-Hope Roadside | 51.51817 | 0.439556 | Urban traffic | Stanford le hope |
| Thurrock | 51.47707 | 0.317969 | Urban Background | Stanford le hope |
| Newcastle Cradlewell Roadside | 54.98639 | -1.598611 | Urban traffic | Newcastle |
| Newcastle Centre | 54.97825 | -1.610528 | Urban Background | Newcastle |
| Sandy Roadside | 52.13242 | -0.300306 | Urban traffic | Sandy |
| Swansea Roadside | 51.6327 | -3.947374 | Urban traffic | Swansea |
| Narberth | 51.78178 | -4.691462 | Rural Background | Swansea |
| York Fishergate | 53.95189 | -1.075861 | Urban traffic | York |
| York Bootham | 53.96751 | -1.086514 | Urban Background | York |
| Haringey Roadside | 51.5993 | -0.068225 | Urban traffic | London |
| London Bloomsbury | 51.52229 | -0.125889 | Urban Background | London |
| London Marylebone Road | 51.52253 | -0.154611 | Urban traffic | London |
| London N. Kensington | 51.52106 | -0.213431 | Urban Background | London |
| Tower Hamlets Roadside | 51.52256 | -0.042164 | Urban traffic | London |
| Camden Kerbside | 51.54421 | -0.175269 | Urban traffic | London |
| Leeds Headingley Kerbside | 53.81997 | -1.576361 | Urban traffic | Leeds |
| Leeds Centre | 53.80378 | -1.546472 | Urban Background | Leeds |

### 2.2.2 Data processing methods and assumptions

Monitored data were processed and displayed using ArcGIS and R version 2.15.1 (R Core Team, 2016) along with the R packages ggplot2 (Wickham, 2009), openair (Carslaw and Ropkins, 2012), and mcgv (Wood, 2003). The data were de-seasonalised to acquire better trend signal (see Figure 2.2), by applying the smoothing

LOESS function, which is a non-parametric regression method that combines multiple regression models in a k-nearest-neighbor-based meta-model (Cleveland et al., 1990). A seasonal trend decomposition based on LOESS is a filtering procedure for decomposing a time series into three components: trend, seasonal and remainder (residual). This method has flexibility in specifying the amounts of variation in the trend and seasonal components and the ability to decompose series with missing values. The approach produces a robust trend and seasonal components that are not distorted by transient, abnormal behaviour in the data and provides fast computation even for long time series (Cleveland et al., 1990). The approach consists of a sequence of smoothing operations each of which employs the same smoother: locally-weighted regression (LOWESS), or LOESS. The seasonal component is found by LOESS smoothing the seasonal sub-series (*i.e.* the series of all January values). The LOESS regression curve, $\hat{f}(x)$, is a smoothing of *y* given *x* that can be computed for any value *x* along the scale of the independent variable. That is, LOESS is defined everywhere and not just at the $x_i$ and this is an important feature that will allow the method to deal with missing values and de-trend the seasonal component in a straightforward way (see Figure 2.2). LOESS can be used to smooth *y* as a function of any number of independent variables but for the trend de-seasonalisation with LOESS only a single variable is needed (Cleveland and Grosse 1990; Cleveland and Devlin 1988; Cleveland et al., 1988).

The statistical approach that we followed for trend calculation is a non-parametric Mann-Kendall approach, while the trend slope is calculated with the Theil-Sen method (Sen, 1968; Theil, 1950) available in the R-openair package. In this method, for a given set of n x, y pairs, the slopes between all pairs of points are

calculated and the median is taken as an estimate of the most probable slope (trend). This method is robust to outliers and can be used in both non-normal and heteroscedastic (non-constant error variance) data series. Bootstrap re-sampling was then used for the calculation of confidence intervals at the 95% level and p-values. A statistically significant trend was assumed when $p < 0.1$ (represented with a '+' symbol), meaning that the trend was not random at a 90% chance; p-values of: $p < 0.05$, $p < 0.01$ and $p < 0.001$, marked by '*', '**' and '***', respectively, indicate very highly significant trends, while $p > 0.1$ shows insignificant trends.

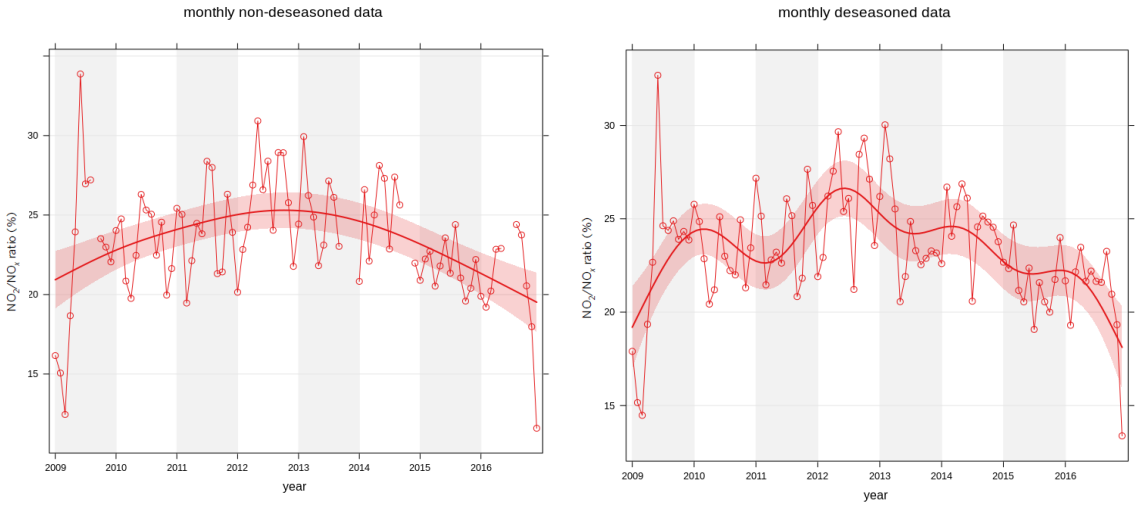


Figure 2.2: Mean monthly $NO_2/NO_x$ ratio in Cambridge, before (left) and after (right) the de-seasonalisation of the data. The solid red line shows the best fit. The shaded red area indicates the 95% confidence intervals.

To derive the inferred primary $NO_2/NO_x$ ratio from ambient monitoring data we used the total oxidant ($O_x = NO_2 + O_3$) approach (Clapp and Jenkin, 2001). It is well

known that in the daytime atmosphere the interconversion of $O_3$ to $NO_2$ and vice versa is generally dominated by the following reactions which also constitute a null cycle:

$$NO + O_3 \rightarrow NO_2 + O_2 \quad (1)$$

$$NO_2 + h\nu \rightarrow NO + O \quad (2)$$

$$O + O_2 + M \rightarrow O_3 + M \quad (3)$$

Reactions (1) - (3) result in the cycling of $NO_x$ between NO and $NO_2$ and total $O_x$ between $O_3$ and $NO_2$, however the total mixing ratios of both $NO_x$ and $O_x$ remain constant. During daylight, the equilibrium that occurs in the above reactions determines the photo-stationary steady state (PSS). Clapp and Jenkin, (2001) illustrated that when in PSS there is a linear relation between $O_x$ and $NO_x$ for roadside station data, which may be interpreted as a $NO_x$ - independent and a $NO_x$ - dependent contribution to $O_x$. The former is the regional contribution which corresponds to the regional background $O_3$ level, whereas the latter is effectively a local contribution that is associated with additional $NO_2$ (i.e. primary $NO_2$ emissions, under the assumption that no other sources are significant). While this analysis only holds in volume mixing ratio space, it should be noted that the AURN data-series are reported in $\mu g/m^3$, therefore before we apply the total oxidant approach, data were converted from $\mu g/m^3$ to ppb by applying EU/DEFRA conversion factors (20 $^oC$ temperature and 1013

hPa pressure). For the analysis presented here, “Daytime” was defined as all whole hours between sunrise and sunset, based on the local time in London.

In the case of vehicle emissions from ambient urban traffic monitoring data, Jenkin, (2004), demonstrated that by considering the ‘total oxidant’ slope, ($NO_2 + O_3$) / $NO_x$, estimates could be drawn for the primary (direct) $NO_2/NO_x$ ratio emitted from vehicle emissions. However, most of the AURN urban traffic monitoring sites in the UK do not have $O_3$ measurements which poses a limitation to the total oxidant approach and to the estimation of the primary $NO_2/NO_x$ emission ratio. In such cases, and whenever $O_3$ data are not available at urban traffic sites, Carslaw and Beevers, (2005) suggested a methodology that calculates the $NO_2/NO_x$ ratio without the need of $O_3$ observations from the urban traffic site, but with additional observations (of $NO_2$, $NO_x$ and $O_3$) from a nearby urban background site. In general, this approach assumes that the increment in $NO_2$ mixing ratio between a given urban traffic monitoring site and a nearby urban background site is partitioned into $NO_2$ that is chemically derived through the reaction between NO and $O_3$, and $NO_2$ which is emitted directly by road vehicles. Therefore, data from paired sites (roadside and background/rural site) are used. The method uses a simple constrained model and a simple basic set of chemical reactions to explain the time-dependent variation in NO, $NO_2$ and $O_3$ as vehicle plumes mix with background air. Carslaw and Beevers (2005), showed that the primary $NO_2/NO_x$ ratio may then be obtained from fitting the observed $NO_2$ - $NO_x$ data to that predicted, whilst optimizing the primary $NO_2$ fraction, and mixing time between emission and observation at the urban site. This chapter follows this approach, but some limitations are noted. Specifically, the approach assumes that the increment in

$NO_2$ mixing ratio above a local background site is controlled by the availability of $O_3$ and directly emitted NO and $NO_2$ only and does not include additional chemical reactions (e.g. of peroxy radicals with NO). Furthermore, it should be mentioned that because the AURN analysers employ a heated molybdenum converter to detect $NO_2$ (as NO), other $NO_y$ species will be detected as $NO_2$. The influence of those interferences might lead to overestimation of $NO_2$ in urban areas (Dunlea et al., 2007; Harrison et al., 2012). In addition, direct emissions of HONO, thought to comprise a small, but still significant and uncertain, component of vehicle exhaust (Crilley et al., 2016; Jenkin et al., 2008; Kurtenbach et al., 2001), is also a potential interferent in $NO_2$ measurements. However, in our analysis (see 2.2.3 below) all the above interferences co-vary with $NO_2$ and do not affect the derived inferred primary $NO_2/NO_x$ ratio, therefore they can be considered negligible.

### 2.2.3 Investigation of cold-start emissions under low ambient temperature conditions

To assess evidence for altered emissions under conditions of low ambient temperatures, the total oxidant approach was applied during rush hour periods during the morning (06:00 - 10:00) and afternoon (16:00 - 19:00) during winter time (November, December, January, February), with the a temperature condition

threshold of 5 $^{o}$C ($T \leq 5$ $^{o}$C). Rush hours were selected because the vehicle fleet experiences less (and known) variations during those hours with respect to the rest of daytime. It should be noted here that the total oxidant approach was used, by including morning pre-sunrise and evening post-sunset periods (notionally daylight only, Clapp and Jenkin, 2001), however sensitivity tests showed that this introduced a very small difference in the overall results (less than a 2% change in the inferred primary $NO_2/NO_x$ emission ratio; less than 3.2 ppb difference in the ozone background). According to European regulations, the bench/laboratory tests for standard vehicle emissions are made under an (air) temperature range of 20 – 30 $^{o}$C (EC, 91/441/ECC) and normally at the fixed temperature value of 23 $^{o}$C (DfT, 2016). The vehicle is given a standard pre-conditioning in a temperature control room so that the whole vehicle including engine oil and coolant is 'soaked' to the regulated temperature range. As a result, the selected temperature threshold method ($T \leq 5$ $^{o}$C), is well below that for the tested/regulated range, and very close to the winter mean temperature in the UK (4.4 $^{o}$C). Results for days that satisfied the temperature criterion were compared with those that did not (Matthaios et al., 2017), in order to examine any potential difference in emissions-driven air quality.

# 2.3 Results and discussion

## 2.3.1 Ambient $NO_x$ and $NO_2$ trends and relationships

The annual averaged ambient $NO_x$ and $NO_2$ values for each urban traffic station are shown in Figure 2.3, normalised to their mean value (2009 - 2016). A clear decline in the levels of both $NO_x$ and $NO_2$ is evident, which based on the overall average from all sites is 11.3(±0.6)% for $NO_x$ (black dashed line, Figure 2.3a) and 17.2(±0.4)% for $NO_2$ (black dashed line, Figure 2.3b) across the time period considered (2009 - 2016). The greater $NO_2$ than $NO_x$ relative decline in the UK urban traffic sites might be due to an alteration in PSS, emissions or in the background ozone that contributes to the photochemical cycle. Figure 2.4 shows how the monthly mean rush hour $NO_2$ mixing ratios (normalized to 100 on 1/1/2009) vary for the examined period. An overall mean reduction of approximately 20% (see black line) in the $NO_2$ mixing ratios is apparent. This sharper $NO_2$ decrease cannot be explained by the changes in background ozone, since the background ozone has not changed significantly during the examined years (0.5% increase – see Figure 2.5). This decrease in $NO_2$ is somewhat counter-intuitive to that expected when considering the increase in the number of licensed diesel vehicles in the UK, which, according to the Department for Transport, have increased from about 39% (2009) to 52% (2016) in urban areas of Wales, Scotland, Northern Ireland

and England, and which are associated with higher $NO_2$ emissions than petrol vehicles. However, it should be highlighted that during the period studied here, new Euro limits came into force for the reduction of $NO_x$ and $NO_2$ vehicle emissions. Briefly, Euro 5 limits, first introduced in 2009, introduced a limit value of 0.18 g/km for $NO_x$ in passenger cars, while the tighter limits of Euro 6 for passenger cars (0.08 g/km for $NO_x$) came into force around 2014, driving the introduction of new after-treatment technologies such as SCR and LNT. Depending upon fleet penetration, these changes are beginning to play an important role in the (fleet averaged) primary $NO_2/NO_x$ ratio from vehicles (Carslaw et al., 2016b).

a)

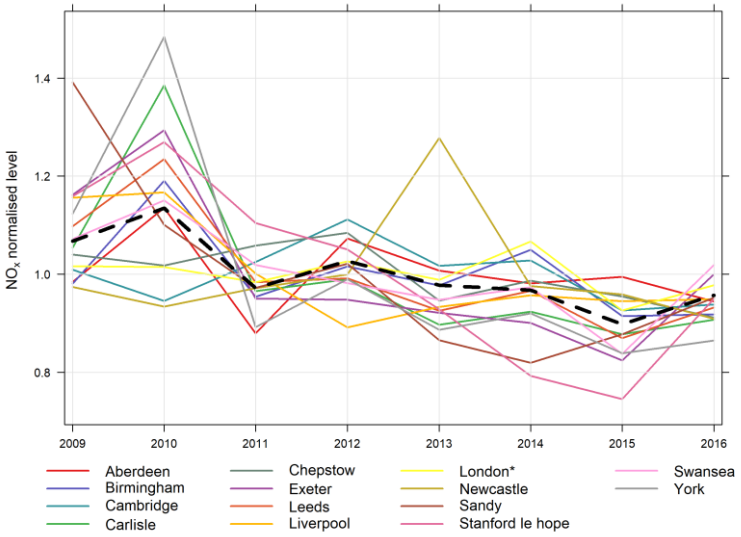


b)

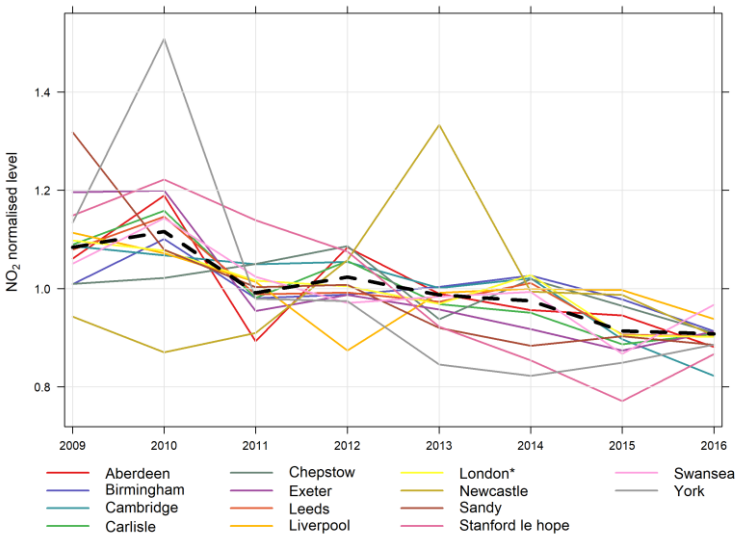


Figure 2.3: Annual average $NO_x$ (a) and $NO_2$ (b) values for urban traffic stations in the UK normalized to their mean value. Black dashed line is the average from all sites used.

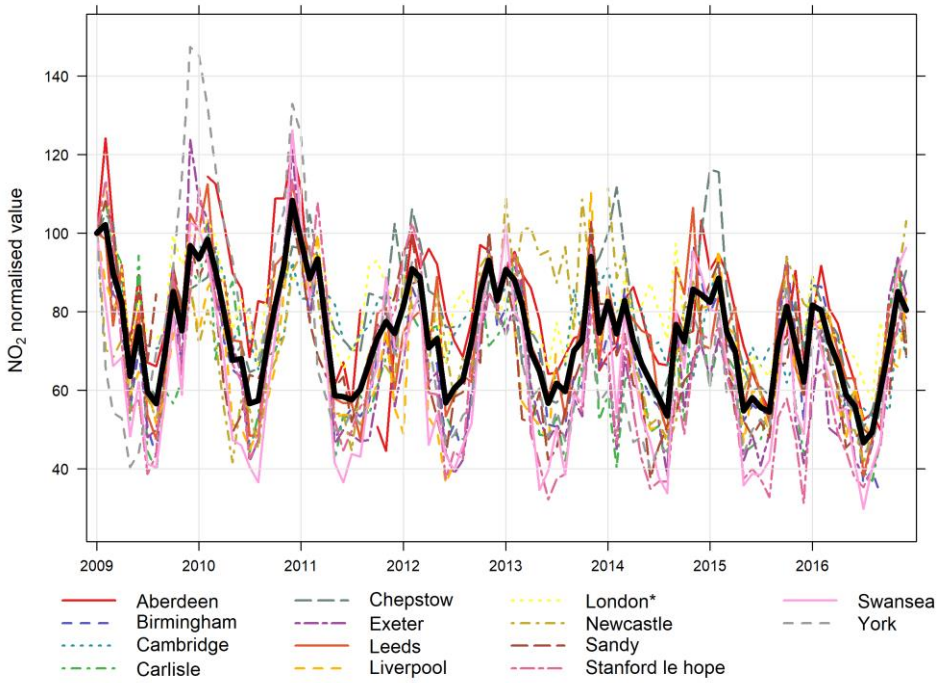


Figure 2.4: Monthly $NO_2$ mixing ratios during rush hour periods (06:00-10:00, 16:00-19:00), normalized to their 1/1/2009 value, for urban traffic monitoring sites across the UK. The black line indicates the mean value across all stations used.

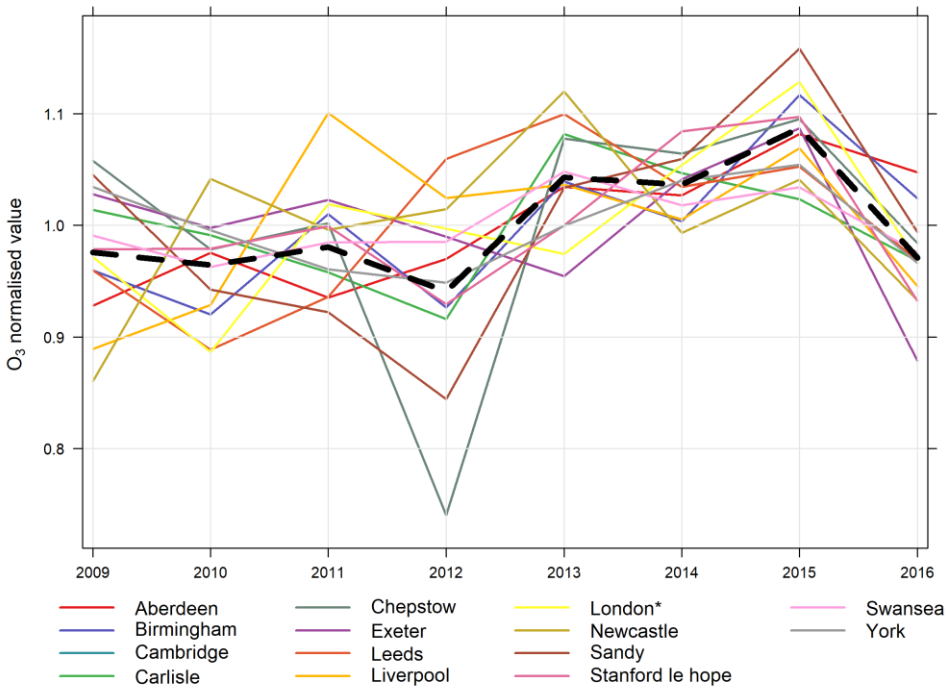


Figure 2.5: Yearly mixing ratios of ozone (normalized to the mean value) for each urban traffic monitoring station between 2009 and 2016. The black dashed line indicates the mean mixing ratio from all the sites.

Figure 2.6 illustrates the variation in the ambient $NO_2/NO_x$ ratio over time, as a function of $NO_x$ abundance, for the ambient monitoring data from urban traffic locations. Figure 2.6a (top) shows the distribution of hourly mean $NO_x$ mixing ratios for 2009 and 2016; Figure 2.6b (right) shows the distribution in hourly mean $NO_2/NO_x$ ratios for the same years and Figure 2.6c (centre) shows the hourly mean $NO_2/NO_x$ ratio as a function of $NO_x$ abundance. The values of $NO_2/NO_x$ as a function of $NO_x$ (Figure 2.6c) tend towards a minimum value, which approximates the primary $NO_2/NO_x$ emission ratio. This asymptote can be used as an alternative to the total oxidant approach described above in order to estimate the primary $NO_2/NO_x$ emission fraction. Itano et al., (2007) used a similar approach to estimate the primary $NO_2/NO_x$ ratio from an urban traffic site in Osaka, Japan. From the distribution in Figure 2.6b (right) it can be seen that the $NO_2/NO_x$ ratio has reduced slightly between 2009 and 2016 (median falling from 0.46 to 0.43), while from the asymptotes in Figure 2.6c (centre) the primary $NO_2/NO_x$ emission ratio can be seen to have fallen from 0.175 to 0.125. Figure 2.6d shows the absolute changes in $NO_2/NO_x$ ratio as a function of the change in total $NO_x$ mixing ratio (hourly mean for corresponding date / time / location) between 2009 and 2016, for each urban traffic location. The greatest reduction in $NO_2/NO_x$ ratio has occurred in the locations where $NO_x$ mixing ratio has increased (i.e. sites which have become more polluted, or busy, with positive values on the x axis), while for the majority of sites where $NO_x$ abundance has decreased (negative x axis values), the $NO_2/NO_x$ ratio has increased. To assess whether the observed changes in $NO_2/NO_x$ could be explained by $NO_x$ - $O_3$ PSS chemistry alone a simple PSS model, based on reactions (1) - (3), was used. In the first instance the model was initiated with

baseline conditions of 30 ppb of $O_3$, 100 ppb of $NO_x$ (75:25% NO:$NO_2$). In the subsequent runs only the initial $NO_x$ mixing ratio was adjusted. In each case the model was run until NO, $NO_2$ and $O_3$ reached PSS and the difference in the final $NO_2/NO_x$ ratio between the baseline run and all other runs was plotted against the change in initial $NO_x$ (see Figure 2.6d – blue line). It is observed that as the $NO_x$ abundance grows (positive x axis values), the PSS-chemistry-derived changes in the $NO_2/NO_x$ ratio (blue line) deviate from the observed ambient behaviour (black points). Further model runs demonstrated that if the PSS model was initiated with a higher $NO_2$ fraction of 0.45 (i.e. similar to the mean $NO_2/NO_x$ ratio observed in 2013 from Figure 2.6a) then the difference between PSS-only predicted and ambient observed $NO_2/NO_x$ differences becomes even larger. Additional model PSS simulations for different initial ozone values e.g. $O_3$ = 100 ppb (extreme case) also showed deviation from observations. Therefore, the results of the model runs suggest that the response of the PSS-chemistry to changes in overall $NO_x$ emissions cannot, in isolation, explain the variation in the $NO_2/NO_x$ ratio observed between 2009 and 2016.

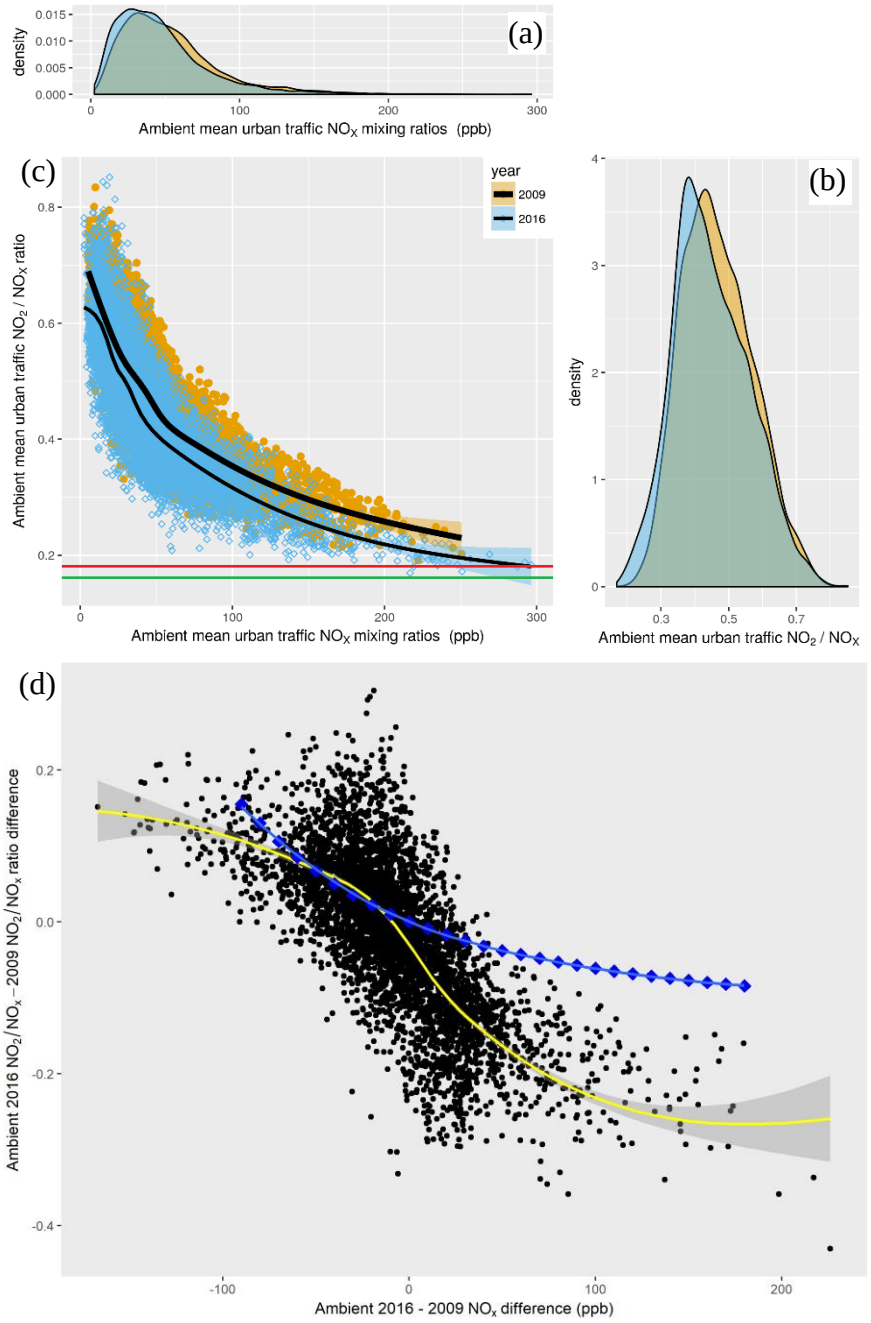


Figure 2.6: Daytime hourly mean ambient (a) $NO_x$ and (b) $NO_2/NO_x$ distributions for 2009 (orange) and 2016 (light blue) from all urban traffic monitoring sites in the UK. (c) $NO_2/NO_x$ ratio vs $NO_x$: the green (2016) and red (2009) lines indicate the baselines of the distributions and can be used to estimate the primary $NO_2$ (see text). (d) ambient $NO_2/NO_x$ ratio as a function of the difference in $NO_x$ mixing ratio for each location, between 2009 and 2016. The yellow line indicates the locally fitted regression (LOESS) line with associated 95% confidence interval, while the blue line indicates the variation in $NO_2/NO_x$ expected, for a change in overall $NO_x$ abundance, on the basis of the $NO_x$-$O_3$ PSS chemistry alone (see text in 2.3.1 for details).

The observed changes in $NO_2/NO_x$ therefore are likely to be influenced primarily by changes in vehicle emissions, which might have resulted from the combined changes in: (1) policy, where new Euro limits came into force for new car passenger models (Euro 5 in 2009 and Euro 6 in 2014), and for London (4 stations included here), a low emission zone came into effect, and daily charges for the London congestion zone increased. (2) Diesel cars, where in 2009, 90% of diesel cars in the UK were Euro 3 and Euro 4, while in 2016, 69% of UK diesel cars were Euro 5 and Euro 6, according to the DfT/National Atmospheric Emissions Inventory NAEI, 2016). (3) After-treatment technologies, where new technologies such as LNT and SCR have been introduced (see chapter 1) and factors such as 'catalyst thrifting', where catalyst developers and manufacturers reduce the amount of platinum group metal (which will potentially affect the amount of $NO_2$ formed), or catalyst deactivation over time (where aged DOC catalyst technologies may have reduced oxidative capacity through thermal deactivation or poisoning and therefore less efficient conversion of NO to $NO_2$, Carslaw et al., 2016b). These results are in accordance with other monitoring observations which show trends from eight long-running urban traffic stations (1995 - 2015), and highlight that six out of eight stations show a downward trend in the ambient $NO_2$ concentrations (DEFRA, 2017). In a recent study across Europe, Grange et al. (2017), conclude that the ambient $NO_2$ levels measured at roadside monitoring sites are dropping, and that the primary $NO_2/NO_x$ emission ratio is lower than assumed by some key emission inventories. This result is also in agreement with the findings of Font and Fuller (2016), who analysed trends from ambient measurements in London and found that $NO_2$ and PM show a declining trend from 2010 to 2015, attributed to a

variety of factors, including a reduction of the primary $NO_2/NO_x$ emission ratio due to the absolute and relative reduction in numbers of older diesel passenger cars in the overall fleet. These studies represent a growing body of evidence that there has been a recent reduction in the ambient and primary emitted $NO_2/NO_x$ ratio in UK urban environments.

### 2.3.2 Trends in inferred primary $NO_2/NO_x$ ratio

The trend in inferred primary $NO_2/NO_x$ ratio is presented in Figure 2.7 (monthly daytime values from all urban traffic sites, calculated using the methodology of Palmgren et al., (1996)/Carslaw and Beevers, (2005), after removing the observed seasonality (see section 2.2.2; Carslaw, 2016a)). Despite some individual monthly increases (mainly in 2011), the inferred primary $NO_2/NO_x$ ratio, shows a clear downward trend, with a change (median value) of -0.32%/year with 95% confidence interval from -0.45% to -0.2% per year, significant to the 0.001 level ($p < 0.001$).

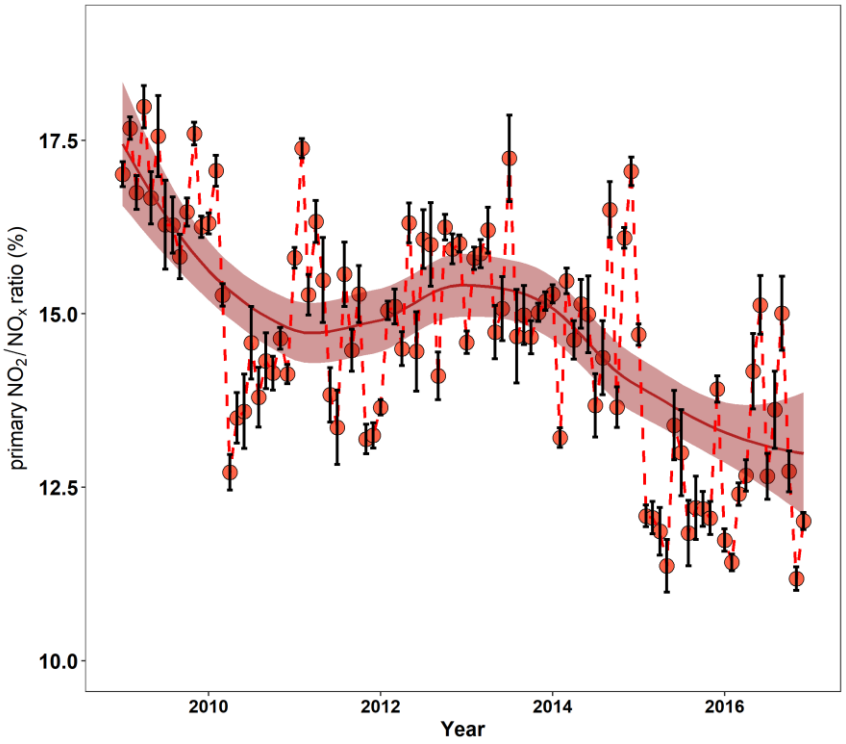


Figure 2.7: Mean overall trend of the inferred primary $NO_2/NO_x$ ratio averaged over all UK urban traffic monitoring sites. The error bars indicate the standard error of the slope estimates. The local regression fitted line (red solid line) is weighted by taking into account the standard errors of the individual slopes. The shaded area indicates the 95% confidence intervals.

Figure 2.7 shows an overall reduction in the inferred primary $NO_2/NO_x$ ratio from 17.5% to 12.5% between 2009 and 2016. Despite the increases reported in the urban traffic monitoring sites in the UK, before 2009 (AQEG, 2004; 2007), the inferred primary emitted $NO_2/NO_x$ experiences an overall reduction of 5 percentage points over the 2009 – 2016 period. In detail, from 2009 until 2011, a small reduction in the emissions is evident (from 17.5% to 15%). From 2011 until mid-2013 no significant changes are observed and the mean inferred primary $NO_2/NO_x$ ratio is steady. At that period the Euro 5a and Euro 5b limits for passenger and light duty vehicles, as well as

the Euro IV standards for heavy duty vehicles came into force for sales of new vehicles in September 2011 and January 2013 for light and heavy-duty vehicles respectively. Standards, which set a prerequisite for diesel vehicles to have a DPF after-treatment system (Euro 5 diesel cars constituted 20% of the diesel fleet in 2011 and they reached 52% by 2014 according to NAEI, (2016)). This technology, as discussed in Chapter 1, uses $NO_2$ in order to burn the collected soot/PM in the filters, thus can also impact $NO_2$ emissions in the exhaust. In September 2014, the most recent and stricter limits of Euro 6 came into force. The introduction of new Euro-limit-driven emissions control technologies and their penetration through the fleet (Euro 5 and Euro 6 passenger cars) may therefore have contributed to this decrease of 2.5 percentage points in the mean primary $NO_2/NO_x$ ratio from early 2014, and the overall decrease of 5 percentage points that is apparent from early 2009. This 29% relative decrease in inferred primary $NO_2/NO_x$ ratio in the last period has to be taken into account in the emission inventories for future modelling estimates of exposure and policy making which currently they estimate an increase until 2015 for UK (NAEI, 2016) and Europe (Kiesewetter et al., 2014; Grange et al., 2017). This decrease for the most polluted $NO_2$ sites, such as those in London, means that these cities are going to meet the EU annual targeted value of 40 $\mu g/m^3$ (for $NO_2$) sooner than initially predicted.

The change in inferred primary $NO_2/NO_x$ ratio between 2009 and 2016 shows some variability with geographic region across the UK (Figure 2.8). With few exceptions, the primary $NO_2/NO_x$ ratio has fallen in the majority of the regions, by a range from 0.5 to 10% (Table 2.2). The observed increases in the ratio in some regions (e.g. York, Swansea) are difficult to explain individually as they may be associated with

other local factors such as changing road layouts and urban infrastructure. A decline in the median inferred primary $NO_2/NO_x$ emission for London of 5% is apparent, in agreement with Carslaw et al., (2016b), who found a decrease of about 7% in the primary $NO_2/NO_x$ ratio for inner London from 2009/10 to 2014/15. However, these variations were not always consistent with the monthly primary $NO_2/NO_x$ trend (calculated for the whole data series) (Table 2.2), indicating that the trends are not significant in every area and more data (i.e. a longer time series) are needed in order for a clear conclusion to be drawn. This potentially reflects that the oxidant analysis assumptions (essentially, that the $NO_x$ - $O_3$ PSS represents a fully closed system) may be less valid for some locations and highlights the complexity and the heterogeneity in the implementation and outcome of policy interventions to control air pollution.

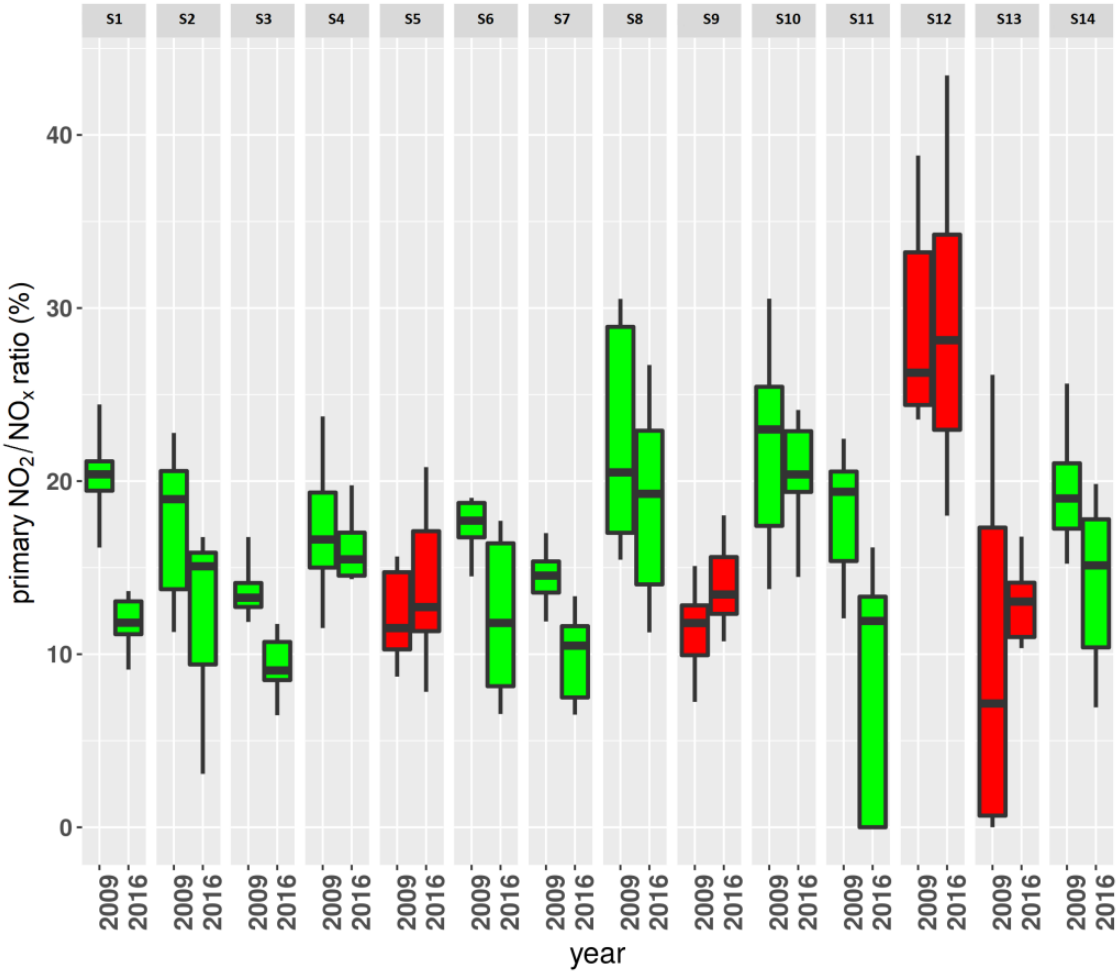


Figure 2.8: Box-whisker plots for the inferred primary $NO_2/NO_x$ ratio for the individual urban traffic monitoring sites considered in this study, during 2009 and 2016. Green indicates a reduction in the median value between the two dates for each location, red an increase, between 2009 and 2016. S1: Aberdeen, S2: Birmingham, S3: Cambridge, S4: Carlisle, S5: Chepstow, S6: Exeter, S7: Leeds, S8: Liverpool, S9: Newcastle, S10: Sandy, S11: Stanford le Hope, S12: Swansea, S13: York, S14: London.

Table 2.2: Median primary $NO_2/NO_x$ difference and monthly trend (percentage points/year) for individual urban traffic monitoring sites in the UK from 2009 to 2016. Symbols (***, **, *, +) indicate the level of significance p (0.001, 0.01, 0.05, 0.1). Note that the median primary $NO_2/NO_x$ values were acquired with a localised fitted regression model, while the monthly trend was calculated with a fitted linear regression model.

| Region | Median 2009 primary $NO_2/NO_x$ (%) | Median 2016 primary $NO_2/NO_x$ (%) | Difference primary $NO_2/NO_x$ (%) | Monthly trend with 95% confidence limits (%/year) |
|---|---|---|---|---|
| Aberdeen | 19 | 10 | -9 | -1.33 (-1.52, -1.1) *** |
| Birmingham | 20 | 10 | -10 | 0.24 (-0.29, 0.78) |
| Cambridge | 12 | 8 | -4 | -0.83 (-1.04, -0.6) *** |
| Carlisle | 21.5 | 17 | -4.5 | -0.16 (-0.51, 0.18) |
| Chepstow | 14 | 16 | 2 | 0.06 (-0.28, 0.34) |
| Exeter | 18 | 15 | -3 | -0.45 (-0.75, -0.13) ** |
| Leeds | 16 | 13 | -3 | -0.17 (-0.5, 0.2) |
| Liverpool | 21 | 19 | -2 | 0.42 (-0.13, 1.01) |
| London | 15 | 10 | -5 | -0.78 (-1.08, -0.38) ** |
| Newcastle | 11 | 10 | -1 | -0.5 (-1.26, 0.37) |
| Sandy | 10 | 15 | 5 | 0.68 (0.39, 0.96) *** |
| Stanford le hope | 20 | 17.5 | -2.5 | -1.79 (-2.45, -1.13) *** |
| Swansea | 27 | 26.5 | -0.5 | 0.16 (-0.12, 0.43) |
| York | 8 | 15 | 7 | -0.8 (-1.61, -0.06) * |

### 2.3.3 Low temperature primary $NO_2$ emissions – evidence for "cold start" effects

The inferred $NO_2/NO_x$ emission ratios for cold ($T \leq 5\ ^oC$) and non-cold/normal ($T > 5\ ^oC$) conditions during winter (November, December, January, February) morning and evening rush hours are depicted in Figure 2.9. The change in gradient between cold (Figure 2.9b, 2.9d) and non-cold/normal (Figure 2.9a, 2.9c) conditions is clearly apparent, with the $O_x$ - $NO_x$ analysis indicating an increase of 64.5% (mornings) and 75% (evenings) in the inferred primary $NO_2/NO_x$ ratio for the former compared with

the latter. The increase in overall $NO_x$ abundance (greater x-axis range, most likely arising primarily from lower and more stable atmospheric boundary layer/mixing heights under cold conditions, alongside reduced winter month $NO_2$ photolysis) is also apparent. The 64.5% increase in inferred primary $NO_2/NO_x$ ratio is statistically significant ($p < 0.001$), changing by over 4 percentage points from 6.2(±0.4)%, for normal winter mornings to 10.2(±0.1)%, for cold winter mornings. Similar behaviour is observed for evenings (75% increase from normal to cold conditions), where the difference is slightly higher at 4.2 percentage points, from 5.6(±0.4) to 9.8(±0.1)% (values in the parenthesis indicate the standard error). For individual locations, the difference between cold and normal conditions varies over a factor of 1.6 to 3.8 fold (Table 2.3).

Table 2.3: Primary $NO_2/NO_x$ ratio during cold weather rush hours (representing cold start emissions) and normal weather rush hours (representing normal emissions) and the corresponding increment for individual areas across the UK. Symbols (***, **, *, +) indicate the level of significance of the slope p (0.001, 0.01, 0.05, 0.1).

| Region | Cold start primary $NO_2$ emissions (%) | | Primary $NO_2$ emissions (%) | | Relative increment (%) | |
|---|---|---|---|---|---|---|
| | Morning | Evening | Morning | Evening | Morning | Evening |
| Aberdeen | 12.3± 0.17*** | 13.1 ± 0.18*** | 12.0±0.3 | 13.0±0.3 | 2.5 | 0.1 |
| Birmingham | 10±0.14*** | 10.4±0.23*** | 7.2±0.4 | 8.2±0.3 | 38.8 | 26.8 |
| Cambridge | 8.5±0.36*** | 7.2±0.36*** | 3.6±0.7 | 4.7±0.5 | 136.1 | 53.2 |
| Carlisle | 12.6±0.43*** | 13.2±0.47*** | 10.1±0.8 | 7.0±0.5 | 24.8 | 88.5 |
| Chepstow | 9.7±0.62*** | 11.9±0.1*** | 9.9±0.9 | 12.0±0.8 | - | 0.1 |
| Exeter | 12.1±0.19*** | 11.7±0.33*** | 6.5±0.3 | 6.8±0.4 | 86.2 | 72.1 |
| Leeds | 8.5±0.2*** | 8.0±0.3*** | 4.6±0.4 | 3.2±0.3 | 84.8 | 150 |
| Liverpool | 9.4±0.3*** | 11.3±0.48*** | 7.8±0.7 | 11.2±0.6 | 20.5 | 0.1 |
| London Camden | 15±0.2*** | 14.2±0.4*** | 12.2±0.3 | 11.1±0.3 | 22.9 | 27.9 |
| London Haringey | 6.8±0.2*** | 6.9±0.04*** | 1.4±0.5 | 3.3±0.3 | 385.7 | 109.1 |
| London Marylebone | 12.3±0.1*** | 13.7±0.2*** | 12±0.2 | 13.7±0.2 | 2.5 | - |
| London tower hamlet | 13.5±0.3*** | 13.8±0.7*** | 12.6±0.6 | 13.8±0.5 | 7.1 | - |
| Newcastle | 10.7±0.1*** | 11.4±0.2*** | 7.9±0.4 | 8.3±.0.3 | 35.4 | 25.3 |
| Sandy | 16.3±0.3*** | 15.1±0.3*** | 15±0.7 | 13.2±0.6 | 8.7 | 14.3 |
| Stanford le hope | 7.0±0.3*** | 8.2±0.4*** | 4.8±0.9 | 7.8±0.6 | 45.8 | 12.8 |
| Swansea | 24.4±0.3*** | 23.4±0.4*** | 15±0.4 | 13.2±0.4 | 62.7 | 77.2 |
| York | 13.8±0.3*** | 13.5±0.4*** | 5.7±0.7 | 5.3±0.4 | 142.1 | 158.4 |

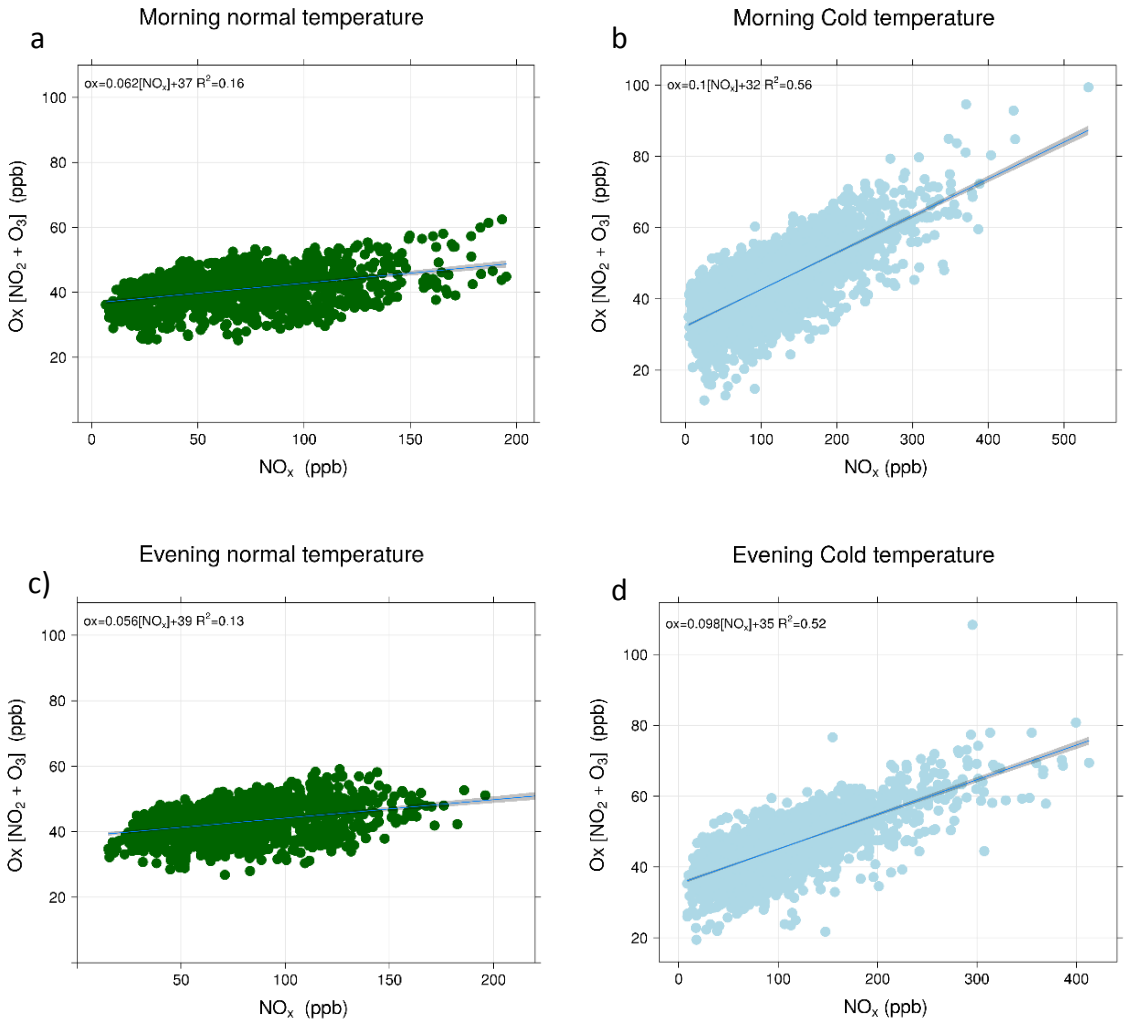


Figure 2.9: $O_x$ - $NO_x$ mean UK plots during normal winter morning and evening rush hours (green) and during cold ($T \leq 5$ $^{o}C$) morning and evening rush hours (blue), representing normal and cold start emissions. The shaded areas indicate the 95% confidence intervals of the linear regression fit.

The morning and evening ambient $NO_2/NO_x$ ratios can be affected by atmospheric chemistry (i.e. reactions involving $HNO_3$, $NO_3$, $N_2O_5$ and HONO) especially during the pre-sunrise and post-sunset rush hours in winter. To examine in detail the impact of the temperature dependence of photochemical processes (alone) upon the

ambient $NO_2/NO_x$ ratio, a simple chemical box-model including a full inorganic chemical mechanism was applied. The model was built using AtChem2, an open source atmospheric chemistry model designed to be used with the Master Chemical Mechanism (MCM). The chemical mechanism used in this study was taken from the MCM version 3.3.1 and included 48 inorganic gas-phase reactions. For the detailed chemical mechanism see appendix A. The photolysis rates were calculated using the MCM parametrization (Saunders et al., 2003) using the latitude and longitude of London (51.51 $^{o}$N, 0.13 $^{o}$W) for the date of 15$^{th}$ of December 2012. The initial concentrations for $O_3$, NO and $NO_2$ were the mean December values from the Marylebone Road (London) roadside monitoring site. The initial concentrations were taken from Dunlea et al., (2007) for $HNO_3$ and from Harrison et al., (2012) for $NO_3$ and $N_2O_5$ (maximum measured hourly values observed in London) and from Kurtenbach et al., (2001) for HONO (from measurements in a traffic tunnel). The model was run for a period of 24 hours starting at midnight of 15$^{th}$ of December 2012 (the first output being 15 minutes after the start time): the concentrations of all species in the model were calculated from the initial values. The model was run 9 times, each with a different temperature in the range from -10 $^{o}$C to +30 $^{o}$C. During each model run, temperature was kept constant. The $NO_2/NO_x$ ratios calculated at each temperature are shown in Figure 2.10.

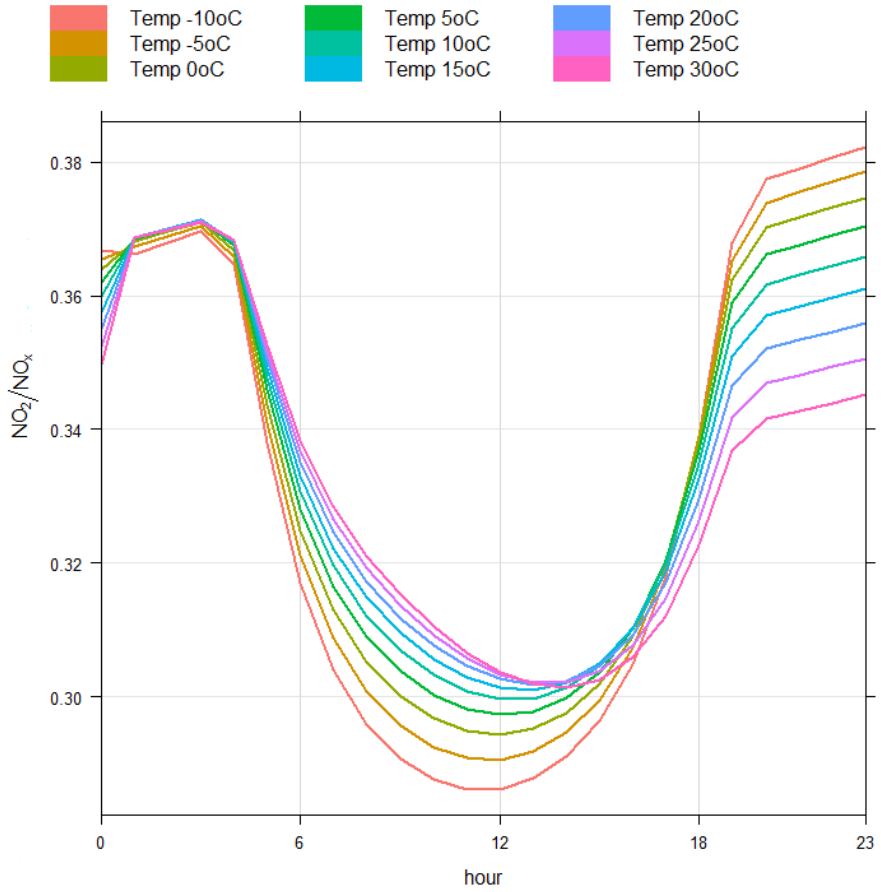


Figure 2.10: Diurnal $NO_2/NO_x$ ratio calculated using a box-model at different temperatures. Note the y-axis ($NO_2/NO_x$) values are highly compressed.

The results showed that the daytime and night time average primary $NO_2/NO_x$ ratios during the rush hour period (i.e., the period examined here for the cold starts) varied by between 0.5% and 8.4%, with a mean relative change of 2.4%, due to the effect of temperature on the chemical reaction kinetics (Figure 2.11). The model results indicate that the observed increments in the inferred primary $NO_2/NO_x$ ratio with low temperatures, of 64.5% and 75%, are much larger than can be accounted for by the temperature-dependence of the atmospheric photochemistry alone. Therefore

it can be suggested that altered vehicle emissions with operating temperature are contributing towards this observation.

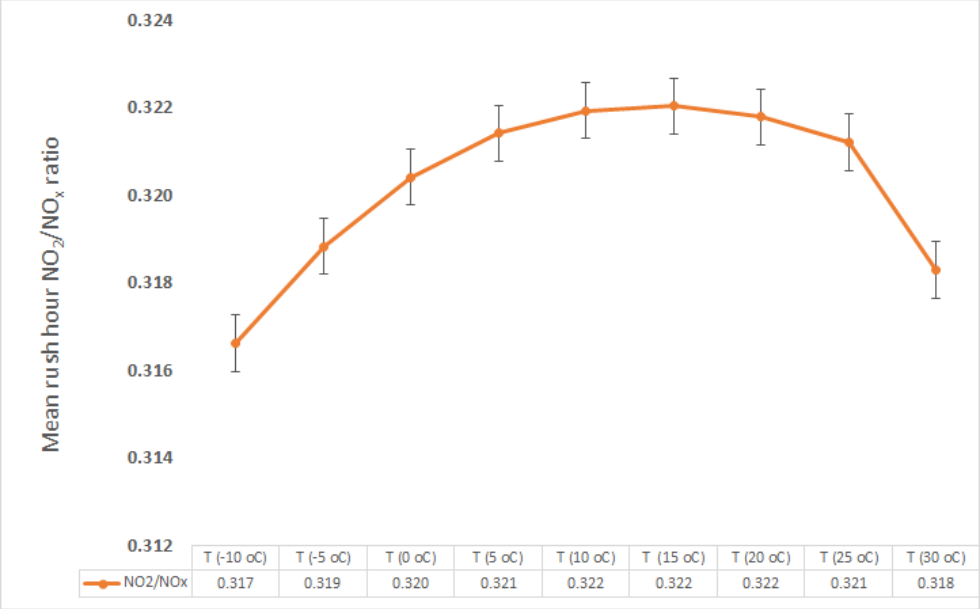


Figure 2.11: Mean rush hour (06:00-10:00 & 16:00-19:00) $NO_2/NO_x$ ratio for different temperatures during winter period, calculated using hourly values from the box-model runs shown in Figure 2.10. The bars indicate the standard error of the mean rush hour ratio.

While the ambient data will contain contributions from vehicles which have been operating for some time and hence are not under "cold-start" conditions, statistics on mode of transport from the DfT National Travel Survey in 2016 indicate that 20% of all trips under 1 mile (1.6 km), were by car (either as driver or passenger), this increased to 77% for trips between 1 and 5 miles (1.6 – 8 km) (DfT, 2017). For urban journeys, distances tend to be shorter than these UK mean values suggest. Short urban trip duration alongside the reduced efficiency or designed deactivation of

emission control systems at temperatures below 250 $^{o}$C, may contribute to the substantial increase in the inferred primary $NO_2/NO_x$ ratio, and hence reduced attainment of $NO_2$ air quality standards, under cold conditions.

Recent testing of vehicles in Germany conducted in 2016 found that over half of ca. 50 vehicles tested had their EGR system inoperative under low ambient temperatures, for engine protection purposes (BMVI, 2016). Such differences in the vehicle $NO_x$ emissions under low temperatures are observed in Euro 6 passenger cars (Suarez-Bertoa and Astorga, 2018). During regulated laboratory tests Suarez-Bertoa and Astorga (2018) observed that Euro 6 gasoline and diesel vehicles emitted two to more than three times more $NO_x$ at pre-conditioned initial engine temperatures of -7 $^{o}$C, compared to emissions at 23 $^{o}$C. These results underline the lower effectiveness in the performance of the after-treatment systems under low initial operating temperatures found in real driving conditions. However, the relative contribution of gasoline and diesel vehicles, or passenger cars vs light- and heavy-goods vehicles, to the change in inferred primary $NO_2/NO_x$ rate cannot be readily determined from these data. At intermediate temperatures (5 – 15 $^{o}$C) reduced changes in the inferred primary $NO_2/NO_x$ ratio were found (see Figure 2.12).

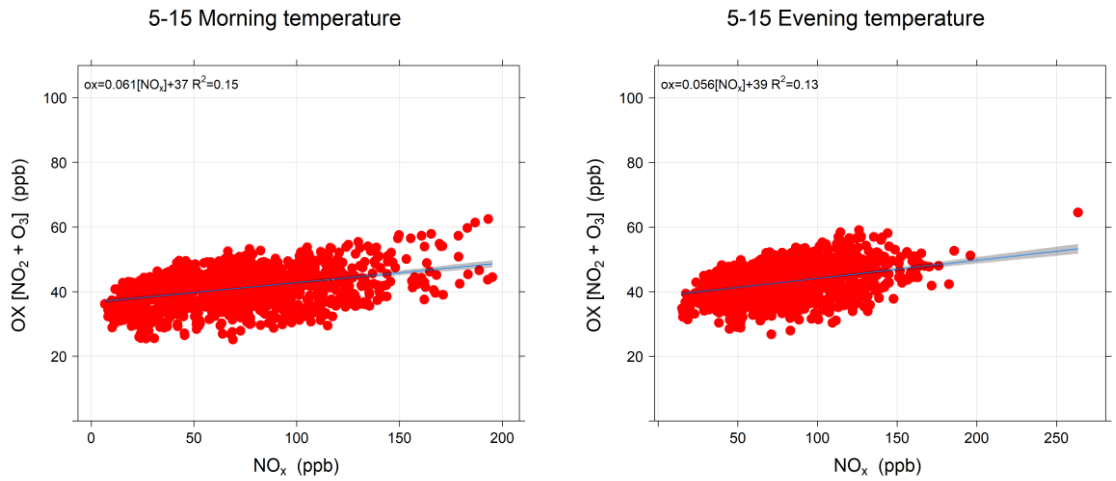


Figure 2.12: Winter period (Nov, Dec, Jan, Feb) Mean UK $O_x$ - $NO_X$ plots for the temperature range of 5-15 $^{o}$C during morning (left) and evening (right) rush hours. The gradient uncertainty is ± 0.004 and ± 0.005 for morning and evening respectively.

Figure 2.13 shows the relationship between inferred mean primary $NO_2/NO_x$ ratio and mean ambient temperature, for the cold months (November, December, January and February). The primary $NO_2/NO_x$ ratio is significantly negatively correlated with temperature ($R^2$ = 0.54), according to the inverse relationship $fNO_2$ = 15% – [0.77 ± 0.15] x (T / $^{o}$C). Similar results to those presented here were reported by Degraeuwe and Weiss (2017), who found that for on-road tests, Euro 5 and Euro 6 cars emit four and three times higher $NO_x$ at low ambient temperatures than the legislative limits, respectively. For Euro 6 cars, similar results were reported by Kwon et al. (2017), who compared $NO_x$ emissions at lower ambient temperatures (0 - 5 $^{o}$C) with higher ambient temperatures (15 - 20 $^{o}$C) and found a difference of 82–192%.

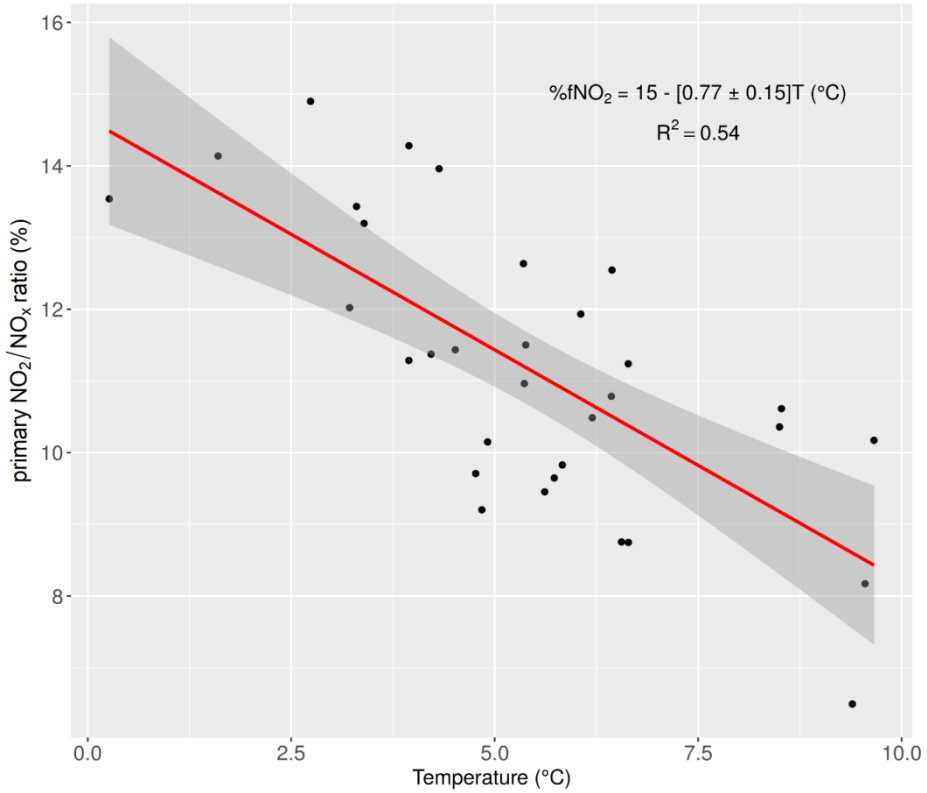


Figure 2.13: Inferred mean monthly primary $NO_2/NO_x$ ratio ($\%fNO_2$) and its dependence on mean ambient temperature in the UK. The grey shaded areas indicate the 95% confidence intervals of the regression relationship.

These literature results, along with the analysis presented here, support the finding that higher vehicle emissions at lower ambient temperatures may have a measurable impact upon ambient air quality. Vehicle emissions effects are likely exacerbated by meteorology during wintertime (lower boundary layer height, and increasing tendency to stable conditions (temperature inversions) during the worst pollution episodes and coldest weather); reduced photolysis frequencies (shifting the $NO_x$ PSS towards $NO_2$), and potentially greater vehicle use during low temperature conditions in the UK, relative to other travel options.

In the analysis the investigation of $NO_2/NO_x$ ratio under warmer weather was attempted. Specifically the primary $NO_2/NO_x$ ratio was calculated for temperatures > 23 $^oC$ in order to investigate the vehicle emissions under high temperatures. 23 $^oC$ was selected as a threshold since this is the regulated temperature of the vehicle laboratory tests. Figure 2.14 shows the inferred mean monthly primary $NO_2/NO_x$ ratio in UK as a function of temperature. As the Figure 2.14 shows, no clear relationship can be discerned between primary $NO_2/NO_x$ ratio and temperature in this range, and the uncertainty, given by the 95% confidence intervals of the linear model, is very big. It should be noted that only ten places in the UK had temperatures higher than 23 $^oC$ and roadside air quality measurements that met the criteria of NO, $NO_2$ and $O_3$ namely, Greater London (5 sites), Birmingham and Cambridge (2 sites) and Exeter, while out of the initial 3,155,000 hours of NO, $NO_2$ and $O_3$ that were included in the analysis only 30,190 hours satisfied the criterion (T > 23 $^oC$) and could be used to investigate the high temperature emissions.

Despite not being able to draw a conclusion of high temperature vehicle primary $NO_2$ emissions in the UK, it would be interesting to apply the same approach in southern European countries such as Spain, Italy and Greece, where temperatures reach 35 $^oC$ in the summer months. A study in Paris which analysed vehicle emissions with remote sensing techniques in 2019 found an increase of 25 - 30% in $NO_x$ for temperatures over 28 $^oC$ (Dallman et al., 2019). A potential increase in $NO_x$ emissions in the roadside atmosphere during summer months or heatwaves would be of particular importance to human health, especially under the current highly abnormal climate. An additional $NO_x$ loading during hot weather might result in poor air quality

periods which in conjunction with the elevated ambient temperature might in turn have a significant consequence to the health condition of people with asthma or elderly people.

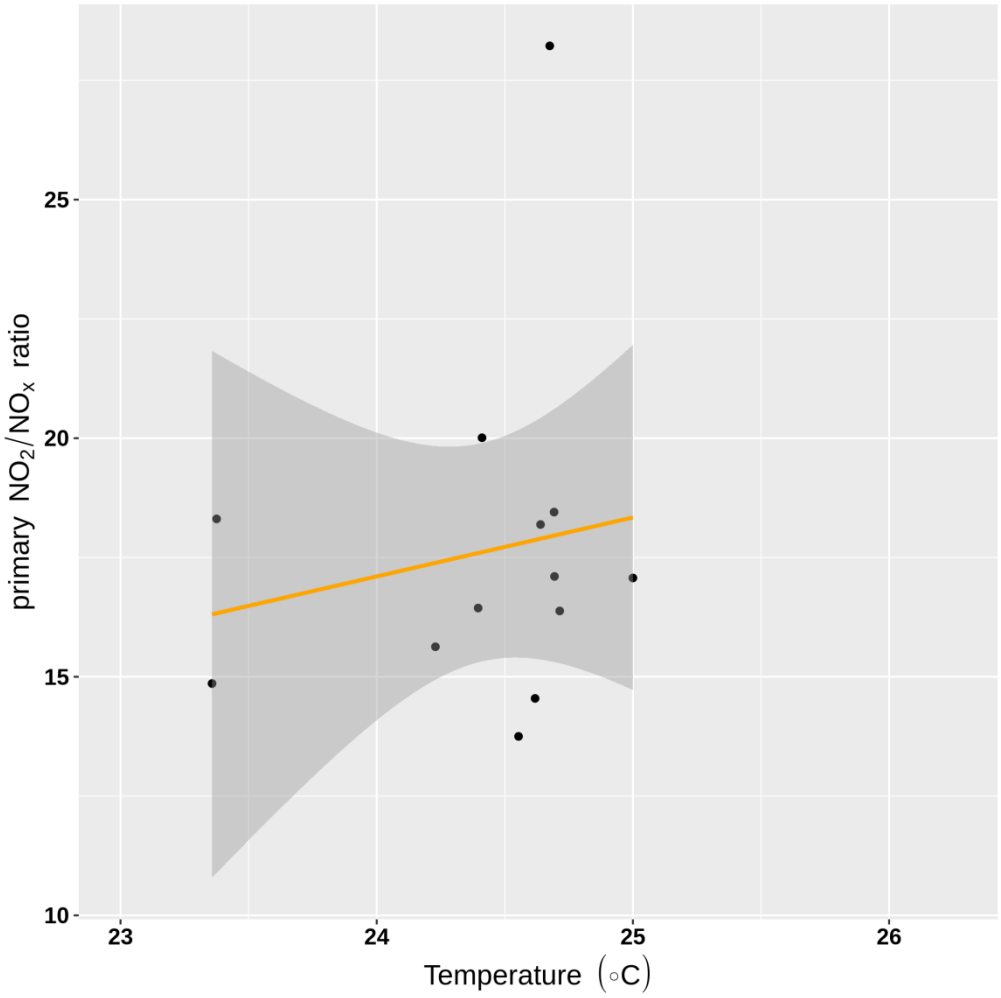


Figure 2.14: Inferred mean monthly primary $NO_2/NO_x$ ratio vs ambient temperature > 23 $^{o}$C in the UK. The grey shaded areas indicate the 95% confidence intervals of the regression relationship.

## 2.4 Summary and concluding remarks

This chapter presents an analysis of ambient $NO_x$ and $NO_2$ mixing ratios, to derive inferred $NO_2/NO_x$ emission ratios from urban traffic monitoring stations in the UK, for the period from 2009 until 2016. The analysis showed:

In keeping with other recent results, a decrease in the mean ambient $NO_2$ mixing ratio at selected urban roadside measurement sites between 2009 and 2016, alongside a smaller reduction in $NO_x$ mixing ratios. Direct emissions were not measured in this work, and a number of assumptions were made in deducing emitted $NO_x$ ratios from ambient data for a number of measurement stations. The mean inferred primary $NO_2/NO_x$ ratio shows an overall reduction of 3 percentage points from 17% to 14%, with a calculated reduction of -0.32 percentage points/year (95% confidence interval of -0.2 to -0.45 percentage points/year), over this time period. The period of this reduction corresponds to the combined application of policies (new Euro limits), changes in fleet composition and, to some extent, to the initial penetration of new after-treatment technologies introduced in the last eight years. However, this reduction is not evident in every location, underling the complexity of the problem and implying that more stringent measures may be needed to further reduce ambient $NO_2$ in urban environments, a challenge that will be heightened by increasing vehicle numbers.

Potential “cold-start” emissions, inferred from ambient monitoring data under low temperature conditions. The results imply that the overall vehicle primary $NO_2/NO_x$ ratios increase on average by 64.5% and 75% for morning and evening rush hours under cold (≤ 5 $^oC$) conditions, compared with (for the UK) normal conditions (> 5 $^oC$), while this difference can be 1.6 - 3.8 times greater when examining individual urban traffic monitoring stations. An inverse relationship was found between ambient temperature and primary $NO_2/NO_x$ ratio.

These results suggest that the combination of typical driving patterns and the temperature dependence of the current after-treatment systems under low ambient temperatures lead to measurable impacts upon ambient air quality. They also highlight the importance of test cycles which consider cold-start emissions, as these may cause a measurable deterioration in air quality in urban areas in the UK. Assessment of the related health burden, which must integrate personal exposure considerations, should combine the impact of meteorological factors on both vehicle performance and public behaviour versus transport choices.

Chapter 2 addresses some key research questions regarding the impact of vehicle emissions on urban air quality in the UK. However, there are still uncertainties that need to be investigated; especially around the within-vehicle and on-road air pollution exposure of individuals and their air pollution inhaled doses under different urban activities such as driving, walking and cycling. These areas are investigated further in the following chapter (3) of the thesis.

# Chapter 3. Within-vehicle air pollution exposure: variation with outside air quality, route choice and ventilation options

This chapter reports simultaneous within-vehicle and directly outside vehicle measurements of various air pollutants, to determine the ratios of inside to outside ($I/O_{VEH}$) levels of particulate matter ($PM_{10}$, $PM_{2.5}$, $PM_1$), ultrafine particle number (UFP), lung surface deposited area (LSDA), NO and $NO_2$ for different vehicles and roads, under different ventilation settings. It further provides a spatial analysis of within-vehicle measurements and $I/O_{VEH}$ ratios to identify potential hotspots by route category/road type. Finally, the chapter includes an analysis of air pollution exposure by activity, by calculating the air pollution inhalation dose of the aforementioned pollutants for male, female and child vehicle occupants following similar routes, and comparing these to other activities such as cycling and walking in a typical urban environment. The material presented in this chapter has been published as:

*Matthaios N. V., Kramer J. L., Crilley R. L., Sommariva R., Pope D. F., Bloss J. W., 2020. Quantification of within-vehicle exposure to NOx and particles: variation with outside air quality, route choice and ventilation options. Atmospheric Environment, 117810, 10.1016/j.atmosenv.2020.117810.*

## Graphical abstract

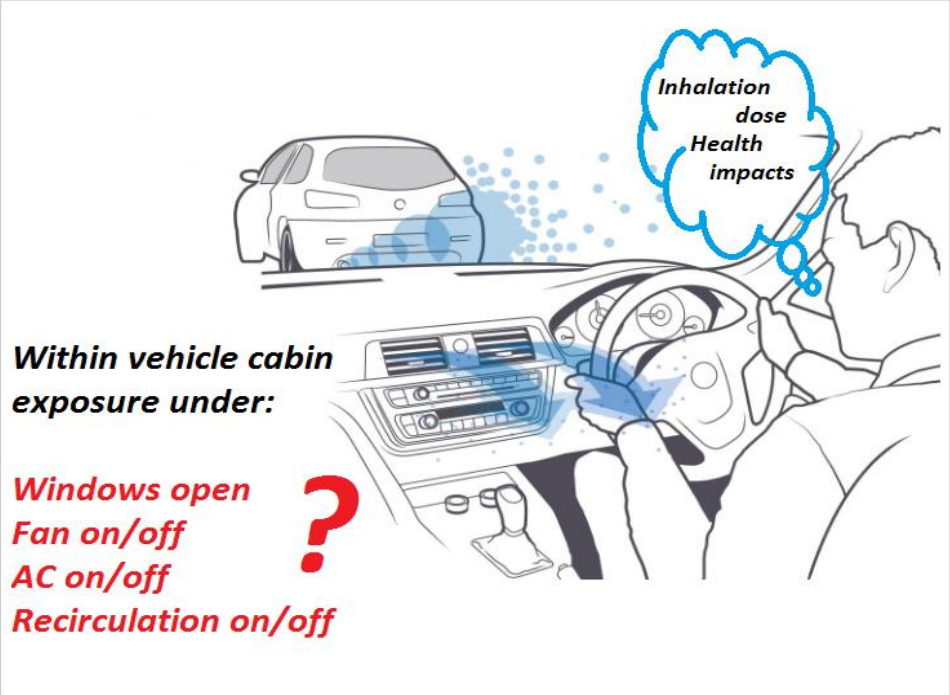


# 3.1 Introduction

Emissions from road transport are an important and often dominant source of ambient air pollution in urban areas, with direct and indirect detrimental impacts on human and environmental health. Increasing urbanisation, and (in many societies)

growth in vehicle ownership and passenger-journeys, contribute to growth in traffic-related ambient air pollution abundance, counteracting in some cases improvements in emissions abatement technologies. The predominant primary air pollutant emissions from vehicles include nitrogen oxides ($NO_x$), particulate matter (PM) including ultrafine particles (UFP), volatile organic compounds (VOCs) and carbon monoxide (CO), derived primarily from exhaust (tailpipe) sources, alongside mechanical (brake, tyre) inputs in the case of PM. A number of studies have demonstrated an association between traffic-related air pollutants and detrimental health outcomes such as asthma, exacerbation of adverse respiratory symptoms (e.g. McConnell et al., 2006; Gan et al., 2011), cardiovascular diseases (Delfino et al., 2005), coronary artery atherosclerosis (e.g. Künzli et al., 2011), and an increase in mortality (e.g. Stölzel et al., 2007; RCP, 2016). Adverse health effects due to elevated exposure to PM or UFP have been associated with cardiovascular problems (e.g. Delfino et al., 2005), while exposure to $NO_2$ is known to lead to reduced lung function and increased risk of cancer (Adam et al., 2015; Hamra et al., 2015; WHO, 2013).

Air pollution health impacts are mediated by personal exposure of the individual in question and vulnerability of that individual to a given dose, which in turn is a function of behaviour in a commuting context of journey, route selection, time of day, transport type, respiration rate and (in the case of vehicles) ventilation options. A significant proportion of the population commute to and from their working environment by car, and, as the outside air undergoes exchange with the air inside vehicle cabins, vehicle occupants may suffer elevated exposure to ambient air pollutants of varying extents during this time. In most cases, the dominant contributor

to within-vehicle exposure originates from the intake of outside, ambient air pollution. Most exposure studies within vehicles reported so far have focussed primarily on particulate pollution (Boogaard et al., 2009; Int Panis et al., 2010; Zuurbier et al., 2010; De Nazelle et al., 2012), typically performing within-vehicle measurements using personal exposure instruments without coupling them with simultaneous on-road (ambient) levels or taking into account the air exchange that occurs between the cabin and the ambient air. Personal exposure instruments often have high measurement uncertainties, while the air exchange defines the amount of pollution that enters the vehicle from outside. Both are critical components to accurately estimate and develop predictive capability for the air pollution exposure of the vehicle occupants.

Air exchange is a key aspect of within-vehicle chemical processes (Weschler and Shields, 2000), in particular $NO_x$ and $O_3$ abundance, alongside the photo-stationary steady state reactions (Weschler et al., 1994). In cases where air exchange has been taken into consideration (regarding the vehicle cabins), species have been treated separately by measuring inside to outside ($I/O_{VEH}$) levels only for UFP (Knibbs et al., 2010; Hudda et al., 2011) or $NO_2$ (Chan and Chung 2003; Martin et al., 2016; Yamada et al., 2016). However, vehicle exhaust emits both particles and nitrogen oxides, therefore, vehicle occupants are exposed to both exhaust particles and gases such as $NO_2$. Consequently, it is essential to know the exposure levels of multiple pollutants simultaneously in order to implement accurate exposure estimates and risk assessment calculations, as the concurrent impact of multiple species upon human health is known to be of great importance (e.g. COMEAP, 2018).

## 3.2 Methods

Measurements of $NO_x$, PM, UFP and LSDA were performed simultaneously inside and directly outside of the studied vehicles in order to determine the absolute ratio of inside/outside air pollution abundance ($I/O_{VEH}$). More specifically, measurements of NO, $NO_2$, $PM_{10}$, $PM_{2.5}$, $PM_1$, UFP and LSDA were performed using four different vehicles, during various daytime driving hours in the city of Birmingham, U.K. The measurements were accompanied by GPS-derived position (latitude, longitude) and vehicle speed and within-vehicle temperature (T) and relative humidity (RH). Figure 3.1 shows a schematic example of the experimental set up, while Figure 3.2 shows a tested vehicle used for the experiments. Two measurement campaigns were performed, from 7$^{th}$ to 16$^{th}$ of February 2017 (with one vehicle only, 2-seater Light duty vehicle) and 26$^{th}$ of October until 9$^{th}$ of November 2017. The vehicles that were included in the two campaigns and their details are shown in Table 3.1. A total of eighty three hours of data collection are used for this analysis.

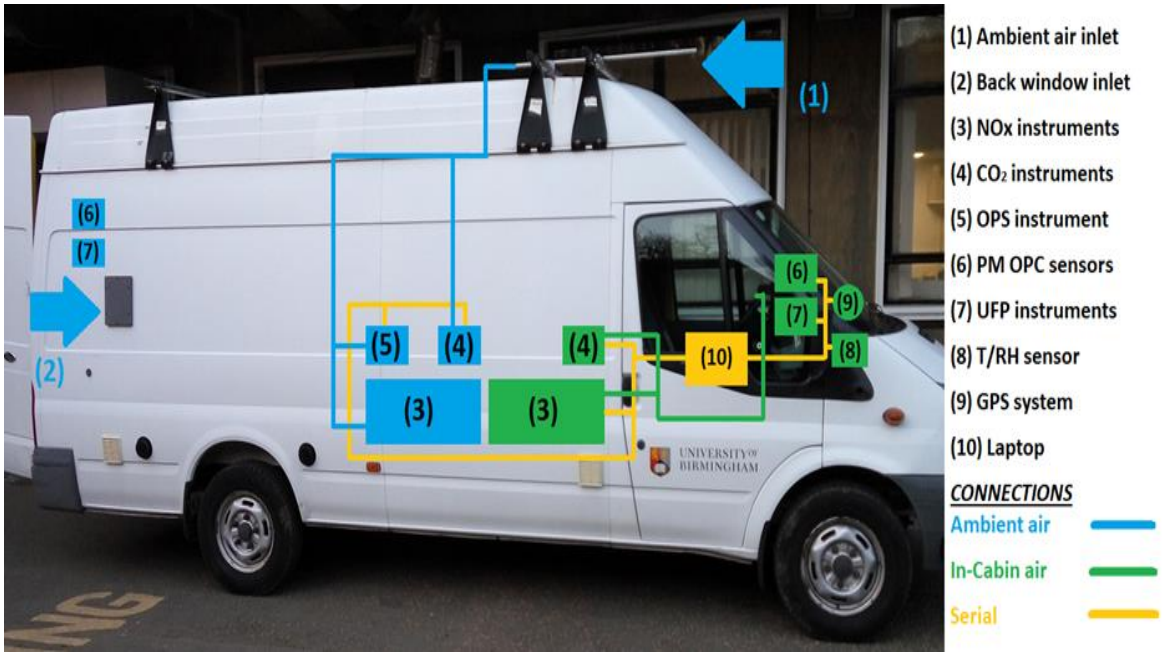


Figure 3.1: Schematic of the configuration of the instruments and connections applied in the tested vehicles.

Table 3.1: Characteristics of the tested vehicles; All vehicles had pollen filter apart from Ford transit that had no air filter. LDV: Light Duty Vehicle.

| Model | Type | Fuel | Year | Engine size (L) | Odometer (km) | Est. Cabin size ($m^3$) |
|---|---|---|---|---|---|---|
| Ford Focus | Estate | Diesel | 2013 | 1.6 | 107282 | 3.46 |
| Vauxhall Insignia | Estate | Diesel | 2016 | 2.0 | 42982 | 3.28 |
| Hyundai i800 | Van (9 seats) | Diesel | 2017 | 2.5 | 17650 | 7.89 |
| Ford Transit | LDV (2 seats) | Diesel | 2009 | 2.4 | 112569 | 2.16 |

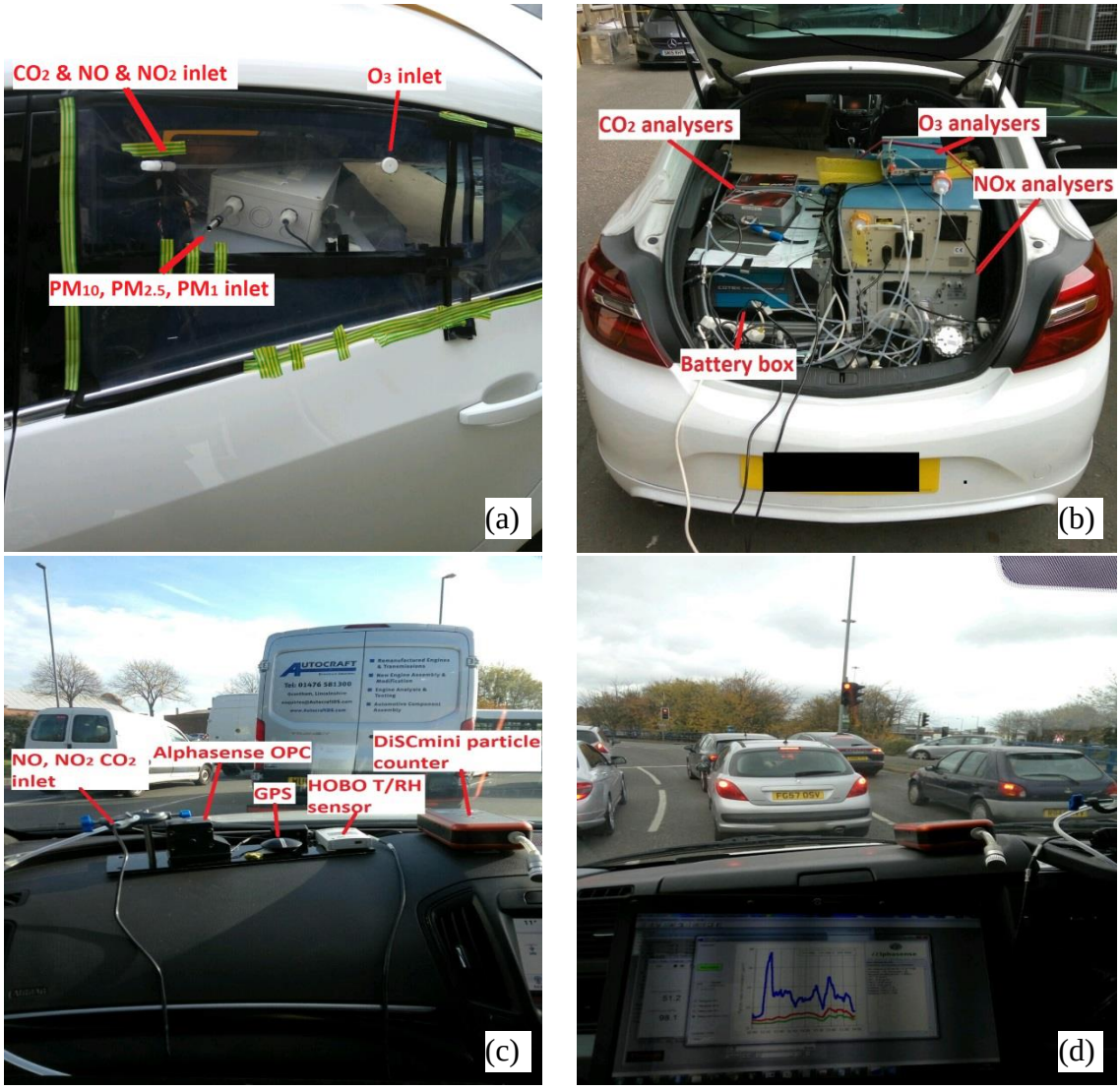


Figure 3.2: Experimental setup of mobile campaign. (a) Inlet of the ambient $NO_2$, NO, $CO_2$, PM, UFP; (b) instrument setup in the boot of a tested Vauxhall Insignia; (c) inlet and instrument setup inside the vehicle close to the breathing area of the driver and co-driver; (d) real time measurements and validity of measurements in the laptop of the co-driver.

All instruments were powered through a specifically designed battery box that provided energy supply for 2.5 hours (see Figure 3.2). The instruments were logged via a single laptop and all measurements were averaged to a 1-minute time resolution and their times were adjusted for different inlet residence times/sampling times to ensure

consistency between the pairs of measurements (see 3.2.4). For each vehicle, we used the same inlet lengths for the gas and particle measurements both indoor and outdoor measurements. All instruments were co-calibrated before and after each campaign, with an observed change of less than 5% between the two calibrations. The calibration, use of identical instrumentation, experimental setup and route to perform the measurements of this campaign is in agreement with the high-quality assured mobile measurements criteria reported in Alas et al., (2019). Table 3.2 shows information about the instrument detection limits, sampling periods and associated measurement uncertainties.

Table 3.2: Instrument details and overview of measurements

| Instrument | Measurement | Method | Sampling time (s) | Uncertainty | Flow (l/min) | Manufacturer |
|---|---|---|---|---|---|---|
| TEI: 42c, 42i | NO, $NO_2$, $NO_X$ | Chemiluminescence | 60 | ±10 % | 0.7 | Thermo Scientific |
| OPS: TSI 3330 | PM10, PM2.5, PM1 | Optical scattering | 10 | - | 1 | TSI Incorporated |
| Minidisc | UFP, LSDA, Particle size | Electrical diffusion | 1 | ±30 % | 1 | NANEOS |
| LI-820 | CO2 | Infrared absorption | 1 | ±3 % | 1 | Licor |
| TEI: 49i | O3 | UV absorption | 60 | <2 ppb | 1 | Thermo Scientific |
| Globsat BU-535 GPS | Latitude, longitude, altitude, speed | Remote sensing | 1 | - | - | Globalsat |
| HOBO | T/RH | - | 60 | ±0.35 $^{O}$C (T) ±2.5% (RH) | - | Onset |

## 3.2.1 Instrumentation

### 3.2.1.1 Nitrogen oxides analyser

For NO and $NO_2$ measurements, two Thermo Scientific chemiluminescent (EN14211:2012 $NO_x$) analysers – models 42i-TL (inside) and 42C (outside) were used. The Models 42C and 42i are based on the principle that nitric oxide (NO) and ozone ($O_3$) react to produce a characteristic luminescence with intensity linearly proportional to the NO concentration. The chemiluminescent mechanism involves electronically excited $NO_2$ molecules which are detected in the range $600 < \lambda < 3000$ nm and are measured in a temperature controlled red sensitive photomultiplier tube. Specifically, $NO_2$ must first be transformed into NO before it can be measured using the chemiluminescent reaction. $NO_2$ is converted to NO, thus giving a NO + $NO_2$ combined signal. Then, $NO_2$ concentration is derived by the difference between the NO and the $NO_x$ signals. The detection limit of the 42i and 42C instruments was determined by 3 times the standard deviation of the measurement in zero air and was calculated to be approximately 0.24 and 0.30 ppb respectively for a 1 minute averaging period. For both $NO_x$ monitors, we employed a multi-point calibration for NO and $NO_2$. The total uncertainty of the mobile measurements for the 42i and 42C was calculated to be 10% and 12% respectively. This uncertainty was derived from the propagation of errors in

the mass flow controllers, NO standard (calibration gas), sampling, reproducibility of the calculations due to the sensitivity of the instrument, losses in the conversion of NO to $NO_2$ due to the molybdenum converter and the losses in the inlets following the recommendations of Minarro and Ferradas, (2012). For the mobile $NO_x$ sampling we used a 6mm teflon tubing to avoid catalytic conversion of NO and $NO_2$ in the tubing.

#### 3.2.1.2 Ozone analyser

For the $O_3$ measurements a Thermo Scientific ozone analyser model 49i was used. The Model 49i operates on the principle that ozone ($O_3$) molecules absorb UV light at a wavelength of 254 nm. Briefly, a mercury lamp (with light intensity $\lambda$ = 254 nm) and photodiodes are located on opposite sides of two absorption cells. Sample analyte is drawn into the instrument, where a pair of valves, send by turns $O_3$ scrubbed/unscrubbed analyte through the two cells. The degree to which the UV light is absorbed from the $O_3$ scrubbed analyte and unscrubbed analyte is then measured and the $O_3$ concentration is calculated, according to the Lambert-Beer law.

### 3.2.1.3 Carbon dioxide analyser

For $CO_2$ measurements we used two LI-820 $CO_2$ gas analysers. The LI-820 is an absolute, non-dispersive, infrared gas analyser based upon a single path, dual wavelength, infrared detection subsystem. The $CO_2$ measurement is a function of the absorption of IR energy as it travels through the optical path. Concentration measurements are based on the difference ratio in the IR absorption between a reference and sample signal.

### 3.2.1.4 Particle number personal monitor

For UFP and LSDA measurements, two DiSCmini (Matter Aerosol AG) units were used. DiSCmini is a portable miniature diffusion size classifier that measures particle number concentration and size. Figure 3.3 shows the DiSCmini size and deployment during the mobile experiments. DiSCmini measuring principle is based on the electrical charging of the aerosol. Positive air ions generated in a corona discharge are mixed with the aerosol. The charged particles are then detected in two stages by electrometers. The first detector stage is a pile of steel grids; small particles will

preferably deposit on it by diffusion and detected as an electrical current. The remaining particles end up in a second stage, the filter stage, and are also detected as an electrical current. The ratio of these two currents is a measure of the average particle size determined during the instrument calibration. Because the charge per particle is a function of particle diameter, once this is known, the particle number concentration can be computed from the total current detected together with the flow rate of the instrument. Both DiSCmini's were operated sampling adjacent to a reference instrument, a condensation particle counter (CPC) before the campaign for 2 days. The 30 sec resolution data plotted together and showed good agreement (Pearson correlation coefficient > 0.8) for the whole 2 day time series. DiSCmini's were then corrected to match the reference instrument according to the slope of the fitted regression in CPC vs DiSCmini data. Figure 3.4 shows the comparison between CPC and DiSCmini 1 and 2.


Figure 3.3: Illustration of DiSCmini particle counter (left) and DiSCmini deployment during the mobile experiments (right).

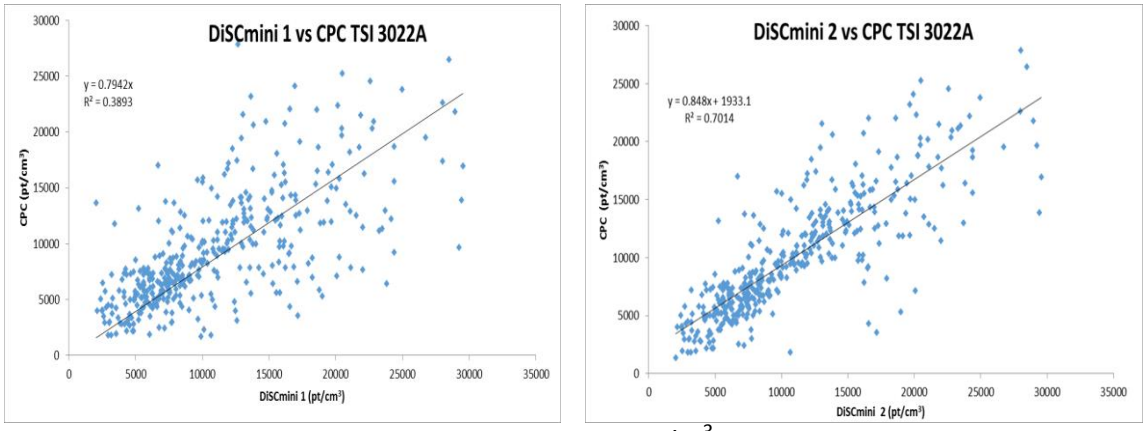

Figure 3.4: Lab comparison of particle number (pt/$m^3$) between DiSCmini and CPC TSI 3022A.

### 3.2.1.5 Particle counter

Two Alphasense optical particle counter (OPC) -N2 sensors were used to measure $PM_{10}$, $PM_{2.5}$ and $PM_1$ mass concentrations. Figure 3.5 shows the sensor and the within-vehicle deployment. The OPC-N2 can be considered as a miniaturised OPC as it measures 75 mm × 60 mm × 65 mm and weighs under 105 g, and as such is significantly cheaper. The OPC-N2 contains a laser (25 mW max) that normally operates at a single power between 5 mW and 8 mW and samples via small fan aspirator and measures particle number concentration over a reported size range of 0.38 to 17 µm across 16 size bins, and maximum particle count of 10 000 $s^{-1}$. The minimum time resolution is 10 s. The measured particle number concentration is converted via on-board factory calibration to particle mass concentrations for $PM_1$,

$PM_{2.5}$ and $PM_{10}$ size fraction according to European Standard EN481. The OPC-N2 are known suffer from influences of RH (Crilley et al., 2018), therefore co-located measurements of RH (performed in vehicle with a HOBO sensor) were used to correct the data when humidity was within the range from 60 to 90% following Crilley et al. (2018). The OPC-N2 sensors used in this study were previously calibrated in the field with reference particle mass instruments, described in detail in Crilley et al. (2018). Briefly, the response of the OPC-N2 were found to be linear with respect to reference instrumentation (e.g. TEOM-FDMS), with a positive artefact observed during times of high RH. This positive artefact has been shown to be related to bulk particle hygroscopicity (Crilley et al., 2020). Therefore, we applied the correction factor developed in Crilley et al., (2018) to the reported particle mass concentrations by the OPC-N2 to reduce any bias between indoor and outdoor measurements. For protection against vibrations we used specifically designed boxes (see Figure 3.2a). For the outdoor particle measurements, we wanted to keep the inlet line as short as possible (6.5 cm) to minimise particle losses. As the study predominantly used normal rental vehicles, we were limited to placing the instruments at a side window (Figure 3.2a). As this inlet location was not ideal and at $45^{o}$ angle, the aerosol sampling was anisokinetic, therefore we had to calculate the particle losses using the method of von der Weiden et al., (2009). For this inlet set up particle losses were found to be minimal, with coarser particles having greater losses than fine and ultrafine particles (11% for $PM_{10}$, 3.5% for $PM_{2.5}$, 1.8% for $PM_1$ and 6% for particles < 300 nm). For the correction of the OPC-N2 mass concentration we also operated a reference optical particle sizer instrument (TSI 3330). The collected data from the OPC-N2 and TSI 3330 were plotted

against each other and the acquired slope of the regression was used to correct the data from OPC-N2 in order to match the reference instrument as in Crilley et al., 2018; 2020. Two test runs were made to calibrate/validate the OPC performance under the experimental conditions of this study. One tested the OPC performance against the reference instrument for within-vehicle conditions, while the other validated the OPC against outdoor/on-road concentrations. Both test runs performed in mobile mode while driving. The calibration of within-vehicle and on-road comparison is shown in Figure 3.6. A third test run around campus was also performed and tested the sampling angle at $45^{o}$ and $90^{o}$ of the side window. The comparison between OPC-N2 and TSI 3330 at $45^{o}$ and $90^{o}$ angle is shown in Figure 3.7. TSI 3330 optical particle spectrophotometer (OPS), which was used a reference instrument, measures particles number concentrations between 0.3 and 10 µm across 16 size bins, with a maximum particle count of 3000 particles $cm^{-3}$.

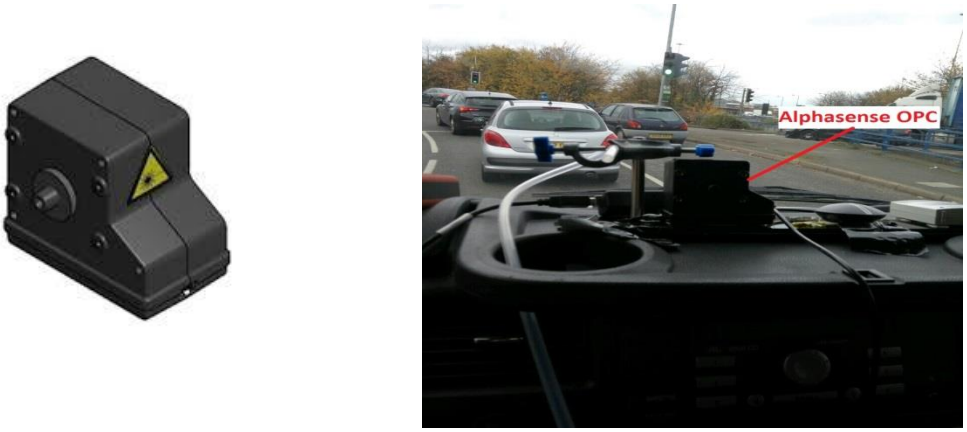


Figure 3.5: Alphasense PM sensor used for the mobile experiments (left) and the within-vehicle deployment (right).

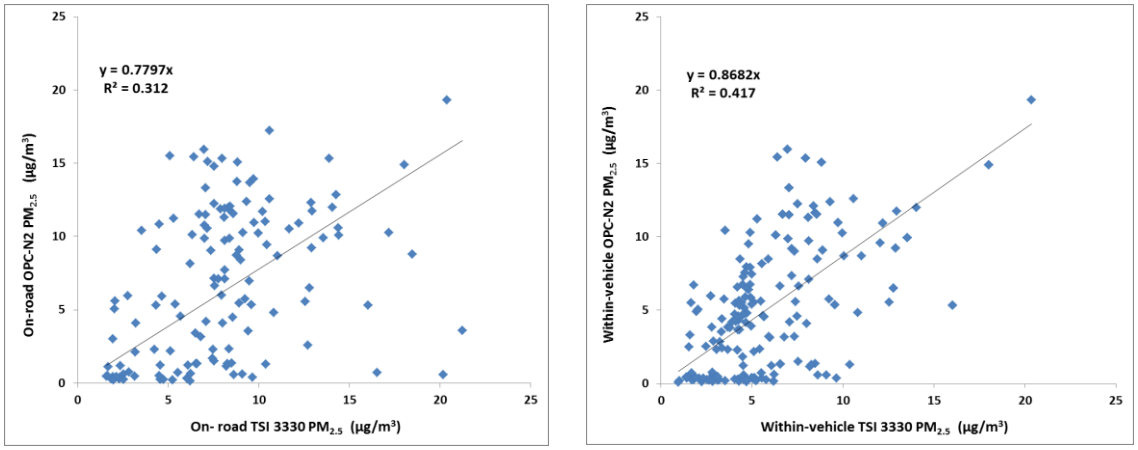


Figure 3.6: Comparison of $PM_{2.5}$ concentrations between OPC-N2 sensors and TSI 3330. (left) for on-road data, (right) for within-vehicle data.

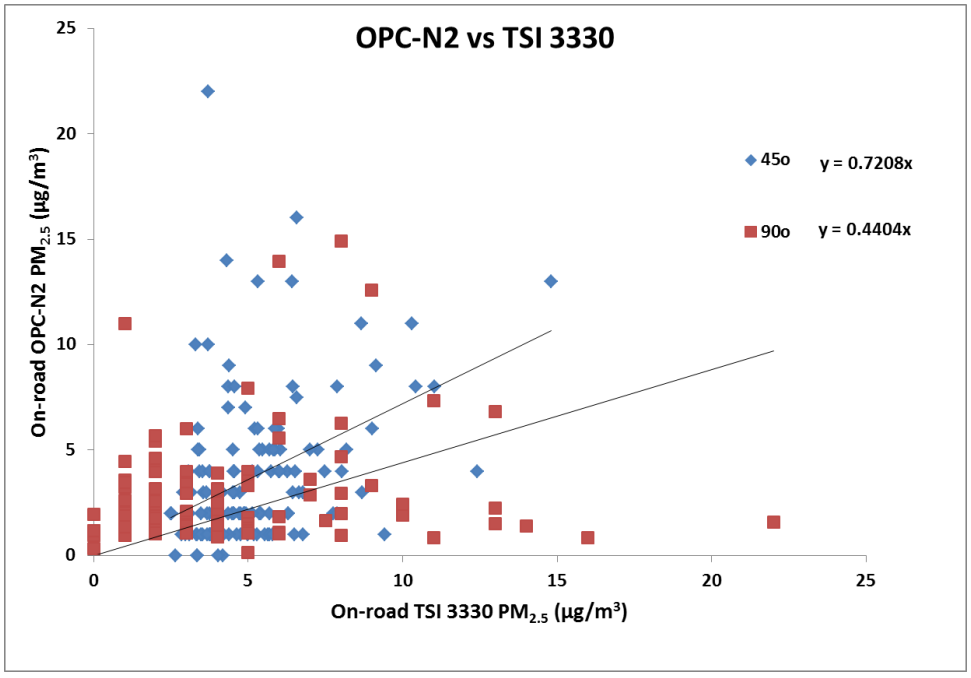


Figure 3.7: Comparison of $PM_{2.5}$ concentrations between OPC-N2 sensors and TSI 3330 at $45^{o}$ and $90^{o}$ sampling angle.

### 3.2.2 Vehicle details and choice of routes

Four vehicles were used in this study. The first was the University of Birmingham Mobile Air Monitoring Laboratory, a long-wheel base, Ford Transit closed cabin 2 seater light duty vehicle (LDV) van (see Figure 3.1). The passenger cabin area for this vehicle is physically separate from the instrument/cargo area, and in this respect typical of front-cabin passenger and light goods vehicles. The other three vehicles were different large passenger cars; a nine seater vehicle and two estate cars (see Table 3.1). For the passenger vehicles, instruments were mounted within the body of each vehicle, with two pairs of inlets protruding into ambient air, and into the cabin volume. For ambient/on-road measurements, one inlet was used for gases (NO, $NO_2$), while $PM_{10}$, $PM_{2.5}$, $PM_1$ and UFP and LSDA had their own separate sampling inlet. The within-cabin sampling inlets were located in the breathing area of the driver/passenger in the front of each vehicle, to permit assessment of exposure inside the car. For the van configuration see information in Figure 3.1. Figure 3.1 also gives an example schematic of the instrument configuration. Both indoor and outdoor measurements were conducted concurrently. The vehicles tested here are representative of the UK fleet as 11% of the UK's fleet is LDV, while the manufacturers and models are amongst the most popular ones in the UK (DfT, 2019).

All vehicles were equipped with standard particle pollen filters as provided by the manufacturer apart from the Ford transit which had no filter (as standard); no

alternative filters such as activated carbon filters were tested. Particle pollen filters stop small particles from entering the interior part of the vehicle, effectively capturing pollen, dust, mould spores and debris, while activated carbon filters have the potential (additionally to the pollen filters) to absorb gases such as CO and $NO_x$.

All four vehicles were driven along a consistent set of driving routes in Birmingham, UK (see Figure 3.8 for routes). Three different roads were chosen to examine the difference in exposure by area/road type. The routes included a sub-urban road (2 side carriage way, 8 m width, 40 mph speed limit, average daily traffic flow 30,000 vehicles), illustrated in red in Figure 3.8, an urban section (via an underground city centre tunnel) (2 to 4 lane road, 8 m width, 30 mph speed limit, average daily traffic flow 51,000 vehicles), depicted in green in Figure 3.8 and a ring road section highlighted in purple in Figure 3.8 (4 to 5 lane road, 8-9 m width, 50 mph speed limit, average daily traffic flow 40,000 vehicles) around the city of Birmingham. The driving schedule for the October campaign was repeated between 12:00 - 16:00 (weekdays only), which accounts for normal daytime traffic, while for the February campaign, more driving patterns including morning/evening rush hours were covered. All the experiments with vehicles were performed by two people namely a dedicated driver and documenter who recorded details of the journeys.

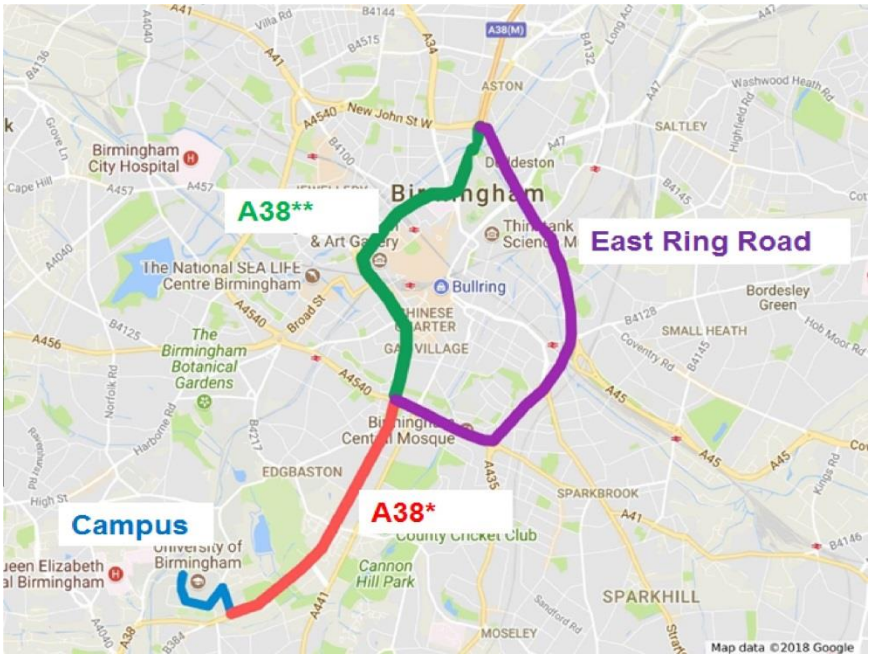


Figure 3.8: Map illustrating the route that was followed during the mobile experiments. A38*: is a suburban road, A38**: is an urban part that includes an underground city tunnel.

### 3.2.3 Ventilation Settings

The vehicle ventilation options that were tested varied amongst the vehicles, however we performed four core and comparable settings. Depending on the available ventilation options a fifth option was explored in two of the vehicles (Vauxhall Insignia and Hyundai i800). See Table 3.3 for detailed information about the tested ventilation settings; in brief measurements in all three road sections was performed with (1) Windows open (OPEN), (2) Fan on, recirculation off, windows closed (FAN), (3) Fan plus

air conditioning on, recirculation off, windows closed (AC), (4) Fan on, recirculation on, windows closed (FAN_R), (5) Fan plus AC on, recirculation on, windows closed (AC_R), (6) No ventilation (Fan or AC), windows closed (NONE). When a ventilation option was tested including fan operation, these were set at the maximum speed. We note that although limited, air exchange within vehicles does occur under the "NONE" setting via leaks. Each ventilation setting in every vehicle was tested over the same route segments, and had approximately the same time duration (20 - 22 min loop completion depending on the traffic - see Figure 3.8) assuring equivalent weight in ventilation setting data analysis.

Table 3.3: Ventilation settings tested in individual vehicles.

| Ventilation | Acronym | Vehicles |
|---|---|---|
| Windows open | OPEN | Ford Focus, Vauxhall insignia, Hyundai i800, Ford Transit |
| Fan on, recirculation off, windows closed | FAN | Ford Focus, Vauxhall insignia, Hyundai i800, Ford Transit |
| AC on, windows closed | AC | Ford Focus, Vauxhall insignia, Hyundai i800 |
| Fan on, recirculation on, windows closed | FAN_R | Ford Focus, Vauxhall insignia, Hyundai i800, Ford Transit |
| AC on, recirculation on, windows closed | AC_R | Vauxhall insignia, Hyundai i800 |
| No ventilation, windows closed | NONE | Ford Focus, Vauxhall insignia, Hyundai i800, Ford Transit |

### 3.2.4 Data processing

All measurements were averaged to a 1 minute time resolution, with instrument and inlet residence times (60 sec for the $NO_x$ analysers and 5 sec for the inlet residence time) taken into consideration. The measurements were applied in three ways: 1) to determine the measured concentrations while driving, 2) to calculate the $I/O_{VEH}$ ratios (ratio of concentrations measured inside the vehicles to the concentrations measured immediately outside, on-road) with different ventilation settings and 3) to calculate the exposure and inhalation dosage of vehicle occupants. For the comparison of cases we used descriptive statistics and a two sample Welch t-test to illustrate the significance at 0.95 and 0.90 confidence intervals.

### 3.2.5 Inhalation dosage calculation

The amount of air pollutants inhaled is dependent not only on the concentration of the pollutant to which a commuter is exposed to but also the duration of exposure and the breathing rate. The inhaled lung dose (ID) is calculated by Equation 1:

$$ID = C_i \times \Delta t \times V_E \quad (1),$$

where $C_i$ is the concentration of pollutant *i* at a given location/time, $\Delta t$ is the exposure time (min) and $V_E$ is the ventilation rate (breathing rate x tidal volume) of an individual ($m^3$/min). As it was discussed in Chapter 1, inhalation dose is a product of the ambient air concentration of pollutants inhaled and exhaled, their breathing rate, which depends upon age and the level of the physical activity of individuals, and deposition fraction, which is the actual proportion of the inhaled amount that is deposited within the human lungs. The ventilation rates used for different exposed groups, namely male, female and children (ages 6 to 13 years - male/female combined) were based on the driving/riding a car exercise category combined (for males and females) or sitting exercise category (for children) taken from Adams (1993) and were 0.62 $m^3$/h, 0.52 $m^3$/h and 0.44 $m^3$/h respectively. The breathing rates that were used to calculate the inhalation dosage for both cyclists and pedestrians were 1.38 ($m^3$/h), 1.16 ($m^3$/h) and 0.77 ($m^3$/h) for males, females and children respectively adopting that they are under light exercise mode (Adams 1993). Light exercise conditions were assumed for both cyclists and pedestrians since the study of Zuurbier et al., (2010) that measured breathing rates in cyclists, reported average breathing rates for men and woman cyclists of 1.41 $m^3$/h (ranging from 0.7- 2.5 $m^3$/h), which fall into the light exercise breathing rates reported in Adams (1993). Cyclists were presumed to be exposed to concentrations measured directly outside the vehicle (*i.e.* assuming that they are cycling on the same roads), while pedestrians who are walking at certain distance from

the road were assumed to be exposed to concentrations measured by air quality stations at representative locations.

## 3.3 Results

### 3.3.1 Exposure variability between vehicles

An example of $PM_{2.5}$ timeseries with a Vauxhall Insignia 2016 is illustrated in Figure 3.9, while the equivalent $NO_2$ time series are shown in Figure 3.10. For Figure 3.6 it can be seen that the inside levels are almost equal to outside/on-road levels with windows open (OPEN ventilation setting, light blue colour). Notable is the fact that under recirculation mode on (FAN_R, green colour), although the outside/on-road levels remain relatively high, a sudden decrease to the within-vehicle levels is observed. Regarding $NO_2$ timeseries (Figure 3.10), the within-vehicle levels experience similar variation to the on-road levels and they remain relatively high across the tested ventilations. Figure 3.11 shows the within-vehicle variation of concentrations across the tested vehicles. Some cross-pollutant variability exists between the vehicles,

however median exposure is very similar in most cases apart from the UFP and LSDA. It is further noted although the median exposure within Ford Focus vehicle (red boxplot) is similar to the other vehicles, its distribution is significantly different ($p < 0.05$) from the other vehicles and is most likely related to the leakage of the vehicle. The median values of all PM classes for the 2-seater van were elevated in comparison to the other vehicles. This discrepancy can be attributed to the fact that the February campaign included driving during morning and evening rush-hours which means different numbers/types of vehicles, thus more particles generated from tailpipe and tyres/brakes, thus the elevation in the median. This can also be seen from the on-road measurements. A further notable finding for the 2 seater van is that the range of the outside pollutants is much smaller compared to the other vehicles. This is likely related to the vertical dispersion dynamics of pollutants and to the sampling inlet of the van being elevated compared to the inlet at the side windows of the passenger cars (see further discussion in 3.4). As expected, in general higher levels were measured outside than inside, while for the individual vehicles the inside levels were observed to following similar temporal patterns to outside levels. This finding is explored more quantitatively later (sections 3.3.3 and 3.3.4).

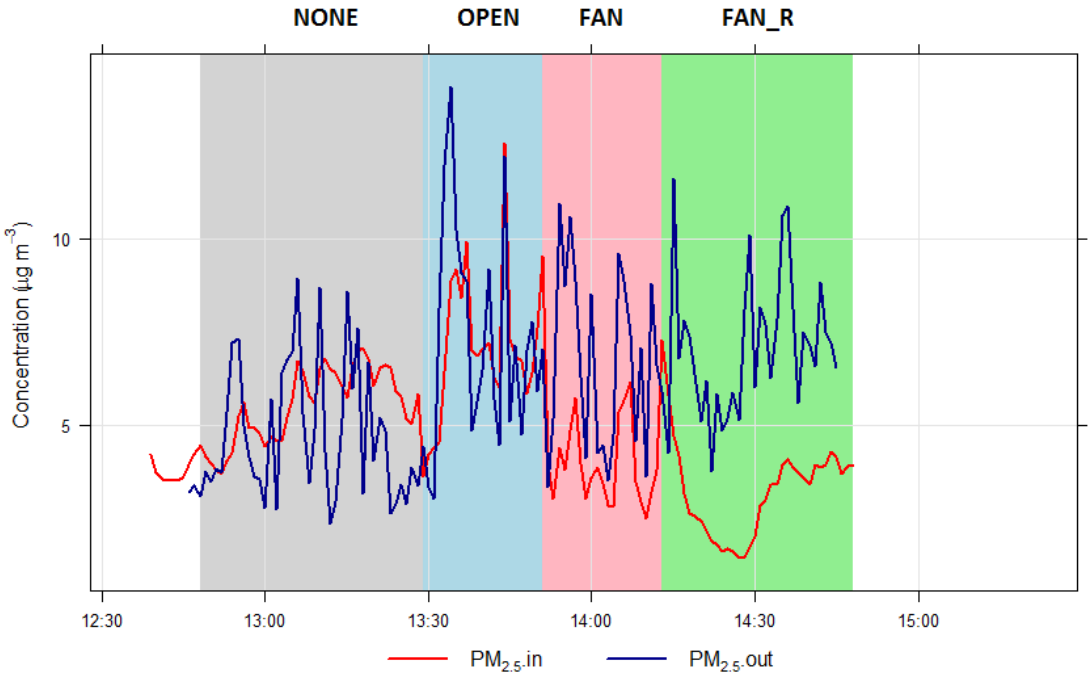


Figure 3.9: Timeseries of inside and ambient, on-road $PM_{2.5}$ concentrations under different ventilation settings for Vauxhall Insignia 2016. Time in x-axis is in GMT.

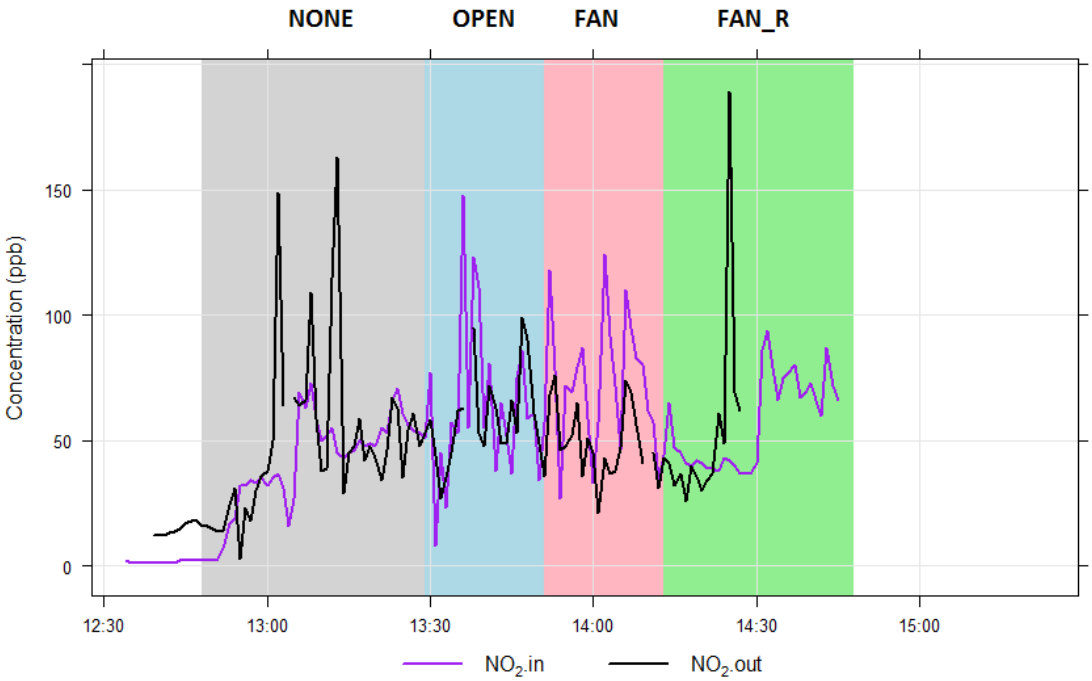


Figure 3.10: Timeseries of inside and ambient, on-road $NO_2$ concentrations under different ventilation settings for Vauxhall Insignia 2016. Time in x-axis is in GMT.

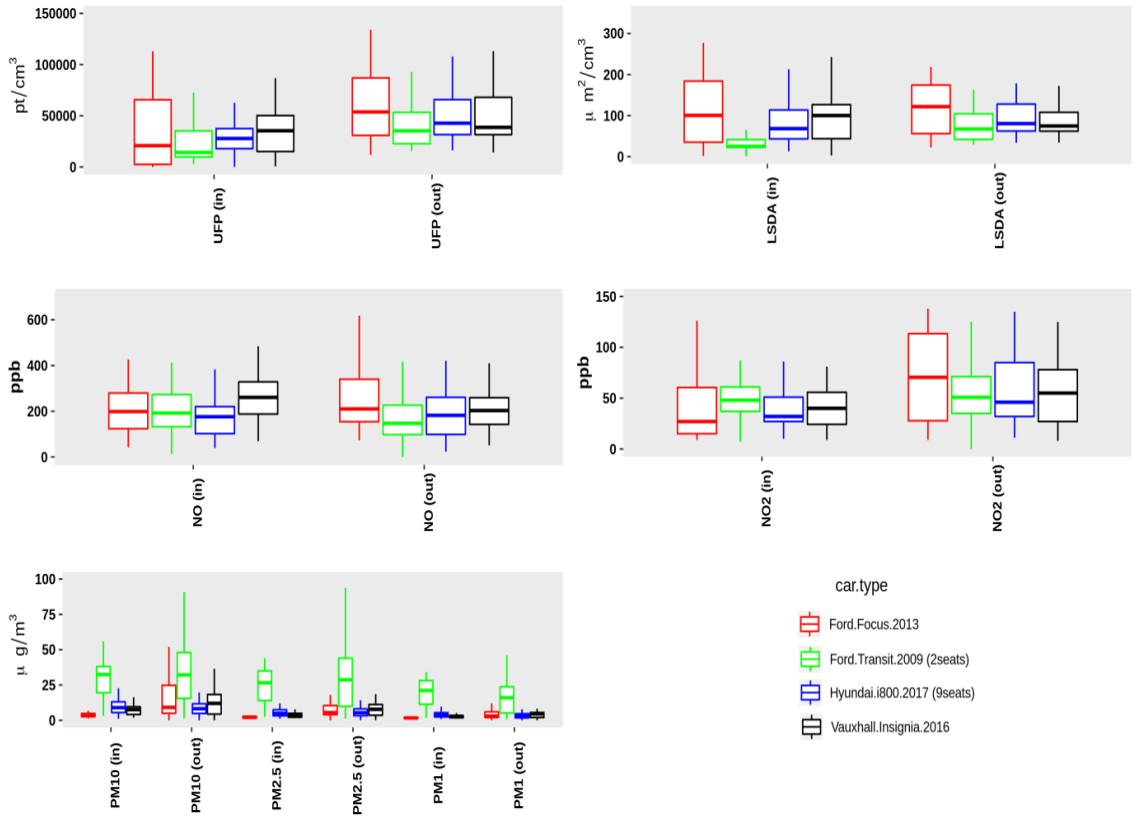


Figure 3.11: Within-vehicle and on-road pollutant levels averaged across all ventilation settings for different vehicles. The boxplot percentile values are 0.05 – 0.95 (line) and 0.25 – 0.75 (box) with the heavy line marking 0.5.

### 3.3.2 Short time exposure variability by road type

High outdoor/on-road levels lead to high indoor levels, mediated to an extent by the selected ventilation option (see later sections 3.3.3 and 3.3.4). Figure 3.12 illustrates the within-vehicle variation of measured species for the three different types of roads explored. Within-vehicle concentrations for both PM and $NO_x$ were

found to be significantly greater ($p < 0.05$) on the urban roads, followed by the ring road and sub-urban roads. The exception (for both within-vehicle and outdoor/on-road levels) was UFP, where higher levels were observed for the ring road and sub-urban roads. The higher UFP measured on the ring-road and sub-urban sections might reflect an emission source (e.g. prevalence of buses or of heavy duty vehicles) (see section 3.4). The LSDA were found to be not statistically different and the median values are almost equal in urban and ring road environments, while being lower for sub-urban roads. $PM_{10}$ values varied significantly ($p < 0.05$) and had median within-vehicle exposure variation of 26, 17 and 15 $\mu g/m^3$ for urban, sub-urban and ring road locations respectively. Similarly, $PM_{2.5}$ median within-vehicle exposure varied between 22, 14 and 8 $\mu g/m^3$ across the same locations respectively, while $PM_1$ median exposure ranged between 18, 11 and 6 $\mu g/m^3$ across the same locations respectively. For $NO_2$, the median within-vehicle abundance was 54, 46 and 32 ppb for urban roads, ring-roads and sub-urban roads respectively. Equally, NO values were found significantly lower ($p < 0.05$) for sub-urban and ring-roads, while urban roads levels were considerably elevated. Analogous variations to within-vehicle species are evident for the outside (ambient, on-road) data (see Figure 3.13; also section 3.2.2 for road characteristics). The highest outdoor/on-road median abundances for PM ($PM_{10}$, $PM_{2.5}$, and $PM_1$) and $NO_x$ (NO and $NO_2$), other than UFP and LSDA, were observed in the urban followed by ring road and sub-urban roads.

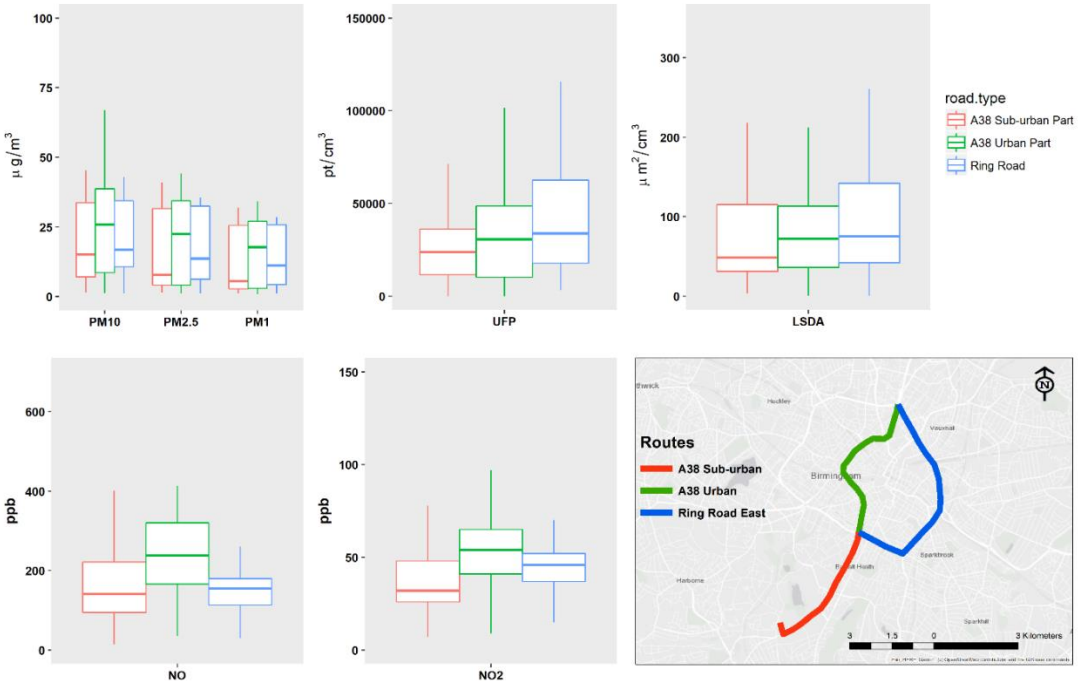


Figure 3.12: Within-vehicle $PM_{10}$, $PM_{2.5}$, $PM_1$, UFP, LSDA, NO and $NO_2$ in sub-urban (red), urban (green) and ring roads (blue) as per map. The boxplot percentile values are 0.05 (starting line), 0.25 (lower box boundary), 0.50 (mid box line), 0.75 (upper box boundary), 0.95 (ending line).

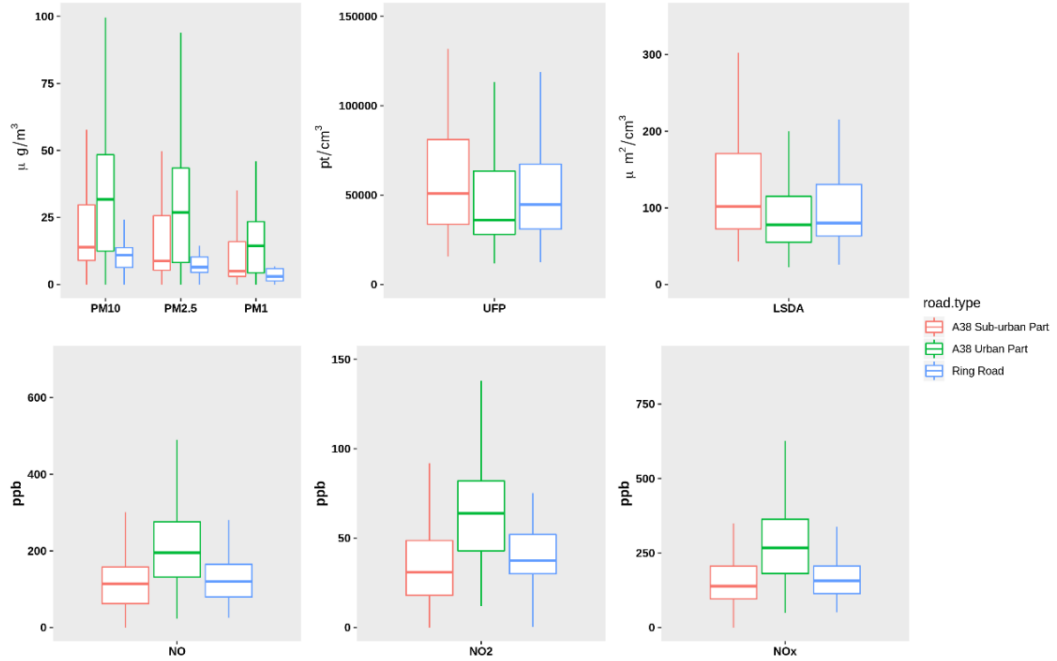


Figure 3.13: Outside levels of $PM_{10}$, $PM_{2.5}$, $PM_1$, UFP, LSDA, NO and $NO_2$ in sub-urban (red), urban (green) and ring roads (blue).

### 3.3.3 Differences in I/O between ventilation modes

Figure 3.14 shows the boxplots of $I/O_{VEH}$ ratio (aggregated and weighted for the values of individual vehicles) for the measured species under different ventilation settings, while the median values are listed in Table 3.4. When pollutant levels for different vehicles were compared under the same ventilation options, no clear difference was observed between tested vehicles, cabin size, ventilation or species in terms of the median variation. However, there are some differences observed regarding the interquartile range of the $I/O_{VEH}$ values, likely related to the different leakage or manufacturing and age of the tested vehicles. For the variation of these $I/O_{VEH}$ ratios separated by vehicle see Figure 3.15.

From the four vehicles tested here, the median $I/O_{VEH}$ ratios for $PM_{10}$ and $PM_{2.5}$ were found to be below 1 for all the tested ventilation settings (see Table 3.4). The lowest ratio was observed when the recirculation option was switched on (FAN_R); however there are settings (e.g. OPEN) where the $75^{th}$ percentile of the $PM_{10}$ and $PM_{2.5}$ $I/O_{VEH}$ ratios is ~1 (see Figure 3.14). $PM_1$, UFP and LSDA $I/O_{VEH}$ median ratios were also below one for the majority of the ventilation settings. However, for some ventilation settings (FAN, OPEN), the median $I/O_{VEH}$ ratios fluctuated between 0.9 and 1.05, while the median LSDA $I/O_{VEH}$ ratio was significantly greater than 1, at 1.14 with the windows open (Table 3.4). The $75^{th}$ percentile of the $I/O_{VEH}$ ratios in those cases was around 1.5 (Figure 3.14). NO and $NO_x$ ($I/O_{VEH}$ median) ratios were always higher

than 1 (range 1.06 - 1.33) for all the ventilation options, and were statistically significantly (p = 0.05) higher than 1 under AC, FAN, FAN_R, OPEN. For $NO_2$, the median $I/O_{VEH}$ ratio was 1.02 with the windows open (OPEN) and 0.9 with fan on (FAN) and recirculation on (FAN_R).

Table 3.4: Median I/O ratios of $PM_{10}$, $PM_{2.5}$, $PM_1$, UFP, LSDA, NO, $NO_2$ and $NO_x$ for different ventilation settings derived from overall vehicles and road types. OPEN: Windows open, FAN: Fan on, recirculation off, windows closed, AC: Fan plus Air condition on, recirculation off, windows closed, FAN_R: Fan on, recirculation, windows closed, AC_R: Fan plus AC on, recirculation, windows closed, NONE: No ventilation Fan or AC, windows closed. * and ** denote p = 0.10 and p = 0.05 level of significance.

| Species | AC | AC_R | FAN | FAN_R | NONE | OPEN |
|---|---|---|---|---|---|---|
| $PM_{10}$ | 0.73 | 0.42 | 0.79** | 0.40** | 0.80 | 0.71 |
| $PM_{2.5}$ | 0.71 | 0.51 | 0.74 | 0.38 | 0.74 | 0.73 |
| $PM_1$ | 0.72 | 0.61 | 1.05 | 0.48 | 1.04 | 0.94 |
| UFP | 0.62 | | 0.90 | 0.14 | 0.45 | 1.03 |
| LSDA | 0.79 | | 0.94 | 0.40 | 0.65 | 1.14 |
| NO | 1.23** | 1.10 | 1.25** | 1.33** | 1.06 | 1.20** |
| $NO_2$ | 0.69 | 0.66 | 0.92 | 0.89 | 0.74 | 1.02* |
| $NO_x$ | 1.06* | 0.98 | 1.14** | 1.21** | 0.96 | 1.15** |

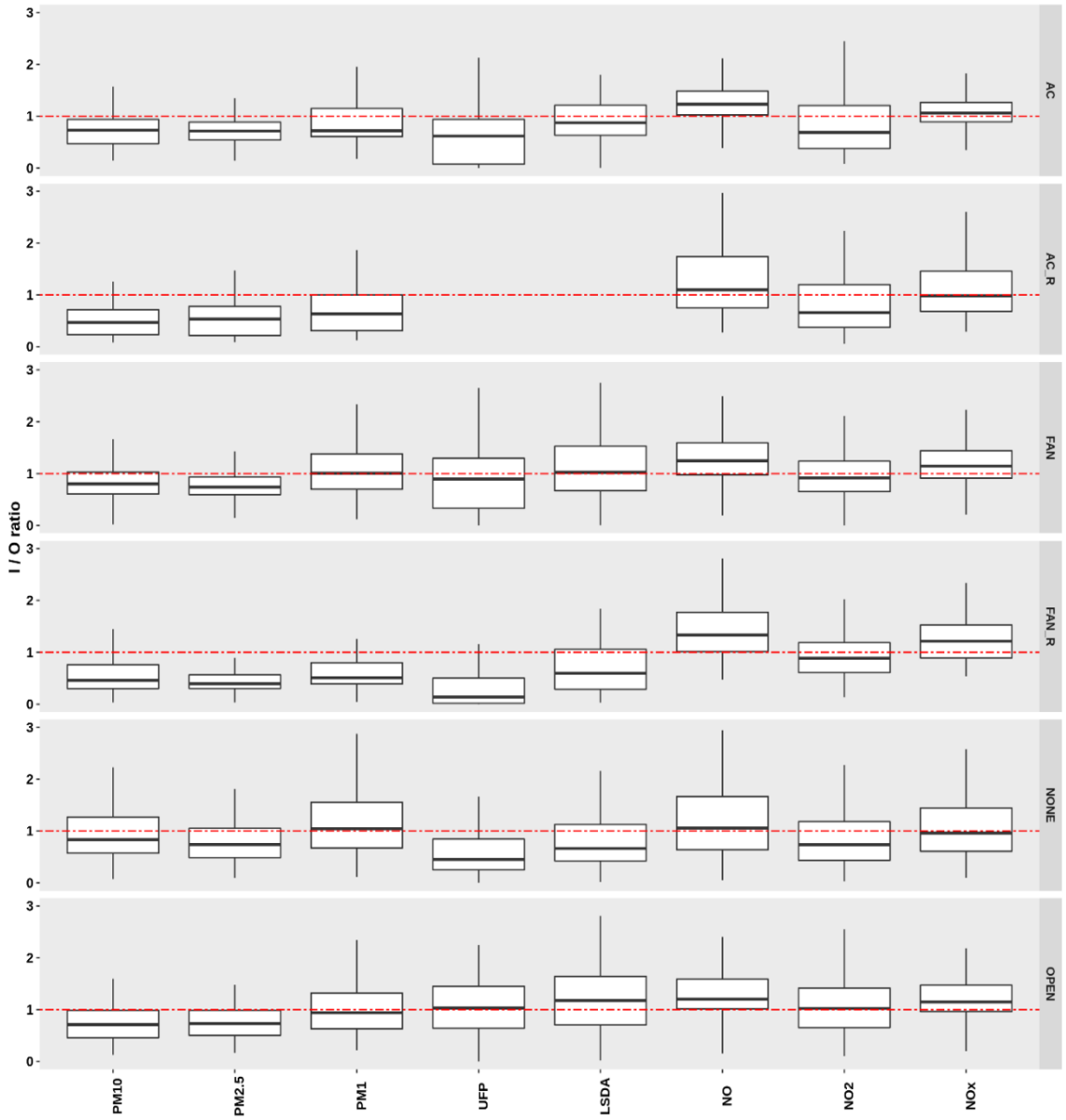


Figure 3.14: Inside/Outside (I/O) boxplot ratios of $PM_{10}$, $PM_{2.5}$, $PM_1$, UFP, LSDA, NO, $NO_2$ and $NO_x$ under different ventilation options aggregated across all vehicles/locations. OPEN: Windows open, FAN: Fan on, recirculation off, windows closed, AC: Fan plus Air condition on, recirculation off, windows closed, FAN_R: Fan on, recirculation, windows closed, AC_R: Fan plus AC on, recirculation, windows closed, NONE: No ventilation Fan or AC, windows closed. The boxplot percentile values are 0.05 (starting line), 0.25 (lower box boundary), 0.50 (mid box line), 0.75 (upper box boundary), 0.95 (ending line).

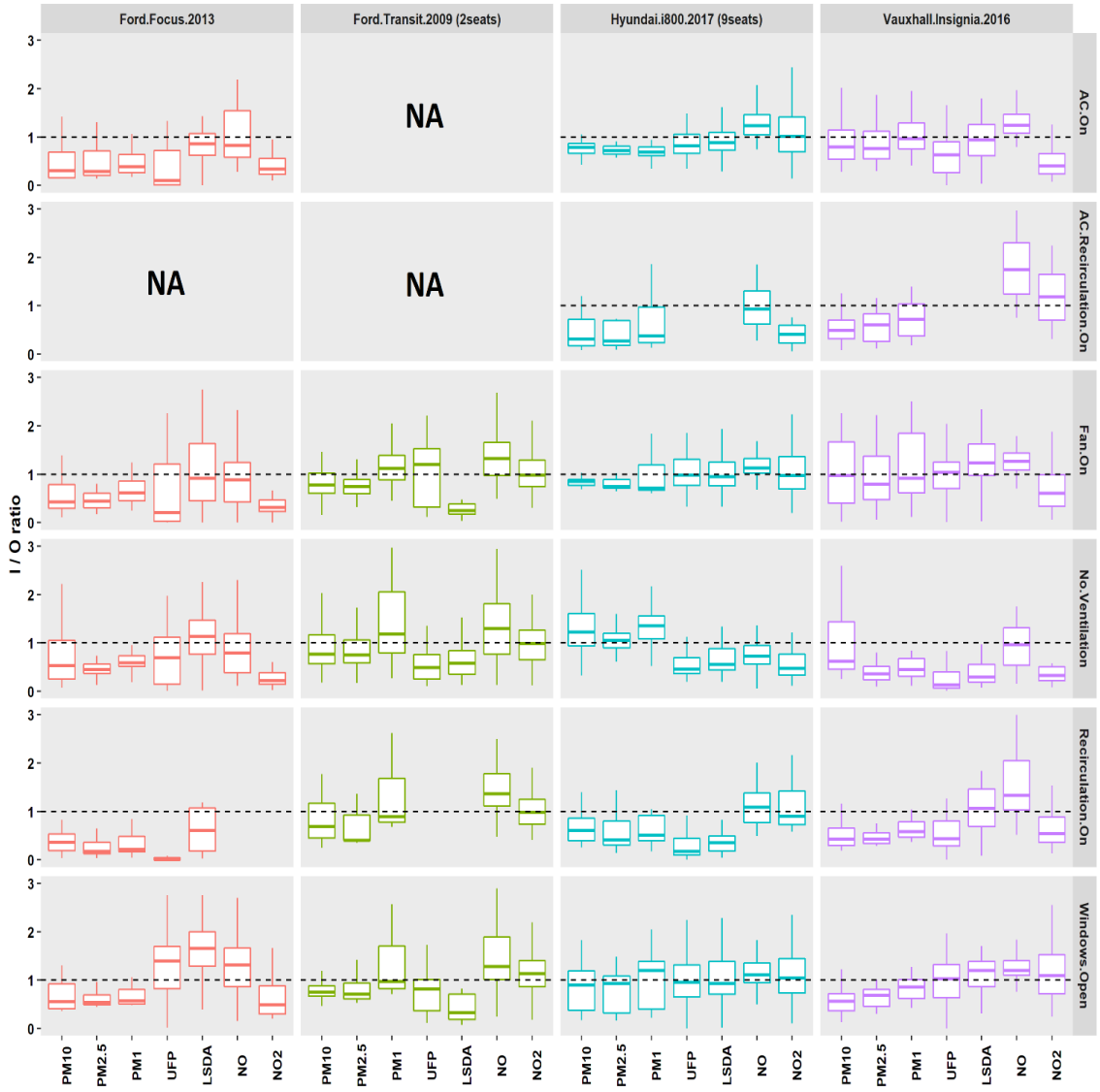


Figure 3.15: I/O boxplot ratios of $PM_{10}$, $PM_{2.5}$, $PM_1$, UFP, LSDA, NO and $NO_2$ for different vehicles under different ventilation options. The dotted black line indicates the ratio of 1. NA: Not available vehicle ventilation option. The boxplot percentile values are 0.05 (starting line), 0.25 (lower box boundary), 0.50 (mid box line), 0.75 (upper box boundary), 0.95 (ending line).

### 3.3.4 Spatial within-vehicle exposure variability

Figure 3.16 shows the within-vehicle levels of $NO_2$ and $PM_{2.5}$ for different ventilation settings as measured over the whole test route. These spatial exposure maps are the average concentrations across all the tested vehicles at each point on the route. It can be observed that within-vehicle concentrations of $NO_2$ are elevated in certain areas, pinpointing potential exposure hotspots. The $NO_2$ spatial analysis showed variability for each ventilation setting across all the routes, where both low on-road and within-vehicle levels (below 30 ppb) were on occasion followed by high on-road and within-vehicle levels (70 ppb or greater) indicating that $NO_2$ is more dependent on the traffic and the identity of the surrounding/leading vehicles (e.g. heavy duty vehicles) rather than the ventilation setting itself (Figure 3.16a, also see Figure A3.1 in appendix for outside pollutant levels). Exposure to particulate pollution is more ventilation dependent than is observed to be the case for $NO_2$, as illustrated from Figure 3.16b. The observed within-vehicle PM concentrations are relatively low (in general less than 10 $\mu g/m^3$) compared to outdoor levels, and only when the windows were open (OPEN), were relatively elevated within-vehicle concentrations observed. The within-vehicle $PM_{10}$ and $PM_1$ concentrations showed a similar spatial variation to those of $PM_{2.5}$ (see appendix Figures A3.2 and A3.3). Spatial maps of within-vehicle UFP and LSDA levels revealed an analogous behaviour to $NO_2$, showing low levels (both within-vehicle and on-road) were followed by high levels across the

tested ventilation indicating that these species are also more traffic than ventilation dependent. The distribution of both within-vehicle and outside air levels of NO showed no clear spatial pattern (e.g. increase as moving from sub-urban road to urban roads) and no systematic hotspots/patterns could be identified. The spatial exposure maps for the other pollutants (both within vehicle and on-road) can be found in Figures A3.1-A3.11 in the appendix.

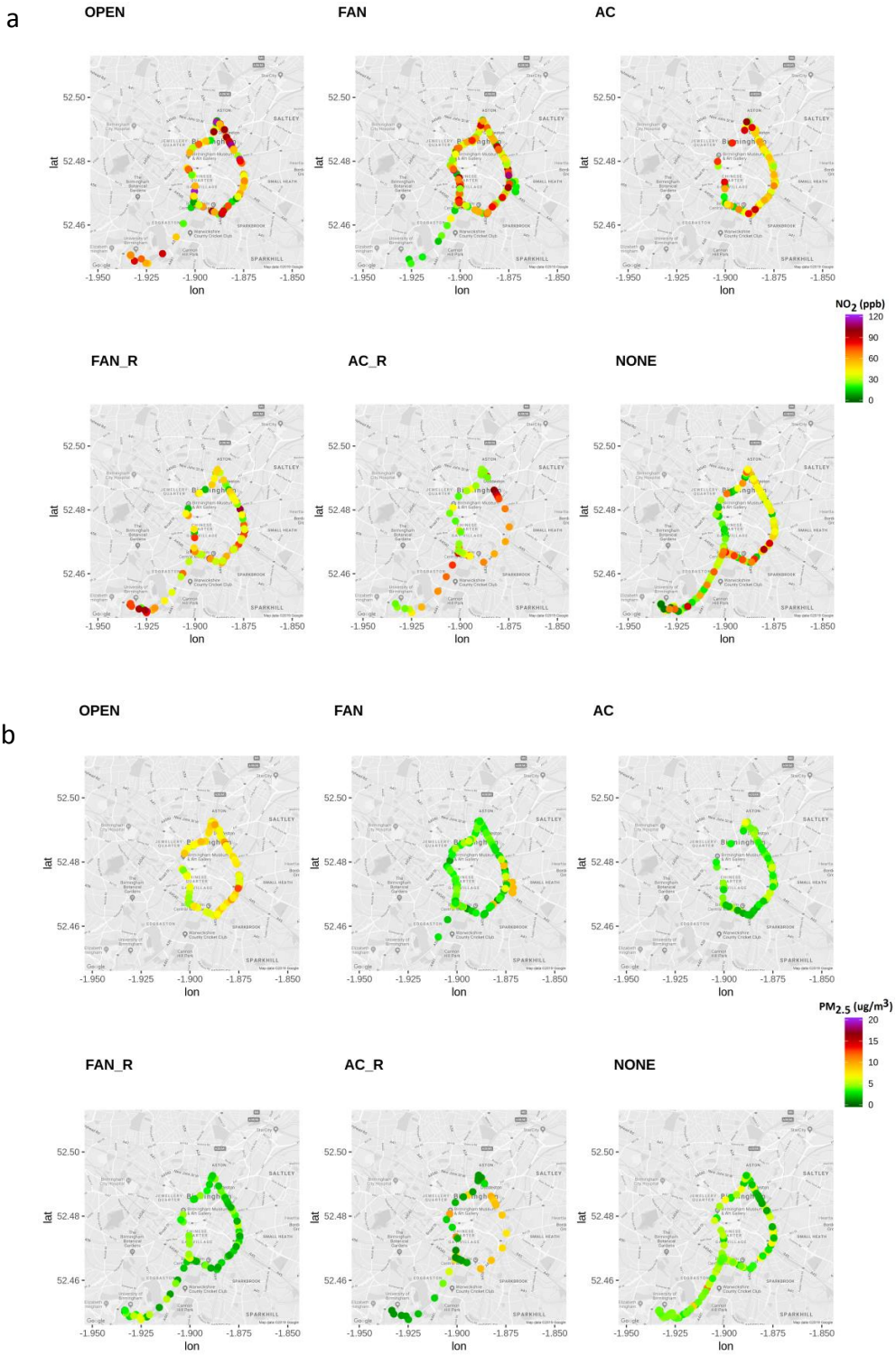


Figure 3.16: Within-vehicle spatial exposure maps for (a) $NO_2$ and (b) $PM_{2.5}$ under different ventilation options (average values from all vehicles). OPEN: Windows open, FAN: Fan on, recirculation off, windows closed, AC: Fan plus Air condition on, recirculation off, windows closed, FAN_R: Fan on, recirculation, windows closed, AC_R: Fan plus AC on, recirculation, windows closed, NONE: No ventilation Fan or AC, windows closed.

### 3.3.5 Inhaled dose

Table 3.5 shows the median hourly calculated inhalation doses (averaged and weighted over all ventilation settings, study vehicles/observation periods) for males, females and children on urban, suburban and ring roads, for vehicle occupants (see letter I in Table 3.5), cyclists or people doing light mode activities close to the road (see letter O in Table 3.5) or pedestrians at an urban background and roadside location (see letter B in Table 3.5). A higher dosage of both particulate and gaseous air pollutants was determined for occupants of vehicles driving on urban roads compared to sub-urban and ring roads. It is also shown that vehicle occupants will inhale less $PM_{2.5}$ and $NO_2$ per unit time than the pedestrians (people doing light activities at a certain distance from the source, represented with B in Table 3.5) and less than the cyclists (people walking or doing activities at a close proximity from source, represented with O, see Table 3.5), as a consequence of lower activity hence breathing rate. Figure 3.17 provides the within-vehicle doses for different ventilation settings for the same roads. As it is illustrated male individuals inhale more air pollutants on a median level due to having bigger lungs and therefore greater tidal volume than females and children. However, there are cases (see Figure 3.17 – $NO_2$ under AC & recirculation on and UFP) where both the median and the interquartile range of the inhalation dose between children and male individuals vary similarly. As discussed in chapter 1, pollutant uptake per mass body weight is normally larger for children than adults, while there are

studies that highlighted that children who are being exposed to elevated air pollution levels might have serious problems in their lung development (Gauderman et al., 2004).

Table 3.5: Median hourly $PM_{10}$, $PM_{2.5}$, $PM_1$, UFP, $NO_2$ and NO inhalation dose for male, female and children vehicle occupants in different roads. I: inside vehicle inhalation dose; representing vehicle occupants, O: directly outside vehicle inhalation dose; representative for cyclists, or people doing light mode activities close to the road, B: air quality based inhalation dose; representative for pedestrians. The inhalation dose for UFP is $10^9$ particles/h for all the other species is μg/h. * and ** indicate hourly median inhalation doses as calculated by the mean campaign hourly concentrations from an urban traffic (*) and an urban background (**) air quality stations in Birmingham. The breathing rates used for cyclists and pedestrians were for light exercise mode. For all the details about the breathing rates see section 3.2.5.

| Road type | Species | Median | | | | | | | | |
|---|---|---|---|---|---|---|---|---|---|---|
| | | Male | | | Female | | | Children | | |
| | | I | O | B | I | O | B | I | O | B |
| Urban | $PM_{10}$ | 16 | 44 | | 13 | 37 | | 11 | 25 | |
| | $PM_{2.5}$ | 14 | 37 | 20* | 12 | 31 | 17* | 10 | 21 | 11* |
| | $PM_1$ | 11 | 20 | | 9 | 17 | | 8 | 11 | |
| | UFP | 19.1 | 58 | | 16.0 | 48.7 | | 13.5 | 32.3 | |
| | $NO_2$ | 64 | 172 | 78* | 54 | 145 | 65* | 45 | 96 | 46* |
| | NO | 184 | 337 | | 154 | 283 | | 131 | 188 | |
| Sub-urban | $PM_{10}$ | 9 | 19 | | 8 | 16 | | 7 | 11 | |
| | $PM_{2.5}$ | 5 | 12 | 18** | 4 | 10 | 15** | 3 | 7 | 10** |
| | $PM_1$ | 3 | 7 | | 3 | 6 | | 2 | 4 | |
| | UFP | 15.4 | 49.6 | | 12.8 | 41.7 | | 10.9 | 27.7 | |
| | $NO_2$ | 38 | 84 | 43** | 32 | 71 | 36** | 24 | 47 | 27** |
| | NO | 109 | 193 | | 91 | 162 | | 77 | 108 | |
| Ring-road | $PM_{10}$ | 10 | 12 | | 9 | 10 | | 7 | 7 | |
| | $PM_{2.5}$ | 8 | 7 | | 7 | 6 | | 6 | 4 | |
| | $PM_1$ | 7 | 4 | | 6 | 3 | | 5 | 2 | |
| | UFP | 20.9 | 70.2 | | 17.5 | 59 | | 14.8 | 39.2 | |
| | $NO_2$ | 55 | 132 | | 46 | 111 | | 39 | 74 | |
| | NO | 120 | 259 | | 101 | 218 | | 85 | 145 | |

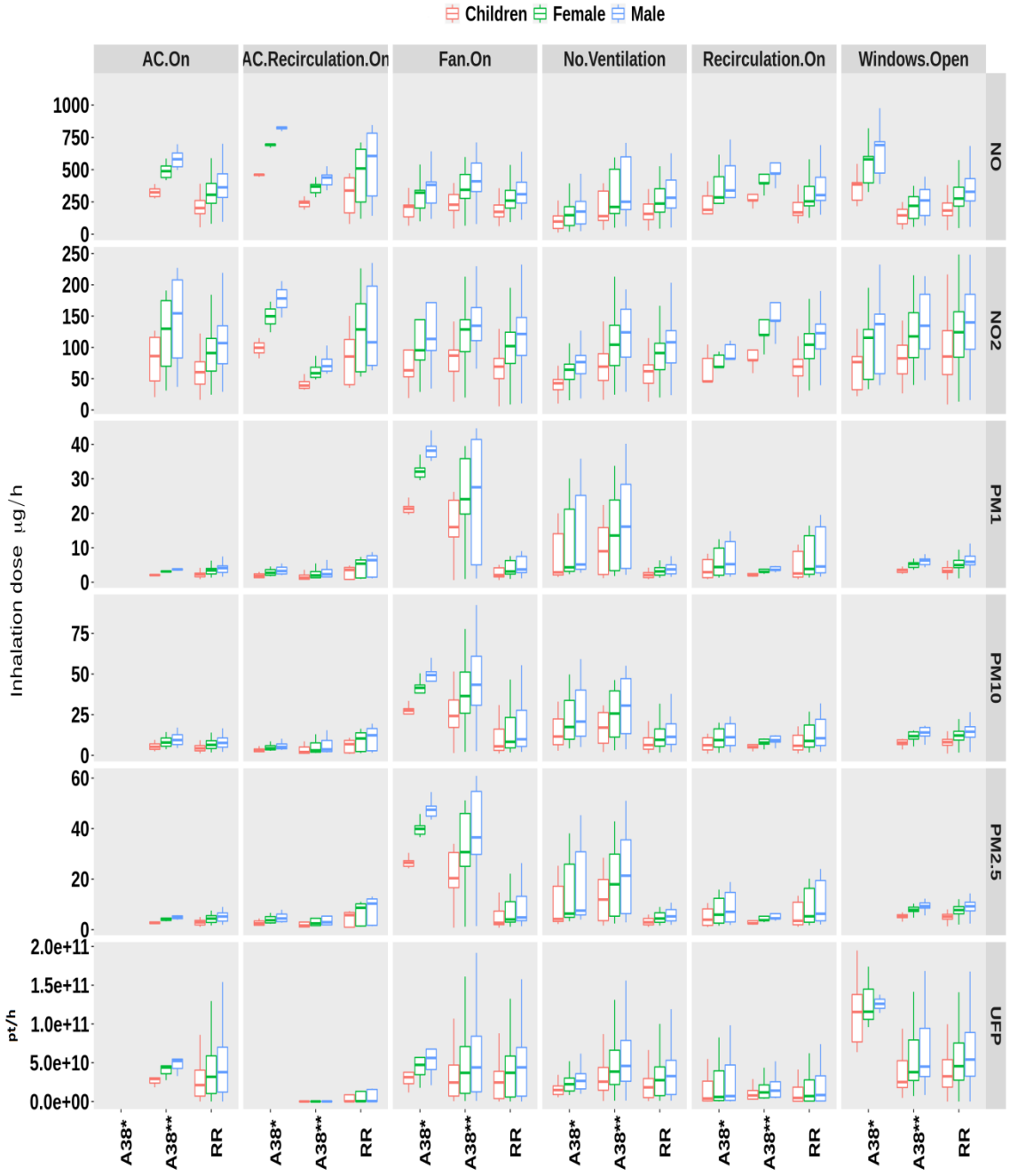


Figure 3.17: Air pollutant inhalation doses of male, female and children vehicle occupants under different ventilations settings and road types. A38*: sub-urban road part; A38**: urban road part; RR: Ring road part. The boxplot percentile values are 0.05 (starting line), 0.25 (lower box boundary), 0.50 (mid box line), 0.75 (upper box boundary), 0.95 (ending line).

# 3.4 Discussion

Exposure of vehicle occupants to $PM_{10}$, $PM_{2.5}$, $PM_1$, UFP, LSDA, NO and $NO_2$ was notably elevated when driving on sub-urban compared to urban roads, however no difference was observed regarding the different days of the week; this is also illustrated by the similar median $I/O_{VEH}$ levels between the four vehicles (see Figure 3.15). When driving from sub-urban to urban and ring-roads, the median within-vehicle exposure (across all ventilation options), increased significantly by 73% and 13% for $PM_{10}$, 175% and 75% for $PM_{2.5}$ and 200% and 83% for $PM_1$ respectively. For UFP and LSDA the exposure was increased by 24% (sub-urban to urban) and 36% (sub-urban to ring road), and (LSDA) 32% and 52%, respectively. $NO_x$ was also significantly higher with a 69% (sub-urban to urban) and 44% (sub-urban to ring road) increase in median exposure for $NO_2$ and 70% (sub-urban to urban) and 11% (sub-urban to ring road) for NO. This reveals that route choice has a significant impact on vehicle occupant's personal exposure to urban air pollution. As illustrated in Figure 3.11 the within-vehicle air pollution levels follow similar variations to the outside levels, as we drive along different types of roads, *i.e.* personal within-vehicle exposure co-varies to some extent with the outside exposure levels. However, a difference in the range of the outside concentrations of the van can be seen in Figure 3.11 (green boxplot). This probably due to the location of the sampling inlet which was located 1 meter higher than that of the passenger vehicles. Past studies suggest an exponential decay of

pollutants with increasing height within street canyons (Kumar et al., 2008) and signalised traffic intersections (Goel and Kumar, 2016), while no such vertical decay has been reported at the sides of highway or motorways (Nakashima et al., 2014). As $I/O_{VEH}$ ratios change with different outside levels which in turn vary with height, the sampling location in an urban mobile measurement campaign (mainly because the side dispersion is blocked by building infrastructure) can play a role to $I/O_{VEH}$ pollutant exposure estimations. Thus the sampling location should be chosen carefully and depending on the needs of the campaign a closer to the road sampling location should be considered where possible.

The higher median exposure levels for both particles and gases measured within-vehicles in the city centre can be explained by the greater outside pollution levels, which in turn reflect traffic density. Elevated levels of ambient gases and particles were also observed close to all junctions and roundabouts. In our case, the route through the city centre also includes transects via an underground tunnel, where the highest concentrations were measured, due to limited dispersion. Similar elevated levels have been reported in other studies (Martin et al., 2016; Yamada et al., 2016). The slightly higher exposure to UFP and LSDA that was observed for the ring road (in comparison to the urban and sub-urban roads) may reflect the greater percentage of heavy goods vehicles (on a daily basis 10 times more heavy goods vehicles on the ring road than urban and sub-urban journey), which are strongly associated with on-road UFP concentrations (Crilley et al., 2012; Fruin et al., 2008; Knibbs et al., 2009).

Some systematic variation in $NO_2$ and $NO_x$ concentrations (see Figure 3.12) may also arise from different operating levels of vehicle emissions control

technologies/after treatment systems – if there is a different preponderance of very short vs longer journeys between the road types, and hence different proportions of vehicles running at normal operating temperature vs under cold start conditions (Matthaios et al., 2019; Grange et al., 2019).

### 3.4.1 The impact of ventilation on air pollution exposure of vehicle occupants

The vehicle ventilation setting makes a significant difference to $I/O_{VEH}$ ratios, hence to the impact of outdoor pollution levels upon personal exposure within vehicles. More specifically, the "AC" ventilation setting reduced significantly the levels of $PM_{10}$, $PM_{2.5}$, $PM_1$, by 27-29%, UFP by 38% and $NO_2$ by 31% compared to on-road levels. Part of this may arise from surface losses as the outside air, following cabin air-filter filtration, passes from the condenser to the evaporator via a heat exchanger.

Under the ventilation condition of "air conditioning with recirculation enabled" (AC_R), the greatest and most significant reductions in air pollution exposure were observed, with the lowest $I/O_{VEH}$ ratios; reductions relative to outside/ambient levels ranged from 37% ($PM_1$) to 53% ($PM_{10}$), while $NO_2$ was also 30% lower (but similar to other ventilation settings) inside the cabin. It should be noted here that modern vehicles normally recirculate a portion of cabin air alongside fresh intake before the

evaporator, which may also play a role in the reduction. We note that there is additional energy requirement to operate AC systems, increasing fuel consumption and hence both air pollutant and $CO_2$ emissions (for internal combustion engine vehicles), worsening overall ambient air quality.

With the "fan on" ventilation setting (FAN), vehicle passengers are exposed to levels of within-vehicle coarse particles ($PM_{10}$ - $PM_{2.5}$) ca. 20% lower than those found immediately outside the vehicle, while levels of fine particles ($PM_1$) and UFP, LSDA as well as $NO_x$ are similar to or occasionally higher than outside levels (see Figure 3.14, Table 3.4). The dominant sources of the fine and lung-deposited particles, and $NO_x$, are expected to be vehicle tailpipe emissions in urban areas, although non-exhaust particles (mainly $PM_{2.5}$ and $PM_{10}$ from brakes/tyres), other gases and evaporative fuel and oil related VOCs such as those coming from the engine can also contribute to occupant exposure where ambient air enters the vehicle cabin (Fedoruk and Kerger, 2003).

When the "fan recirculation" ventilation setting (FAN_R) was in operation, $PM_{10}$, $PM_{2.5}$, $PM_1$, UFP and LSDA exposure were significantly reduced for vehicle occupants relative to outside levels, by about 50% across all PM classes and by more than 80% for UFP and 60% for LSDA. This result is in accordance with previous studies (Knibbs et al., 2010; Hudda et al., 2011; Yamada et al., 2016). The FAN_R option reduces within-vehicle particulate pollution and exposure inside vehicles by circulating the air inside the vehicle, since cabin air passes through the particulate pollen filter multiple times (by allowing only a very small portion of air from outside to penetrate inside). Recirculation settings will increase within-cabin residence time, as only a small

fraction of fresh air enters to be mixed with the recirculated air. This in turn provides more time for the $NO_x$ - $O_3$ photo-stationary steady state to evolve away from that determined in the outside/ambient environment – leading to elevated $NO_2$ due to the production of $NO_2$ via reactions of NO with $O_3$. This is supported by the measurements of $NO_2$ and $O_3$ species inside the cabin as illustrated in Figure 3.18, where for a given within-vehicle $NO_x$ mixing ratio when the within-vehicle $NO_2$ increases the within-vehicle $O_3$ deceases. This chemistry will contribute to the observation of an elevated $I/O_{VEH}$ ratio for $NO_2$ if compared with AC ventilation settings (see Table 3.4). Over time, the impact of other processes (notably, $O_3$ deposition to surfaces) may alter and eventually reverse this effect. The timescale for the $NO_x$ photo-stationary steady state is of the order of 50 seconds (under typical continental boundary layer daytime conditions), while the volume residence time (volume/inflow) can be as little as 30 seconds (calculated from 0.10 $m^3$/s flow rate for a typical 3 $m^3$ cabin under full fan power operation), indicating that inflow of external air will typically dominate over photo-stationary steady state effects in non-recirculatory full ventilation modes, and to a lesser extent under reduced ventilation.

As illustrated in Figure 3.19, the $I/O_{VEH}$ ratio of different pollutants varies notably with different fan setting/speed, as also observed by Martin et al., (2016), where changing fan power from 0 to 50% and 100%, increased the median $NO_2$ I/O ratio from 0.21 to 0.64 and 0.83 respectively.

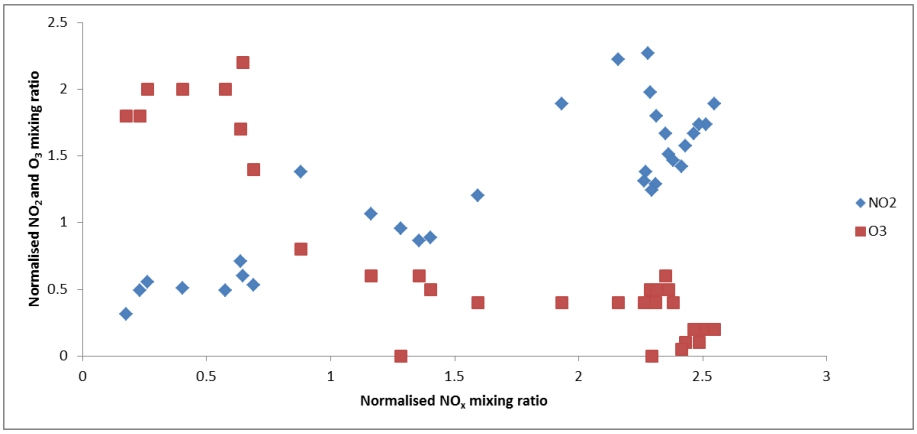


Figure 3.18: Normalised (to the mean) variation of within-vehicle $NO_2$ and $O_3$ mixing ratios under FAN_R (fan on, recirculation on, AC off and windows closed) ventilation setting in Vauxhall Insignia.

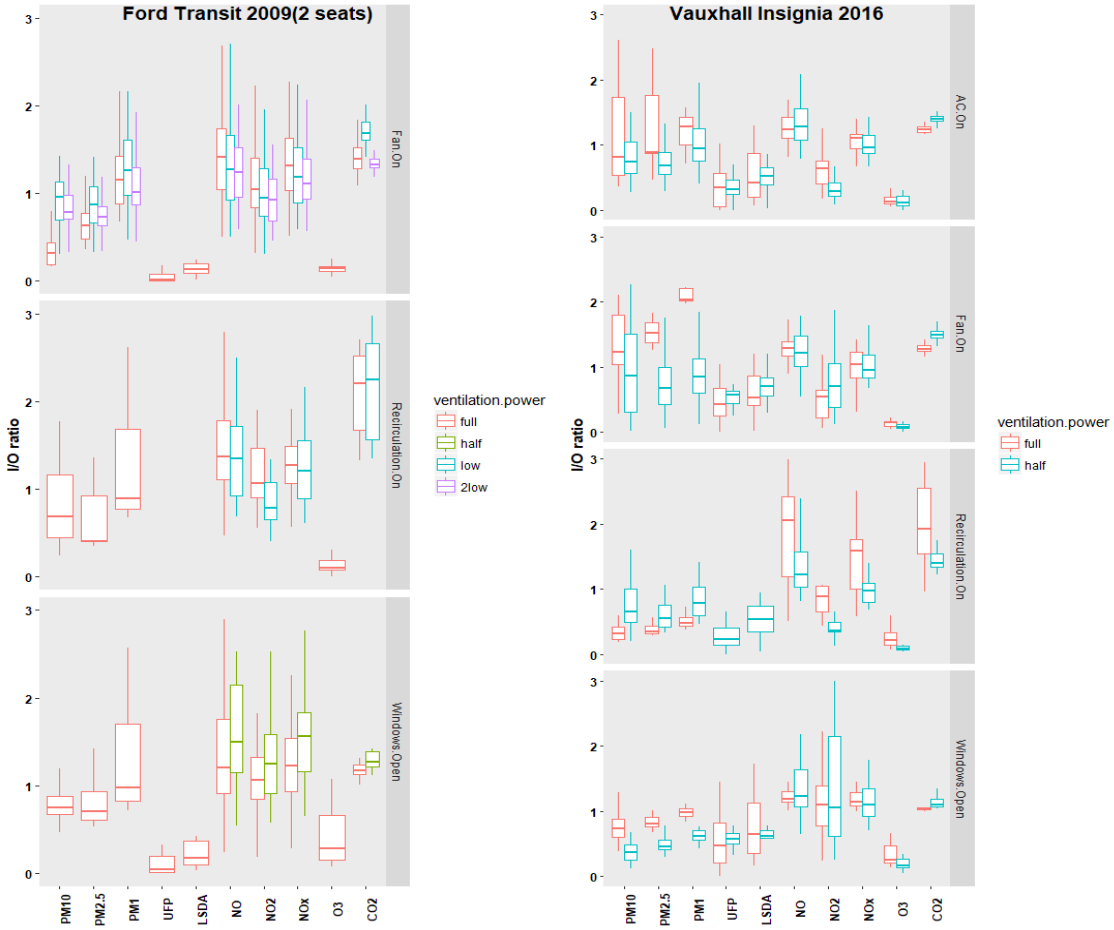


Figure 3.19: Ventilation power impact in the I/O ratios of species under different ventilation settings.

Under the "open windows" ventilation setting (OPEN), we observe elevated $I/O_{VEH}$ ratios of $PM_1$, UFP, LSDA and NO, $NO_2$ and lower ratios for $PM_{10}$ and $PM_{2.5}$ compared to the other ventilation settings, with levels approaching ambient. If the vehicle under consideration is following traffic ahead, it will enter the leading vehicle's exhaust plume; for the prevalent low-level exhaust pipe, larger particles of that exhaust plume are deposited faster (Ning et al., 2005) and only a fraction may reach the height of the following vehicle's windows and enter the cabin. This is reflected in almost all ventilation settings where we see about 30% smaller $I/O_{VEH}$ ratios relative to outdoor levels for $PM_{10}$ and $PM_{2.5}$ (Table 3.4). On the contrary, finer particles ($PM_1$, UFP) and gases like $NO_2$ may be more readily dispersed over greater distances due to the vehicle's mechanical turbulent kinetic energy (Wang et al., 2006) and thus more readily enter the cabin of the vehicle behind, depending upon the precise plume dynamics and driving conditions.

With no ventilation active and windows closed (NONE), vehicle occupants were exposed to approximately 20% lower $PM_{10}$ and $PM_{2.5}$ concentrations in comparison to outside levels. The within-vehicle exposure to ultrafine particles and LSDA (of greatest importance for some health effects - Oberdorster et al., 2007) and to $NO_2$ was also reduced by 63%, 44% and 30% respectively. However under this ventilation option, and depending on the number of the vehicle occupants, a quick build-up of $CO_2$ inside the cabin, from 1000-2500 ppm, might have an impact in decision making performance or cause other cognitive effects (Satish et al., 2012). Figure 3.20, shows that the $CO_2$ builds-up quickly up to 3500 ppm for the first 60 min of driving under fan off, while $NO_2$ and PM remain relatively low. After the first 60 min and the change in ventilation

to fan on, $CO_2$ levels are dropping to ambient levels, however, PM raise substantially inside the vehicle's cabin.

These results suggest that the $I/O_{VEH}$ ratios for particles increased towards 1 (outdoor) when bringing a greater quantity of air from outside, as anticipated, while when recirculating the air inside the cabin they are reduced up to 80% relatively to the outdoor levels. However, under recirculation mode, there is potentially a trade-off between benefits in terms of reduced PM, but also a penalty in terms of increased $NO_2$. This suggestion needs further investigation due to the modest sample size reported here and potentially confounding factors such as concentration of within-vehicle VOC, ambient weather conditions, sunlight and within-vehicle photolysis rates.

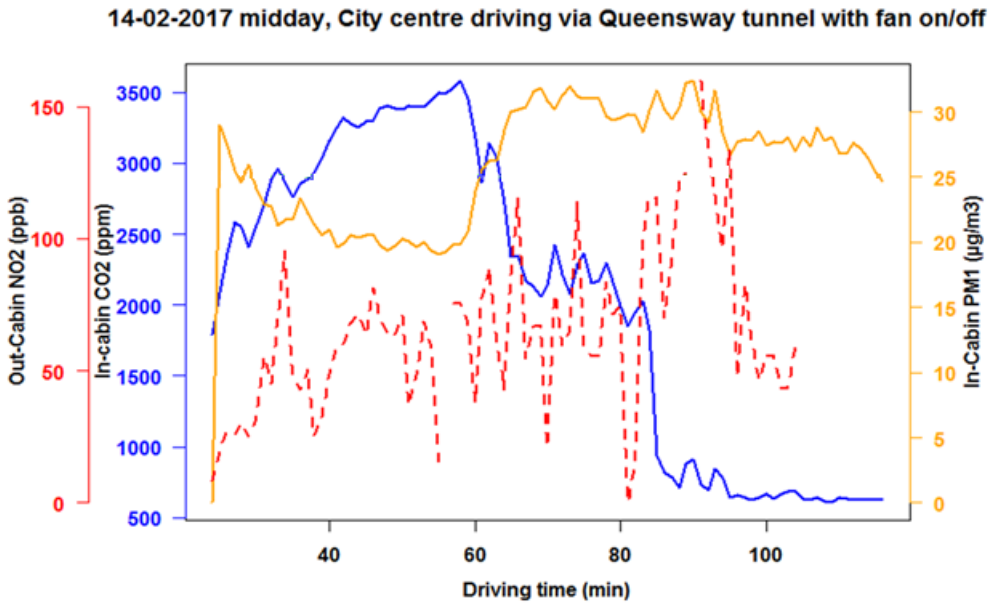


Figure 3.20: Within-vehicle cabin variation of $CO_2$, $NO_2$ and $PM_1$ with fan on and off. Blue: $CO_2$ concentrations, Orange: within-vehicle $PM_1$ concentrations, Red: On-road $NO_2$ levels.

### 3.4.2 Inhalation doses

Calculated inhalation doses for vehicle occupants in urban, sub-urban and ring road locations provide insights to the dynamic exposure that vehicle occupants undergo. Comparison of inhalation doses within-vehicles, directly outside vehicles and from the air quality stations at an urban traffic location and an urban background location (where most human exposure occurs) can give an insight into exposure. Under the assumption that the outside vehicle levels measured here represent the exposure that cyclists or people that do light exercise (e.g. road construction workers, runners) have, and that for those exposed at a greater distance from roads the data obtained from roadside and background air quality station levels are representative of pedestrian exposure, the median hourly air pollution inhalation dose of vehicle occupants is the least of the three activities. Regarding the regulated air pollutants $PM_{2.5}$ and $NO_2$, people driving in urban areas inhale a lower total mass (averaged in all ventilation options), compared to pedestrians by a range of 10% to 30% for $PM_{2.5}$ and 5% to 18% for $NO_2$, for all categories (male, female and children). Vehicle occupants also (across all categories) inhale less than cyclists (or people that do light exercise nearby the road) at about 52% to 63% for both $PM_{2.5}$ and $NO_2$. For sub-urban roads, vehicle occupants were found to inhale about 70% less $PM_{2.5}$ and 12% less $NO_2$ (across all categories) when compared to pedestrians, while when compared to cyclists (or people performing other light outdoor activities), car passengers (all categories) inhale

about 60% less $PM_{2.5}$ and about 50% less $NO_2$. For the ring road type environment, it was calculated that vehicle occupants inhale 60% less $NO_2$ and 12.5% to 33% less $PM_{2.5}$ than those exercising outside. However, it should be noted that these comparisons might vary if the activity comparison was performed for congested periods or in specific places (e.g. while waiting at traffic signals). Although in this study we did not measure any activity based personal exposure, according to the study of Dons et al., (2012), who performed activity based personal exposure experiments, commuting was accountable for 30% of our total daily dose to air pollution in comparison to 22% that was attributed to home-based activities. From the amount attributable to commuting, moving by car presents greater dose contribution compared to bus or train.

In terms of exposure variation as a function of road type, those driving on urban roads inhale significantly elevated $NO_2$ and particles compared to those driving on sub-urban and ring-roads. Specifically, vehicle passengers in an urban driving route inhale 56% and 100% more $PM_{10}$, 225% and 550% more $PM_{2.5}$, 233% and 250% more $PM_1$, 25% and 13% more UFP, and 71% and 18% more $NO_2$ compared to those driving on sub-urban and ring-roads, respectively. Vu et al. (2018) reported UFP doses of 16.8 × $10^9$ particles/h for males living close to roads, in good agreement with the experimental observations, where male vehicle occupants inhaled 19.1 × $10^9$ particles/h.

The short-term health impacts of $NO_2$ and $PM_{2.5}$ can be compared via calculation of their effect on all-cause mortality (Harrison and Beddows, 2017). The Hazard Ratios for all-cause mortality according to the World Health Organisation HRAPIE report (WHO, 2013) are 1.037 for $NO_2$ per 10 μg/$m^3$ and 1.062 for $PM_{2.5}$ per 10

$\mu g/m^3$. This gives a relative impact of the two species per unit mass of $NO_2/PM_{2.5}$ = 0.037/0.062 = 0.60. It is highly likely that there is an overlap between the associations for $NO_2$ and $PM_{2.5}$, although there are considerable uncertainties in estimating the size of this overlap, as most cohorts that are exposed to air pollution, are probably exposed to both $NO_2$ and $PM_{2.5}$ and vice versa (COMEAP, 2018). In our study, the median vehicle occupant's absolute inhalation dose ratio of $NO_2$ to $PM_{2.5}$ is 4.6 for urban, 7.6 for sub-urban and 6.9 for ring road environments. This gives a trip average inhalation dose of 6.4 ($NO_2$ dose/$PM_{2.5}$ dose) meaning that vehicle occupants inhale a greater mass of $NO_2$ than $PM_{2.5}$. Despite the uncertainties around this ratio, the implication for professional drivers is that the premature mortality impact of nitrogen dioxide is currently greater than that of $PM_{2.5}$ under the test conditions assessed in this work. This impact might be even bigger if one considers that NO is quickly oxidised to $NO_2$.

### 3.4.3 Potential implications for public health

The UK-population-average time spent as a vehicle occupant was recently reported as 216 hours per year (DfT, 2016). If this corresponded to solely urban area journeys, and these in turn were equivalent to the study area considered here, a male individual would overall inhale 13,800 µg of $NO_2$ and 3,000 µg of $PM_{2.5}$ per year

(inhalation doses from Table 4), which underpins the higher impact of $NO_2$ over $PM_{2.5}$ for vehicle occupants. Spatial within-vehicle maps under different ventilation settings revealed that $PM_{2.5}$ levels are more ventilation dependant than $NO_2$, potentially due to the efficacy of pollen filters (Vande Hey et al., 2018). This highlights the benefit from using e.g. effective active carbon/charcoal filters to capture $NO_x$ (Yoo et al., 2015) in parallel. The NO $I/O_{VEH}$ ratio was found to be essentially independent of the vehicle size and ventilation preference (in the four tested vehicles, all equipped with pollen filters). Although not a regulated air pollutant, the bioactivity of NO is implicated in elevated blood pressure and in arterial stiffness, a major mechanism of systolic hypertension (Hermann et al., 2006).

The "air-conditioning with recirculation" (AC_R) ventilation option was found to minimise the vehicle occupant exposure to the pollutant species measured here. We note that some within cabin/ambient air exchange still occurs, even under this setting. Air exchange rates are dependent on the vehicle make/model and (to an extent) condition (Hudda et al., 2012).

A number of additional factors related to personal exposure and health impacts from inhaled pollutants could not be considered in this work. In addition to a greater study size (vehicle type, filtration option, road type etc.), these include more in-depth study of the within-vehicle air chemistry and abundance of other species (including VOCs, polycyclic aromatic hydrocarbons, $CO_2$, CO, $O_3$ and other species). We have also not considered the likely contrasting impacts of different PM chemical composition and morphology.

Vehicle occupants are exposed to key detrimental air pollutants of $PM_{2.5}$ and $NO_2$ with overall median inside-vehicle/outside-vehicle ($I/O_{VEH}$) ratios of 0.76 and 0.98 for $PM_{2.5}$ and $NO_2$ respectively. For the optimal (lowest exposure) ventilation setting, within-vehicle exposure to $PM_{2.5}$ and $NO_2$ is reduced by 49% and 34% respectively. Overall, vehicle occupants inhale 45% less $PM_{2.5}$ and 12% less $NO_2$ compared to pedestrians, and 47% and 57% less $PM_{2.5}$ and $NO_2$ than cyclists. Passengers can modify their exposure and inhalation dose through route choice by factors of 1.25 – 3.5 and 0.4 – 0.45 for $PM_{2.5}$ and $NO_2$ respectively. In all the above, the vehicle route and ventilation choice has a significant influence upon occupant personal exposure to air pollution.

Chapter 3 investigated within-vehicle air pollution under different ventilation settings and routes in and around Birmingham (UK) and found significant implications for the elevated $NO_2/PM_{2.5}$ inhalation dose of vehicle passengers. As the results of this chapter might be case specific a more robust approach is needed in order to estimate within-vehicle exposure at any given situation. Therefore, the following chapter (4) explores the development of two complementary modelling approaches that can be used to estimate within-vehicle exposure levels more widely.

# Chapter 4. Prediction of within-vehicle exposure by traditional and machine learning modelling approaches

This chapter reports the development of two complementary approaches to simulate within-vehicle passenger exposure to air pollutants ($PM_{10}$, $PM_{2.5}$, $PM_1$, UFP, LSDA, $NO_2$ and $NO_x$) as a function of outside (ambient) levels, under different vehicle ventilation conditions. The first approach involves the development of a mass-balance model, which explicitly represents physical and (some) chemical processes which drive changes in air pollutant abundance. The second approach uses machine-learning algorithms, which seek to replicate the observed within-vehicle data based upon a training set of observations, and does not include any mechanistic representation. Results from the mass-balance model (a) are compared with time series measurements of within-vehicle concentrations. Results from the machine-learning model (b) are compared with a subset of observations which were excluded from the training dataset. Both models estimated within-vehicle air pollution exposure using different inputs: (i) measurements from directly outside the tested vehicles and (ii) measurements from nearby air quality monitoring stations, thus providing new capability for exposure prediction for vehicle occupants and professional drivers.

## Graphical Abstract

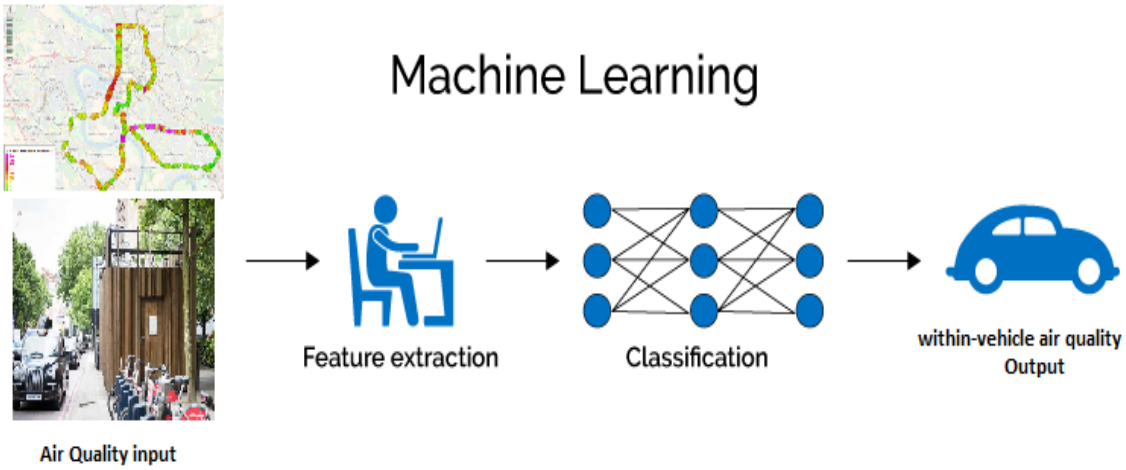


# 4.1 Introduction

Vehicular sources, including both combustion and non-exhaust sources, dominate primary emissions of nitrogen dioxide ($NO_2$) and are significant contributors to particulate matter ($PM_{10}$, $PM_{2.5}$, $PM_1$ and ultrafine particles - UFP) in urban environments. Numerous studies have highlighted the relationship between traffic related particulate air pollution and adverse health effects such as cardiopulmonary

disease, respiratory symptoms, lung function and changes in cardiac function (Heal et al., 2012; Atkinson et al., 2010; De Hartog et al., 2010; Delfino et al., 2005). Traffic related $NO_2$ exposure, in particular, has been associated with increased lung cancer and reduced lung function (Adam et al., 2015; Hamra et al., 2015; IARC, 2014).

High volumes of road traffic within urban areas often dominate sources of urban air pollution, providing strong roadside concentration increments relative to suburban, rural and other residential areas (Harrison, 2018). The interior of vehicles represent a further microenvironment where enhanced or reduced exposure to traffic related air pollution can occur; moderated through air exchange with the ambient environment, and within-vehicle physical and chemical processing which can affect species concentrations. However, given the comparatively short duration of most commuting trips (with vehicles), many fundamental indoor air quality studies have focussed on other microenvironments such as homes, work places and schools.

The significance of within-vehicle exposure varies with travel, commuting behaviours, trip duration and occupant vulnerability. According to TomTom traffic index, congested periods in urban areas globally have increased from 2018 to 2019 by a range of 2% to 18% (TomTom, 2019). As a consequence, the time spent within vehicles in large cities (population > 800 000) worldwide has increased during morning and evening rush hours by up to 42 minutes (TomTom, 2019). In UK, there are approximately 32 million registered full driving license holders, of which 6% are professional drivers (DfT, 2017) who may be particularly subject to extensive exposure to within-vehicle air pollution.

Previous experimental studies exploring exposure inside vehicles while commuting have found within-vehicle concentrations to be a factor of 2-3 larger than in other transport modes (e.g. De Nazelle et al., 2012; Zuurbier et al., 2010). Delgado-Saborit, (2012) reported the ratio of concentrations inside a vehicle to the ambient air concentration as determined from air quality monitoring sites (also known as the ambient air ratio) of 4.5 for BC (a marker for combustion, UFP and PM) and 1.4 for $NO_2$ in Birmingham (UK). Other studies investigated the impact of ventilation settings on within-vehicle exposure and found that exposure was highly dependent on the amount of air intake, age of the vehicle and leaks (Martin et al., 2016; Hudda et al., 2012; Knibbs et al., 2010). Limited studies have also directly compared within-vehicle and immediately outside/adjacent air pollution levels and exposure to both particulate and gaseous species (Matthaios et al., 2020; Yamada et al., 2016); highlighting the potentially greater health impact of $NO_2$ over PM exposure. All the aforementioned studies can be considered limited to their experimental conditions, and in order to predict air pollutant concentrations inside vehicles under any given circumstance, it is essential to develop accurate generalised modelling approaches.

## 4.2 Methods

In this section a brief summary of the measurement data used is explained, followed by an introduction of the processes that affect within-vehicle air quality. A summary of the physical parameters that affect within-vehicle air quality included in the mass balance model (A) is given together with the mass balance model equations, description and initial conditions. A detailed description of the machine-learning model (B), its training and validation process is presented followed by an evaluation of metrics and scenarios which were constructed to test both models in real world situations.

### 4.2.1 Measurements

The model development and validation was supported by measurements of $CO_2$, NO, $NO_2$, $O_3$, $PM_{10}$, $PM_{2.5}$, $PM_1$, ultrafine particle number (UFP) and lung surface deposited area (LSDA). These measurements were performed simultaneously within the vehicle cabins (breathing zone of the driver) and directly outside (in front or at the back window of) the tested vehicle. Measurements were performed during two

periods in 2017 on a consistent route featuring sub-urban, an urban and ring roads around Birmingham (UK). Temperature and relative humidity were also measured inside the vehicle cabin. Information regarding instruments, sampling periods and measurements obtained are presented in chapter 3 and median values are summarised here (Table 4.4) to provide context for the modelling analysis which is the main focus of this chapter.

### 4.2.2 Vehicles and ventilation conditions

Measurements were performed using four vehicles (see Table 4.1). Three of the vehicles were equipped with air conditioning (AC) and fitted with pollen filters (one had no cabin intake air filtering (by specification)). Five core ventilation settings were tested: (a) windows open, fans and AC off; (b) Fans on - AC & recirculation off and windows closed; (c) Fan plus AC on, recirculation off, windows closed (d) Fan plus recirculation on, AC off, windows closed (e) Fan plus AC and recirculation on, windows closed (in two vehicles) and (f) windows closed, AC, fans and recirculation off. Fan power in two of the vehicles was full or off, while in two vehicles intermediate fan power settings were also tested. Each ventilation setting was treated independently within the model (for details see later Table 4.3).

Table 4.1: Vehicles and their characteristics used in this study.

| Characteristics | Ford Focus | Vauxhall Insignia | Hyundai i800 | Ford Transit |
|---|---|---|---|---|
| Vehicle type | Estate | Estate | 9 seater van | Cargo van |
| Model year | 2013 | 2016 | 2017 | 2009 |
| AC | Yes | Yes | Yes | No |
| Est. volume ($m^3$) | 3.46 | 3.28 | 3.92 | 2.16 |
| Est. surface area ($m^2$) | 2.65 | 2.76 | 3.70 | 0.81 |
| Air filter | Pollen | Pollen | Pollen | None |

### 4.2.3 Air exchange processes

There are several processes that influence within-vehicle concentrations. Physical air exchange processes are represented schematically in Figure 4.1, and overall give rise to the air exchange rate (AER) from a combination of the ventilation system and/or leaks. AER is an important parameter that accounts for all routes of air exchange and explains overall pollutant transport into the vehicle cabin. A moving vehicle experiences aerodynamic effects, which can affect surface pressures. The surface pressure can increase or decrease as a function of driving speed, but it is also specific to the locations. The surface pressure of a moving vehicle is lower on the side doors than on the rear surfaces (Kang et al., 2012; Song et al., 2012; Tilch et al., 2008). In addition to the driving speed, the leakage airflow rate could also change due to cabin pressurisation under mechanical ventilation conditions (i.e. AC on mode).

Therefore, it is important to take into account the ventilation modes, fan settings, driving speed, and vehicle shape when studying automotive envelope leakage and/or infiltration of pollutant concentrations expressed as μg/m$^3$ to the passenger cabin. From the fluid mechanics perspective, the envelope leakage can be described in a power-law correlation with two parameters: the flow coefficient ($C_f$) and the pressure exponent (*n*) (ASHRAE, 2005; ASTM, 2010). These two parameters can be obtained based on the measurements of supplied ventilation airflow rate ($Q_s$) and the associated changes in differential pressure (*dP*). Within-vehicle pollutant introduction may be modified by filtering (in the case of the ventilation system) or other losses in the case of leaks (referred to as the penetration factor). Inside vehicle cabins, the flow of air that is mechanically supplied via the ventilation system is denoted $Q_S$, and is dependent upon the fan power and air vent surface area (see modelling parameters section 4.2.4). In this case, outside air passes through the air filter (when fitted) which has a specific collection efficiency ($f_{ef}$), depending on the type of filter, to remove particles and gases and only a fraction ($1 - f_{ef}$) of the outside concentrations will enter the cabin. Outside air can also enter the cabin via leaks; driven by the pressure difference between within-vehicle and outdoor environment (denoted $Q_L$) with a penetration factor *P*. Within-vehicle physical losses of air pollutants include: (1) deposition onto internal surfaces (e.g. seats, floor, clothes) with a deposition coefficient ($Dp$) that varies according to the species' aerodynamic properties; and (2) breathing rate of the vehicle occupants, ($Q_R$), where a certain fraction of the within-vehicle concentrations are removed as they are deposited into the human lungs ($RDp$). Exhalation was not considered here as an additional source in the model, as it is a

negligible source for the non-VOC species considered here (Knibbs et al., 2011). All parameters are summarised in Table 4.2.

Table 4.2: Parameters describing the physical processes around air exchange.

| Name | Symbol | Quantity | Units |
|---|---|---|---|
| Mechanical supplied air | $Q_s$ | Flow rate | $m^3/h$ |
| Vehicle leaks | $Q_L$ | Flow rate | $m^3/h$ |
| Breathing rate | $Q_R$ | Flow rate | $m^3/h$ |
| Deposition rate coefficient | $Dp$ | rate | $h^{-1}$ |
| Respiratory deposition coefficient | $RDp$ | dimensionless | - |
| Filter efficiency | $f_{ef}$ | dimensionless | - |
| Penetration factor | $P$ | dimensionless | - |

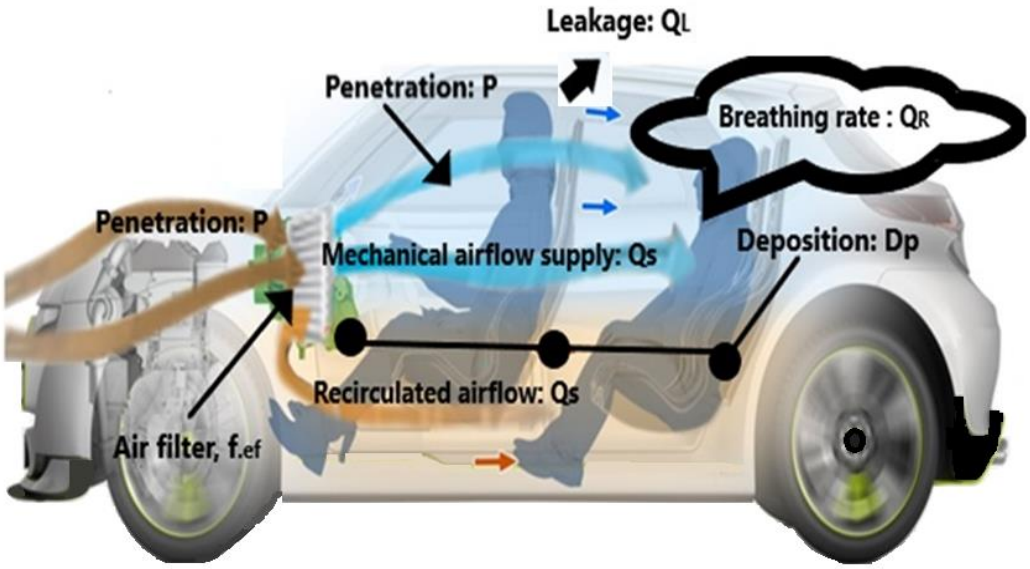


Figure 4.1: Schematic representation of the principal physical air exchange processes inside a typical vehicle cabin. When the Fan/AC are switched on to bring ambient outside air (brown arrow) within-cabin, the outdoor air passes thorough the filter ($f_{ef}$) and is mechanically supplied ($Q_S$) inside the vehicle (blue arrow). When the setting is on recirculation (orange arrow) the air inside the cabin again passes through the filter and is resupplied inside the cabin. While these settings occur, there are processes such as breathing rate of the vehicle occupants ($Q_R$), deposition ($Dp$), penetration of outside air inside ($P$) and vehicle leaks ($Q_L$) that happen in parallel.

## 4.2.4 Within-vehicle modelling

### 4.2.4.1 Mass balance model (A) description and equations

The model developed in this study predicts concentrations within the vehicle cabin arising from outside sources. However, such models can also simulate the impact of internal sources (e.g. resuspension of deposited particles) under the correct modifications. More specifically, for a given time interval, the model will define the rate of change of the within-vehicle concentration (following Xu and Zhu, 2009; Knibbs et al., 2010) by using a mass-balance approach as: the concentration that comes from the outside/on-road air as a function of ventilation, minus the within-vehicle concentration and the losses that occur inside the vehicle cabin. In order for the model to be sensitive to the rapid outside concentration changes (due to congestion, traffic lights, vehicles overtaking) the time step that we used in this study to predict the within-vehicle concentrations was 1 min. This time step is also adequate to capture all the important processes inside a typical car cabin (Xu and Zhu, 2009). The mathematical equation for model (A) that describes the within-vehicle cabin physical processes illustrated in Figure 4.1 is given in Eq (1). Model (A) hypothesizes that the air enters in a well-mixed microenvironment inside the vehicle cabin.

$$\frac{d(C_{inj}V)}{dt} = C_{outj}\left[Q_S(1-f_{ef}) + Q_L P_j\right] - C_{inj}[Q_R RD_p + Dp_j V + (Q_S + Q_L)] \quad [1],$$

The left hand side of Eq (1) represents the rate of change of the within-vehicle mass, where $C_{inj}$ is the j concentration inside the vehicle, $C_{outj}$ is the j concentration outside the vehicle, $Q_S$ is the mechanical supply flow, $Q_L$ is the leakage flow, $Q_R$ is the respiratory breathing rate of the vehicle occupants, $V$ is the volume of the vehicle, $f_{ef}$ is the filtration efficiency, $P_j$ is the penetration factor, $RD_p$ is the deposition rate coefficient of the respiratory system of vehicle occupants, $Dp$ is the deposition rate coefficient inside the vehicle and $t$ is the time.

Under steady state/equilibrium, Equation (2) is the analytical solution for Equation (1), while in order to identify which processes dominate in each ventilation setting, Equation (2) changed accordingly and the analytical solution for each ventilation type is provided in Table 4.3. Outdoor concentrations change dramatically over a short period of time, which is very common for on-road conditions. For that reason Equation (1) can be solved numerically to Equation (3) with respect to outdoor concentration variations by using a time-step approach. In Eq (3) $C'_{inj}$ represents the final concentration after a defined time interval and $C_{inj}$ is the initial concentration inside the vehicle at the start of the time interval $\Delta t$. The different ventilation options of this are described in Table 4.3.

$$\frac{C_{inj}}{C_{outj}} = \frac{[Q_S(1-f_{ef})+Q_L P_j]}{Q_R RDp_j + Dp_j V + (Q_S+Q_L)}, \quad at\ t = \infty \quad [2],$$

$$(C'_{inj} - C_{inj})V = \left[C_{outj}(Q_S(1 - f_{ef}) + Q_L P_j) - C_{inj}\left(Q_R RDp_j + DP_j V + (Q_S + Q_L)\right)\right]\Delta t \quad [3],$$

For gases, no heterogeneous reactions from surfaces etc. were taken into account, since their impact is considered insignificant with respect to the external sources and Equation (3) was modified to Equation (4) for $NO_x$ considering only PSS reactions, where $R_{ij}$ is the reaction rate between species *i* and *j*.

$$(C'_{inj} - C_{inj})V = \left[C_{outj}(Q_S(1 - f_{ef}) + Q_L P_j) - C_{inj}(Q_R RDp_j + DP_j V + (Q_S + Q_L) + \sum_{j=1}^{n} R_{ij})\right]\Delta t \quad [4],$$

Table 4.3: Equations used to predict within-vehicle concentrations with different ventilation settings. (a) Air condition (AC) on with fan a full power, (b) Fans on without AC or recirculation on, (c) recirculation on, fan low power, (d) windows open, fans and AC off and (e) windows closed, AC fans and recirculation off.

| | Ventilation setting | Equations | Predominant factors |
|---|---|---|---|
| Analytical solution | (e) | $\frac{C_{ij}}{C_{oj}} = \frac{Q_L + P_j}{Q_R R D p_j + D p_j S + Q_L}$ | Penetration factor ($P_j$), Deposition coefficient ($Dp_j$), Leakage rate ($Q_L$) |
| | (a), (b), (d) | $\frac{C_{ij}}{C_{oj}} = \frac{[Q_S(1 - f_{ef}) + Q_L P_j]}{Q_R R D p_j + D p_j S + (Q_S + Q_L)}$ | Mechanical airflow ($Q_S$), Filter efficiency ($f_{ef}$) |
| | (c) | $\frac{C_{ij}}{C_{oj}} = \frac{Q_L + P_j}{Q_R R D p_j + D p_j S + (Q_S f_{ef} + Q_L)}$ | Leakage rate ($Q_L$), Penetration factor ($P_j$), Deposition coefficient ($Dp_j$) |

| | Ventilation setting | explicit Euler forward approximation |
|---|---|---|
| Numerical approach | (e) | $(C'_{inj} - C_{inj})V = [C_{outj}(Q_L + P_j) - C_{inj}(Q_R R D p_j + DP_j V + Q_L)]\Delta t$ |
| | (a), (b), (d) | $(C'_{inj} - C_{inj})V = \left[C_{outj}(Q_S(1 - f_{ef}) + Q_L P_j) - C_{inj}\left(Q_R R D p_j + DP_j V + (Q_S + Q_L)\right)\right]\Delta t$ |
| | (c) | $(C'_{inj} - C_{inj})V = \left[C_{outj}(Q_L + P_j) - C_{inj}\left(Q_R R D p_j + DP_j V + (Q_S f_{ef} + Q_L)\right)\right]\Delta t$ |

#### 4.2.4.2 Model (A) initial conditions

The initial conditions for penetration and filtration removal for different species in model (A) were taken from Table 4.4, and were values reported in the literature and adopted accordingly to our experiments. Deposition coefficient rates for each species were taken from the literature and adjusted for each vehicle according to their surface to volume ratio reported in Table 4.5. Leaks were taken for each vehicle from Figure 4.3 for 40 kmh, while for mechanical flow a single value was used throughout the simulations and adjusted for intermediate or full fan power (see Table 4.5). Respiration deposition and breathing rates were adjusted for two vehicle occupants. The initial concentrations (both inside and on-road) were the first values of the each vehicle run. Model (A) was run four times, each for every vehicle's measured timeseries, with the first output being 1 minute after the start time. The concentrations of all species in the model were calculated from the initial values. To further test for any dependence upon the applied conditions, the measured within-vehicle concentration was replaced with a median overall within-vehicle concentration and the model re-run again with all the other parameters remaining the same (for details see 2.7 case i).

Table 4.4: Parameters used for the eq (1), (2), (3) and (4); a) from Ott et al., 2008, b) Calculated in the study according to the ratio of $PM_{2.5}/PM_{10}$ and $PM_1/PM_{2.5}$, c) Values from Gong et al., (2009) for the median UFP (50nm) size in this study d) Values from Nazaroff and Cass, (1987) for indoor $NO_2$ decay rates in a house e) Values from Thatcher et al., (2003), f) Values from Williams et al., (2003), g) average value from the studies reported in Chen and Zhao, (2011), h) According to light exercise and sitting from Hinds (1999) for UFP size 50nm, i) Postlethwait and Bidani, (1990) j) Values from Qi et al., (2008); +: Values used for Windows open, ++: Values used for Fan on, AC on, +++: Values used for All closed, Recirculation on; *: Full fan power, **: Low fan power; ‡: No filter efficiency was applied since all the cars were equipped with pollen filters.

| Species | Deposition rate coefficient (Dp) | Penetration factor (P) | Respiratory deposition coefficient (RDp) | Filter efficiency (f.ef) |
|---|---|---|---|---|
| $PM_{10}$ | $123.76^{b+}$, $27.03^{b++}$, $13.26^{b+++}$ | $0.6^{e}$ | $0.65^{h}$ | $0.8^{j*}$, $0.6^{j**}$ |
| $PM_{2.5}$ | $72.8^{a+}$,$15.9^{a++}$,$7.8^{a+++}$ | $0.72^{f}$ | $0.65^{h}$ | 0.65j*, 0.45j** |
| $PM_1$ | $54.82^{b+}$,$11.93^{b++}$, $5.85^{b+++}$ | $0.8^{g}$ | $0.55^{h}$ | $0.4^{j}$ |
| UFP | $10^{c}$ | $0.8^{g}$ | $0.6^{h}$ | $0.25^{j}$ |
| LSDA | $10^{c}$ | $0.8^{g}$ | $0.6^{h}$ | $0.25^{j}$ |
| $NO_2$ | $39.6^{d}$ | 0.7 | $0.65^{i}$ | $0^{‡}$ |
| $NO_x$ | $39.6^{d}$ | 0.7 | $0.65^{i}$ | $0^{‡}$ |

Table 4.5: Parameters changed during the modelling between different vehicles. $Q_s$: Mechanical supplied air, $Q_L$: vehicle leakage, V: vehicle volume, S vehicle surface area. **: full fan strength; *: intermediate fan strength; $^{++}$: leakage at 30 kmh; $^{+}$ leakage at 40 kmh.

| | Ford Focus | Vauxhall Insignia | Hyundai i800 | Ford Transit |
|---|---|---|---|---|
| $Q_s$ ($m^3$/h) | 648** | 648** / 270* | 648** | 648** / 270* |
| $Q_L$ ($m^3$/h) | $30^{++}$ / $37.5^{+}$ | $26^{++}$ / $35^{+}$ | $25^{++}$ / $28^{+}$ | $38^{++}$ / $50^{+}$ |
| V ($m^3$) | 3.46 | 3.28 | 3.92 | 2.16 |
| S ($m^2$) | 2.65 | 2.76 | 3.70 | 4.81 |

## 4.2.5 Description of within-vehicle modelling parameters

### 4.2.5.1 Mechanical supply flow ($Q_S$)

Vehicle ventilation systems govern air exchange between the interior cabin air and the outside ambient air. The mechanical supply flow is calculated by multiplying the number of vents by the surface area of the air vent and the air flow speed. In general, the size of a typical vent depends on the manufacturer's design and varies in

vehicle with sizes from 30 to 60 $cm^2$. In this study, the model assumed four vents with constant sizes of 50 $cm^2$. For full fan power 6 m $s^{-1}$ airflow velocity was selected, while for intermediate fan power 2.5 m $s^{-1}$ was applied (Xu and Zhu, 2009). The calculated mechanical flows were 648 $m^3$/h, and 270 $m^3$/h for full and intermediate fan power levels, respectively.

#### 4.2.5.2 Leakage flow ($Q_L$)

Leakage flow out of the vehicles is driven by the pressure difference between the interior and outdoor environment and/or turbulence around the vehicle. The leakage flow depends on the ventilation settings, the vehicle manufacturer, as well as the model, age and the driving speed of the vehicle. The best approach for quantifying the leakage flow is to use a tracer gas to determine how much air enters a given space over time. In this study, $CO_2$ was used as a tracer gas for two reasons: 1) it can be used as a tracer for the outside sources (vehicle exhaust) and 2) the vehicle occupants can be used as a source (via breathing), and thus, individual ventilation setting can be estimated after subtracting the breathing rates of the occupants. To estimate the $CO_2$ generation rate of the occupants (2.3 ppm/s or 8,300 ppm/h) we used a simple linear regression model of $CO_2$ vs time inside the vehicles across all vehicles with no ventilation at 0 km/h assuming that under these conditions leakage was negligible. For

a given vehicle speed (strictly speaking, the vehicle air speed), the air exchange rate (AER) is nearly constant and the $CO_2$ concentrations inside the car will eventually reach an equilibrium value. Assuming a small air exchange rate when the car is stationary, with interior air well mixed, the vehicle-specific source term can be determined by the initial build-up rate of $CO_2$ when inside and outside $CO_2$ concentrations are similar. Therefore, $CO_2$ generation can be estimated by the gradient, as recommended by Fruin et al., 2011. Figure 4.2 shows the $CO_2$ generation rate of two vehicle occupants during the ford focus vehicle tests.

The leakage tests were conducted under real-world traffic conditions, with each test vehicle being driven at different speeds in urban, sub-urban and ring-road driving cycles. Nominal speeds of 30 to 40 mph were used, although the absolute speed varied according to the test conditions at the time of measurement. Testing under real-world traffic conditions was seen as the most appropriate approach given the purpose of the leakage test, which was to determine the validity of an existing model for cars, as reported in Hudda et al., (2012), in the UK fleet. The model equation is given as:

$$\ln(Q_L) = 2.79 + (0.019 \times S) + (0.015 \times v.age + 3.3 \times 10^{-3}\, v.age^2) + (-0.023 \times V + 6.6 \times 10^{-5} V^2) + m, \quad [1]$$

where, *S* is the vehicle speed, *V* is the volume of the cabin, *v.age* is the vehicle's age and *m* is the manufacturer adjustment, which is -0.71 for German vehicles and -0.39

for Japanese vehicles. For zero speed, a value of -0.51 factor is recommended by Hudda et al., 2011. $Q_L$: $CO_2$ rate of change for each ventilation after the subtraction of $CO_2$ generated from occupants. In this study, the $CO_2$ leakage: $Q_L$ for individual vehicles at different speeds was calculated by using the model above when there was no ventilation, the windows were closed, AC/Fan and RC was off and $CO_2$ generated from breathing taken into account. Figure 4.3 shows the AER for different vehicles at different speeds with no ventilation.

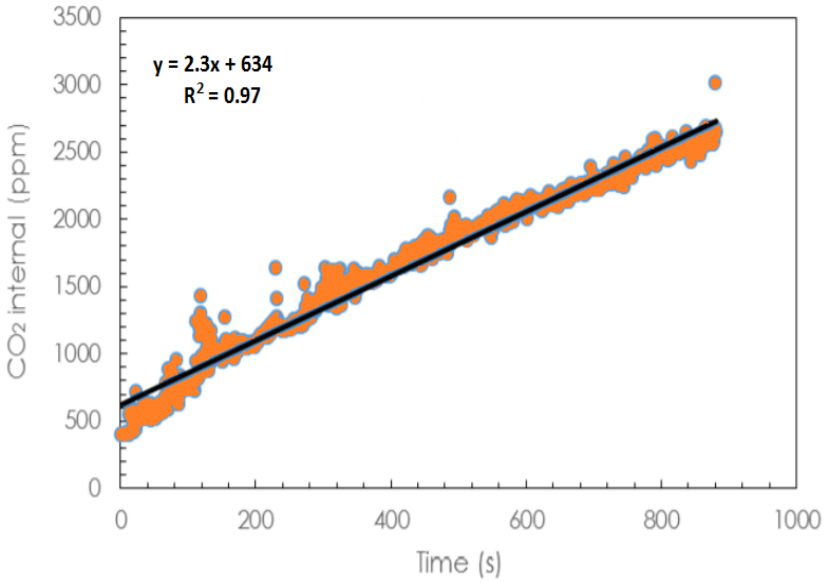


Figure 4.2: Within-vehicle $CO_2$ generation rate due to breathing for the 2013 Ford focus.

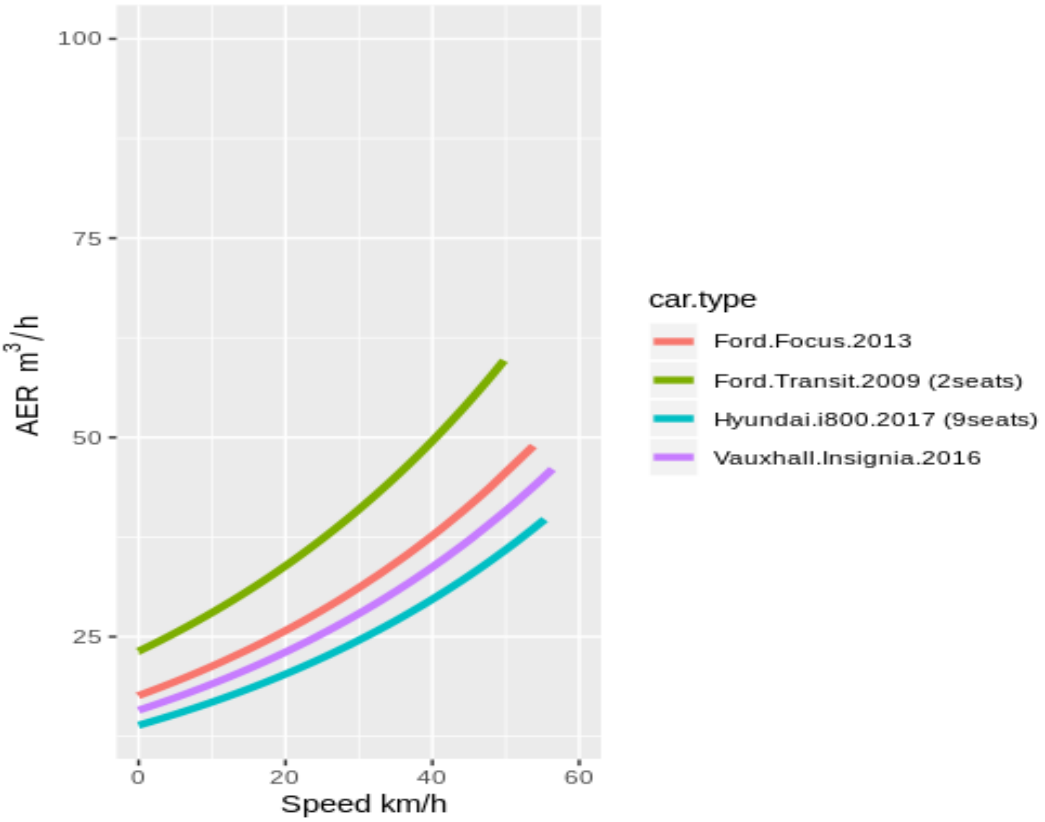


Figure 4.3: Air Exchange rate (or $CO_2$ leakage flow: $Q_L$) for different vehicles under real-world driving conditions and various speed range.

#### 4.2.5.3 Human respiratory inhalation flow ($Q_R$)

The Inhalation flow is the volumetric breathing rate of the vehicle occupants. During the experiments two occupants (one male and one female or two males, aged from 30 to 40) were inside the vehicle. A breathing rate of 1.38 $m^3$/h for males and 1.16 $m^3$/h for female was used, taken from the study of Adams (1993). Exhalation is a

negligible source of non-VOC species considered here, and are therefore it was excluded from the calculations (Knibbs et al., 2011).

#### 4.2.5.4 Respiratory deposition coefficient ($R_{Dp}$)

Respiratory deposition is the net loss of particles in the human respiratory system. Here, the respiratory deposition coefficient can be considered analogous to filtration efficiency, where it represents the fractional loss of pollutant species during breathing. For UFP and LSDA (median measured value of 50 nm) we adopted the RDp from Hinds (1999) for light exercise. For $PM_{10}$ and $PM_{2.5}$ the equivalent RDp is 0.65 while for $PM_1$ is 0.55. For $NO_x$ and $NO_2$ respiratory deposition of 0.65 was used as reported in Postlethwait and Bidani, (1990).

#### 4.2.5.5 Deposition rate coefficient (Dp)

The deposition rate is a loss mechanism inside vehicles and consists of two main factors, fan air velocity and surface area (Thatcher et al., 2002). These factors

differ between within-cabin and indoor microenvironments. Air Exchange rates (AERs) are much greater inside vehicles (Ott et al., 2007; Knibbs et al., 2010; Hudda et al., 2012) compared to buildings (Yamamoto et al., 2010). For UFP (Number) and LSDA (50nm size) we used the deposition rate coefficient of 10 $h^{-1}$, as in Gong et al., (2009), and which was adjusted for each vehicle according to their surface to volume ratio. For $PM_{2.5}$ deposition rate coefficient values provided by Ott et al., 2007 for different ventilation options were adapted for $PM_{10}$ and $PM_1$ according to the measured $PM_{2.5}/PM_{10}$ = 0.7 and $PM_1/PM_{2.5}$ = 0.74 ratios.

#### 4.2.5.6 Filtration efficiency ($f_{ef}$)

The filtration efficiency is a measure of how well the vehicle's air filter can trap particles from penetrating the cabin. Air filtration mechanisms include straining, interception, diffusion, inertial impaction and electrostatic attraction to capture specific range of sizes of the particulate being filtered. The straining, interception, diffusion, and inertial impaction mechanisms rely upon media filters to accomplish filtration, while electrostatic attraction is typically obtained by charging the particulate as part of the filtration mechanism. In commercial filters, straining, inertial impaction, and interception are the dominant collection mechanisms for particles greater than 0.2

microns, and diffusion is dominant for particles less than 0.2 microns. This filtration efficiency varies for $PM_{10}$ and $PM_{2.5}$ in buildings depending on the experimental conditions and is expected also to vary in different vehicles. Qi et al., (2008) tested vehicle particle filter efficiencies for two different velocities, representing low and full power fan settings. Their calculated filter efficiencies were adopted in this study (see Table 4.4). For gas phase pollutants no filtration efficiency was used since the equipped pollen filters had no gas selectivity.

#### 4.2.5.7 Penetration factor (*P*)

Penetration is a mechanism by which air enters the vehicle through cracks, and can be quantified using the penetration factor. The penetration factor is defined as the fraction of atmospheric species which pass through the vehicle with the infiltrating air, and is similar to the factor applied for indoor air quality in buildings, varying for different particle sizes (Chen and Zhao, 2011). The penetration factor for each particle size used in this study is summarized in Table 4.4. No penetration factors for $NO_2$ and $NO_x$ were found in the literature and therefore an equivalent behaviour to fine particles ($PM_{2.5}$ and less) was assumed.

#### 4.2.5.8 Reaction and photolysis rates

The only reactions considered here are the (overall) PSS reactions of $NO_2 + hv \rightarrow NO + O$, $NO + O_3 \rightarrow NO_2 + O_2$ while the reaction rate was calculated using the Arrhenius expression with the measured temperatures within-cabin. The photolysis frequency inside buildings varies depending on the building and window design and lighting, which can lead to large differences in the actinic flux (Carslaw, 2007). This is also true for vehicles since there are different type of windows (e.g. no, light or heavy tint) and also vehicle designs and of course orientation that change the light transmission. For the outdoor photolysis rates, AtChem2, a chemistry box model (Sommariva et al., 2020), ran to calculate the photolysis rates for each experimental day assuming clear-sky conditions. For within-vehicle photolysis rates, a photolysis ratio of 1:10 for $j(NO2)_{indoor}$:$j(NO2)_{outdoor}$ values reported in Carslaw, (2007) for buildings was applied to the outdoor photolysis rates.

### 4.2.6 Machine learning model (B) and cross validation

Machine learning (ML) is a method of data analysis that is based on the concept that systems can learn from data, identify patterns and make decisions with minimal human intervention (Kotsiantis, 2007). The only rule in machine learning is that there is no single algorithm that will work well for all tasks. Each task that needs to be solved has its own idiosyncrasies. Therefore, there are lots of algorithms and approaches to suit each problem's unique oddities. There are several types of machine learning, unsupervised and supervised are well established approaches and the most commonly used. Semi-supervised and Reinforcement learning are newer and more complex but have shown impressive results (Botvinick et al., 2019). Unsupervised learning case is where methods such as clustering are used to recognise patterns in the data without reference to the outputs, while supervised algorithms are used in a known set of input data and output responses in order to combine input variables in such a way as to predict the outcome using classification or regression methods. The majority of practical machine learning uses supervised learning.

Supervised (or often known as inductive) machine learning is the process of learning a set of rules from instances (or examples in a training set), or more generally speaking, creating a classifier that can be used to generalize from new instances. It is called supervised learning because the process of algorithm learning from the training dataset can be thought of as a teacher supervising the learning process of the

students. We know the correct answers, then we let the algorithm iteratively make predictions on the training data and be corrected by the teacher, thus the algorithm learns. This learning stops when the algorithm achieves an acceptable level of performance. In a more scientific context, supervised learning is where we have input variables (x) and an output variable (Y) and we use an algorithm to learn the mapping function from the input to the output Y = f(x). The goal is to approximate the mapping function so well that when we have new input data (x) that we can predict the output variables (Y) for that data. The process of applying supervised ML to a real-world problem is described in Figure 4.4.

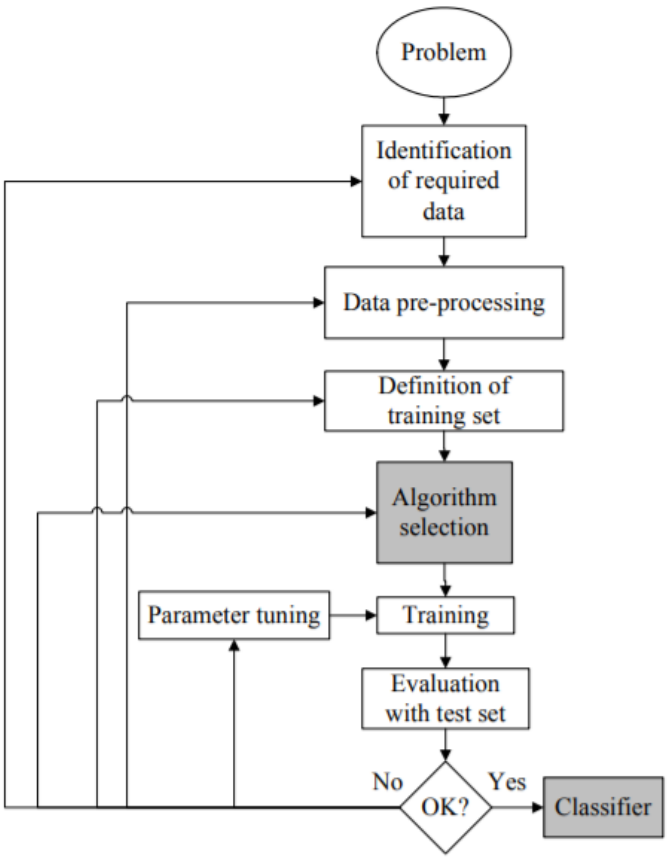


Figure 4.4: The process of supervised machine learning (from Kotsiantis, 2007).

There are several supervised ML algorithms that can be used for model training and prediction. As a rule, no single learning algorithm can uniformly outperform other algorithms over all datasets. However, they can be evaluated for their (1) accuracy, (2) speed of learning (with respect to number of attributes and number of instances), (3) speed of classification, (4) ability to deal with discrete/binary and continuous attributes, (5) danger of overfitting, (6) attempts required for incremental learning, (7) ability to handle model parameters and explain classifications, (8) tolerance to missing values, irrelevant attributes, noise, redundant attributes and highly interdependent attributes (Kotsiantis, 2007). Table 4.6 provides a comparison of the most common supervised ML algorithms.

In this study the k-Nearest Neighbour (kNN) algorithm was used. kNN is a non-parametric statistical instance-based learning method that is used for classification and regression and is based on feature similarity. In both cases, the input consists of the k closest training examples in the feature space; in machine learning and pattern recognition, a feature is an individual measurable property or characteristic of a phenomenon being observed. There the algorithm calculates which already stored instance is mostly similar to the new instance (Cover and Hart, 1975; Weinberger et al., 2006). This is done by storing the training data in an n-dimensional space where each of the n-dimensions corresponds to one n-features that are used to describe an instance (making the model learn). When a new instance is inputted, the algorithm searches similar instances from memory using the Euclidean distance and then assigns the new record by identifying the single most frequent class label. A commonly used

distance metric for continuous variables is Euclidean distance. For discrete variables, another metric (Hamming distance) can be used.

In kNN, the output depends on whether the algorithm was used for classification or regression. In kNN classification, the output is class related, which in principle means that the object is classified by the majority of its neighbours; the object is being assigned to the class most common among its k nearest neighbours (with k being a positive integer). If for example k = 1, then the object is simply assigned to the class of that single nearest neighbour. In kNN regression the algorithm is used for estimating continuous variables and the output is the value related to the property of the object. This value is the average of all the values of k nearest neighbours. kNN regression algorithm uses a weighted average of the k nearest neighbours, which is weighted by the inverse of their distance. The algorithm works as follows: Compute the Euclidean distance from the query example to the labelled examples. Order the labelled examples by increasing distance. Find a heuristically optimal number k of nearest neighbours, based on RMSE. Calculate an inverse distance weighted average with the k-nearest multivariate neighbours. This method is robust to noisy and large training datasets (Wettschereck et al., 1997) since it considers the query instance when generalizing beyond the training data, whereas a more different machine learning method would have chosen the time where the query instance was observed (Aquilina et al., 2018). However, kNN algorithms require large storage for the model training, are sensitive to the choice of the similarity function (function which is used to compare instances) and lack of principled way to choose the best k except through cross-validation (Kotsiantis, 2007).

Table 4.6: Comparison of supervised machine learning algorithms **** stars represent the best and * star the worst performance (adopted from Kotsiantis, 2007).

| | Decision trees | Neural networks | Naïve Bayes | kNN |
|---|---|---|---|---|
| General accuracy | ** | *** | * | ** |
| Speed of learning (with respect to number of attributes and the number of instances) | *** | * | **** | **** |
| Speed of classification | **** | **** | **** | * |
| Tolerance to missing values | *** | * | **** | * |
| Tolerance to irrelevant attributes | *** | * | ** | ** |
| Tolerance to redundant attributes | ** | ** | * | ** |
| Tolerance to highly interdependent attributes | ** | *** | * | ** |
| Dealing with discrete, binary, continuous attributes | **** | *** | *** | *** |
| Tolerance to noise | ** | ** | *** | * |
| Dealing with danger of overfitting | ** | * | *** | *** |
| Attempts for incremental learning | ** | * | **** | **** |
| Explanation ability/transparency of knowledge/classifications | **** | * | ** | *** |
| Model parameter handling | *** | * | **** | *** |

The machine learning applied in this study used the original 80% of the observations of the complete dataset, by using a random number generator. The remaining 20% was reserved to validate and test the model's predictability and response (after the ML training) to fresh random unseen data. In detail, the ML training dataset used concentrations within vehicles, on-road concentrations, ventilation power (expressed from 0 to 100), ventilation type (expressed from 1 to 5) and surface area and cabin volume of the vehicles. The ML training followed the repeated k-fold cross validation approach. In this method, after randomly splitting the training data (80% of the initial dataset) into k-folds (10 in our case), a ML model was built and trained for k-1 folds (training fold) of the dataset and tested on the $k^{th}$ (testing fold). For each fold/subset that is held out, the model is trained on all other subsets. This training process was repeated 1000 times and the final model accuracy is taken as the mean from the number of repeats. More repetitions provide better accuracy for each instance in the dataset, however it should be mentioned that this requires huge computational power. This process maximizes the training and the testing of the ML algorithm and has the advantage that for a single dataset we used all the available values of that dataset (80% of the initial dataset in our case) for training and testing. This method is robust for estimating the accuracy and the size of k and tunes the amount of bias in the predictions; Principles which are critical when using a kNN approach (Kotsiantis, 2007). Finally, the ML model (built from k-1 folds and tested on the $k^{th}$ fold with 1000 repeats) was evaluated against the 20% of the initially excluded data to ensure its predictability. The method that was used here is shown in Figure 4.5.

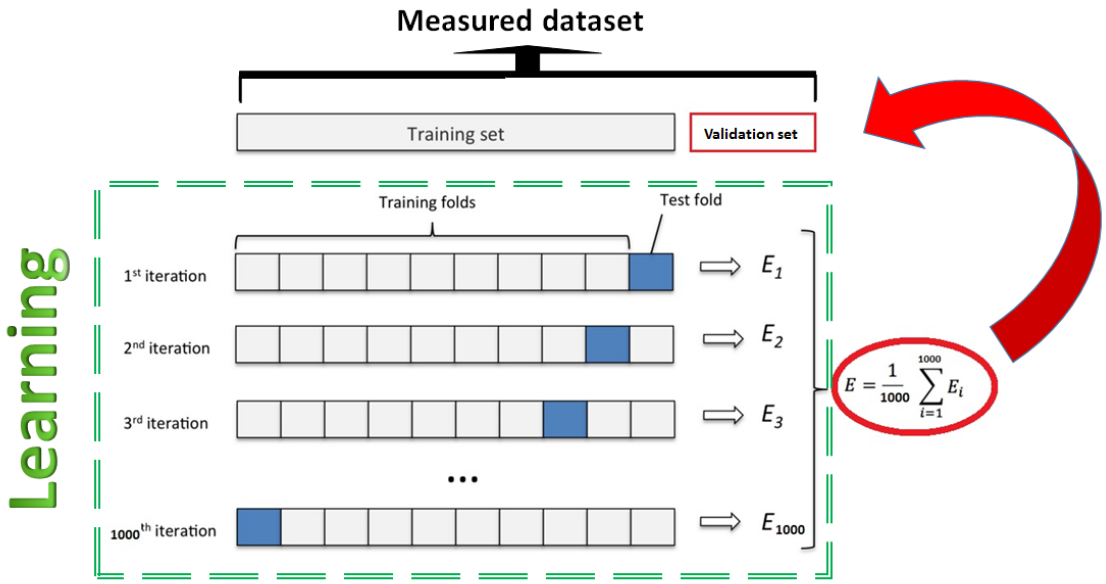


Figure 4.5: Machine learning training process and k-1 cross validation

### 4.2.7 Model evaluation and real world application scenarios

Model (A) was validated against the measurements inside vehicles. As the initial timestep of the model (A) uses 1 min time interval and in order to avoid any potential noise in the initial conditions, modelling prediction tests also included non-consecutive minutes within the same ventilation settings of the same car/run (1 to 3, 2 to 4 etc.), which however did not vary between them. For Model (B), the data were divided to 80:20 and 80% was used for training and 20% for validation of random

observational within-vehicle concentration data, which were excluded before the machine learning training.

For validation of model (B) we used the statistical indices of comparison of means (for observed and predicted values), Root mean square error (RMSE), where the closest the RMSE is to 0 the better the model prediction (Aidaui et al., 2015; Matthaios et al., 2017), defined as:

$$RMSE = \sqrt{\frac{\sum_{i=1}^{n}(M_i - O_i)^2}{n}}$$

where *n* is the sample size and $M_i$ and $O_i$ the individual sample points for modelled and observed indexed with *i*. Factor of two (FAC2), which is the fraction of predictions within a factor of two of observations where the predictions vary between 0.5 ≤ FAC2 ≤ 2 and FAC2 = 1 is the perfect prediction and satisfy:

$$0.5 \leq \frac{M_i}{O_i} \leq 2.0$$

Mean bias (MB), which provides a good indication of the mean over or under estimate of predictions. Mean bias in the same units as the quantities being considered.

$$MB = \frac{1}{n}\sum_{i=1}^{n} M_i - O_i$$

Mean Gross Error (MGE): The mean gross error provides a good indication of the mean error regardless of whether it is an over or under estimate. Mean gross error is in the same units as the quantities being considered.

$$MGE = \frac{1}{n}\sum_{i=1}^{n}|M_i - O_i|$$

Pearson correlation coefficient (r), which is a measure of the strength of the linear relationship between two variables. If there is perfect linear relationship with positive slope between the two variables, r = 1. If there is a perfect linear relationship with negative slope between the two variables r = −1. A correlation coefficient of 0 means, that there is no linear relationship between the two variables. The Pearson correlation coefficient can be defined as:

$$r_{xy} = \frac{\sum_{i=0}^{n}(m_i - \bar{m})(o_i - \bar{o})}{\sqrt{\sum_{i=0}^{n}(m_i - \bar{m})^2}\sqrt{\sum_{i=0}^{n}(o_i - \bar{o})^2}}$$

Index of agreement (IOA), which is a measure of how well the predicted variations are represented around the mean observations and is commonly used in model evaluation (Willmott et al., 2011). It spans between −1 and +1 with values approaching +1 representing better model performance. An IOA of 0.5, for example, indicates that the sum of the error magnitudes is one half of the sum of the observed deviation magnitudes. When IOA = 0.0, it signifies that the sum of the magnitudes of the errors and the sum of the observed deviation magnitudes are equivalent. When

IOA = −0.5, it indicates that the sum of the error magnitudes is twice the sum of the perfect model-deviation and observed deviation magnitudes. Values of IOA near −1.0 can mean that the model estimated deviations are poor estimates of the observed deviations. IOA for c = 2, can be defined as:

$$IOA = \begin{cases} 1 - \dfrac{\sum_{i=0}^{n}|M_i - O_i|}{c\sum_{i=0}^{n}|O_i - \bar{O}|}, & when \quad \sum_{i=0}^{n}|M_i - O_i| \leq c\sum_{i=0}^{n}|O_i - \bar{O}| \\ \dfrac{c\sum_{i=0}^{n}|O_i - \bar{O}|}{\sum_{i=0}^{n}|M_i - O_i|} - 1, & when \quad \sum_{i=0}^{n}|M_i - O_i| > c\sum_{i=0}^{n}|O_i - \bar{O}| \end{cases}$$

To examine the predictability of the mass balance model (A) and the applicability of the ML model (B), we tested two cases: (i) in model (A) we replaced the actual measured within-vehicle concentrations with a median within-vehicle concentration of the examined pollutant for the initial condition and we re-ran the model (A) to ensure that there was minimal dependence upon the initial interior concentrations; the same replacement was applied to the ML model (B), where the training took into account the median interior values instead of the actual observations. This represents a scenario where the concentration outside is known (e.g. from low cost sensor networks running in wifi) but the within-vehicle is unknown. In case (ii), model (B) was trained with median within-vehicle levels and outside levels from the closest roadside air quality station (instead of actual on-road measurements). This case was built to reflect real world situations *i.e.* where only monitoring station data is likely to be available, rather than data from directly outside the vehicle. In both

cases, model (B) followed the 80:20 approach with 1000 iterations. Table 4.7 summarises the constructed cases.

Table 4.7: Cases constructed to test the application of the model. $C'_{inmj}$: denotes predicted median concentration; $C'_{inmj}$: denotes within-vehicle median levels; $C_{outaqj}$: denotes hourly concentration levels from the air quality stations. All the remaining parameters in the model are taken from the values in Table 4.4.

| Case | Equation |
|---|---|
| Initial model | $(C'_{inj} - C_{inj})V = \left[C_{outj}(Q_S(1 - f_{ef}) + Q_L P_j) - C_{inj}\left(Q_R R D p_j + DP_j V + (Q_S + Q_L)\right)\right]\Delta t$ |
| Case (i) | $(C'_{inmj} - C_{inmj})V = \left[C_{outj}(Q_S(1 - f_{ef}) + Q_L P_j) - C_{inmj}\left(Q_R R D p_j + DP_j V + (Q_S + Q_L)\right)\right]\Delta t$ |
| Case (ii) | $(C'_{inmj} - C_{inmj})V = \left[C_{outaqj}(Q_S(1 - f_{ef}) + Q_L P_j) - C_{inmj}\left(Q_R R D p_j + DP_j V + (Q_S + Q_L)\right)\right]\Delta t$ |

# 4.3 Results

## 4.3.1 Measured concentrations

Table 4.8 presents the median of the concentrations measured in our campaigns. The highest exposure to combustion related gaseous ($NO_2$ and $NO_x$) and particulate (UFP and LSDA) pollutants was measured with open windows (ventilation d). The highest mean exposure to particulate combustion pollution ($PM_{10}$, $PM_{2.5}$, $PM_1$) was measured when the fan was on bringing air from outside inside (ventilation b). The lowest mean exposure for $PM_{10}$, $PM_{2.5}$, $PM_1$, UFP and LSDA occurs when the recirculation option is switched on (Ventilation options d and e), however those options have the second highest exposure to $NO_x$ and second highest exposure for $NO_2$. The reason for this is unclear; however a potential shift in the PSS reactions with the remaining amount of ozone within-vehicle might be the reason for that (see Chapter 3). The within-vehicle measurements show different variation of species with different ventilation setting, highlighting in that way the importance to be able to model accurately the species within-vehicles with respect to the ventilation choice.

Table 4.8: Median concentrations of $PM_{10}$, $PM_{2.5}$, $PM_1$, LSDA, $NO_2$, $NO_x$, UFP and $CO_2$ under ventilation settings: (a) windows open, fans and AC off, (b) Fans on - AC &recirculation off, windows closed(c) Fan plus AC on, recirculation off, windows closed (d) Fan plus recirculation on, fan low power, AC off, windows closed (e)Fan plus AC and recirculation on, windows closed and (f) windows closed, AC, fans and recirculation off.

| Species | Ventilation a | Ventilation b | Ventilation c | Ventilation d | Ventilation e | Ventilation f |
|---|---|---|---|---|---|---|
| $PM_{10}$ ($\mu g/m^3$) | 15 | 24 | 6 | 8 | 3 | 13 |
| $PM_{2.5}$ ($\mu g/m^3$) | 8 | 15 | 4 | 4 | 3 | 5 |
| $PM_1$ ($\mu g/m^3$) | 5 | 13 | 3 | 3 | 2 | 3 |
| LSDA ($\mu m^2/cm^3$) | 52 | 39 | 38 | 12 | 6 | 26 |
| $NO_2$ ($\mu g/m^3$) | 101 | 92 | 77 | 92 | 61 | 59 |
| $NO_x$ ($\mu g/m^3$) | 545 | 493 | 476 | 526 | 530 | 298 |
| UFP ($pt/cm^3$) | 44,816 | 31,960 | 27,265 | 5,466 | 400 | 19,110 |
| $CO_2$ ($mg/m^3$) | 974 | 1271 | 1181 | 2551 | 2479 | 2673 |

## 4.3.2 Modelling results – comparison with observations

### 4.3.2.1 Mass-balance model (A) simulations

Figure 4.6 illustrates an example timeseries of the mass-balance model (A) predictions and comparison with measured levels of UFP and $NO_2$ from one of the test

vehicles. For UFP, the model performs well under windows-open, fan-on and AC-on modes, but overpredicts the observed levels under the no-ventilation and recirculation modes. For $NO_2$, the model performs well under no-ventilation and recirculation conditions, but underestimates the observations for windows-open and AC-on, and overestimates for fan-on and AC-with-recirculation. The reason for this difference in UFP might be the assumptions in the initial parameters in the model. Specifically, for the no ventilation and recirculation modes, parameters such as deposition rates or penetration factor of the species play an important role. Here, the deposition rate and the penetration factor as well as the filter efficiency for UFP were adopted according to studies made in homes using 50 nm test particles (median within-vehicle UFP size). However, vehicles are different indoor microenvironments to homes, where different UFP sizes have different deposition rates; an accurate representation of which may improve the model outputs. As for the $NO_2$ differences, in addition to the deposition rate taken from decay rates in a house, another reason for this discrepancy might be the losses from secondary reactions upon vehicle surfaces and the formation of nitrous acid (HONO) which are not included in the model (see limitations).

To examine the performance of model (A) across all the measurements, data were aggregated in Figure 4.7, which shows the measured vs. the mass balance model (A) values for all the data for different vehicles and ventilations. $PM_{10}$, $PM_{2.5}$ and $PM_1$ species are predicted well by the model and are within the ±10% of the 1:1 line, however, a clear under estimation is evident for UFP and LSDA. This is possibly because the model used parameters such as filtration efficiency, deposition etc. that were available from the literature might not be applicable to new vehicle models such as the

ones tested in this study. Furthermore, one should note that internal sources of particle generation were not considered, which might be a further reason for the under-prediction in those species. For $NO_x$ and $NO_2$ some false predictions at high levels are apparent, however the majority of predictions are well within the ±10% of the 1:1 modelled and observed data. The reason for the discrepancy in the high level $NO_x$ and $NO_2$ might be due to specific events such as high emitters overtaking which cannot be captured by the model.

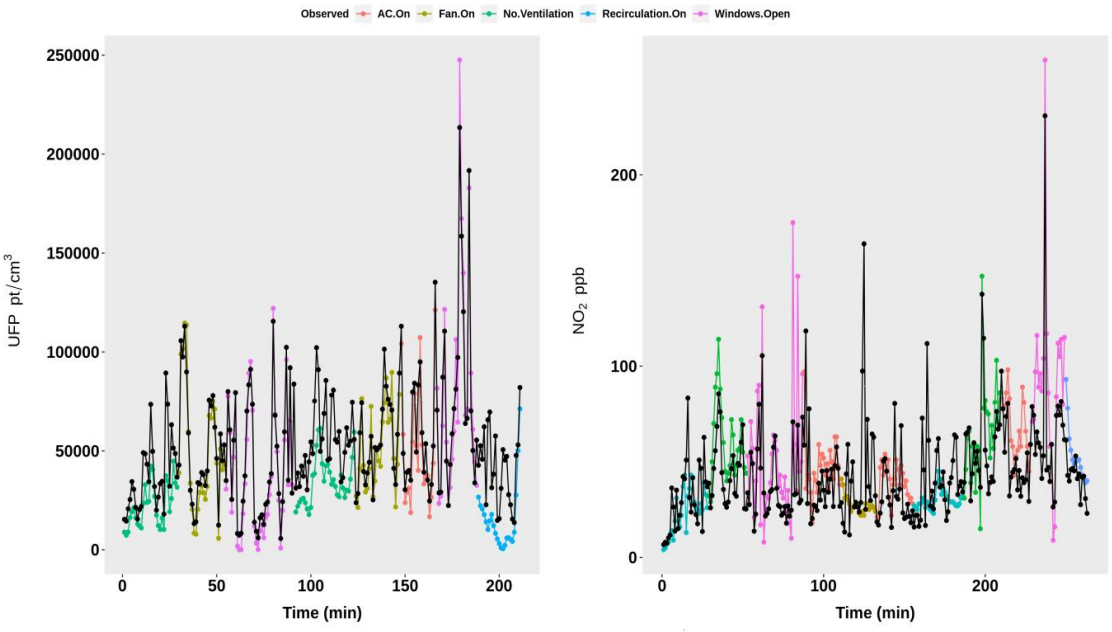


Figure 4.6: Time series of modelled (Model A) and observed values for UFP and $NO_2$ in Vauxhall Insignia. Different colours indicate the different ventilation settings, while the solid black line shows the modelled data.

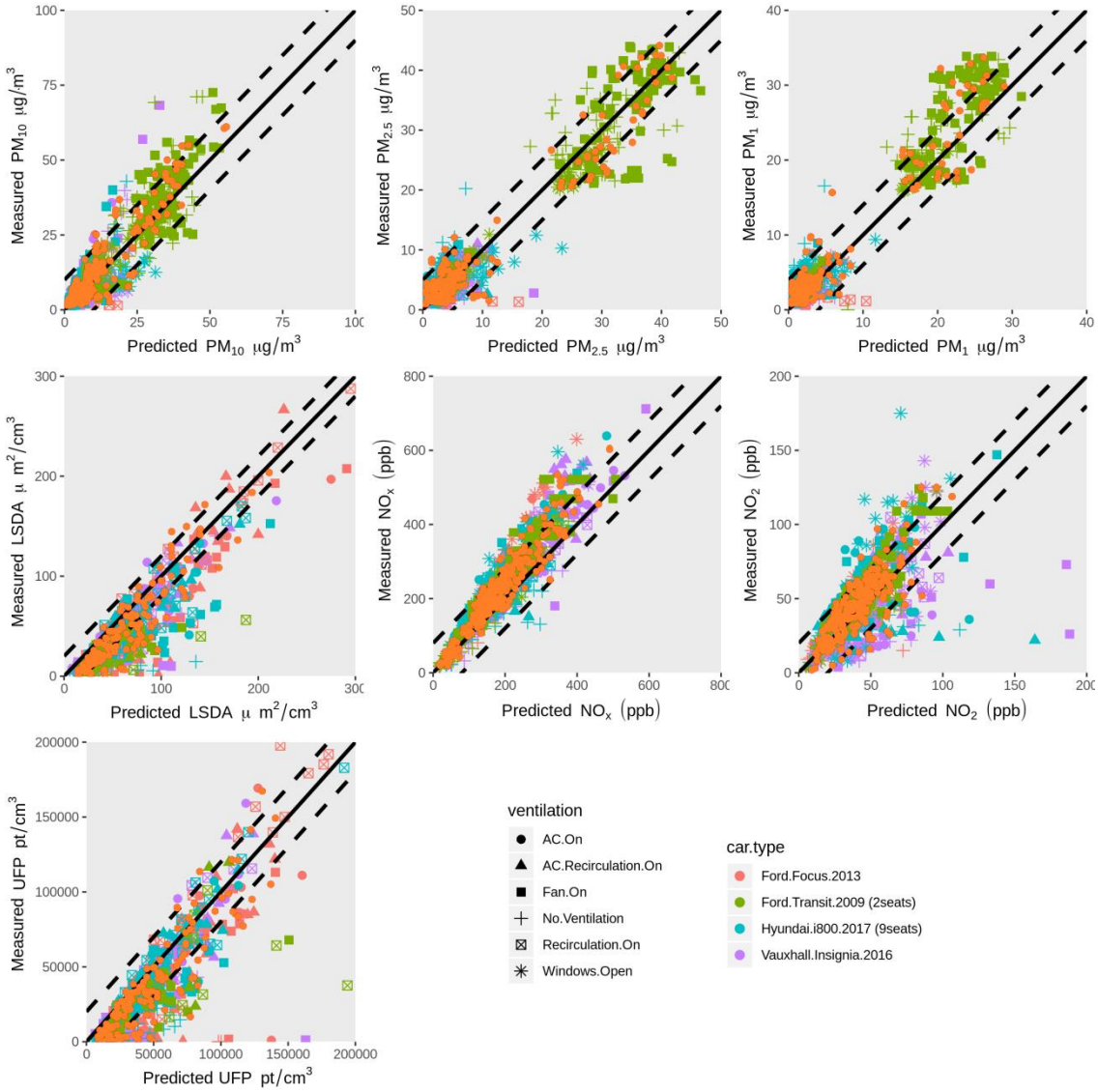


Figure 4.7: Measured vs mass balance model (A) and ML model (B) within-vehicle concentrations of $PM_{10}$, $PM_{2.5}$, $PM_1$, LSDA, $NO_x$, $NO_2$ and UFP. The orange dots indicate the ML predictions (Model B) for 20% of randomly excluded data. The solid line denotes the perfect model 1:1. The dashed lines indicate the ±10% of the perfect model.

#### 4.3.2.2 Machine learning (ML) model predictions (B)

The ML model was trained with 80% of the measured data for which the model performance is, by definition, expected to be generally good and validated against the 20% of test data (within-vehicle and ambient observations) which were randomly selected and excluded from the training algorithm. In Figure 4.7 the orange dots also show the comparison between the observed and the ML modelled values for the 20% of the unseen data. The ML model has as good predictions as the mass balance model and in some cases, such as for $NO_2$, it improves upon the mass-balance model predictions. Most of the ML model predictions in almost all the species are equally spread around the perfect model (1:1), however, an under-prediction still occurs in the LSDA and UFP species.

Table 4.9 summarises the ML model performance statistics against the 20% of randomly removed data. As can be seen the model shows good skill in predicting within vehicle concentrations of different pollutants with the RMSE (root mean squared error) lower than the SD (standard deviation) of the observations for all of the species considered. Pearson correlation coefficients are higher than 0.80, while an IOA (index of agreement) greater than 0.69 for all the species in general indicates good model predictions (Matthaios et al., 2017). The mean gross error (MGE) of the ML model's performance is less than 5 μg $m^{-3}$ for all the particle classes ($PM_{10}$, $PM_{2.5}$ and $PM_1$) and less than 11 ppb for $NO_2$. The biggest error is evidenced in $NO_x$ and UFP which is almost the same as the MB (mean bias). The model's fraction of predictions

within a factor of two of observations (FAC2) is also in good agreement with observations (higher than 0.69 for all the species), while noteworthy is the fact the model's FAC2 score is very high (0.89) for $NO_2$. The MB (mean bias) indicates that the ML model under-predicts the particulate species by less than < 1 μg $m^{-3}$ and the $NO_2$ by less than < 5 ppb. The biggest under-prediction occurs for UFP and $NO_x$, however random events such as overtaking or congestion that can result in greater NO outside and consequently inside, might not be captured fully by the model. Regarding the UFP predictions it has to be noted that particle leaks from the engine or generation of already deposited particles (in the seats or fabrics) due to vibration or movement might cause this discrepancy in UFP predictions and those are terms that were not included in the model. Overall it can be stated that the ML has good skill in predicting the random measurement data with promising applicability in real world as discussed later on in the constructed cases and the use of air quality data.

Table 4.9: Model evaluation statistics against 20% random observation data after machine learning. n: number values. FAC2: predictions within a factor of two of observations, perfect model FAC2 = 1. MB: Mean bias. MGE: Mean gross error – indication of the mean error regardless of over or under estimate. RMSE: Root mean squared error. r: Pearson correlation coefficient, values from -1 to 1; values of 0 no prediction. IOA: Index of Agreement, values from -1 to 1. $\overline{m_O}$, $\overline{m_p}$: Mean values of observations and predictions respectively. SD: Standard Deviation.

| Species | n | FAC2 | MB | MGE | RMSE | R | IOA | $\overline{m_O}$ | $\overline{m_p}$ | $SD_o$ |
|---|---|---|---|---|---|---|---|---|---|---|
| $PM_{10}$ | 196 | 0.76 | -1.06 | 4.4 | 6.82 | 0.89 | 0.80 | 15 | 13.9 | 14.6 |
| $PM_{2.5}$ | 196 | 0.78 | 0.14 | 2.3 | 3.4 | 0.96 | 0.87 | 9.9 | 10.2 | 11.8 |
| $PM_1$ | 196 | 0.81 | -0.8 | 1.6 | 2.33 | 0.97 | 0.89 | 7.6 | 6.8 | 9.02 |
| LSDA | 140 | 0.69 | 20.9 | 22.3 | 28.76 | 0.92 | 0.69 | 48.5 | 69.5 | 50.9 |
| $NO_2$ | 256 | 0.89 | -5.0 | 10.4 | 15.4 | 0.89 | 0.79 | 45.5 | 40.5 | 24.27 |
| $NO_x$ | 256 | 0.83 | -49.9 | 53.9 | 76.9 | 0.84 | 0.75 | 246.8 | 196.95 | 144.7 |
| UFP | 140 | 0.66 | 13405 | 16518 | 23209 | 0.90 | 0.73 | 29841 | 52793 | 43031 |

#### 4.3.2.3 Extended application of mass balance and ML models – data from monitoring stations

In the predictions discussed above, each model utilized external concentrations of air pollutants measured directly outside the vehicle either to drive the calculated pollutant exchange (mass balance model A), or as the training set for the ML predictions (B). In order to check both model's application under real world circumstances two cases were constructed: Case (i), represents a scenario where the concentration outside is known (e.g. from low cost sensor networks) but the within-vehicle level is unknown and tests the performance of both models A and B. Case (ii) tests the application of model (B) in real world situations, where both within and outside vehicle levels are unknown and the only data available is the hourly levels from nearby air quality monitoring stations (see 4.2.7). The air quality levels from the monitoring sites were taken from urban-traffic and urban-background locations representing different locations of the testing route.

Figure 4.8 shows case (i) comparison of the two models against the measurements. The mass balance model (A) does a good job in predicting the low concentrations of $PM_{10}$, $PM_{2.5}$, $PM_1$ and $NO_2$, however the model does not predict well the high level of all the pollutants and has a notable discrepancy in the predictions of LSDA, UFP and $NO_x$. In contrast, the ML model (B) has better overall predictions than the mass balance model for all the species. Specifically for $PM_{10}$, $PM_{2.5}$ and $PM_1$, the model (B) shows a clear improvement in the predictions where it predicts better both

high and low concentrations within ±10% of the 1:1 comparison. However, the ML model (B) also shows (to a lesser extent than the mass balance model A) deviation from the observations for LSDA, UFP and $NO_x$. The fact that ML improves the model's performance was also found in other studies (Ozcift and Gulten, 2011; Aquilina et al., 2018). Figure 4.9 shows case (ii) comparison of ML model B vs observations. The results generally show some notable discrepancies for $NO_x$ and $NO_2$, however for a given outside air quality measurement the ML model provides an acceptable representation of the within-vehicle air quality, giving promising insights about the applicability of the method to provide an indication of within-vehicle exposure with zero additional cost.

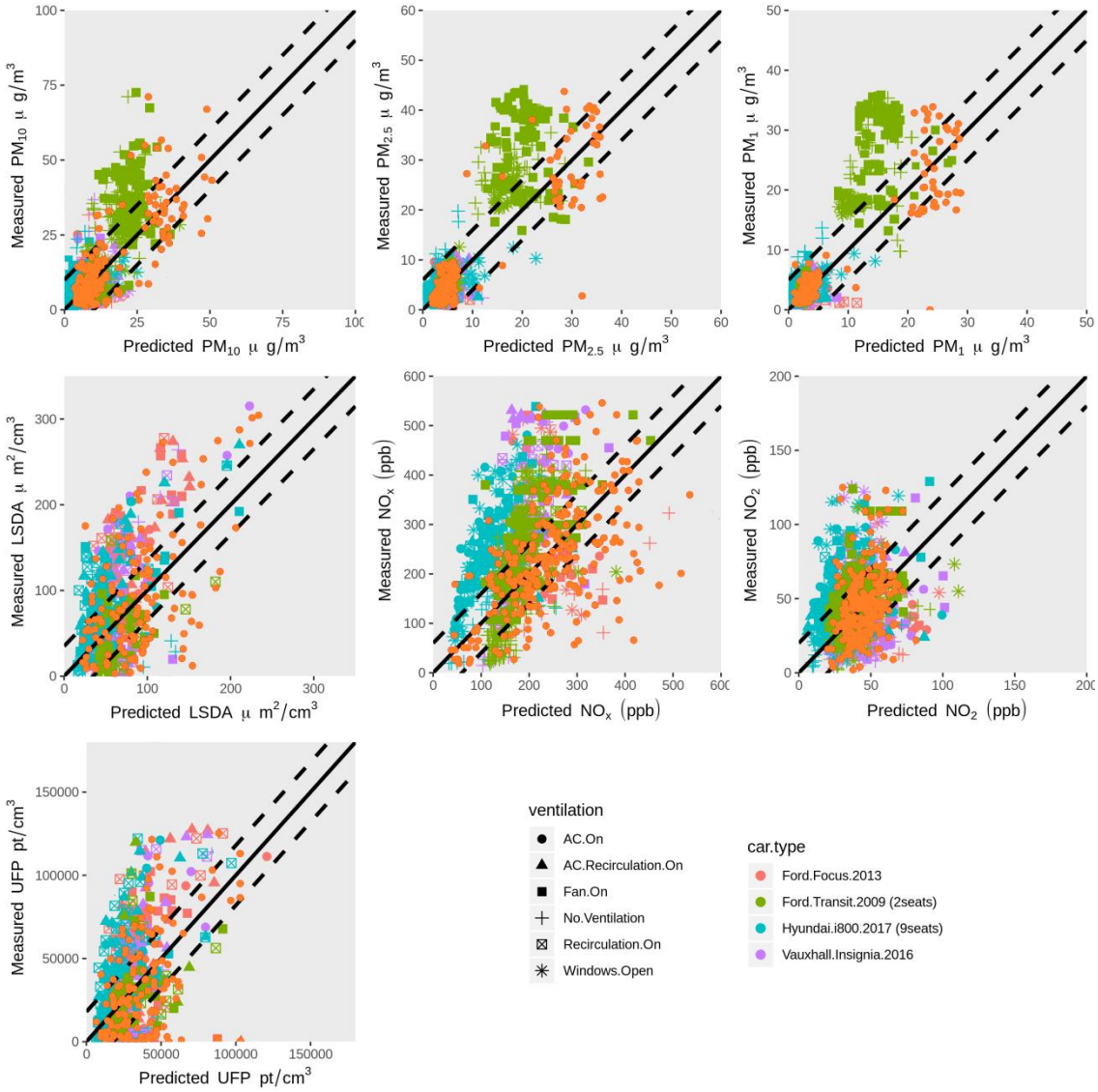


Figure 4.8: Measured vs mass balance model (A) and ML model (B) within-vehicle concentrations of $PM_{10}$, $PM_{2.5}$, $PM_1$, LSDA, $NO_x$, $NO_2$ and UFP. The orange dots indicate the ML predictions for 20% of randomly selected data. The solid line denotes the perfect model 1:1. The dashed lines indicate the ±10% of the perfect model. Both models used median within-vehicle concentrations instead of actual levels (see case (i) Table 5).

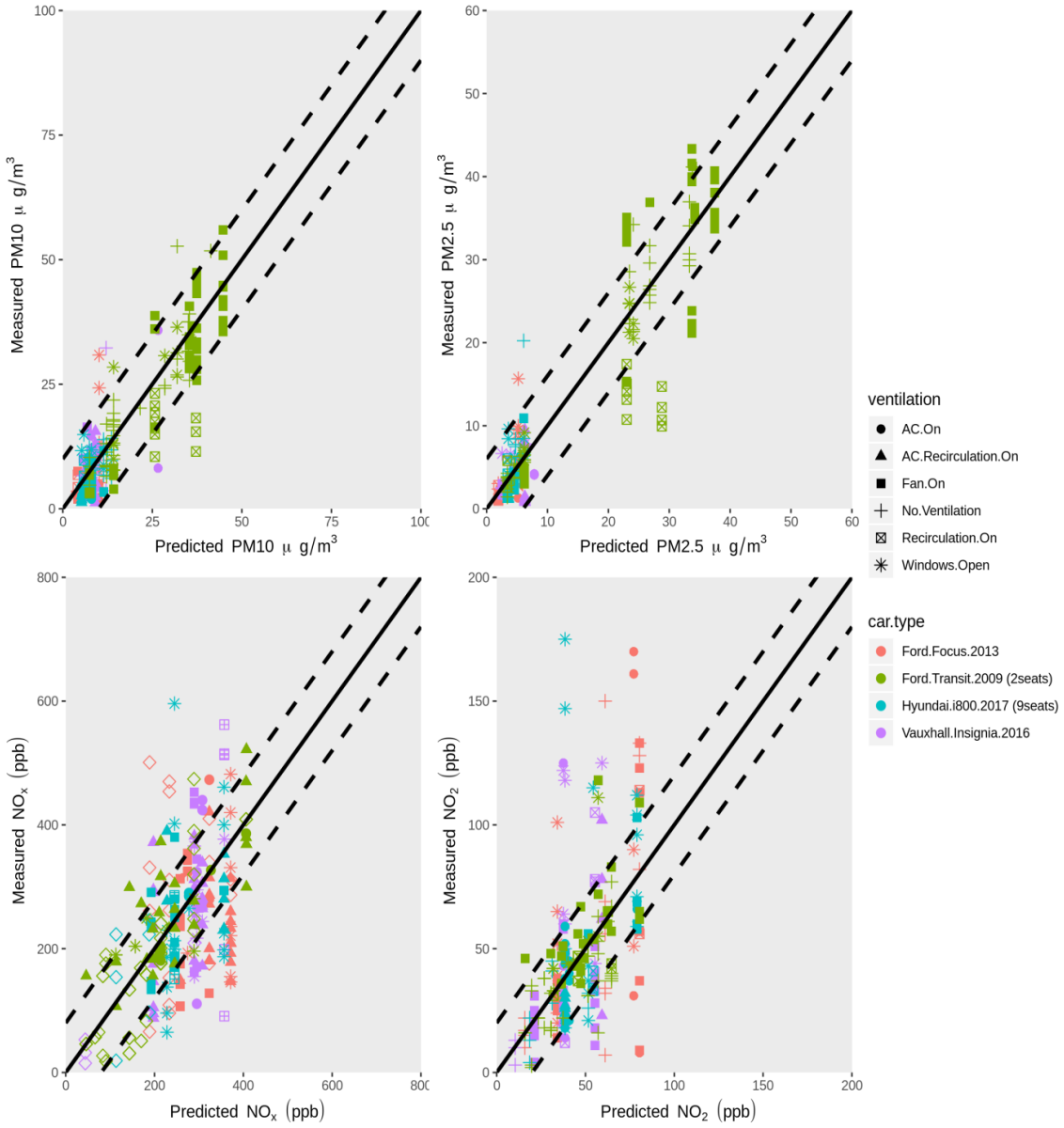


Figure 4.9: Comparison of within-vehicle ML modelled and measured species. For the learning of the ML model, a median within-vehicle level from all vehicles and hourly outdoor air quality measurements were used (see case (ii) in Table 4.7).

# 4.4 Discussion

## 4.4.1 Limitations

Several models have been reported in the literature for the prediction of within-vehicle concentrations of the measured species. However, since the various different within-vehicle studies in the literature have focused on different aspects it was difficult to directly apply one of the models of Hudda et al., (2012); Knibbs et al., (2010) or Xu and Zhu, (2009). The model developed by Hudda et al., 2012, uses a large number of vehicles and multi linear regression approaches and generalized estimating equations to estimate within-vehicle concentrations of UFP, while the models of Knibbs et al., (2010) and Xu and Zhu, (2009) are mass balance based models. The differential equations that we used here are based on the mass balance studies of Knibbs et al., 2010 and Xu and Zhu, (2009), with some modifications in the equations and also by adding key aspects of chemical processing. Another reason for the difference in some modelled vs observed levels might be because values such as deposition coefficients, filtration efficiency and penetration factors were taken from literature. As highlighted in Lee et al., (2015a), those factors depend on the combined effects of the ventilation conditions (i.e., ventilation mode and fan settings) and the aerodynamic changes on the vehicle envelope (i.e., driving speed and vehicle shapes).

The current model and method might have limitations in the prediction of other more reactive species within vehicles and needs to be validated for those species. The model assumes a well-mixed microenvironment which is not always true in real world driving conditions. Furthermore, the ML technique might be dependent upon the initial estimates (e.g. vehicle characteristics, fan power, AERs and other within-vehicle parameters to build the model) and therefore the ML applicability needs to be tested in other cases. In the model the leakage rate/passive ventilation was calculated using the equations of Hudda et al., (2012) to calculate $CO_2$ AER (after excluding the $CO_2$ generated from the occupants) when the cabin had no ventilation setting. However, since that method uses generalized regression models based on vehicle age, driving speed, and fan strength, the method may impose uncertainty across different vehicle models and other equations used to calculate the leakage flow/passive ventilation based on the pressure difference (Lee et al.,2015b) need to be tested for suitability. Engine/fuel leaks can generate gaseous and particulate pollution and other organic gas compounds such as, benzene, toluene, xylene, and methyl-tertiary butyl ether (Fedoruk and Kerger, 2003; Jo and Park, 1998; Duffy and Nelson, 1997) that can enter the interior of the vehicles via the ventilation system. This potent source is not currently included in the model of this study. Finally, carcinogenic/toxic species such as volatile organic compounds which are released from plastics and fabrics on exposure to sunlight and heat (Yoshida and Matsunaga, 2006, You et al., 2007) and heterogeneous surface reactions of species such as HONO or reactions of peroxy radicals with NO, can play a role in the within-vehicle chemistry. The model

currently is limited in omitting representation of such detailed chemistry, secondary aerosol formation and other particle physics processes.

### 4.4.2 Implications

Knowing that despite spending only 6% of our time daily in transport, this accounts for 25% of our total daily exposure (Dons et al., 2011); modelling the within-vehicle concentrations is an important step to assess and hence minimize air pollution exposure. Vehicle use changes not only from region to region but also depending on the meteorological conditions (e.g. more people commute by car under cold weather). This change in the vehicle use results in more vehicle emissions not only due to the higher number of vehicles on road but also due to the way their after-treatment abatement technologies work under cold weather (Matthaios et al., 2019). In turn these elevated vehicle emissions can result in greater exposure for vehicle occupants. Currently, estimating within-vehicle exposure to air pollution with direct methods such as measurements is very challenging, therefore alternative indirect approaches, such as the models of this study, need to be explored.

The modelling methodology presented here can be developed into a useful tool that can be used by policy makers in order to estimate the air pollutant concentration

levels inside vehicles. The approach presented here uses for the first time machine learning algorithms to train a model in order to predict random unseen data giving within-vehicle exposure, with promising applicability elsewhere and for different species. For example, this can also complement a fundamental bottom up approach for modelling, based upon the relevant differential equations and processes. Although the results here might be case dependent (especially the ML algorithm), it has been shown that the method, with the appropriate case-dependent adaptations (e.g. other ML algorithm or more detailed input data in the model), can provide good within-vehicle exposure results.

The use of ambient monitoring data (rather than adjacent to vehicle measurements) to predict within-vehicle concentrations gave promising results highlighting that within-vehicle exposure can be estimated with no additional cost of measurements. Given that commercial/professional drivers (e.g. bus, taxi and van drivers) exposure is a currently debating issue, with very limited to no studies globally according to the systematic review of Lawin et al., (2018), modelling techniques such as those presented here can be proved very useful to estimate the health risks that are associated with this group.

As a future direction, this research can provide the background for more in-depth exposure predictive models for car passengers, where driving conditions (e.g. urban, motorway driving), driving duration, passenger characteristics (e.g. different ventilation rates, metabolism, sex, weight) and pollutant infiltration and penetration pathways, including potential engine leaks, will be taken into consideration. Further investigation of exposure in alternative methods of commuting would be useful to

provide an estimate of the total daily exposure to air pollution, and raise public awareness for alternative ways of commuting. Measurements of carcinogenic organic compounds or other toxic substances such as dioxins will provide insights about which other pollutants are more important for health impact assessments. Such information will be critical for the application of air quality management policies and new technologies such as within-vehicle air purifiers or high selectivity air filters to reduce air pollution exposure.

# Chapter 5. Synthesis

## 5.1 Summary and conclusions

The main research objective of this thesis was to investigate real-world vehicle emissions in an urban environment and their implications for outdoor and within-vehicle air quality, and hence exposure and human health. The thesis focuses on three main research areas and answers a number of key questions concerning:

- Trends in long term ambient air quality measurements at roadsides in the UK from 2009 to 2016, identifying measurable impacts that the vehicle emissions have upon urban air quality.
- Within-vehicle multi air pollutant personal exposure under different ventilation settings on urban, sub-urban and ring-road driving environments and the corresponding activity based exposure and inhalation dose that vehicle occupants, cyclists and pedestrians experience in a typical urban environment.
- Development of a microenvironment model to estimate within-vehicle air pollution exposure and the use of the state-of-the-art machine learning algorithms under real world scenarios to provide within-vehicle exposure estimates from existing conurbation monitoring data.

Several tools were applied/developed including a) data mining of observations, namely hourly air quality concentrations of NO, $NO_2$, $O_3$ together with meteorological observations of temperature, humidity and cloud coverage across the UK from 2009 - 2016, 2) mobile measurement campaigns with different types of vehicles, where a total of 13 instruments were deployed inside vehicles to measure inside to outside concentrations of NO, $NO_2$, $CO_2$, $PM_{10}$, $PM_{2.5}$, $PM_1$, UFP and LSDA and 3) application and development of modelling tools, namely atmospheric chemistry box-models, mass-balance receptor models and state-of-the-art machine learning models. Here the main findings of the aforementioned three key research areas are summarised, alongside a discussion of potential limitations of this study, and identification of remaining research gaps/future research directions.

**Chapter 2 investigated ambient $NO_x$ and $NO_2$ mixing ratios, as well as primary $NO_2$ emissions from road vehicles, via analysis of data from urban traffic monitoring stations in the UK, for the period from 2009 until 2016.** A new methodology was developed to investigate cold temperature vehicle emissions from ambient data which used to report air quality. The analysis found:

An overall decrease in the mean ambient $NO_2$ mixing ratios of 20% between 2009 and 2016, alongside a smaller, 10% reduction in $NO_x$ mixing ratios, implying improvement in the UK's urban air quality in so far as nitrogen oxides are concerned.

The ambient $NO_2/NO_x$ ratio has changed since 2009, and for locations with the same $NO_x$ mixing ratios between 2009 and 2016, the $NO_2$ mixing ratios have fallen,

suggesting that there is a positive impact of applied policies and plans on reducing primary $NO_2$ emissions from vehicles.

The mean inferred primary $NO_2$ emissions show a significant overall reduction of 3 percentage points from 17% to 14% (18% change), with a calculated reduction of -0.32 percentage points/year (95% confidence interval of -0.2 - -0.45 percentage points/year). The timescales for this reduction correspond to the combined application of policies (new Euro limits), the change in the fleet (reduction/change of old diesel vehicles) and to some extent the new after-treatment technologies which were introduced and fitted in vehicles in the last eight years. However, this reduction is not evident in every city/county, underling the complexity of the problem and implying that more critical measures are needed for the reduction of ambient $NO_2$.

The application of the newly introduced methodology for the investigation of "cold-start" emissions, inferred from ambient monitoring data under low temperature conditions, showed an overall primary $NO_2$ emissions increase by 64.5% and 75% on average for morning and evening rush hours respectively. This emission increment under low temperature (≤ 5 $^{o}$C) rises between 1.6 and 3.8 times higher than under normal temperatures (> 5 $^{o}$C) when examining individual urban locations. A significant inverse relationship was found between mean monthly temperature and mean monthly primary $NO_2$ emissions, where the latter can be estimated according to the equation (1):

$$fNO_2 = 15 - [0.77 \pm 0.15]\ T\ (^{O}C), \qquad \text{for } T \leq 0 \qquad (1)$$

In summary, chapter 2 suggests that the current after-treatment systems are lacking in performance under low ambient temperatures. Furthermore, the combination of (short duration) driving patterns and temperature dependence of after-treatment systems lead to measurable impacts upon ambient air quality. This finding needs to be addressed, in order to avoid highly augmented $NO_x$ and $NO_2$ emissions, and thus, air pollution episodes with elevated exposure under cold weather. They also highlight the importance of new regulations with stricter limits to capture all vehicle type cold-start emissions. Finally, the results reported here provide encouraging evidence that with combined and correct/targeted implementation of legislation, policy and technology, the $NO_x$ and $NO_2$ problem in urban areas, which stems from vehicles, can be significantly mitigated.

**Chapter 3 investigated the $PM_{10}$, $PM_{2.5}$, $PM_1$, UFP, LSDA, NO and $NO_2$ exposure within-vehicles in relation to the on-road/ambient air pollution under different ventilation settings and driving routes, through primary data collection/measurements.** The vehicle occupant air pollution uptake (inhalation) was also investigated in this chapter and it was compared with cycling and walking activities. The analysis showed:

The median within-vehicle exposure (aggregated across all vehicle ventilation options tested), when driving from sub-urban to urban and ring-roads, increased by 73% and 13% for $PM_{10}$, 175% and 75% for $PM_{2.5}$ and 200% and 83% for $PM_1$ respectively. UFP exposure increased by 24% (sub-urban to urban) and 36% (sub-urban

to ring-road), and for LSDA by 32% and 52%, respectively. $NO_x$ median exposure increased significantly by 69% (sub-urban to urban) and 44% (sub-urban to ring-road) for $NO_2$, and 70% (sub-urban to urban) and 11% (sub-urban to ring-road) for NO. This highlights the significant effect that the correct choice of route has on vehicle occupant's exposure to air pollution.

The impact of vehicle ventilation setting upon vehicle occupant exposure to air pollution was examined by assessing variations in $I/O_{VEH}$ ratios. The $I/O_{VEH}$ ratios for particles increased towards outdoor levels when introducing greater outside air flow into the vehicle, as would be expected. When recirculating the air within the cabin, $I/O_{VEH}$ median ratios for $PM_{10}$, $PM_{2.5}$, $PM_1$, UFP and LSDA decreased up to 80% relatively to the outdoor levels. However, under recirculation mode, the analysis showed that there might be a potential trade-off between benefits from reduced PM, and a penalty in exposure from increased $NO_2$.

Vehicle occupants, due to reduced breathing rate and activity, inhale less air overall than pedestrians and cyclists on the same roads. On a median level, vehicle occupants inhale 4.6, 7.6 and 6.9 more $NO_2$ than $PM_{2.5}$ by mass in urban, sub-urban and ring-road environments respectively, with a trip average inhalation dose ratio of 6.4 ($NO_2$ dose/$PM_{2.5}$ dose). The implication of this dose ratio for professional drivers is that the influence of $NO_2$ on premature mortality is greater than that of $PM_{2.5}$ (under the conditions assessed in this work) and could be even greater given that within vehicles, NO is quickly oxidised to $NO_2$ in the presence of $O_3$ prior to its loss to surfaces.

To summarise, vehicle occupants are exposed to detrimental concentrations of $PM_{2.5}$ and $NO_2$ with overall median $I/O_{VEH}$ ratios of 0.76 and 0.98 respectively. For the optimal (lowest exposure) ventilation setting, within-vehicle exposure to $PM_{2.5}$ and $NO_2$ is reduced by 49% and 34% respectively. Overall, vehicle occupants inhale 45% less $PM_{2.5}$ and 12% less $NO_2$ compared to pedestrians, and 47% and 57% less $PM_{2.5}$ and $NO_2$ than cyclists. Finally, car passengers can modify their exposure and inhalation dose through route choice by factors of 1.25 – 3.5 and 0.4 – 0.45 for $PM_{2.5}$ and $NO_2$ respectively.

**Chapter 4 used the experimental results reported in chapter 3 and developed a mass balance model for the indirect investigation of within-vehicle air pollution exposure.** In this chapter, alternative modelling methods using the state-of-the-art machine learning algorithms were validated using the experimental data and tested for real world applications where only data from nearby air quality monitoring sites is available.

The mass balance model showed different performance predictions for gases and particles, with most of the species being within the ±10% of the standard error of the 1:1 model. Some systematic discrepancies that occur in the model regarding the UFP and LSDA predictions are probably associated with the infiltration, deposition and penetration parameters of these species, whose values were taken from studies performed in houses/buildings.

The machine learning model showed similar performance to the original mass balance model for the majority of the species considered, and better predicted $NO_2$

levels. The predictions of the machine learning model showed good skill in estimating random unseen within-vehicle concentrations of different pollutants with the RMSE (root mean squared error) lower than the SD (standard deviation) of observations for all species. Furthermore, the machine learning model had a Pearson correlation coefficient greater than 0.80, and IOA greater than 0.69 for all the species, demonstrating good predictions. Finally, the test of the machine learning model with real world cases to predict within-vehicle exposure of $PM_{2.5}$ and $NO_2$ using median within-vehicle concentration and data from the closest air quality monitoring sites (instead of real observations directly adjacent to the vehicle) showed promising results for the application of this approach.

## 5.2 Limitations

The findings presented and discussed in this thesis are not without uncertainty and have their limitations. For example, chapter 2 investigated the primary $NO_2/NO_x$ ratio in UK roadsides with the application of the 'total oxidant' analysis, $(NO_2 + O_3) / NO_x$, to draw conclusions regarding vehicle emissions following Jenkin, (2004). However, most urban traffic monitoring sites in the UK do not have $O_3$ measurements which poses a limitation to the total oxidant approach and to the estimation of the

primary $NO_2/NO_x$ vehicle emissions. In cases where $O_3$ data was not available at urban traffic sites, additional observations from the closest urban background site were included and the methodology of Carslaw and Beevers, (2005) was followed. Carslaw and Beevers, (2005) assume that the increment in $NO_2$ mixing ratio between a given urban traffic monitoring site and a nearby urban background site is partitioned into $NO_2$ that is chemically derived through the reaction between NO and $O_3$, and $NO_2$ which is emitted directly by road vehicles. However, this is not the case in some locations mainly due to the surrounding infrastructure and/or any additional sources. In addition to the above, this indirect total oxidant approach is not a "type approved" method to investigate driving emissions. In order to measure real world driving emissions additional information regarding the vehicle operating temperature and oil temperature are needed (Franco et al., 2013). The method that was introduced in this chapter to estimate the cold-temperature vehicle emissions and their impact on air quality has a main limitation. The method assumes that the ambient temperature was the operational temperature of the vehicle, and cannot distinguish between the number of vehicles operated under cold-start, hot-restart or normal conditions. The implications for the $NO_x$ urban air quality load of only cold-start vehicles might be even greater as shown by recent studies (Grange et al., 2019). Finally, the total oxidant approach has a clear limitation at night, as it assumes PSS, which can only occur during daytime, in the atmosphere. At night the $O_3$ aloft reacts with $NO_2$ to form $NO_3$, a short lived radical, which during daytime due to its rapid photolysis and reaction with NO, can enhance $NO_2$ concentrations in early morning hours (Brown and Stutz, 2012).

The within-vehicle exposure findings for $PM_{10}$, $PM_{2.5}$, $PM_1$, UFP, LSDA, NO and $NO_2$ and the $I/O_{VEH}$ ratios, reported in chapter 3, are limited to the number of vehicles and the ventilation settings and routes tested in this thesis. A broader range of vehicles including new and old vehicles might differentiate the results as the I/O ratios are highly dependent on the manufacturer and age of the vehicle (Hudda et al., 2011). Furthermore, within-vehicle exposure might vary during rush hour periods and night time due to on-road fleet composition and atmospheric processes, and might be greater than the values reported here under normal daytime traffic driving outside of peak periods. The experiments in chapter 3 did not test any air cabin filters other than the standard pollen ones and no further implications for NO and $NO_2$ reductions could be made. Finally, breathing rates or body weight of vehicle occupants were not measured in this study and the calculation and comparison of the inhalation doses were made using the ventilation rates reported in Adams, 1993. The air pollution uptake might vary from the values reported in chapter 3 during driving/commuting by car, cycling and walking activities, as individuals react differently to heavy/light exercise activities, while this uptake might also be different for smoking and non-smoking groups.

The mass balance modelling developed in chapter 4 is, apart from the low number of vehicles available to provide test data, limited by the model physical parameters. Most of the parameters are based on measurement studies performed in residential buildings/houses, and vehicles are typically smaller microenvironments than houses and hence more sensitive to such physical processes. Therefore, the current deposition rates, penetration factors, filtration, leaks might lead to systematic

under or over predictions in the model. The mass balance model also assumes a well-mixed vehicle cabin microenvironment. Finally, the mass balance model does not include any reactive surface chemistry and detailed physical and chemical indoor processes such as particle coagulation, particle phase-change phenomena and heterogeneous reactions (Carslaw, 2007). The ML model that was applied in chapter 4 is dependent on the specific training parameters (e.g. vehicle characteristics, fan power, AERs, concentrations) and therefore the same ML algorithm might not be suited for other applications.

## 5.3 Suggestions for future research

To date, there are several studies reporting discrepancies between legislative vehicle emission limits and cold-start vehicle real world driving emissions (BMVI, 2016; Degraeuwe and Weiss, 2017; Grange et al., 2019; Suarez-Bertoa and Astorga, 2018). However, there are limited studies reporting elevated real world vehicle driving emissions under hot temperatures (Dallman et al., 2019). These studies are either based on PEMS or on remote sensing data and are experimentally expensive regarding their deployments. The methodology reported in chapter 2 could be expanded and applied under hot temperatures to provide insights for vehicle emissions. Plume chase

measurements, which are currently used to estimate fleet average vehicle emissions, could be focused on investigating real world driving emissions under: 1) different road gradients (e.g. uphill/downhill), locations (e.g. traffic lights, roundabouts), conditions (i.e. idling, accelerating, decelerating), 2) investigating ammonia emissions from the new SCR and LNT diesel catalysts (Elser et al., 2018) or 3) non-exhaust emissions from tyre wear of electric vehicles, which might play a critical role in future urban air pollution when this type of vehicle starts to penetrate the fleet.

The experiments in chapter 3 reported exposure to multiple air pollutants within vehicles relative to air quality directly outside and underpinned the greater health impact of $NO_2$ over $PM_{2.5}$ for vehicle occupants, at the levels observed from these data. Dominici et al., (2010), highlighted the necessity of shifting exposure studies from a single-pollutant to a multipollutant approach in order to protect human health from air pollution. The multiple air pollutant exposure approach taken in chapter 3 could be applied in other indoor microenvironments such as schools, offices and houses, where epidemiologists are currently lacking data (COMEAP, 2018). Contrasting impacts of different PM chemical composition and morphology also need to be investigated as they play a critical role in mortality, while additional measurements regarding toxic VOC mixtures such as benzene or toluene need to be performed. In this way, we can improve their understanding regarding the precise weight that each air pollutant has on human health. Future research related to air pollution inside vehicle cabins must be conducted with the use of activated carbon air cabin filters or with air purifiers inside the cabin in order to quantify their associated health benefit. Furthermore, future, within-vehicle exposure campaigns need to

include measurements of the breathing rates and body weight of vehicle occupants and enhance our understanding about the air pollution uptake that specific groups have under this activity. The necessity of this is underpinned by Cepeda et al., 2017, who found that although drivers are exposed to regular air pollution spikes, their overall uptake is much smaller compared to those walking or cycling. Multi-pollutant exposure campaigns should also focus on time activity of individuals, such as the European Physical Activity through Sustainable Transport Approaches - PASTA project (Gascon et al., 2019), and the activity contribution to daily inhalation dose, as highlighted in the meta-analysis of Cepeda et al., (2017). However up to the present date this is still challenging, firstly because different activities might give different air pollutant species dose contributions and secondly since most of the personal exposure campaigns rely on personal exposure monitors, which have significant discrepancies in measuring the actual exposure levels, potentially leading to false estimates. Approaches to tackle this problem include massive air quality monitoring as described by Motlagh et al. (2020), where thousands or hundreds of thousands of sensors can be integrated into the vehicles or carried by pedestrians, which in addition to the reference stations and mid-cost sensors at specific locations, can achieve detailed and accurate coverage.

The development of the mass-balance model for microenvironments in chapter 4 is currently limited to indoor reactive chemistry. Up to date, reactive chemistry is a critical source of chemicals for indoor environments that might not otherwise be present as primary emissions. These chemicals can be responsible for the formation of oxygenated VOCs (such as organic nitrates, carbonyls, etc.) and secondary organic

aerosols (Weschler and Carslaw, 2018). Currently, there is a gap in the literature regarding the air pollutant transformations and detailed chemistry within-vehicles, and properties such as infiltration efficiency, leaks, deposition rates, evaporation and condensation were all taken from indoor house studies (see Table 4.5). Therefore, it is essential to investigate those chemical transformations and missing sources in microenvironments in order to improve the accuracy of the present modelling approaches. In addition to the above, detailed mapping of internal sources such as particle resuspension from seats or other surfaces need to be investigated and included in the models. Such detailed measurements will complement mass balance model approaches which in turn coupled with other air quality models can provide dynamic estimates of our daily exposure based on activity. They will also support improvement of machine learning algorithms in data driven models which can be used as an alternative approach to predict within-vehicle air quality.

# Bibliography

ACEA, (2017), Share of Diesel in New Passenger Cars. Retrieved from http://www.acea.be/statistics/tag/category/share-of-diesel-in-new-passenger-cars

Adams W. C., 1993. Measurement of breathing rate and volume in routinely performed daily activities. Final Report Contract No. A033- 205, Air Resources Board, California Environmental Protection Agency, Sacramento, CA

Adam, M., Schikowski, T., Carsin, A. E., Cai, Y., Jacquemin, B., Sanchez, Met al., 2015. Adult lung function and long-term air pollution exposure. ESCAPE: a multicentre cohort study and meta-analysis. Eur Respir J, 45, 38–50. https://doi.org/10.1183/09031936.00130014

Aidaoui L, Triantafyllou A. G., Azzi A., Garas S. K., Matthaios V. N., 2015. Elevated stacks' pollutants' dispersion and its contributions to photochemical smog formation in a heavily industrialized area. Air Qual Atmos Health 8:213–227

Alas, H. D. C., Weinhold, K., Costabile, F., Di Ianni, A., Müller, T., Pfeifer, S., Di Liberto, L., Turner, J. R., and Wiedensohler, A., 2019. Methodology for high-quality mobile measurement with focus on black carbon and particle mass concentrations, Atmos. Meas. Tech., 12, 4697–4712, https://doi.org/10.5194/amt-12-4697-2019.

Alm, S., Jantunen, M.J., Vartiainen, M., 1999. Urban commuter exposure to particle matter and carbon monoxide inside an automobile. Journal of Exposure Analysis and EnvironmentalEpidemiology 9, 237

Anenberg S.C., Miller J., Minjares R., Du L., Henze D.K., Lacey F., et al., 2017. Impacts and mitigation of excess diesel-related NOx emissions in 11 major vehicle markets, Nature 545, 467–471.

Andersson, J., May, J., Favre, C., Bosteels, D., De Vries, S., Heaney, M., … Mansell, J. (2014). On-Road and chassis dynamometer evaluations of emissions from two Euro 6 diesel vehicles. SAE International Journal of Fuels and Lubricants, 7(3), 1–16. https://doi.org/10.4271/2014-01-2826

Anttila, P., Tuovinen, J., Niemi, J. V. (2011). Primary NO2 emissions and their role in the development of NO 2 concentrations in a traffic environment. Atmospheric Environment, 45(4), 986–992. https://doi.org/10.1016/j.atmosenv.2010.10.050

Apte S. J., Brauer M., J. Cohen J. A., Ezzati M., C. Pope C. A., 2018. Ambient PM2.5 Reduces Global and Regional Life Expectancy. Environmental Science & Technology Letters, 2018; DOI: 10.1021/acs.estlett.8b00360

AQEG. (2004). Nitrogen Dioxide in the UK. Retrieved from http://www.defra.gov.uk/environment/airquality/publications

AQEG. (2007). Trends in Primary Nitrogen Dioxide in the UK. Retrieved from http://archive.defra.gov.uk/environment/quality/air/airquality/publications

Aquilina N., D. S. J. Maria, B. Stefano et al., 2018. Comparison of machine learning approaches with a general linear model to predict personal exposure to benzene. Environmental Science & Technology, vol. 52, 2018.

Atkinson R. W., Fuller G. W., Anderson H. R., Harrison R. M., Armstrong B., 2010. Urban ambient particle metrics and health: a time-series analysis. Epidemiology, 21:501–11.

Attfield, M. D., Schleiff, P. L., Lubin, J. H., Blair, A., Stewart, P. A., Vermeulen, R., … Silverman, D. T. (2012). The Diesel Exhaust in Miners Study : A Cohort Mortality Study With Emphasis on Lung Cancer. Journal of the National Cancer Institute, 104, 869–883. https://doi.org/10.1093/jnci/djs035

Bais, A.F., Lucas, R.M., Bornman, J.F., Williamson, C.E., Sulzberger, B., Austin, A.T., Wilson, S. R., Andrady, A.L., Bernhard, G., McKenzie, R.L., Aucamp, P.J., Madronich, S., Neale, R.E., Yazar, S., Young, A.R., de Gruijl, F.R., Norval, M., Takizawa, Y., Barnes, P.W., Robson, T. M., Robinson, S.A., Ballaré, C.L., Flint, S.D., Neale, P.J., Hylander, S., Rose, K.C., Wängberg, S.-Å., Häder, D.-P., Worrest, R.C., Zepp, R.G., Paul, N.D., Cory, R.M., Solomon, K.R., Longstreth, J., Pandey, K.K., Redhwi, H.H., Torikai, A., Heikkilä, A.M., 2018. Environmental effects of ozone depletion, UV radiation and interactions with climate change: UNEP Environmental Effects Assessment Panel, update 2017. Photochem. Photobiol. Sci. 17, 127–179.

Ben-David T., Waring S. M., 2016. Impact of natural versus mechanical ventilation on simulated indoor air quality and energy consumption in offices in fourteen U.S. cities, Building and Environment 104, DOI: 10.1016/j.buildenv.2016.05.007.

Berges, M. G. M., R. M. Hofmann, D. Scharffe, P. J. Crutzen (1993). Nitrous oxide emissions from motor vehicles in tunnels and their global extrapolation, J. Geophys. Res., 98(D10), 18527–18531, doi:10.1029/93JD01637.

Bielaczyc, P., Szczotka, A., Woodburn, J., (2012). Excess emissions and fuel consumption of modern spark ignition passenger cars at low ambient temperature. SAE paper

2012-01-1070, SAE world congress & exhibition, Detroit Michigan, USA, April 2012. http://dx.doi.org/10.4271/2012-01-1070.

Bielaczyc, P., Szczotka, A., Woodburn, J., (2011). The effect of low ambient temperature on the cold-start emissions and fuel consumption of passenger cars. J Automobile Eng 2011, 225(9), 1253-1264. http://dx.doi.org/10.1177/0954407011406613.

Bishop, G. A., Starkey, J. R., Ihlenfeldt, A., Walter, J. (1989). IR Long-Path Photometry: A Remote Sensing Tool for Automobile Emissions. Analytical Chemistry, 61(10), 0–5.

Bloss, W., 2009. Atmospheric chemical processes of importance in cities. In: Hester, R.E., Harrison, R.M. (Eds.), Air quality in urban environments. Issues in Environmental Science and Technology, vol. 28. Royal Society of Chemistry, London, pp. 42-64.

BMVI. (2016). Bericht der Untersuchungskommission „ Volkswagen “. Www Document, Bundesministerium Für Verkehr Und Digit. Infrastruktur. URL. Https:// www.bmvi.de/SharedDocs/DE/Anlage/VerkehrUndMobilitaet/Strasse/berichtUntersuchungskommission-volkswagen.pdf?__blob¼publicationFile.

Boniardi L., Dons E., Campo L., Van Poppel M., Luc Int Panis L., Fustinoni S., 2019. Is a Land Use Regression Model Capable of Predicting the Cleanest Route to School? Environments, 6, 90; doi:10.3390/environments6080090

Boogaard H, Borgman F, Kamminga J, Hoek G. 2009. Exposure to ultrafine and fine particles and noise during cycling and driving in 11 Dutch cities. Atmos Environ 43:4234–4242.

Both, A. F., D. Westerdahl, S. Fruin, B. Haryanto & J. D. Marshall 2013. Exposure to carbon monoxide, fine particle mass, and ultrafine particle number in Jakarta, Indonesia: Effect of commute mode. Science of the Total Environment, 443, 965-972

Botvinick, M. et al., 2019. Reinforcement Learning, Fast and Slow. Trends Cogn. Sci. 23(5) DOI: 10.1016/j.tics.2019.02.006.

Brantley, H. L., Hagler, G. S. W., Kimbrough, E. S., Williams, R. W., Mukerjee, S., Neas, L. M. 2014. Mobile air monitoring data-processing strategies and effects on spatial air pollution trends. Atmospheric Measurement Techniques, 7(1), 2169–2183. https://doi.org/10.5194/amt-7-2169-2014

Brown, S. S., Stutz, J., 2012. Nighttime radical observations and chemistry, Chem. Soc. Rev., 41, 6405–6447, doi:10.1039/c2cs35181a.

Capri A., Chen Y. F., 2001. Gaseous Elemental Mercury as an Indoor Air Pollutant, Environmental Science and Technology 35(21):4170-3.

Carslaw, D. (2016a). The openair manual.

Carslaw, D. C. (2005). Evidence of an increasing NO2/NOX emissions ratio from road traffic emissions. Atmospheric Environment, 39(26), 4793–4802. https://doi.org/10.1016/j.atmosenv.2005.06.023

Carslaw, D. C., Beevers, S. D. (2005). Estimations of road vehicle primary NO 2 exhaust emission fractions using monitoring data in London. Atmospheric Environment, 39(1), 167–177. https://doi.org/10.1016/j.atmosenv.2004.08.053

Carslaw, D. C., Beevers, S. D., Tate, J. E., Westmoreland, E. J., Williams, M. L. (2011). Recent evidence concerning higher NOx emissions from passenger cars and light duty vehicles. Atmospheric Environment, 45(39), 7053–7063. https://doi.org/10.1016/j.atmosenv.2011.09.063

Carslaw, D. C., Murrells, T. P., Keenan, M. (2016b). Have vehicle emissions of primary NO2 peaked ? Faraday Discussions, 189(0), 439–454. https://doi.org/10.1039/C5FD00162E

Carslaw, D. C., Rhys-Tyler, G. (2013). New insights from comprehensive on-road measurements of NOx, NO2 and NH3 from vehicle emission remote sensing in London, UK. Atmospheric Environment, 81(2), 339–347. https://doi.org/10.1016/j.atmosenv.2013.09.026

Carslaw, D. C., Ropkins, K. (2012). openair - An R package for air quality data analysis. Environmental Modelling and Software, 27–28, 52–61. https://doi.org/10.1016/j.envsoft.2011.09.008

Carslaw N., 2007. A new detailed chemical model for indoor air pollution. Atmos. Environ, 41 (6), 1164−1179.

Cepeda M., Schoufour J., Freak-Poli R., Koolhaas C. M., Dhana K., Bramer W. M., Franco O. H., 2017. Levels of ambient air pollution according to mode of transport: a systematic review. Lancet. https://doi.org/10.1016/S2468-2667(16)30021-4

Chan, A.T., Chung, M.W., 2003. Indoor-outdoor air quality relationships in vehicle: effect of driving environment and ventilation modes. Atmos. Environ. 37, 3,795-3,808.

Chan, C.-C., Ozkaynak, H., Spengler, J.D., Sheldon, L., 1991. Driver exposure to volatile organic compounds, CO, ozone and NO2 under different driving conditions. EnvironmentalScience & Technology 25 (5), 964.

Chan, L.Y., Liu, Y.M., 2001. Carbon monoxide levels in popular passenger commuting modes traversing major commuting routes in Hong Kong. Atmospheric Environment 35, 2637.

Chan, L.Y., Chan, C.Y., Qin, Y., 1999. The effect of commuting microenvironment on commuter exposures to vehicular emission in Hong Kong. Atmospheric Environment 33 (11), 1777.

Chan, L.Y., Lau, W., Lee, S., Chan, C.Y., 2002a. Commuter exposure to particulate matter in public transportation modes in Hong Kong. Atmospheric Environment 36, 3363.

Chan, L.Y., Lau, W., Zou, S., Cao, Z., Lai, S., 2002b. Exposure level of carbon monoxide and respirable suspended particulate in public transportation modes while commuting in urban area of Guangzhou, China. Atmospheric Environment 36, 5831.

Chen, C., Zhao, B., 2011. Review of relationship between indoor and outdoor particles: I/Oratio, infiltration factor and penetration factor. Atmos. Environ. 45, 275–288. https://doi.org/10.1016/j.atmosenv.2010.09.048

Chertok, C., Voukelatos, A., Sheppeard, V., Rissel, C., 2004. Comparison of personal exposures to air pollutants by commuting mode in Sydney—BTEX & NO2. NSW Department of Health, Better Health Centre, Sydney.

Clapp, L. J., Jenkin, M. E. (2001). Analysis of the relationship between ambient levels of O3 , NO2 and NO as a function of NOx in the UK. Atmospheric Environment, 35(2), 6391–6405.

Cleveland, R. B., Cleveland, W. S., McRae, J. E., Terpenning, I. (1990). STL: A seasonal-Trend Decomposition Procedure Based on Loess. Journal of Official Statistics, 6(1), 3–73.

Clifford, M., Clarke, R., Riffat, S., 1997a. Drivers' exposure to carbon monxoide in Nottingham, UK. Atmospheric Environment 31 (7), 1003.

COMEAP, C. O. M. E. A. P. (2010). The Mortality Effects of Long-Term Exposure to Particulate Air Pollution in the United Kingdom.

COMEAP. (2018). Committee on the Medical effects of air pollutants. Associations of long-term average concentrations of nitrogen dioxide with mortality. Retreived from: https://www.gov.uk/government/publications/nitrogen-dioxide-effects-on-mortality.

Correia et al., 2020. Particle exposure and inhaled dose while commuting in Lisbon. Env. Poll. 257, 113547.

Cover T., Hart P., 1967. Nearest neighbor pattern classification. In IEEE Transactions in Information Theory, IT-13, pages 21–27.

Crilley, L. R.; Knibbs, L. D.; Miljevic, B.; Cong, X.; Fairfull Smith, K. E.; Bottle, S. E.; Ristovski, Z. D.; Ayoko, G. A.; Morawska, L., 2012. Concentration and oxidative potential of on-road particle emissions and their relationship with traffic composition: Relevance to exposure assessment. Atmos. Environ., 59 (0), 533−539

Crilley, L. R., Kramer, L., Pope, F. D., Whalley, L. K., Cryer, D. R., Heard, D. E., … Bloss, W. J. (2016). On the interpretation of in situ HONO observations via photochemical steady state. Faraday Discussions, 189, 191–212. https://doi.org/10.1039/C5FD00224A

Crilley, L. R., Singh, A., Kramer, L. J., Shaw, M. D., Alam, M. S., Apte, J. S., Bloss, W. J., Hildebrandt Ruiz, L., Fu, P., Fu, W., Gani, S., Gatari, M., Ilyinskaya, E., Lewis, A. C., Ng'ang'a, D., Sun, Y., Whitty, R. C. W., Yue, S., Young, S., and Pope, F. D., 2020. Effect of aerosol composition on the performance of low-cost optical particle counter correction factors, Atmos. Meas. Tech., 13, 1181–1193, https://doi.org/10.5194/amt-13-1181-2020.

Cames, M., Helmers, E., 2013. Critical evaluation of the European diesel car boom—global comparison, environmental effects and various national strategies. Environ. Sci. Eur. 25, 1–22.

Dallmann, T., Bernard, Y., Tietge, U., Muncrief R., 2019. Remote sensing of motor vehicle emissions in Paris https://www.trueinitiative.org/media/790750/true_paris_rs_report_0905019-1.pdf

Dardiotis, C., Martini, G., Marotta, A., Manfredi, U., (2013). Low-temperature cold-start gaseous emissions of late technology passenger cars. Applied Energy 111, 468-478. http://dx.doi.org/10.1016/j.apenergy.2013.04.093

DEFRA. (2017). Air Pollution in the UK 2016. Retrieved from https://uk-air.defra.gov.uk/library/annualreport/index

DEFRA, 2018. Air pollution in the UK 2017, Department for Environment Food and Rural Affairs. Sep 2018: https://uk-air.defra.gov.uk/assets/documents/annualreport/air_pollution_uk_2017_issue_1.pdf

Degraeuwe, B., Weiss, M. (2017). Does the New European Driving Cycle (NEDC) really fail to capture the NOX emissions of diesel cars in Europe? Environmental Pollution, 222, 234–241. https://doi.org/10.1016/j.envpol.2016.12.050

Delfino, R.J., Malik, S., Sioutas, C., 2005. Potential role of ultrafine particles in associations between airborne particle mass and cardiovascular health. Environmental Health Perspectives 113 (8), 934-946.

Delgado-Saborit, J.M., 2012. Use of real-time sensors to characterise human exposures to combustion related pollutants. J. Environ. Monit. 14, 1824–1837.

Dennekamp, M., Mehenni, O., Cherrie, J., Seaton, A., 2002. Exposure to ultrafine particles and PM2.5 in different microenvironments. Annals of Occupational Hygiene 46 (Suppl. 1), 412

De Hartog, J.J., Ayres, J., Karakatsani, A., Analitis, A., ten Brink, H., Hameri, K., Harrison, R., Katsouyanni, K., Kotronarou, A., Kavouras, I., Meddings, C., Pekkanen, J., Hoek, G., 2010. Lung function and indicators of exposure to indoor and outdoor particulate matter among asthma and COPD patients. Occupational and Environmental Medicine 67, 2-10.

De Nazelle A, Seto E, Donaire-Gonzalez D, Mendez M, Matamala J, Nieuwenhuijsen MJ. et al. 2013. Improving estimates of air pollution exposure through ubiquitous sensing technologies. Environ Pollut; 176: 92-9.

De Nazelle, A., Fruin, S., Westerdahl, D., Martinez, D., Ripoll, A., Kubesch, N., Nieuwenhuijsen, M., 2012. A travel mode comparison of commuters' exposures to air pollutants in Barcelona. Atmos. Environ. 59, 151–159.

DfT, Department for Transport. (2016). Vehicle Emissions Testing Programme - Moving Britain Ahead, (April 2016).

DfT, Department for Transport (2017). National Travel Survey: England 2016, (July 2017) retrieved from https://www.gov.uk/government/statistics/national-travel-survey-2016.

Dickens, C., 2000. In-Car Particle Exposure. A report produced for DETR, vol. AEAT/EEQA-0125, issue 2. AEA Technology

Dominici F., Peng R. D., Barr C. D., Bell M. L., 2010. Protecting human health from air pollution: shifting from a single pollutant to a multipollutant approach. Epidemiology 21:187–194.

Dons, E., Int Panis, L., Van Poppel, M., Theunis, J., Willems, H., Torfs, R., Wets, G., 2011. Im-pact of time–activity patterns on personal exposure to black carbon. Atmos. Environ. 45, 3594–3602. https://doi.org/10.1016/j.atmosenv.2011.03.064.

Duci, A., Chaloulakou, A., Spyrellis, N., 2003. Exposure to carbon monoxide in the Athens urban area during commuting. The Science of the Total Environment 309 (1–3), 47.

Duffy, B. L., Nelson, P. F., 1997. Exposure to emissions of 1,3-butadiene and benzene in the cabins of moving motor vehicles and buses in Sydney, Australia, Atmos. Environ., 31, 3877–3885.

Dunlea, E. J., Herndon, S. C., Nelson, D. D., Volkamer, ... Molina, M. J.: Evaluation of nitrogen dioxide chemiluminescence monitors in a polluted urban environment, Atmos. Chem. Phys., 7, 2691–2704, doi:10.5194/acp-7-2691-2007, 2007.

E. E. A. (2016). Air quality in Europe — 2016 report.

EC Commission, E. (2011). Commission Regulation (EU) No 582/2011, of 25 May 2011. Implementing and amending Regulation (EC) No 595/2009 of the European parliament and of the council with respect to emissions from heavy duty vehicles (Euro VI) and amending Annexes I and III to Directive 2007/46/EC of the European Parliament and of the Council. Official Journal of the European Union, 2011, L 167/1-168.

EC Commission, E. (2008a). Directive 2008/50/EC of the European Parliament and the Council of 21 May 2008. On ambient air quality and cleaner air for Europe. Official Journal of the European Union, 2008, L152/1-44.

EC Commision, E., (2008b). Commission Regulation (EC) No 692/2008 of 18 July 2008. Implementing and amending Regulation (EC) No 715/2007 of the European Parliament and of the Council on type-approval of motor vehicles with respect to emissions from light passenger and commercial vehicles (Euro 5 and Euro 6) and on access to vehicle repair and maintenance information. Official Journal of the European Union, 2008, L199/1-136.

EC Commision, E. (1998). Directive 98/68/EC of the European Parliament and of the Council of 13 October 1998. Relating to measures to be taken against air pollution by emissions from motor vehicles and amending Council Directive 70/220/EEC. Official Journal of the European Communities, (L), 1-56.

EC Commission, E. (1996). On ambient air quality assessment and management. Official Journal of the European Communities, 1995(L), 55–63.

EC Commission, E. (1991). Council Directive (91/441/EEC). On the approximation of the laws of the Member States relating to measures to be taken against air pollution by emissions from motor vehicles. Official Journal of the European Communities, (L), 1–103.

Edwards, P. N. 2011. History of climate modeling, Wiley Interdisciplinary Reviews, Climate Change, 2, 128–139.

El-Fadel, M., Abi-Esber, L., 2009. In-vehicle exposure to carbon monoxide emissions from vehicular exhaust: a critical review. Critical Reviews in Environmental Science and Technology 39, 585-621.

Elser, M., El-Haddad, I., Maasikmets, M., Bozzetti, C., Wolf, R., Ciarelli, G., Slowik, J. G., Richter, R., Teinemaa, E., Hüglin, C., Baltensperger, U., and Prévôt, A. S. H., 2018. High contributions of vehicular emissions to ammonia in three European cities derived from mobile measurements, Atmos. Environ., 175, 210– 220, https://doi.org/10.1016/j.atmosenv.2017.11.030

Fedoruk M. J., Kerger B. D., 2003. Measurement of volatile organic compounds inside automobiles. Journal of Exposure Analysis and Environmental Epidemiology, 13: 31–41.

Fernandez-Bremauntz, A.A., Ashmore, M.R., 1995. Exposure of commuters to carbon monoxide in Mexico city—I. Measurement of in-vehicle concentrations. Atmospheric Environment 29 (4), 525

Fiorello, D.; Martino, A.; Zani, L.; Christidis, P.; Navajas-Cawood, E. Mobility data across the EU 28 member states: Results from an extensive CAWI survey.Transp. Res. Procedia2106,14, 1104–1113.

Font, A., Fuller, G. W. (2016). Did policies to abate atmospheric emissions from traffic have a positive effect in London? Environmental Pollution, 218, 463–474. https://doi.org/10.1016/j.envpol.2016.07.026

Franco V., Kousoulidou M., Muntean M., Ntziachristos L., Hausberger S., Dilara P., 2013. Road vehicle emission factors development: A review. Atmospheric Environment, 70, 84–97. https://doi.org/10.1016/j.atmosenv.2013.01.006

Fromme, H., Lahrz, T., Piloty, A., Gebhardt, H., Oddoy A., and Ruden, H.,Sci. Total Environ., 2004, 326(1–3), 143–149.

Fruin S. A., Hudda N., Sioutas C., Delfino R. J., 2011. Predictive Model for Vehicle Air Exchange Rates Based on a Large, Representative Sample. Environmental Science and Technology, Vol. 45, pp. 3,569-3,575.

Fruin, S., Westerdahl, D., Sax, T., Sioutas, C., Fine, P. M., 2008. Measurements and predictors of on-road ultrafine particle concentrations and associated pollutants in Los Angeles. Atmos. Environ. 42, 207–219. http://dx.doi.org/10.1016/j.atmosenv.2007.09.057

Gan, W., Tamburic, L., Davies, H.W., Demers, P.A., Koehoorn, M., Brauer, M., 2011. Long-term exposure to traffic-related air pollution and the risk of coronary heart disease hospitalization and mortality. Environmental Health Perspectives 119 (4), 501-507.

Gascon M., Götschi T., de Nazelle A., Gracia E., Ambròs A., Márquez S., Marquet O., Avila-Palencia I., Brand C., Iacorossi F., Raser E., Gaupp-Berghausen M., Dons E., Laeremans M., Kahlmeier S., Sánchez J., Gerike R., Anaya-Boig E., Int Panis L., Nieuwenhuijsen M., 2019. Correlates of Walking for Travel in Seven European Cities: The PASTA Project, Vol. 127, No. 9. https://doi.org/10.1289/EHP4603

Gauderman W. J., Avol E., Gilliland F., Vora H., Thomas D., Berhane K., McConnell R., Kuenzli N., Lurmann F., Rappaport E., Margolis H., Bates D., Peters J. The effect of air pollution on lung development from 10 to 18 years of age. N Engl J Med. 2004;351:1057-67.

Giechaskiel, B., Vlachos, T., Riccobono, F., Forni, F., Colombo, R., Montigny, F., Le-Lijour, P., Carriero, M., Bonnel, P., Weiss, M., 2016. Implementation of portable emissions measurement systems (PEMS) for the real-driving emissions (RDE) regulation in Europe.J. Vis. Exp., 118.

Goel, A., & Kumar, P. (2016). Vertical and horizontal variability in airborne nanoparticles and their exposure around signalised traffic intersections. Environmental Pollution, 214, 54–69. doi:10.1016/j.envpol.2016.03.033

Gomez-Perales, J.E., Colvile, R.N., Nieuwenhuijsen, M.J., Fernandez-Bremauntz, A., Gutierrez-Avedoy, V.J., Paramo-Figueroa, V.H., et al., 2004. Commuters exposure to PM2.5, CO, and benzene in public transport in the metropolitan area of Mexico City. Atmospheric Environment 38 (8), 1219.

Gong L., Xu B., Zhu Y., 2009. Ultrafine particles deposition inside passenger vehicles. Aerosol Sci. Technol., 43, 544–553

Grange, S.K., Lewis, A.C., Moller, S.J., et al., 2017. Lower vehicular primary emissions of NO2 in Europe than assumed in policy projections. Nat Geosci 2017; 10: 914-918

Grange S. K., Farren N. J., Vaughan A. R., Rose R. A., Carslaw D. C., 2019. Strong Temperature Dependence for Light-Duty Diesel Vehicle NOx Emissions, Environmental Science & Technology 53(11): 6587-6596. https://pubs.acs.org/doi/10.1021/acs.est.9b01024

Grice, S., Stedman, J., Kent, A., Hobson, M., Norris, J., Abbott, J., Cooke, S. (2009). Recent trends and projections of primary NO2 emissions in Europe. Atmospheric Environment, 43(13), 2154–2167. https://doi.org/10.1016/j.atmosenv.2009.01.019

Gulliver, J., Briggs, D.J., 2004. Personal exposure to particulate air pollution in transport microenvironments. Atmospheric Environment 38 (1), 1.

Hamra, G. B., Laden, F., Cohen, A. J., Raaschou-Nielsen, O., Brauer, M., Loomis, D. 2015. Lung cancer and exposure to nitrogen dioxide and traffic: A systematic review and meta-analysis. Environmental Health Perspectives, 123 (11), 1107–1112. https://doi.org/10.1289/ehp.1408882

Harrison, R.M., 2018. Urban atmospheric chemistry: a very special case for study. npjClim. Atmos. Sci. 1, 5. https://doi.org/10.1038/s41612-017-0010-8.

Harrison, R. M., Beddows, D. C. 2017. Efficacy of Recent Emissions Controls on Road Vehicles in Europe and Implications for Public Health. Scientific Reports, March, 1–5. https://doi.org/10.1038/s41598-017-01135-2

Harrison, R. M., Dall'Osto, M., Beddows, D. C. S., Thorpe, A. J., Bloss, W. J., Allan, J. D., … Smith, S. (2012). Atmospheric chemistry and physics in the atmosphere of a developed megacity (London): An overview of the REPARTEE experiment and its conclusions. Atmospheric Chemistry and Physics, 12(6), 3065–3114. https://doi.org/10.5194/acp-12-3065-2012

Harrison, R.M. Deacon, A.R. and Jones, M.R. et al. (1997) Sources and processes affecting concentrations of PM10 and PM2.5 particulate matter in Birmingham (U.K.). Atmos. Environ. 31, 24, 4103-4117.

Han, X., Aguilar-Villalobos, M., Allen, J., Carlton, C.S., Robinson, R., Bayer, C., et al., 2005. Traffic-related occupational exposures to PM2.5, CO and VOCs in Trujillo, Peru. International Journal of Occupational and Environmental Health 11 (3), 276

Heal M. R., Kumar P., Harrison R. M, 2012. Particles, air quality, policy and health. Chem Soc Rev 41:6606–30.

Hermann M., Flammer A., and Lüscher F. T., 2006. Nitric oxide in hypertension. Journal of Clinical Hypertension, vol. 8, no. 12, supplement 4, pp. 17–29, 2006.

Hinds W. C., 1999. Aerosol Technology: Properties, Behavior, and Measurement of Airborne Particles. Wiley, New York.

Holloway, A.M. and Wayne, R.P. 2010. Atmospheric chemistry. Royal Society of Chemistry.

Hueglin, C., Buchmann, B., Weber, R. O. (2006). Long-term observation of real-world road traffic emission factors on a motorway in Switzerland. Atmospheric Environment, 40 (June), 3696–3709. https://doi.org/10.1016/j.atmosenv.2006.03.020

Hudda, N., Kostenidou, E., Sioutas, C., Delfino, R.J., Fruin, S.A., 2011. Vehicle and driving characteristics that influence in-cabin particle number concentrations. Environ. Sci. Technol. 45, 8,691-8,697.

Hudda, N., Eckel, S.P., Knibbs, L.D., Sioutas, C., Delfino, R.J., Fruin, S.A., 2012. Linking in-vehicle ultrafine particle exposures to on-road concentrations. Atmos. Environ. 59, 578-586.

ICCT, The International Council On Clean Transportation (2016). Pocketbook, European Vehicle Market Statistics. (http://www.theicct.org/sites/default/files/publications/ICCT_Pocketbook_2016.pdf)

Int Panis, L., De Geus, B., Vandenbulcke, G., Willems, H., Degraeuwe, B., Bleux, N., Mishra, V., Thomas, I., Meeusen, R., 2010. Exposure to particulate matter in traffic: a comparison of cyclists and car passengers. Atmos. Environ. 44, 2263–2270.

Itano, Y., Bandow, H., Takenaka, N., Saitoh, Y. (2007). Impact of NOx reduction on long-term ozone trends in an urban atmosphere. Science of The Total Environment, 379(2), 46–55. https://doi.org/10.1016/j.scitotenv.2007.01.079

IARC, (2014). Diesel and Gasoline engine exhausts and some nitroarenes. Volume 105 IARC monographs on the evaluation of carcinogenic risks to humans. https://monographs.iarc.fr/wp-content/uploads/2018/06/mono105.pdf (accessed June 2019)

Jacobson, M. Z., 2012. Air Pollution and Global Warming, Cambridge Univ. Press, Cambridge, U. K.

Jenkin, M. E. (2004). Analysis of sources and partitioning of oxidant in the UK — Part 2 : contributions of nitrogen dioxide emissions and background ozone at a kerbside location in London. Atmospheric Environment, 38, 5131–5138. https://doi.org/10.1016/j.atmosenv.2004.05.055

Jenkin, M. E. Ã., Utembe, S. R., Derwent, R. G. (2008). Modelling the impact of elevated primary NO2 and HONO emissions on regional scale oxidant formation in the UK. Atmospheric Environment, 42(2), 323–336. https://doi.org/10.1016/j.atmosenv.2007.09.021

Jerrett M., Arain A., Kanaroglou P., B. Beckerman, Potoglou D., Sahsuvaroglu T., Morrison J., Giovis C., 2005. J. Exposure Anal. Environ. Epidemiol., 15(2), 185–204

Jimenez, J. L., McManus, J. B., Shorter, J., H., Nelson, D., D., Zahniser, M., S., Koplow, M., McRae, G. J.,Kolb, C. E., (2000). Cross road and mobile tunable infrared laser measurements of nitrous oxide emissions from motor vehicles, Chemosphere - Global Change Science, Volume 2, Issues 3–4, Pages 397-412, ISSN 1465-9972, https://doi.org/10.1016/S1465-9972(00)00019-2

Jo W. K., Choi S. J., 1996. Vehicle occupants' exposure to aromatic Volatile Organic Compounds while commuting on an urban-suburban route in Korea. J Air Waste Manage Assoc 46: 749-754

Kang B. H., Lee H. J., 2017. A review of recent research on automotive HVAC systems for EVs. Int J Air Cond Refrig 24(4):1720003. https://doi.org/10.1142/S2010132517300038

Kaur, S., Nieuwenhuijsen, M.J., Colvile, R.N., 2007. Fine particulate matter and carbon monoxide exposure concentrations in urban street transport microenvironments. Atmospheric Environment 41, 4781-4810.

Kiesewetter, G., Borken-Kleefeld, J., Schopp, W., Heyes, C., Thunis, P., Bessagnet, B., € Terrenoire, E., Gsella, A., Amann, M., 2014. Modelling NO2 concentrations at the street level in the GAINS integrated assessment model: projections under current legislation. Atmos. Chem. Phys. 14, 813e829. http://dx.doi.org/10.5194/ acp-14-813-2014

Knibbs, L.D., de Dear, R.J., Morawska, L., Mengersen, K.L., 2009. On-road ultrafine particle concentration in the M5 east road tunnel, Sydney, Australia. Atmospheric Environment 43, 3510-3519.

Knibbs, L.D., de Dear, R.J., Morawska, L., 2010. Effect of cabin ventilation rate on ultrafine particle exposure inside automobiles. Environmental Science Technology 44 (9), 3546-3551.

Knibbs L. D., Cole-Hunter T., Morawska L., 2011. A review of commuter exposure to ultrafine particles and its health effects, Atmos. Env., 45, 2611-2622.

Koetse, M. J., Hoen, A., 2014. Preferences for alternative fuel vehicles of company car drivers. Resour. Energy Econ. 37, 279–301.

Kolluru, S. S. R., Patra, A. K., 2020. Personal exposures to PM during short distance highway travel in India. Transportation Research Part D, 81, 102315.

Kotsiantis S. B., 2007. Supervised machine learning: A review of classification techniques. Informatica, 31, 249–268.

Koushki, P.A., Al-Dhowalia, K.H., Niazi, S.A., 1992. Vehicle occupant exposure to carbon monoxide. Journal of Air and Waste Management Association 42 (12), 1603

Krausse, B., Mardaljevic, J., 2005. Patterns of drivers' exposure to particulate matter. In: Williams, K. (Ed.), Spatial Planning, Urban Form and Sustainable Transport. Ashgate, Aldershot, UK.

Kumar, P., Fennell, P. S., Hayhurst, A. N., & Britter, R. E. (2008). Street Versus Rooftop Level Concentrations of Fine Particles in a Cambridge Street Canyon. Boundary-Layer Meteorology, 131(1), 3–18. doi:10.1007/s10546-008-9300-3

Künzli, N., Perez, L., von Klot, S., Baldassarre, D., Bauer, M., Basagana, X., Breton, C., Dratva, J., Elosua, R., de Faire, U., Fuks, K., de Groot, E., Marrugat, J., Penell, J., Seissler, J., Peters, A., Hoffmann, B., 2011. Investigating air pollution and atherosclerosis in humans: concepts and outlook. Progress in Cardiovascular Diseases 53 (5), 334-343.

Kurtenbach, R., Spittler, M., Wiesen, P., Ackermann, R., Geyer, A., Platt, U. (2001). Investigations of emissions and heterogeneous formation of HONO in a road traffic tunnel. Atmospheric Environment, 35, 3385–3394.

Kurti, S. P., Kurti, A. N., Emerson, S. R., Rosenkranz, R. R., Smith, J. R., Harms, C. A., & Rosenkranz, S. K., 2016. Household Air Pollution Exposure and Influence of Lifestyle on Respiratory Health and Lung Function in Belizean Adults and Children: A Field Study. Int. J. Env. Res. & Pub Hth, 13 (7)

Kwon, S., Park, Y., Park, J., Kim, J., Choi, K., Cha, J. (2017). Characteristics of on-road NO x emissions from Euro 6 light-duty diesel vehicles using a portable emissions

measurement system. Science of the Total Environment, 576(x), 70–77. https://doi.org/10.1016/j.scitotenv.2016.10.101

Lawin H., Fanou L. A., Hinson A. V., Stolbrink M., Houngbegnon P., Kedote N. M., Fayomi B., Kagima J., Katoto P., Ouendo E. M. D., Mortimer K., 2018. Health Risks Associated with Occupational Exposure to Ambient Air Pollution in Commercial Drivers: A Systematic Review. Int. J. Environ. Res. Public Health, 15, 2039; doi:10.3390/ijerph15092039.

Lee E. S., Stenstrom M. K., Zhu Y.F., 2015a. Ultrafine particles infiltration into passenger vehicles Part I: experimental evidences. Transp. Res. Part D.: Transp. Environ. 38, 156–165.

Lee E. S., Stenstrom M. K., Zhu Y.F.,2015b. Ultrafine particle infiltration into passenger vehicles, Part II: model analysis. Transp Res D.; 38: 144–155.

Lelieveld J, Klingmüller K, Pozzer A, Pöschl U, Fnais M, Daiber A and Münzel T (2019) Cardiovascular disease burden from ambient air pollution in Europe reassessed using novel hazard ratio functions, European Heart Journal, 1–17. Available at: https://academic.oup.com/eurheartj/advanceticle/doi/10.1093/eurheartj/ehz135/5372326

Liu, W., Zhang, J., Zhang, L., Turpin, B. J., Welsel, C. P., Morandi, M. T., Stock, T. H., Colome S., and Korn, L. R., 2006, Atmos. Environ., 40(12), 2202–2214.

Liu, J., Chan, C., Jeng, F., 1994. Predicting personal exposure levels to carbon monoxide (CO) in Taipei, based on actual CO measurements in microenvironments and a Monte Carlo simulation method. Atmospheric Environment 28 (14), 2361.

Louis, C., Liu, Y., Martinet, S., D'Anna, B., Valiente, A.M., Boreave, A., R'Mili, B., Tassel, P., Perret, P., André, M., 2017. Dilution effects on ultrafine particle emissions from Euro 5 and Euro 6 diesel and gasoline vehicles, Atmospheric Environment doi: 10.1016/j.atmosenv.2017.09.007.

Mackay, E., 2004. An investigation of the variation in personal exposure to carbon monoxide and particulates on the A660 in Leeds. M.Sc. Thesis, University of Leeds

Mandin, C., Trantallidi, M., Cattaneo, A., Canha, N., Mihucz, V.G., Szigeti, T., Mabilia, R., Perreca, E., Spinazze, A., Fossati, S., De Kluizenaar, Y., Cornelissen, E., Sakellaris, I., Saraga, D., Hänninen, O., De Oliveira Fernandes, E., Ventura, G., Wolkoff, P., Carrer, P., Bartzis, J.G., 2017. Assessment of indoor air quality in office buildings across Europe — the OFFICAIR study. Sci. Total Environ. 579, 169–178. http://dx.doi.org/10.1016/j.scitotenv.2016.10.238.

Martin, A.N., Boulter, P.G., Roddis, D., McDonough, L., Patterson, M., Rodriguez del Barco, M., Mattes, A., Knibbs, L.D., 2016. In-vehicle nitrogen dioxide concentrations in road tunnels. Atmos. Environ. 144:234–248. http://dx.doi.org/10.1016/j.atmosenv.2016.08.083

Matthaios, V. N., Kramer, L. J., Pope, F. D., Bloss, W. J., 2019. Investigation of vehicle cold start primary NO2 emissions from ambient monitoring data in the UK and their implications for urban air quality. Atmos. Environ. 199, 402-414. https://doi.org/10.1016/j.atmosenv.2018.11.031

Matthaios, V. N., Triantafyllou, A. G., Koutrakis, P., 2017. PM10 episodes in Greece: Local sources versus long-range transport—observations and model simulations. Journal of the Air and Waste Management Association, 67(1), 105–126. https://doi.org/10.1080/10962247.2016.1231146

Matthaios V. N., Triantafyllou A. G., Albanis T. A., Sakkas V., Garas S., 2018. Performance and evaluation of a coupled prognostic model TAPM over a mountainous complex terrain industrial area. Theor Appl Climatol, 132(3–4):885–903.

Mavroidis, I., Chaloulakou, A. (2011). Long-term trends of primary and secondary NO2 production in the Athens area . Variation of the NO2/ NOx ratio. Atmospheric Environment, 45(38), 6872–6879. https://doi.org/10.1016/j.atmosenv.2010.11.006

McConnell, R., Berhane, K., Yao, L., Jerrett, M., Lurmann, F., Gilliland, F., Kunzli, N., Gauderman, J., Avol, E., Thomas, D., Peters, J., 2006. Traffic, susceptibility, and childhood asthma. Environmental Health Perspectives 114 (5), 766-772.

Miñarro, M. D. and Ferradás, E. G., 2012. Performance evaluation of two commercial chemiluminescence NOx analysers according to European Standard EN 14211, J. Environ. Monit., 14, 383–390, https://doi.org/10.1039/c1em10601e.

Motlagh N. H., Lagerspetz E., Nurmi P., Li X., Varjonen S., Mineraud J., Siekkinen M., Rebeiro-Hargrave A., Hussein T., Petaja T., Kulmala M., Tarkoma S., 2020. Toward massive scale air quality monitoring. IEEE Communications Magazine, vol. 58, no. 2, pp. 54–59, 2.

Morawska, L., Afshari, A., Bae, G.N., Buonanno, G., Chao, C.Y.H., Hanninen, O., Hofmann, W., Isaxon, C., Jayaratne, E.R., Pasanen, P., Salthammer, T., Waring, M. and Wierzbicka, A., 2013. Indoor aerosols: from personal exposure to risk assessment, Indoor Air, 23, 462–487.

Munir, S., Chen, H., Ropkins, K., (2013). Quantifying temporal trends in ground level ozone concentration in the UK. Science of the Total Environment, 458-460, 217-227.

NAEI (2016). National Atmospheric Emission inventory emission factors for transport http://naei.beis.gov.uk/resources/rtp_fleet_projection_NAEI_2015_Base_2016_v4.0_Final.xlsx

Nazaroff, W.N., Cass, G.R., 1986. Mathematical modeling of chemically reactive pollutants in indoor air. Environmental Science and Technology 20 (9), 924–934.

Nine R D, Clark N N, J, D. J., M, A. C. (1999). Development of a heavy-duty chassis dynamometer driving route. Proceedings of the Institution of Mechanical Engineers, Part D: Journal of Automobile Engineering, (December 1998), 561–574.

Nieuwenhuijsen M., Paustenbach D., and Duarte-Davidson R., Environ. Int., 2006, 32(8), 996–1009.

Ning Z, Cheung C. S., Lu Y., Liu M. A., Hung W.T., 2005. Experimental and numerical study of the dispersion of motor vehicle pollutants under idle condition. Atmospheric Environment 39, 7880-7893.

Oberdorster, G., Stone, V., Donaldson, K., 2007. Toxicology of nanoparticles: A historical perspective. Nonotoxicology 1:1 2-25. https://doi.org/10.1080/17435390701314761

O'Driscoll, R., et al., 2018. Real World CO2 and NOx Emissions from 149 Euro 5 and 6 Diesel, Gasoline and Hybrid Passenger Cars. Science of The Total Environment, 621 pp. 282-290.

Ott, W., Switzer, P., Willitis, N., 1994. Carbon monoxide exposures inside an automobile traveling on an urban arterial highway. Journal of Air and Waste Management Association 44, 1010

Ott W., Klepeis N., Switzer P., 2008. Air change rates of motor vehicles and in-vehicle pollutant concentrations from secondhand smoke. J. Exposure Sci. Environ. Epidemiol., 18, 312–325

Ozcift, A., Gulten, A., 2011. Classifier Ensemble Construction with Rotation Forest to Improve Medical Diagnosis Performance of Machine Learning Algorithms. Comput. Methods Programs Biomed. 552, 104 (3), 443–451

Palmgren, F., Berkowicz, R.,Hertel, O., Vignati, E., 1996. Effects of reduction of NOX on the NO2 levels in urban streets. The Science of The Total Environment 189–190, 409–415.

Papapostolou, V., Lawrence, J. E., Diaz, E. A., Wolfson, J. M., Ferguson, S. T., Long, M. S., … Koutrakis, P. (2011). Laboratory evaluation of a prototype photochemical chamber designed to investigate the health effects of fresh and aged vehicular exhaust emissions Laboratory evaluation of a prototype photochemical chamber designed to investigate the health effects of fr. Inhilation Toxicology, 23(August 2017), 495–505. https://doi.org/10.3109/08958378.2011.587034

Papalexiou S., Moussiopoulos N., 2006. Wind flow and photochemical air pollution in Thessaloniki, Greece. Part II: statistical evaluation of European zooming Model's simulation results. Environ Model Softw 21:1752–1758

Petersen GA, Sabersky RH (1975) Measurements of pollutants inside an automobile. J Air Pollut Control Assoc 25:1028–1032. https://doi.org/10.1080/00022470.1975.10470174

Pfeifer, G., Harrison, R., Lynam, D., 1999. Personal exposures to airborne metals in London taxi drivers and office workers in 1995 and 1996. The Science of the Total Environment 235, 253.

Postlethwait, E. M., and Bidani, A., 1990. Reactive uptake governs the pulmonary airspace removal of inhaled nitrogen dioxide. J. Appl. Physiol. 68:594-603.

Qi, C.; Stanley, N.; Pui, D. Y. H.; Kuehn, T. H. Laboratory and on-road evaluations of cabin air filters using number and surface area concentration monitors. Environ. Sci. Technol. 2008, 42, 4128–4132.

RCP, 2016. Royal College of Physicians Every breath we take: the lifelong impact of air pollution. Report of a working party. London: RCP, 2016. https://www.rcplondon.ac.uk/projects/outputs/every-breath-we-take-lifelong-impact-air-pollution (accessed June 2019)

R Core Team. (n.d.). R Language Definition. Retrieved from http://web.mit.edu/~r/current/arch/amd64_linux26/lib/R/doc/manual/R-lang.pdf

Requia, W. J., Dalumpines, R., Adams, M. D., Arain, A., Ferguson, M., & Koutrakis, P. (2017). Modeling spatial patterns of link-based PM2.5 emissions and subsequent human exposure in a large canadian metropolitan area. Atmospheric Environment, 158(X), 172–180. https://doi.org/10.1016/j.atmosenv.2017.03.038

Riediker, M., Cascio, W.E., Griggs, T.R., Herbst, M.C., Bromberg, P.A., Neas, L., Williams, R.W., Devlin, R.B., 2004. Particulate matter exposure in cars is associated with cardiovascular effects in healthy young men. American Journal of Respiratory and Critical Care Medicine 169, 934-940.

Rodes, C., Sheldon, L., Whitaker, D., Clayton, A., Fitzgerald, K., Flanagan, J., et al., 1998. Measuring concentrations of selected air pollutants inside California vehicles: Final Report, ARB Contract No. 95-339, prepared for California Environmental Agency & South Coast Air Quality Management District.

Romagnoli, P., Balducci, C., Perilli, M., Gherardi, M., Gordiani, A., Gariazzo, C., Gatto, M.P., Cecinato, A., 2014. Indoor PAHs at schools, homes and offices in Rome, Italy. Atmos. Environ. 92, 51–59

Ropkins, K., Defries, T. H., Pope, F., Green, D. C., Kemper, J., Kishan, S., … Hager, J. S. (2017). Science of the Total Environment Evaluation of EDAR vehicle emissions remote sensing technology. Science of The Total Environment, 609, 1464–1474. https://doi.org/10.1016/j.scitotenv.2017.07.137

Russell A., Dennis R., 2000. NARSTO critical review of photochemicalmodels and modeling. Atmos Environ 34:2283–2324

Salmond J. A., McKendry I. G., 2005. A review of turbulence in a very stable nocturnal boundary layer and its implications for air quality. Prog Phys Geogr 29 (2):171–188

Salonen H., Salthammer T., Morawska L., 2019. Human exposure to NO2 in school and office indoor environments, Environment International 130:104887

San Jose R., Stohl A., Karatzas K., Bohler T., James P., Perez J. L., 2005. A modelling study of an extraordinary night time ozone episode over Madrid domain. Environmental modeling & Software 20:587–59

Satish, U., Mendell, M.J., Shekhar, K., Hotchi, T., Sullivan, D., Streufert, S., Fisk, W.J., 2012. Is CO2 an indoor pollutant? Direct effects of low-to-moderate CO2 concentrations on human decision-making performance. Environ. Health Perspect. 120, 1671

Saunders, S. M., Jenkin, M. E., Derwent, R. G., and Pilling, M. J., 2003. Protocol for the development of the Master Chemical Mechanism, MCM v3 (Part A): tropospheric degradation of nonaromatic volatile organic compounds, Atmos. Chem. Phys., 3, 161–180, https://doi.org/10.5194/acp-3-161-2003, 2003.

Schieweck, A., Uhde, E., Salthammer, T., Salthammer, L. C., Morawska, L., Mazaheri, M., and Kumar, P., 2018. Smart homes and the control of indoor air quality. Renewable and Sustainable Energy Reviews 94, 705–718.

Schneider, P., Gebefugi, I., Richter, K., Wolke, G., Schnelle, J., Wichmann H. E., and Heinrich J., 2001. Sci. Total Environ., 267(1–3), 41–51.

Seaman L. N., 2000. Meteorological modeling for air-quality assessments. Atmos Environ 34:2231–2259

Sen, K. P. (1968). Estimates of the Regression Coefficient Based on Kendall ' s Tau. Journal of the American Statistical Association, 63(324), 1379–1389.

Seinfeld, J. H. and Pandis, S. N.: Atmospheric Chemistry and Physics: from Air Pollution to Climate Change, John Wiley, New York, 1998.

Silverman, D. T., Samanic, C. M., Lubin, J. H., Blair, A. E., Stewart, P. A., Vermeulen, R., … Attfield, M. D. (2012). The Diesel Exhaust in Miners Study : A Nested Case – Control Study of Lung Cancer and Diesel Exhaust. Journal of the National Cancer Institute, 104, 855–868. https://doi.org/10.1093/jnci/djs034

Singer B. C., Hodgson A. T., Hotchi T., Kim J. J., 2004. Atmos. Environ., 2004, 38(3), 393–403.

Sokhi R. S., San Jose R, Kitwiroon N, Fragkou E, Perez JL, Middleton DR(2006) Prediction of ozone levels in London using the MM5-CMAQ modelling system. Environ Model Softw 21:566–576

Sommariva, R., Cox, S., Martin, C., Borońska, K., Young, J., Jimack, P. K., Pilling, M. J., Matthaios, V. N., Nelson, B. S., Newland, M. J., Panagi, M., Bloss, W. J., Monks, P. S., and Rickard, A. R., 2020. AtChem (version 1), an open-source box model for the Master Chemical Mechanism, Geosci. Model Dev., 13, 169–183, https://doi.org/10.5194/gmd-13-169-2020.

Stölzel, M., Breitner, S., Cyrys, J., Pitz, M., Wölke, G., Kreyling, W., Heinrich, J., Wichmann, H.-E., Peters, A., 2007. Daily mortality and particulate matter in different size classes in Erfurt, Germany. Journal of Exposure Analysis and Environmental Epidemiology 17, 458e467.

Stingone JA, Pandey OP, Claudio L, Pandey G., 2017. Using machine learning to identify air pollution exposure profiles associated with early cognitive skills among us children. Environ Pollut.; 230: 730–40.

Stull R., 1988. An introduction to boundary layer meteorology. Kluwer Academic Publishers, London

Suarez-Bertoa, R., Astorga, C., (2018). Impact of cold temperature on Euro 6 passenger car emissions. Environmental Pollution, 234, 318-329. https://doi.org/10.1016/j.envpol.2017.10.096

Thatcher, T.L., Lunden, M.M., Revzan, K.L., Sextro, R.G., Brown, N.J., 2003. A concentration rebound method for measuring particle penetration and deposition in the indoor environment. Aerosol Sci. Technol. 37, 847-864.

Theil H. (1950). A rank-invariant method of linear and polynomial Regression analysis. Ned. Akad. Wetenchappen, (53), 386–392. https://doi.org/http://dx.doi.org/10.1007/ 978-94-011-2546-8

TomTom, 2018. World traffic index, measuring congestion worldwide https://www.tomtom.com/en_gb/trafficindex/list?citySize=LARGE&continent=ALL&country=ALL

Van de Hey, J. D., Sonderfeld, H., Jeanjean, A. P. R., Panchal, R., Leigh, R. J., Allen, M. A., … Monks, P. S., 2018. Experimental and modeling assessment of a novel automotive cabin PM2.5 removal system. Aerosol Science and Technology, 52(11), 1249–1265. doi:10.1080/02786826.2018.1490694

Vardoulakis, S., 2009. Human Exposure: Indoor and Outdoor. In: Hester, R.E., Harrison, R.M. (Eds.), Air quality in urban environments. Issues in Environmental Science and Technology, vol. 28. Royal Society of Chemistry, London, pp. 42-64.

Velasco et al., 2019 Particle exposure and inhaled dose while commuting by public transport in Mexico City. Atmos. Env., 219, 117044

von der Weiden, S.-L., Drewnick, F., and Borrmann, S., 2009. Particle Loss Calculator – a new software tool for the assessment of the performance of aerosol inlet systems, Atmos. Meas. Tech., 2, 479–494, https://doi.org/10.5194/amt-2-479-2009.

Vu, T.V., Zauli-Sajani, S., Poluzzi, V. Harrison R. M., 2018. Factors controlling the lung dose of road traffic-generated sub-micrometre aerosols from outdoor to indoor environments. Air Quality Atmosphere and Health https://doi.org/10.1007/s11869-018-0568-2

Wang, J. S., Chan, T. L., Cheung, C. S., Leung, C. W., and Hung, W. T., 2006. Three-dimensional pollutant concentration dispersion of a vehicular exhaust plume in the real atmosphere, Atmos. Environ., 40, 484–497

Weiss, M., Bonnel, P., Hummel, R., Provenza, A., Manfredi, U. (2011). On-Road Emissions of Light-Duty Vehicles in Europe. Environmental Science and Technology, 45, 8575–8581.

Weinberger K. Q., Blitzer J., Saul L. K., 2006. Distance metric learning for large margin nearest neighbor classification. In NIPS. MIT Press 2, 3

Weschler C. J., Shields H.C., 2000. The influence of ventilation on reactions among indoor pollutants: modeling and experimental observations. Indoor Air 10:92–100.

Weschler C. J., Shields H. C., Naik D. V., 1994. Indoor chemistry involving O3, NO, and NO2 as evidenced by 14 months of measurements at a site in California. Environ Sci Technol 28:2120–2132

Weschler, C. J., Carslaw, N., 2018. Indoor Chemistry. Environ. Sci. Technol., 52 (5), 2419−2428

Wettschereck D., Aha D. W., Mohri T., 1997. A Review and Empirical Evaluation of Feature Weighting Methods for a Class of Lazy Learning Algorithms. Artificial Intelligence Review 10:1–37.

WHO, Report, T. 2013. Review of evidence on health aspects of air pollution – REVIHAAP Project.

WHO, Report 2013. Health Risks of Air Pollution in Europe (HRAPIE), WHO, Copenhagen (2013)

Wickham, H. (2009). ggplot2 : elegant graphics for data analysis. Springer.

Williams, R., Suggs, J., Rea, A., Sheldon, L., Rodes, C., Thornburg, J., 2003. The Research Triangle Park particulate matter panel study: modeling ambient source contribution to personal and residential PM mass concentrations. Atmos. Environ. 37, 5365-5378.

Wilks D. S., 2005. Statistical Methods in the Atmospheric Sciences, Volume 91, Second Edition (International Geophysics). 2nd ed. Academic Press (cit. on p. 238).

Willmott, C. J., Robeson S. M., Matsuura K., 2011. A refined index of model performance. Int. J. of Clim. 32(13), DOI: 10.1002/joc.2419

Wood, S. N. (2003). Thin plate regression splines. Journal Royal Statistical Society, 95–114.

Xu B., Zhu Y., 2009. Quantitative analysis of the parameters affecting in-cabin to on-roadway (I/O) ultrafine particle concentration ratios. Aerosol Sci. Technol., 43, 400–410.

Yamada, H., Hayashi, R., Tonokura, K., 2016. Simultaneous measurements of on road/in-vehicle nanoparticles and NOx while driving: actual situations, passenger exposure and secondary formations. Sci. Total Environ. 563, 944-955.

Yamamoto, N., Shendell, D.G., Winer, A.M., Zhang, J., 2010. Residential air exchange rates in three major US metropolitan areas: results from the relationship among indoor, outdoor, and personal air study 1999-2001. Indoor Air 20, 85-90.

Yanowitz J., McCormick, R. L., Graboski M., S., (2000). In-Use Emissions from Heavy-Duty Diesel Vehicles. Environmental Science and Technology, 729–740.

Yokomura, H., Kohketsu, S., Mori, K., (2003). EGR System in a Turbocharged and Intercooled Heavy-Duty Diesel Engine. Expansion of EGR Area with Venturi EGR System, Technical review, 2003. Mitsubishi Motors Corporation

Yoo, J.Y., Park, C.J., Kim, K.Y., Son, Y.-S., Kang, C.-M., Wolfson, J.M., Jung, I.-H., Lee, S.- J., Koutrakis, P., 2015. Development of an activated carbon filter to remove NO2 and HONO in indoor air, J. Hazard. Mater. 289 184–189, https://doi.org/10.1016/j.jhazmat.2015.02.038

Yoshida, T., Matsunaga, I., 2006. A case study on identification of airborne organic compounds and time courses of their concentrations in the cabin of a new car for privateuse. Environ. Int. 32:58–79. http://dx.doi.org/10.1016/j.envint.2005.04.009.

You, K., Ge, Y., Hu, B., Ning, Z., Zhao, S., Zhang, Y., Xie, P., 2007. Measurement of in-vehiclevolatile organic compounds under static conditions. J. Environ. Sci. 19:1208–1213.http://dx.doi.org/10.1016/S1001-0742(07)60197-1.

Zagury, E., Le Moullec, Y., Momas, I., 2000. Exposure of Paris taxi drivers to automobile air pollutants within their vehicles. Occupational and Environmental Medicine 57, 406.

Zuurbier, M., Hoek, G., Oldenwening, M., Lenters, V., Meliefste, K., van den Hazel, P., Brunekreef, B., 2010. Commuters' exposure to particulate matter air pollution is affected by mode of transport, fuel type, and route. Environ. Health Perspect. 118, 783–789.

# Appendix A

## MCM Mechanism

```
* MCMv3.3.1 Subset generated for the following species:   ;
*  ;
*;
* Variable definitions.  All species are listed here.;
*;
VARIABLE
 N2O5 H2O2 NO H2 NA HONO OH SO2 O HNO3 SO3 O1D HO2 HO2NO2 CO SA O3
HSO3 NO2 NO3 ;
****************************************************** ;
*;
* Generic Rate Coefficients ;
*;
KRO2NO = 2.7D-12*EXP(360/TEMP) ;
KRO2HO2 = 2.91D-13*EXP(1300/TEMP) ;
KAPHO2 = 5.2D-13*EXP(980/TEMP) ;
KAPNO = 7.5D-12*EXP(290/TEMP) ;
KRO2NO3 = 2.3D-12 ;
KNO3AL = 1.4D-12*EXP(-1860/TEMP) ;
KDEC = 1.00D+06 ;
KROPRIM = 2.50D-14*EXP(-300/TEMP) ;
KROSEC = 2.50D-14*EXP(-300/TEMP) ;
KCH3O2 = 1.03D-13*EXP(365/TEMP) ;
K298CH3O2 = 3.5D-13 ;
K14ISOM1 = 3.00D7*EXP(-5300/TEMP) ;
*;
* Complex reactions ;
*;
KD0 = 1.10D-05*M*EXP(-10100/TEMP) ;
KDI = 1.90D17*EXP(-14100/TEMP) ;
KRD = KD0/KDI ;
FCD = 0.30 ;
NCD = 0.75-1.27*(LOG10(FCD)) ;
FD = 10@(LOG10(FCD)/(1+(LOG10(KRD)/NCD)**2)) ;
KBPAN = (KD0*KDI)*FD/(KD0+KDI) ;
KC0 = 3.28D-28*M*(TEMP/300)@-6.87 ;
KCI = 1.125D-11*(TEMP/300)@-1.105 ;
KRC = KC0/KCI ;
FCC = 0.30 ;
NC = 0.75-1.27*(LOG10(FCC)) ;
FC = 10@(LOG10(FCC)/(1+(LOG10(KRC)/NC)**2)) ;
KFPAN = (KC0*KCI)*FC/(KC0+KCI) ;
K10 = 1.0D-31*M*(TEMP/300)@-1.6 ;
K1I = 5.0D-11*(TEMP/300)@-0.3 ;
KR1 = K10/K1I ;
FC1 = 0.85 ;
NC1 = 0.75-1.27*(LOG10(FC1)) ;
F1 = 10@(LOG10(FC1)/(1+(LOG10(KR1)/NC1)**2)) ;
```

```
KMT01 = (K10*K1I)*F1/(K10+K1I) ;
K20 = 1.3D-31*M*(TEMP/300)@-1.5 ;
K2I = 2.3D-11*(TEMP/300)@0.24 ;
KR2 = K20/K2I ;
FC2 = 0.6 ;
NC2 = 0.75-1.27*(LOG10(FC2)) ;
F2 = 10@(LOG10(FC2)/(1+(LOG10(KR2)/NC2)**2)) ;
KMT02 = (K20*K2I)*F2/(K20+K2I) ;
K30 = 3.6D-30*M*(TEMP/300)@-4.1 ;
K3I = 1.9D-12*(TEMP/300)@0.2 ;
KR3 = K30/K3I ;
FC3 = 0.35 ;
NC3 = 0.75-1.27*(LOG10(FC3)) ;
F3 = 10@(LOG10(FC3)/(1+(LOG10(KR3)/NC3)**2)) ;
KMT03 = (K30*K3I)*F3/(K30+K3I) ;
K40 = 1.3D-3*M*(TEMP/300)@-3.5*EXP(-11000/TEMP) ;
K4I = 9.7D+14*(TEMP/300)@0.1*EXP(-11080/TEMP) ;
KR4 = K40/K4I ;
FC4 = 0.35 ;
NC4 = 0.75-1.27*(LOG10(FC4)) ;
F4 = 10@(LOG10(FC4)/(1+(LOG10(KR4)/NC4)**2)) ;
KMT04 = (K40*K4I)*F4/(K40+K4I) ;
KMT05 = 1.44D-13*(1+(M/4.2D+19)) ;
KMT06 = 1 + (1.40D-21*EXP(2200/TEMP)*H2O) ;
K70 = 7.4D-31*M*(TEMP/300)@-2.4 ;
K7I = 3.3D-11*(TEMP/300)@-0.3 ;
KR7 = K70/K7I ;
FC7 = 0.81 ;
NC7 = 0.75-1.27*(LOG10(FC7)) ;
F7 = 10@(LOG10(FC7)/(1+(LOG10(KR7)/NC7)**2)) ;
KMT07 = (K70*K7I)*F7/(K70+K7I) ;
K80 = 3.2D-30*M*(TEMP/300)@-4.5 ;
K8I = 3.0D-11 ;
KR8 = K80/K8I ;
FC8 = 0.41 ;
NC8 = 0.75-1.27*(LOG10(FC8)) ;
F8 = 10@(LOG10(FC8)/(1+(LOG10(KR8)/NC8)**2)) ;
KMT08 = (K80*K8I)*F8/(K80+K8I) ;
K90 = 1.4D-31*M*(TEMP/300)@-3.1 ;
K9I = 4.0D-12 ;
KR9 = K90/K9I ;
FC9 = 0.4 ;
NC9 = 0.75-1.27*(LOG10(FC9)) ;
F9 = 10@(LOG10(FC9)/(1+(LOG10(KR9)/NC9)**2)) ;
KMT09 = (K90*K9I)*F9/(K90+K9I) ;
K100 = 4.10D-05*M*EXP(-10650/TEMP) ;
K10I = 6.0D+15*EXP(-11170/TEMP) ;
KR10 = K100/K10I ;
FC10 = 0.4 ;
NC10 = 0.75-1.27*(LOG10(FC10)) ;
F10 = 10@(LOG10(FC10)/(1+(LOG10(KR10)/NC10)**2)) ;
KMT10 = (K100*K10I)*F10/(K100+K10I) ;
K1 = 2.40D-14*EXP(460/TEMP) ;
K3 = 6.50D-34*EXP(1335/TEMP) ;
K4 = 2.70D-17*EXP(2199/TEMP) ;
K2 = (K3*M)/(1+(K3*M/K4)) ;
```

```
KMT11 = K1 + K2 ;
K120 = 2.5D-31*M*(TEMP/300)@-2.6 ;
K12I = 2.0D-12 ;
KR12 = K120/K12I ;
FC12 = 0.53 ;
NC12 = 0.75-1.27*(LOG10(FC12)) ;
F12 = 10@(LOG10(FC12)/(1.0+(LOG10(KR12)/NC12)**2)) ;
KMT12 = (K120*K12I*F12)/(K120+K12I) ;
K130 = 2.5D-30*M*(TEMP/300)@-5.5 ;
K13I = 1.8D-11 ;
KR13 = K130/K13I ;
FC13 = 0.36 ;
NC13 = 0.75-1.27*(LOG10(FC13)) ;
F13 = 10@(LOG10(FC13)/(1+(LOG10(KR13)/NC13)**2)) ;
KMT13 = (K130*K13I)*F13/(K130+K13I) ;
K140 = 9.0D-5*EXP(-9690/TEMP)*M ;
K14I = 1.1D+16*EXP(-10560/TEMP) ;
KR14 = K140/K14I ;
FC14 = 0.36 ;
NC14 = 0.75-1.27*(LOG10(FC14)) ;
F14 = 10@(LOG10(FC14)/(1+(LOG10(KR14)/NC14)**2)) ;
KMT14 = (K140*K14I)*F14/(K140+K14I) ;
K150 = 8.6D-29*M*(TEMP/300)@-3.1 ;
K15I = 9.0D-12*(TEMP/300)@-0.85 ;
KR15 = K150/K15I ;
FC15 = 0.48 ;
NC15 = 0.75-1.27*(LOG10(FC15)) ;
F15 = 10@(LOG10(FC15)/(1+(LOG10(KR15)/NC15)**2)) ;
KMT15 = (K150*K15I)*F15/(K150+K15I) ;
K160 = 8D-27*M*(TEMP/300)@-3.5 ;
K16I = 3.0D-11*(TEMP/300)@-1 ;
KR16 = K160/K16I ;
FC16 = 0.5 ;
NC16 = 0.75-1.27*(LOG10(FC16)) ;
F16 = 10@(LOG10(FC16)/(1+(LOG10(KR16)/NC16)**2)) ;
KMT16 = (K160*K16I)*F16/(K160+K16I) ;
K170 = 5.0D-30*M*(TEMP/300)@-1.5 ;
K17I = 1.0D-12 ;
KR17 = K170/K17I ;
FC17 = 0.17*EXP(-51/TEMP)+EXP(-TEMP/204) ;
NC17 = 0.75-1.27*(LOG10(FC17)) ;
F17 = 10@(LOG10(FC17)/(1.0+(LOG10(KR17)/NC17)**2)) ;
KMT17 = (K170*K17I*F17)/(K170+K17I) ;
KMT18 = 9.5D-39*O2*EXP(5270/TEMP)/(1+7.5D-29*O2*EXP(5610/TEMP)) ;
KPPN0 = 1.7D-03*EXP(-11280/TEMP)*M ;
KPPNI = 8.3D+16*EXP(-13940/TEMP) ;
KRPPN = KPPN0/KPPNI ;
FCPPN = 0.36 ;
NCPPN = 0.75-1.27*(LOG10(FCPPN)) ;
FPPN = 10@(LOG10(FCPPN)/(1+(LOG10(KRPPN)/NCPPN)**2)) ;
KBPPN = (KPPN0*KPPNI)*FCPPN/(KPPN0+KPPNI) ;
************************************************** ;
*;
* Peroxy radicals. ;
*;
```

```
* WARNING: The following species do not have SMILES strings in the
database. ;
*          If any of these are peroxy radicals the RO2 sum will be
wrong!!! ;
************************************************** ;
*  ;
RO2 =  ;
*;
* Reaction definitions. ;
*;
% 5.6D-34*N2*(TEMP/300)@-2.6*O2 : O = O3 ;
% 6.0D-34*O2*(TEMP/300)@-2.6*O2 : O = O3 ;
% 8.0D-12*EXP(-2060/TEMP) : O + O3 = ;
% KMT01 : O + NO = NO2 ;
% 5.5D-12*EXP(188/TEMP) : O + NO2 = NO ;
% KMT02 : O + NO2 = NO3 ;
% 3.2D-11*EXP(67/TEMP)*O2 : O1D = O ;
% 2.0D-11*EXP(130/TEMP)*N2 : O1D = O ;
% 1.4D-12*EXP(-1310/TEMP) : NO + O3 = NO2 ;
% 1.4D-13*EXP(-2470/TEMP) : NO2 + O3 = NO3 ;
% 3.3D-39*EXP(530/TEMP)*O2 : NO + NO = NO2 + NO2 ;
% 1.8D-11*EXP(110/TEMP) : NO + NO3 = NO2 + NO2 ;
% 4.50D-14*EXP(-1260/TEMP) : NO2 + NO3 = NO + NO2 ;
% KMT03 : NO2 + NO3 = N2O5 ;
% 2.14D-10*H2O : O1D = OH + OH ;
% 1.70D-12*EXP(-940/TEMP) : OH + O3 = HO2 ;
% 7.7D-12*EXP(-2100/TEMP) : OH + H2 = HO2 ;
% KMT05 : OH + CO = HO2 ;
% 2.9D-12*EXP(-160/TEMP) : OH + H2O2 = HO2 ;
% 2.03D-16*(TEMP/300)@4.57*EXP(693/TEMP) : HO2 + O3 = OH ;
% 4.8D-11*EXP(250/TEMP) : OH + HO2 = ;
% 2.20D-13*KMT06*EXP(600/TEMP) : HO2 + HO2 = H2O2 ;
% 1.90D-33*M*KMT06*EXP(980/TEMP) : HO2 + HO2 = H2O2 ;
% KMT07 : OH + NO = HONO ;
% KMT08 : OH + NO2 = HNO3 ;
% 2.0D-11 : OH + NO3 = HO2 + NO2 ;
% 3.45D-12*EXP(270/TEMP) : HO2 + NO = OH + NO2 ;
% KMT09 : HO2 + NO2 = HO2NO2 ;
% 3.2D-13*EXP(690/TEMP)*1.0 : OH + HO2NO2 = NO2 ;
% 4.0D-12 : HO2 + NO3 = OH + NO2 ;
% 2.5D-12*EXP(260/TEMP) : OH + HONO = NO2 ;
% KMT11 : OH + HNO3 = NO3 ;
% 4.0D-32*EXP(-1000/TEMP)*M : O + SO2 = SO3 ;
% KMT12 : OH + SO2 = HSO3 ;
% 1.3D-12*EXP(-330/TEMP)*O2 : HSO3 = HO2 + SO3 ;
% 6.00D-06 : HNO3 = NA ;
% 4.00D-04 : N2O5 = NA + NA ;
% 1.20D-15*H2O : SO3 = SA ;
% J<1> : O3 = O1D ;
% J<2> : O3 = O ;
% J<3> : H2O2 = OH + OH ;
% J<4> : NO2 = NO + O ;
% J<5> : NO3 = NO ;
% J<6> : NO3 = NO2 + O ;
% J<7> : HONO = OH + NO ;
% J<8> : HNO3 = OH + NO2 ;
```

```
% KMT04 : N2O5 = NO2 + NO3 ;
% KMT10 : HO2NO2 = HO2 + NO2 ;
*;
* End of Subset.  No. of Species = 21, No. of Reactions = 48 ;
```

# Inside – Outside spatial plots

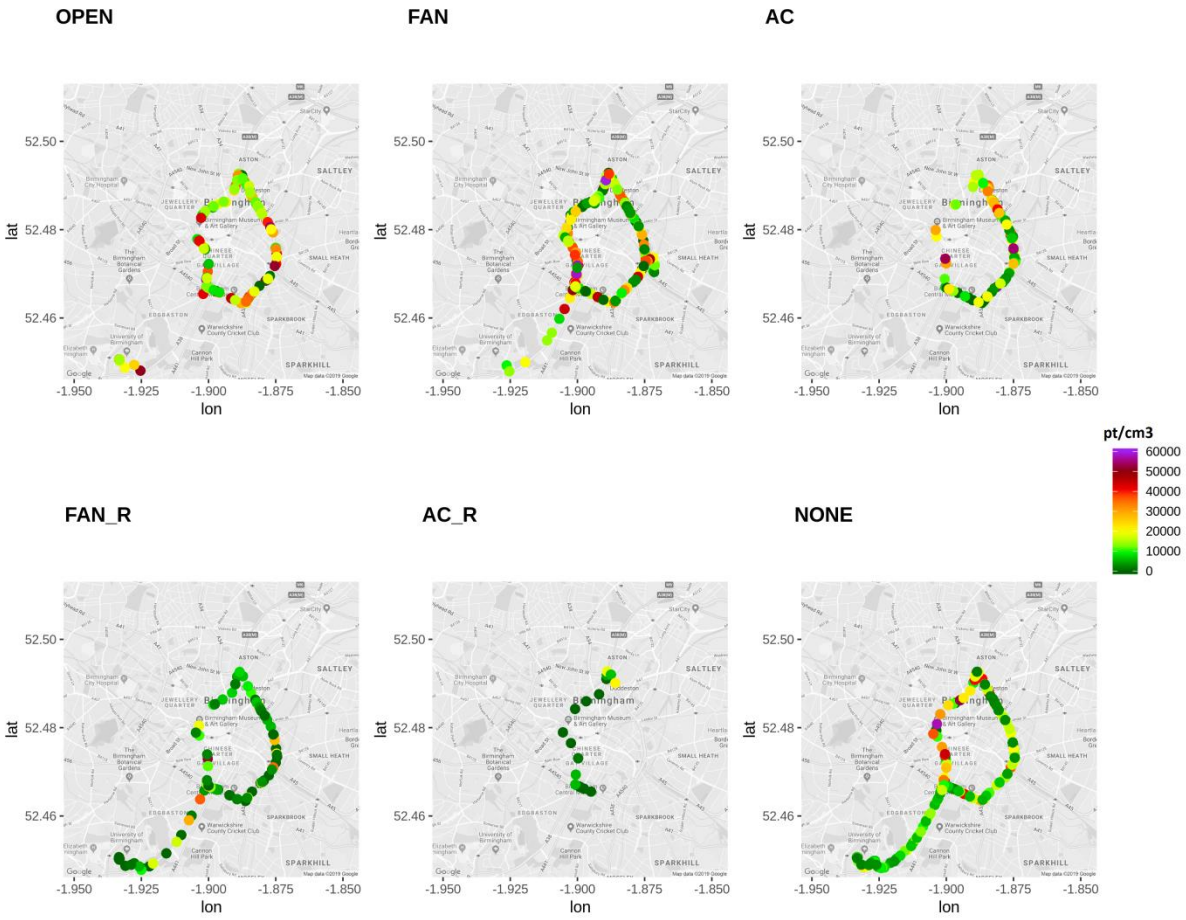


Figure A4. Within-vehicle spatial exposure map for UFP under different ventilation options. OPEN: Windows open, FAN: Fan on, recirculation off, windows closed, AC: Fan plus Air condition on, recirculation off, windows closed, FAN_R: Fan on, recirculation, windows closed, AC_R: Fan plus AC on, recirculation, windows closed, NONE: No ventilation Fan or AC, windows closed.

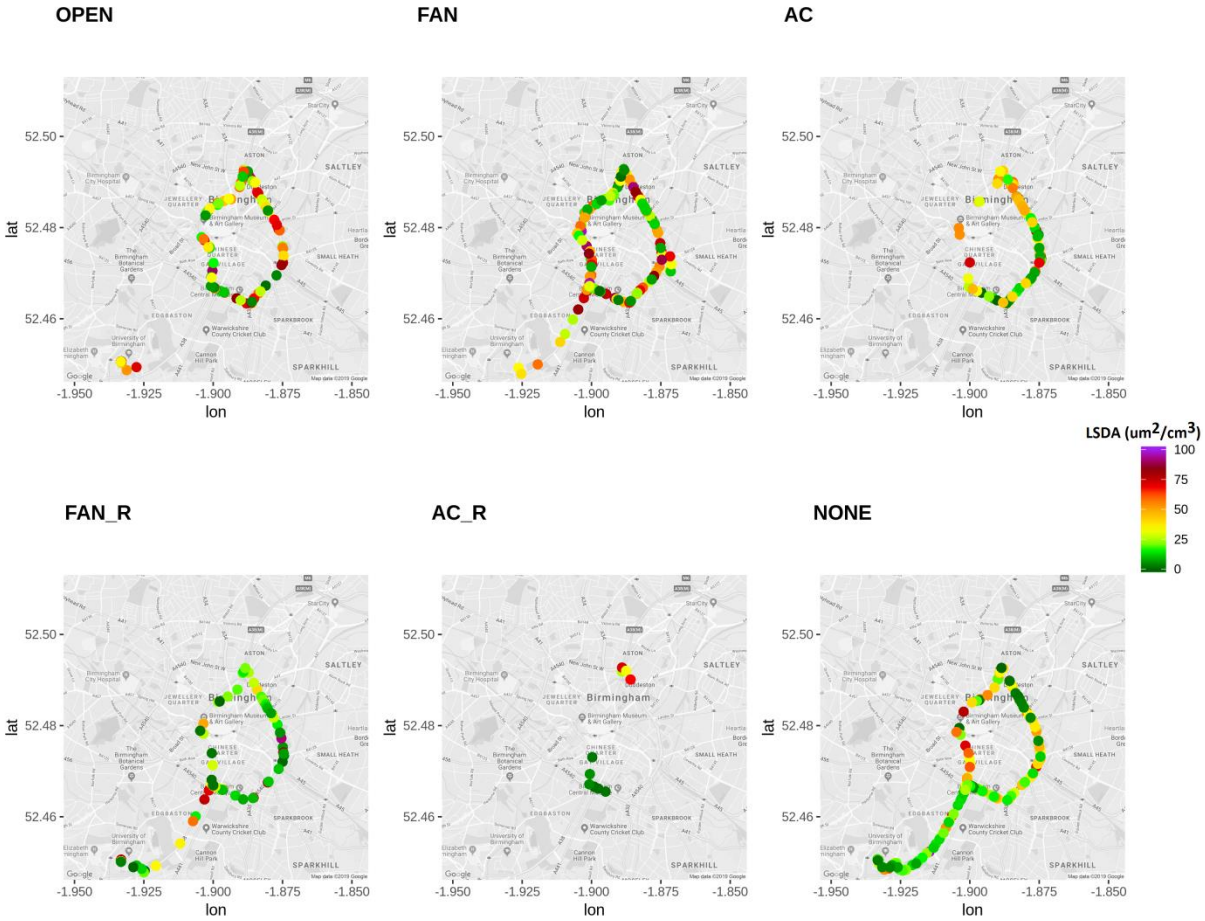


Figure A5. Within-vehicle spatial exposure map for LSDA under different ventilation options. OPEN: Windows open, FAN: Fan on, recirculation off, windows closed, AC: Fan plus Air condition on, recirculation off, windows closed, FAN_R: Fan on, recirculation, windows closed, AC_R: Fan plus AC on, recirculation, windows closed, NONE: No ventilation Fan or AC, windows closed.

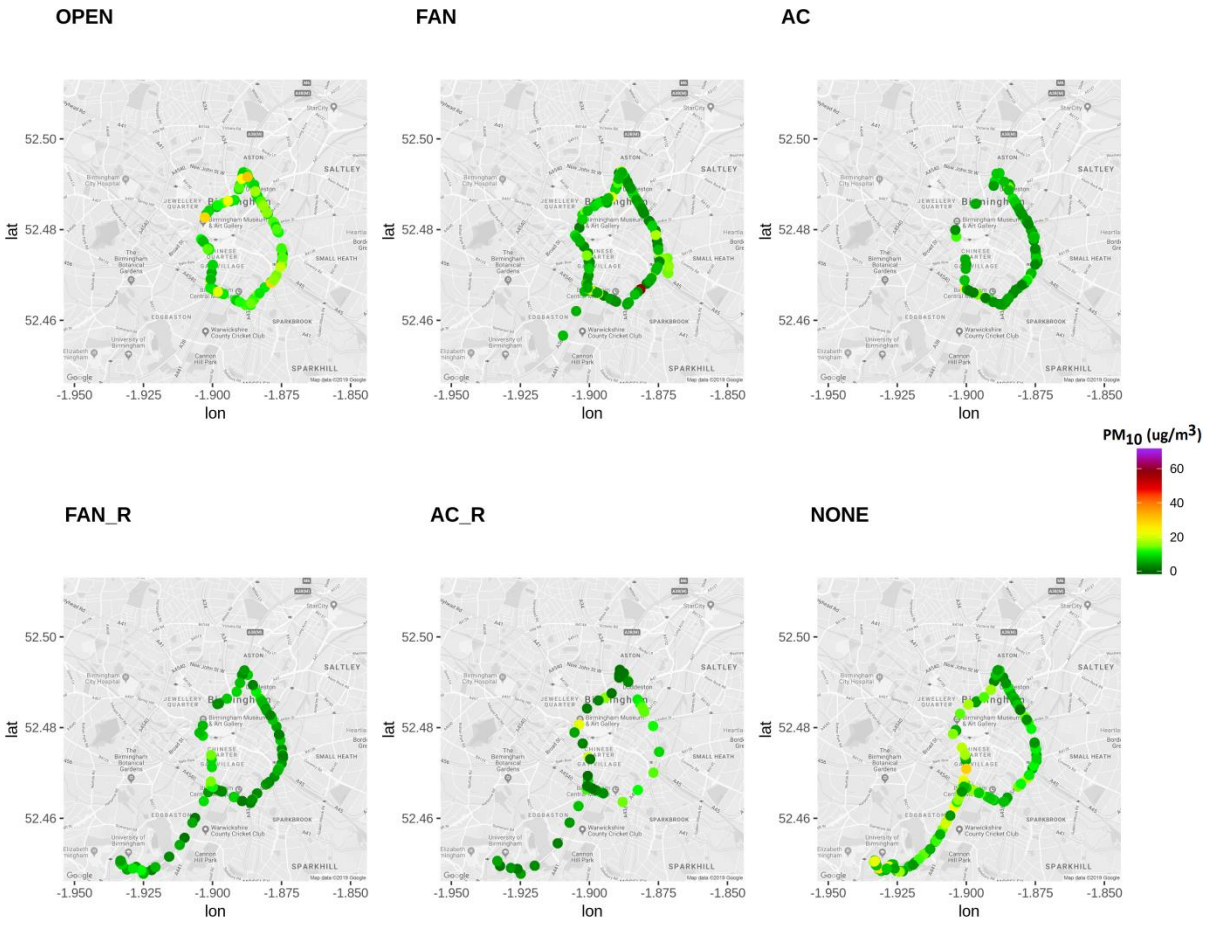


Figure A6. Within-vehicle spatial exposure map for $PM_{10}$ under different ventilation options. OPEN: Windows open, FAN: Fan on, recirculation off, windows closed, AC: Fan plus Air condition on, recirculation off, windows closed, FAN_R: Fan on, recirculation, windows closed, AC_R: Fan plus AC on, recirculation, windows closed, NONE: No ventilation Fan or AC, windows closed.

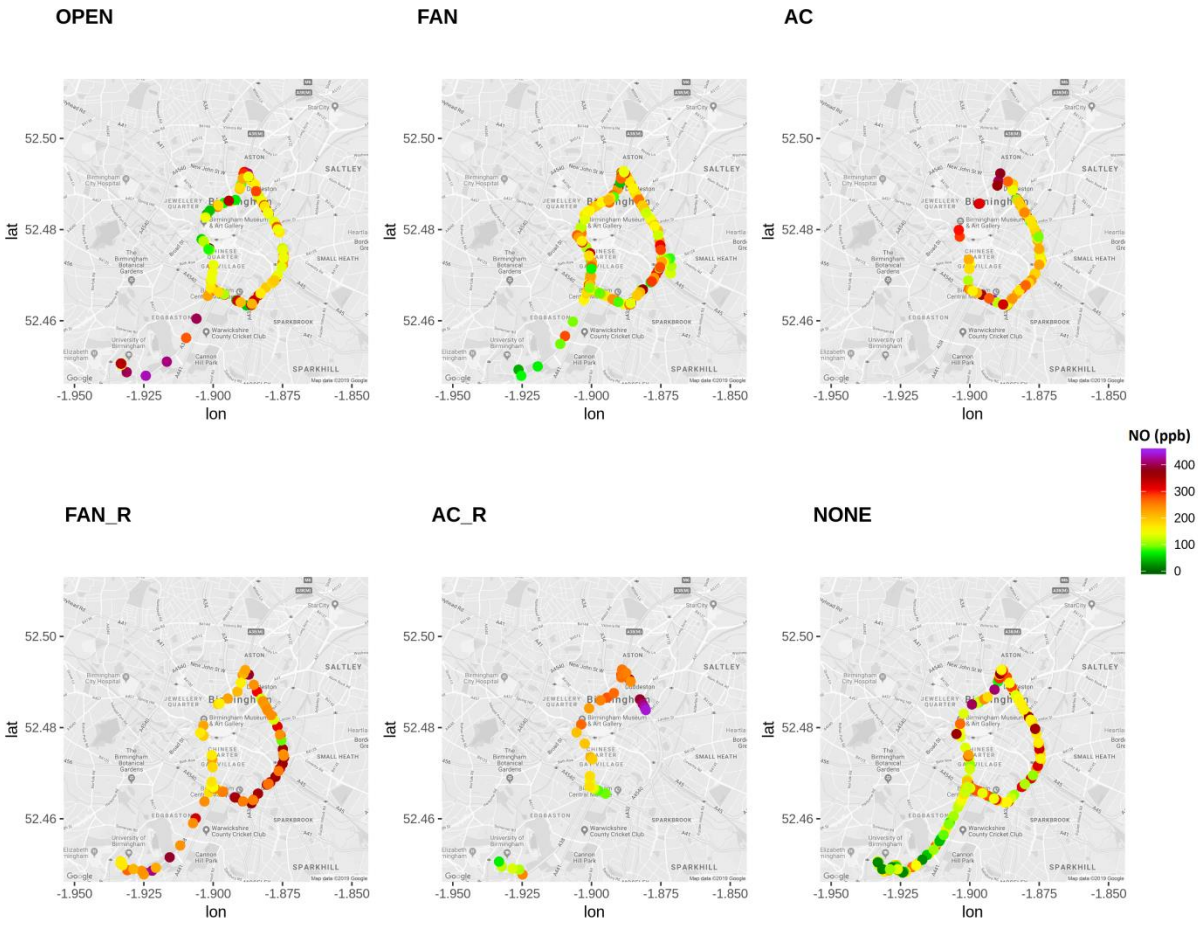


Figure A7. Within-vehicle spatial exposure map for NO under different ventilation options. OPEN: Windows open, FAN: Fan on, recirculation off, windows closed, AC: Fan plus Air condition on, recirculation off, windows closed, FAN_R: Fan on, recirculation, windows closed, AC_R: Fan plus AC on, recirculation, windows closed, NONE: No ventilation Fan or AC, windows closed.

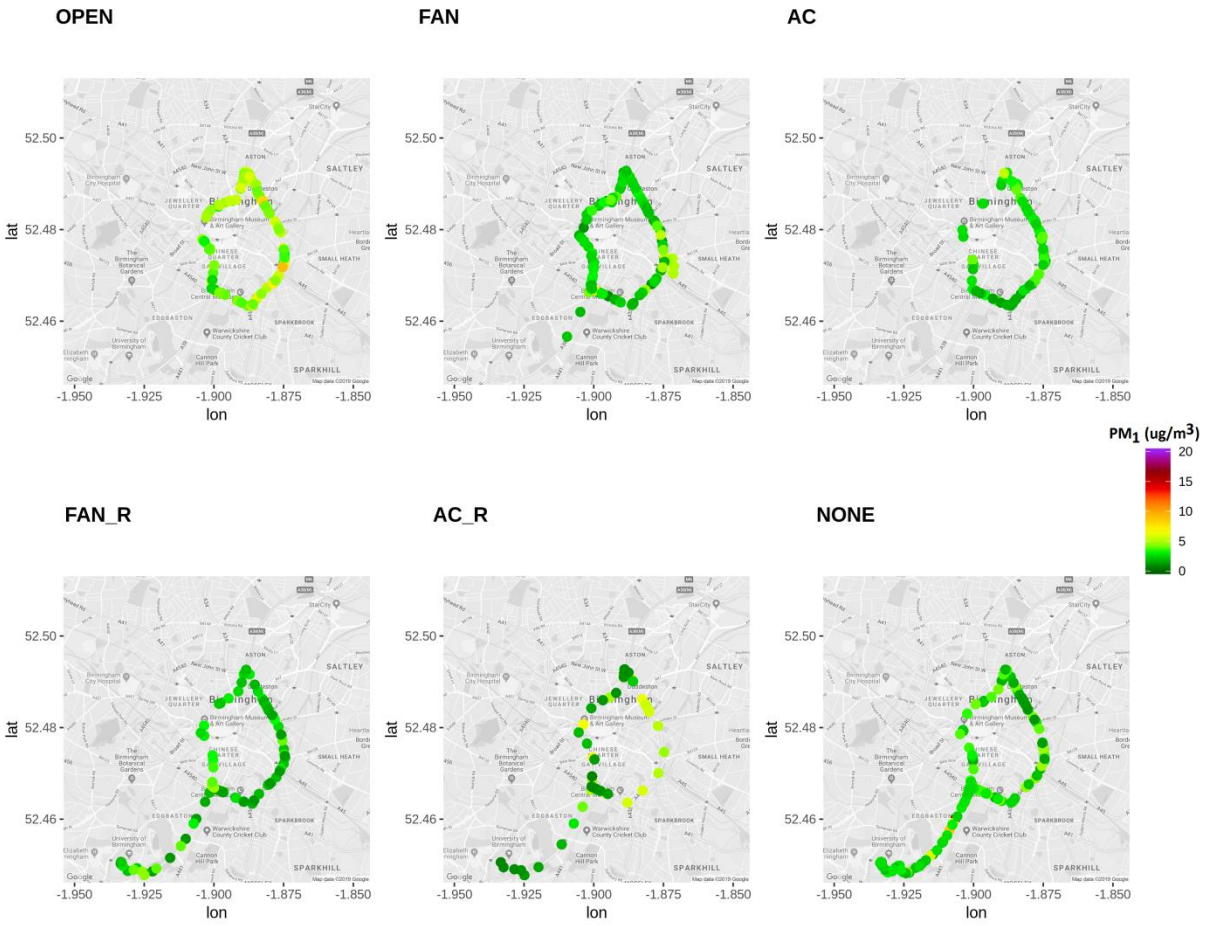


Figure A8. Within-vehicle spatial exposure map for $PM_1$ under different ventilation options. OPEN: Windows open, FAN: Fan on, recirculation off, windows closed, AC: Fan plus Air condition on, recirculation off, windows closed, FAN_R: Fan on, recirculation, windows closed, AC_R: Fan plus AC on, recirculation, windows closed, NONE: No ventilation Fan or AC, windows closed.

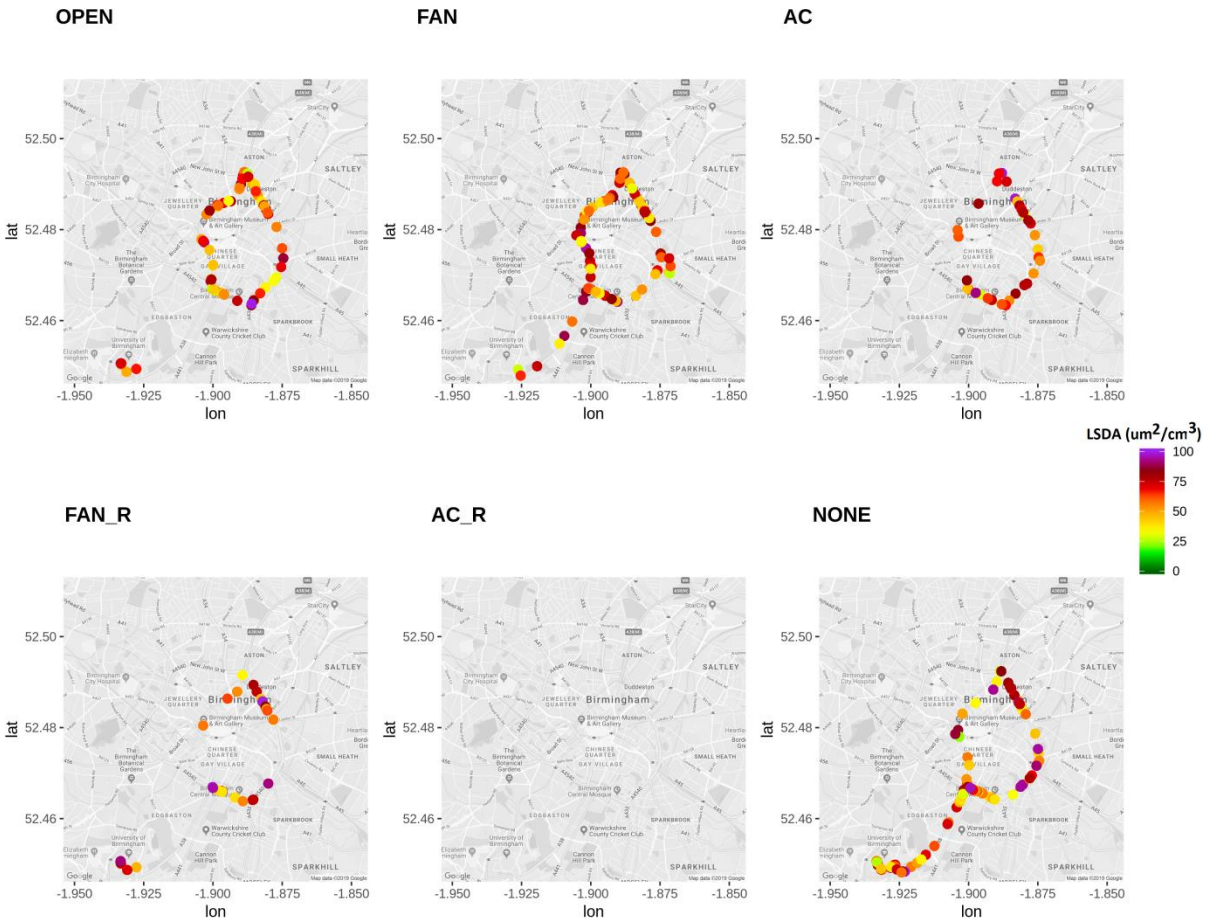


Figure A9. LSDA outside spatial exposure maps (as resulted by all vehicle trips) under different ventilations OPEN: Windows open, FAN: Fan on, recirculation off, windows closed, AC: Fan plus Air condition on, recirculation off, windows closed, FAN_R: Fan on, recirculation, windows closed, AC_R: Fan plus AC on, recirculation, windows closed, NONE: No ventilation Fan or AC, windows closed.

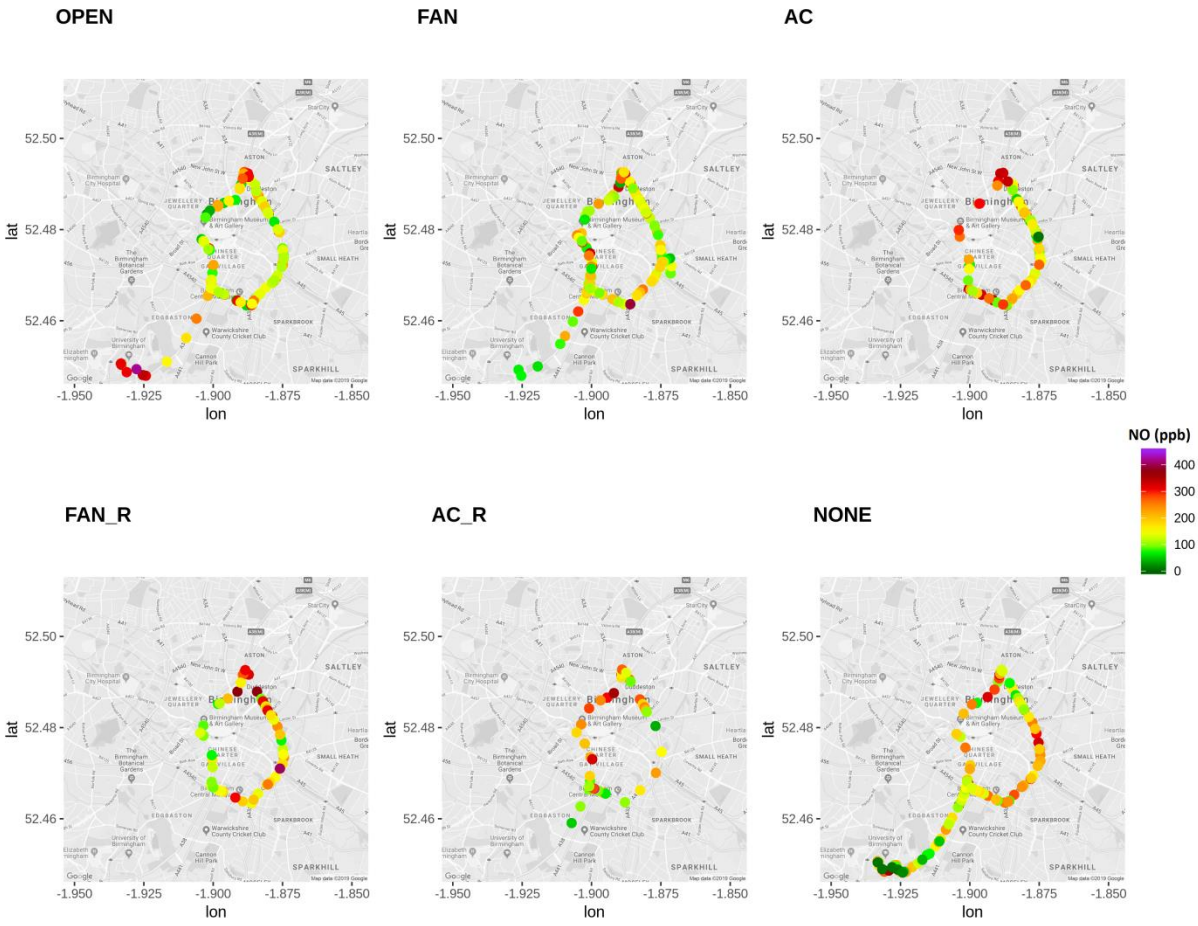


Figure A10. NO levels outside spatial exposure maps (as resulted by all vehicle trips) under different ventilations OPEN: Windows open, FAN: Fan on, recirculation off, windows closed, AC: Fan plus Air condition on, recirculation off, windows closed, FAN_R: Fan on, recirculation, windows closed, AC_R: Fan plus AC on, recirculation, windows closed, NONE: No ventilation Fan or AC, windows closed.

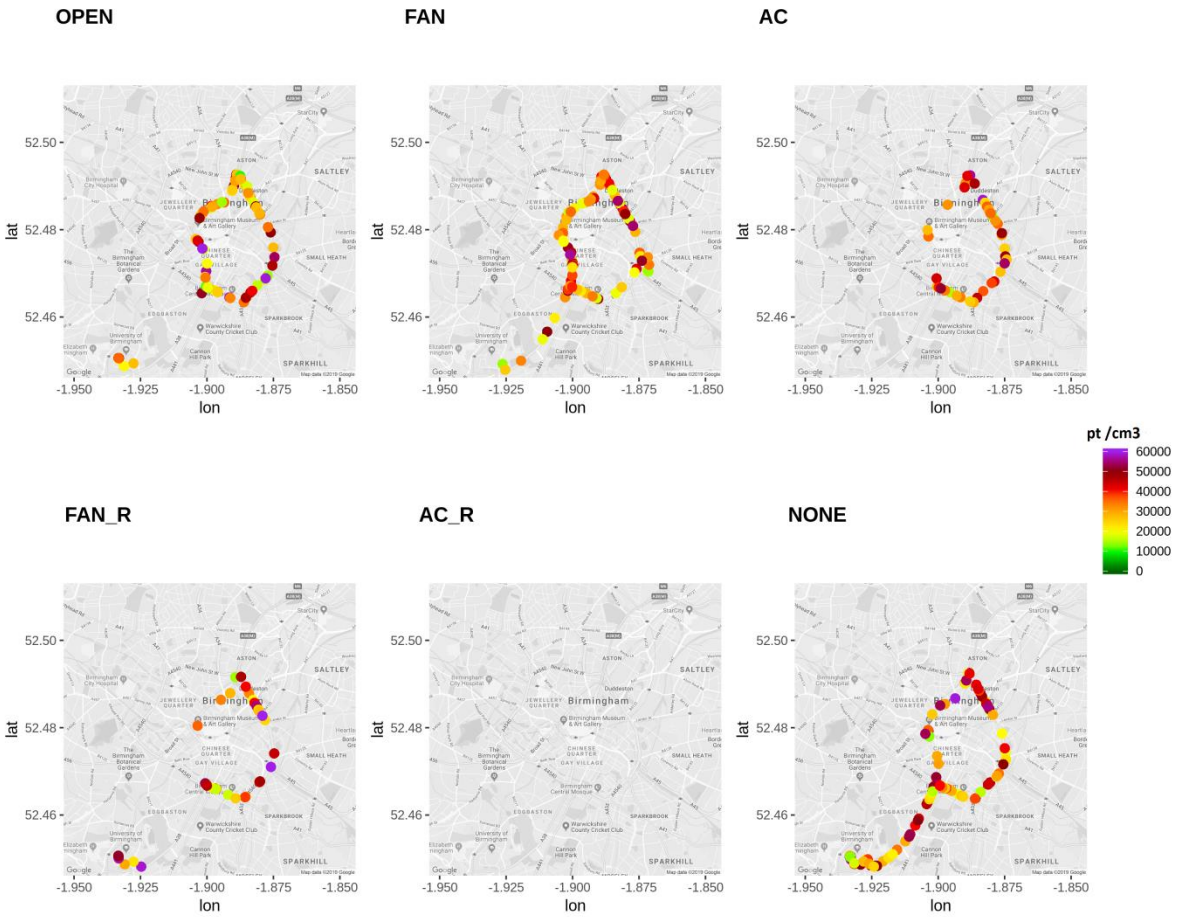


Figure A11. UFP number outside spatial exposure maps (as resulted by all vehicle trips) under different ventilations OPEN: Windows open, FAN: Fan on, recirculation off, windows closed, AC: Fan plus Air condition on, recirculation off, windows closed, FAN_R: Fan on, recirculation, windows closed, AC_R: Fan plus AC on, recirculation, windows closed, NONE: No ventilation Fan or AC, windows closed.

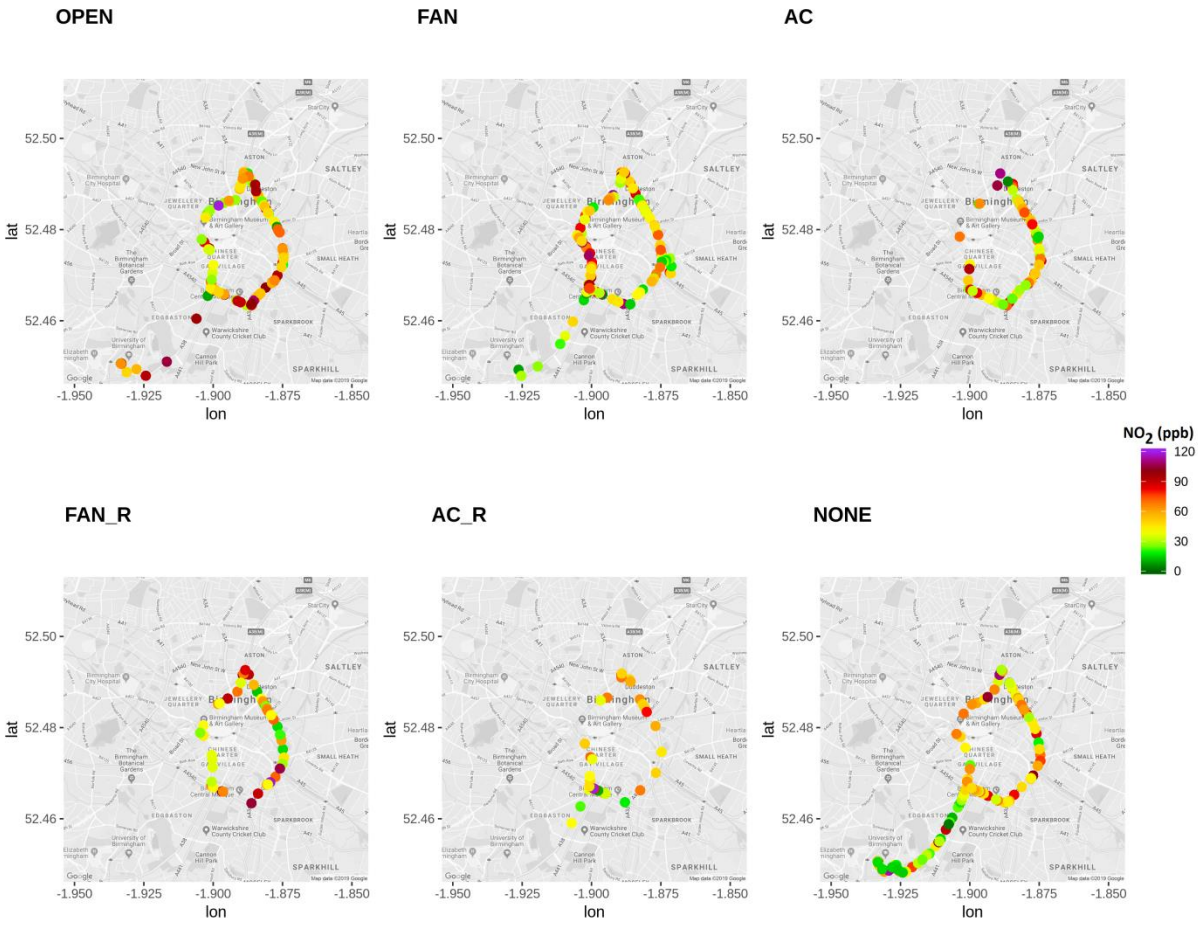


Figure A12. $NO_2$ levels outside spatial exposure maps (as resulted by all vehicle trips) under different ventilations OPEN: Windows open, FAN: Fan on, recirculation off, windows closed, AC: Fan plus Air condition on, recirculation off, windows closed, FAN_R: Fan on, recirculation, windows closed, AC_R: Fan plus AC on, recirculation, windows closed, NONE: No ventilation Fan or AC, windows closed.

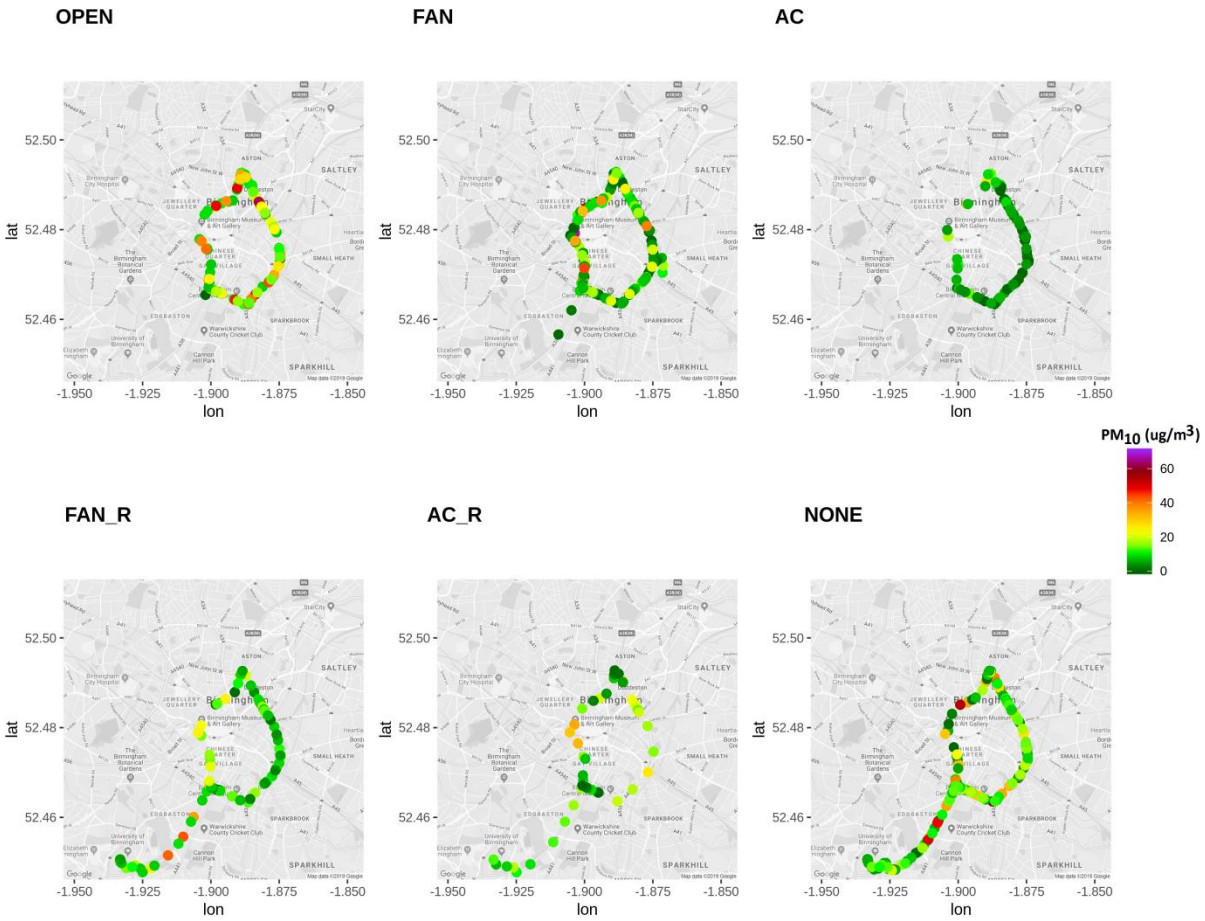


Figure A13. $PM_{10}$ levels outside spatial exposure maps (as resulted by all vehicle trips) under different ventilations OPEN: Windows open, FAN: Fan on, recirculation off, windows closed, AC: Fan plus Air condition on, recirculation off, windows closed, FAN_R: Fan on, recirculation, windows closed, AC_R: Fan plus AC on, recirculation, windows closed, NONE: No ventilation Fan or AC, windows closed.

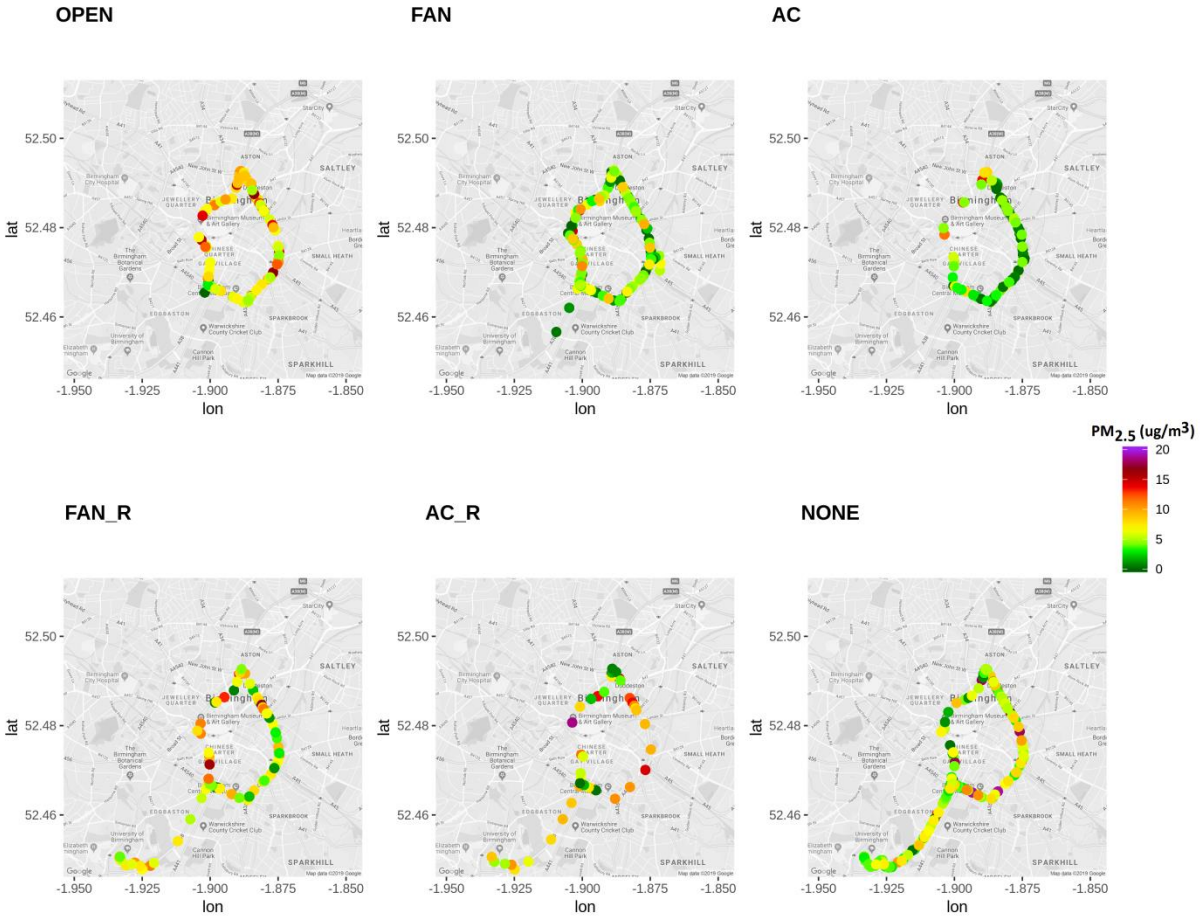


Figure A14. $PM_{2.5}$ levels outside spatial exposure maps (as resulted by all vehicle trips) under different ventilations OPEN: Windows open, FAN: Fan on, recirculation off, windows closed, AC: Fan plus Air condition on, recirculation off, windows closed, FAN_R: Fan on, recirculation, windows closed, AC_R: Fan plus AC on, recirculation, windows closed, NONE: No ventilation Fan or AC, windows closed.

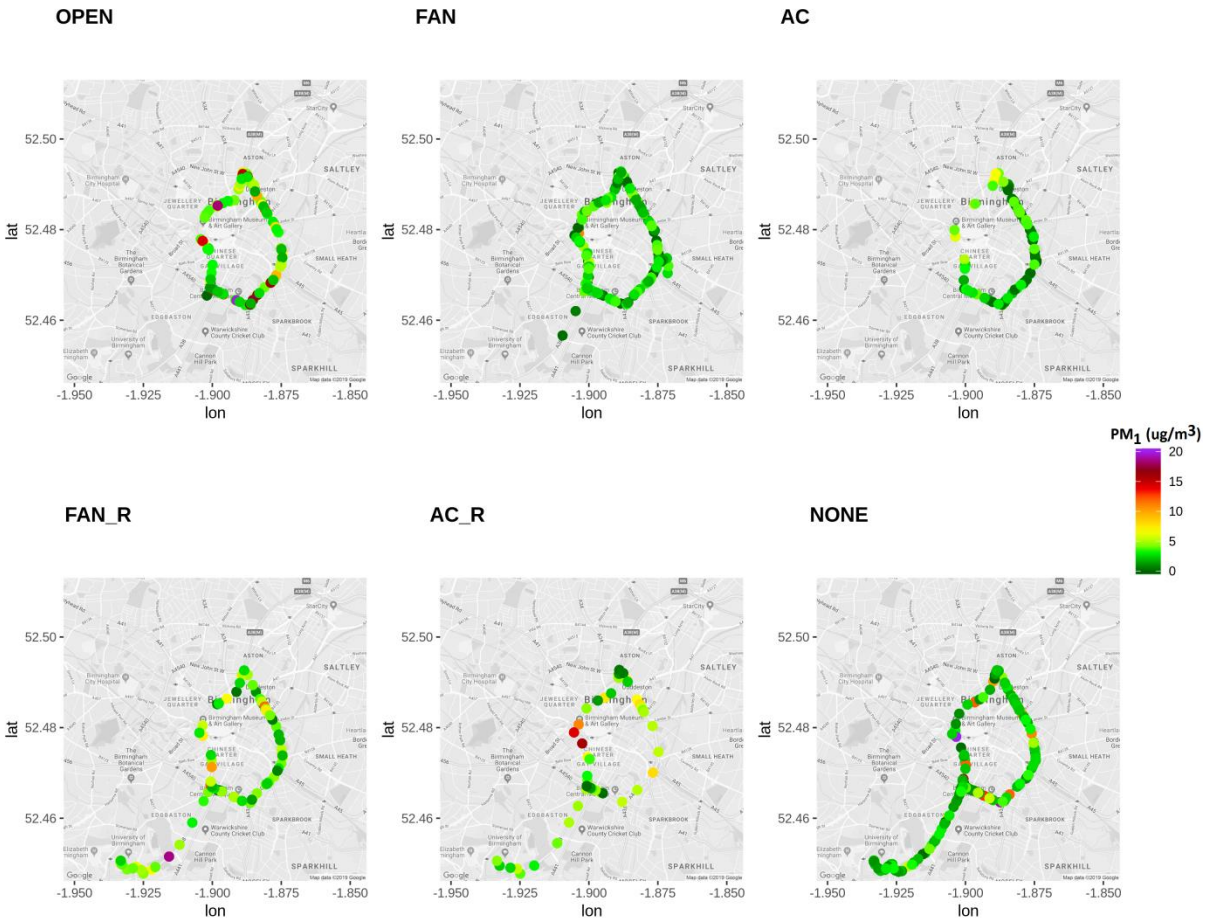


Figure A15. $PM_1$ levels outside spatial exposure maps (as resulted by all vehicle trips) under different ventilations OPEN: Windows open, FAN: Fan on, recirculation off, windows closed, AC: Fan plus Air condition on, recirculation off, windows closed, FAN_R: Fan on, recirculation, windows closed, AC_R: Fan plus AC on, recirculation, windows closed, NONE: No ventilation Fan or AC, windows closed.

# Appendix B

## Published articles